AD 255820

RADC-TR-61-70

PRECISE LONG RANGE RADAR DISTANCE MEASURING TECHNIQUES

C. K. RUTLEDGE

R. A. BOWERS J. C. MALLORY

J. T. CULVER G. H. NOBLE

CONVAIR (ASTRONAUTICS) DIVISION
GENERAL DYNAMICS CORPORATION
San Diego, California

CONVAIR REPORT NO. AE61-0114
15 February 1961

CONTRACT NO. AF30(602)-2115

Prepared For

ROME AIR DEVELOPMENT CENTER
AIR RESEARCH AND DEVELOPMENT COMMAND
UNITED STATES AIR FORCE
GRIFFISS AIR FORCE BASE
New York

RADC-TR-61-70

PRECISE LONG RANGE RADAR DISTANCE MEASURING TECHNIQUES

C. K. RUTLEDGE

R. A. BOWERS

J. X. MULVEY

J. L. CULVER

G. H. NOWAK

CONVAIR (ASTRONAUTICS) DIVISION
GENERAL DYNAMICS CORPORATION
San Diego, California

CONVAIR REPORT NO AE61-0061
13 February 1961

CONTRACT NO. AF30(602)-2196

RDF 60-006

Prepared For

ROME AIR DEVELOPMENT CENTER
AIR RESEARCH AND DEVELOPMENT COMMAND
UNITED STATES AIR FORCE
GRIFFISS AIR FORCE BASE
New York

FOREWORD

This report was prepared under Contract Number AF 30(602)-2196, Project Number 5703, Task Number 55040, to present the results of a study of very-long baseline radio tracking systems with baseline ranges of 200 nautical miles to 3000 nautical miles.

ABSTRACT

An analytical investigation of 200- to 3,000-nautical-mile baseline radio tracking systems was conducted. The evaluation considered the use of the systems in tracking and guiding earth satellites and lunar spacecraft. Representative error models for several tracking systems were formulated and compared. The comparison showed that systems which measure slant range only, contain fewer sources of error. A tracking system simulation employing computer programs and a high-speed digital computer is described. Use of the tracker simulation to depict the error model of a range-only tracking system, together with representative spacecraft trajectories is discussed. The results of the tracker simulation are presented for a system including survey (tracker location) errors and a system without survey errors. The comparison of these results shows that the survey errors are the limiting factor in the performance of long-baseline tracking systems in the measurement of spacecraft position and velocity.

An analysis of a geodetic satellite method of survey in the tracking system is presented. The method considers the problem of determining the distance of each tracking station from the earth's center of mass on an oblate earth.

An evaluation of tropospheric propagation effects on the radio measurement of slant range is presented. A technique based on regression analysis is described for determining the amount of the error in the measurement of slant range. The technique is suitable for highly accurate automatic real-time calculation of the correction for tropospheric propagation effects.

TABLE OF CONTENTS

TABLE OF CONTENTS (Continued)

LIST OF ILLUSTRATIONS

LIST OF ILLUSTRATIONS (Continued)

LIST OF ILLUSTRATIONS (Continued)

LIST OF ILLUSTRATIONS (Continued)

LIST OF TABLES

LIST OF APPENDICES

SECTION I

INTRODUCTION

1.1 GENERAL

This report presents the analytical results of a six month's evaluation of radio/radar tracking and guidance techniques. The objective of the study was to analyze the capability of long baseline, earth-based radar systems for tracking and guiding vehicles in cislunar space. (Short baseline systems and angle-measuring systems, e.g., azimuth and elevation of a "tracking" radar, have not been considered in this study.) The primary mission of the long baseline systems is to track and guide manned and unmanned lunar-orbiting vehicles and lunar-landing vehicles. A secondary mission is to track and guide earth satellites and near-earth spacecraft. The minimum accuracy objective in guiding these vehicles is to attain a spherical error of probability (SEP) of one nautical mile for ranges up to 10,000 nautical miles, or an SEP of 1/10,000 of the range beyond 10,000 nautical miles. However, a review of operational requirements for 1965-70 cislunar vehicles indicates that an order of magnitude improvement in the guidance accuracy is desirable (SEP = 1/100,000 of radial distance from the earth). To accommodate variations in the performance of the spacecraft propulsion and flight control systems, the tracking accuracy must exceed this guidance accuracy requirement.

1.2 STUDY SCOPE

The baseline length considered in the study was restricted to distances of 200 to 3000 nautical miles. Analytical models representing the radar tracking systems were formulated for ground station complexes to measure the following basic parameters:

(1) three ranges,
(2) three range sums,
(3) three range differences, and
(4) range rates.

In addition, hybrid systems were considered which employ combinations of these basic parameters, e.g., one range and two range sums.

A tracking complex measuring three ranges is the most fundamental of these systems. In this system the distances R_1, R_2, and R_3 (Figure 1) are measured separately. This is accomplished by measuring the time lapse in propagating a radio signal from station T_1 to the spacecraft and back to T_1, by measuring the time lapse in propagating a second radio signal from station T_2 to the spacecraft and back to T_2, and similarly for the third distance. The spacecraft position is the intersection of the three spherical surfaces determined by the three range measurements.

Ir a range sum system the spacecraft location is determined from three sets of measurements of the time lapse in propagating a radio signal from one station to the spacecraft and then to a second station. Thus, the measurements represent the set:

$$R_1 + R_2$$

$$R_2 + R_3$$

$$R_3 + R_1.$$

The spacecraft position is the intersection of the three ellipsoidal surfaces determined by these range sum measurements, see Figure 2.

In a three range difference system, a signal from the spacecraft is received at each of four ground stations and the times of arrival of the signal are noted at each station. From these four time observations three independent time differences can be formed which represent the set of three range differences:

$$\Delta R_1 \propto t_1 - t_4$$
$$\Delta R_2 \propto t_2 - t_4$$
$$\Delta R_3 \propto t_3 - t_4$$

The spacecraft position is the intersection of the three hyperbolic surfaces determined by these range difference measurements.

In analyzing these systems it was assumed that: 1) in the measurement of position parameters, radio signals are propagated over the appropriate paths and one or more "clocks" are used to measure the elapsed time on the paths; 2) the range rate is derived from the Doppler effect on signal frequency; 3) the signal reflected or retransmitted at the spacecraft was undelayed or delayed by a known amount. These assumptions permitted a maximum of flexibility and realism in depicting error models for the tracking systems and in analyzing the errors in tracking typical spacecraft.

The geometrical figure involved in locating a spacecraft relative to three ground stations can be visualized as a tetrahedron with the vehicle at the apex and the three stations at the corners of the tetrahedron base. However, in describing the motion of a spacecraft, it is necessary to relate its position to the earth's gravitational field. This, requires that the position of the tracking stations be known, relative to the earth's center of mass. This in turn, establishes a second tetrahedron whose apex is at the center of mass. The situation is represented in Figure 1. From the figure it can readily be seen that acquiring accurate knowledge of spacecraft position and motion entails an accurate knowledge of the three coordinates of each station, as well as the three slant ranges from the stations to the spacecraft.

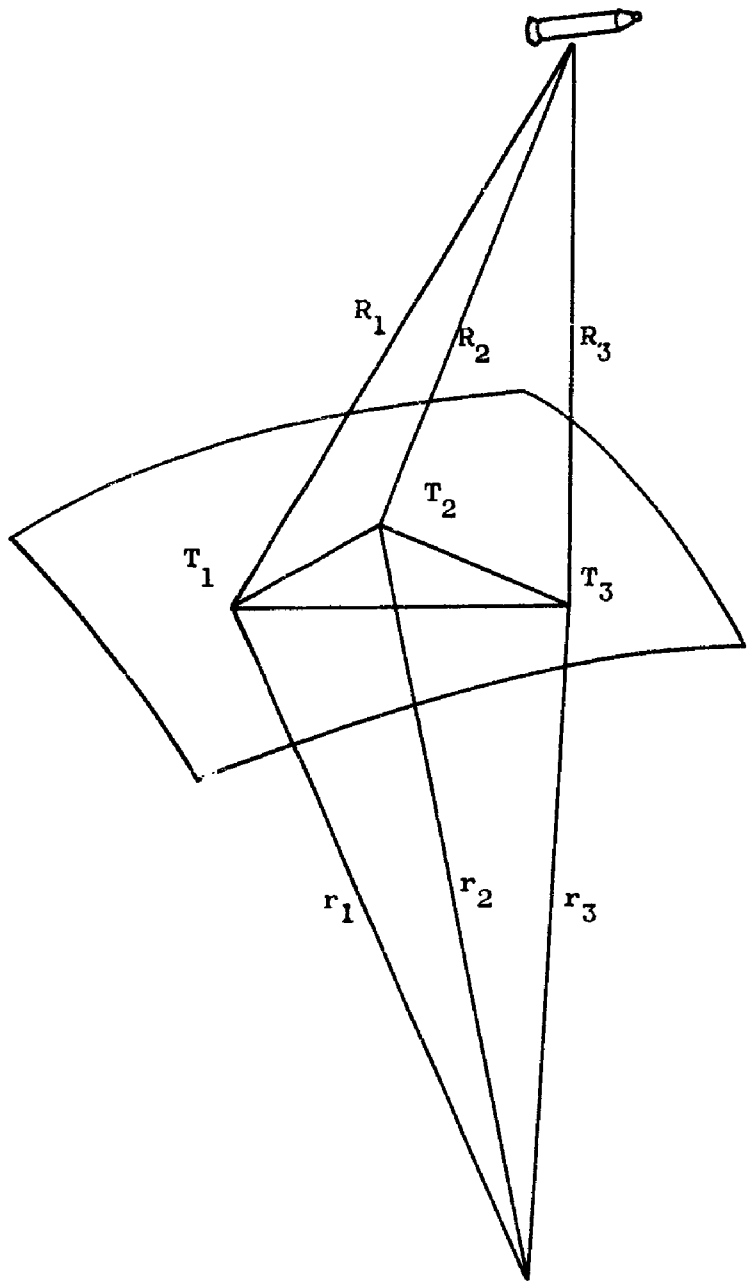

Figure 1. Tracking System Geometry

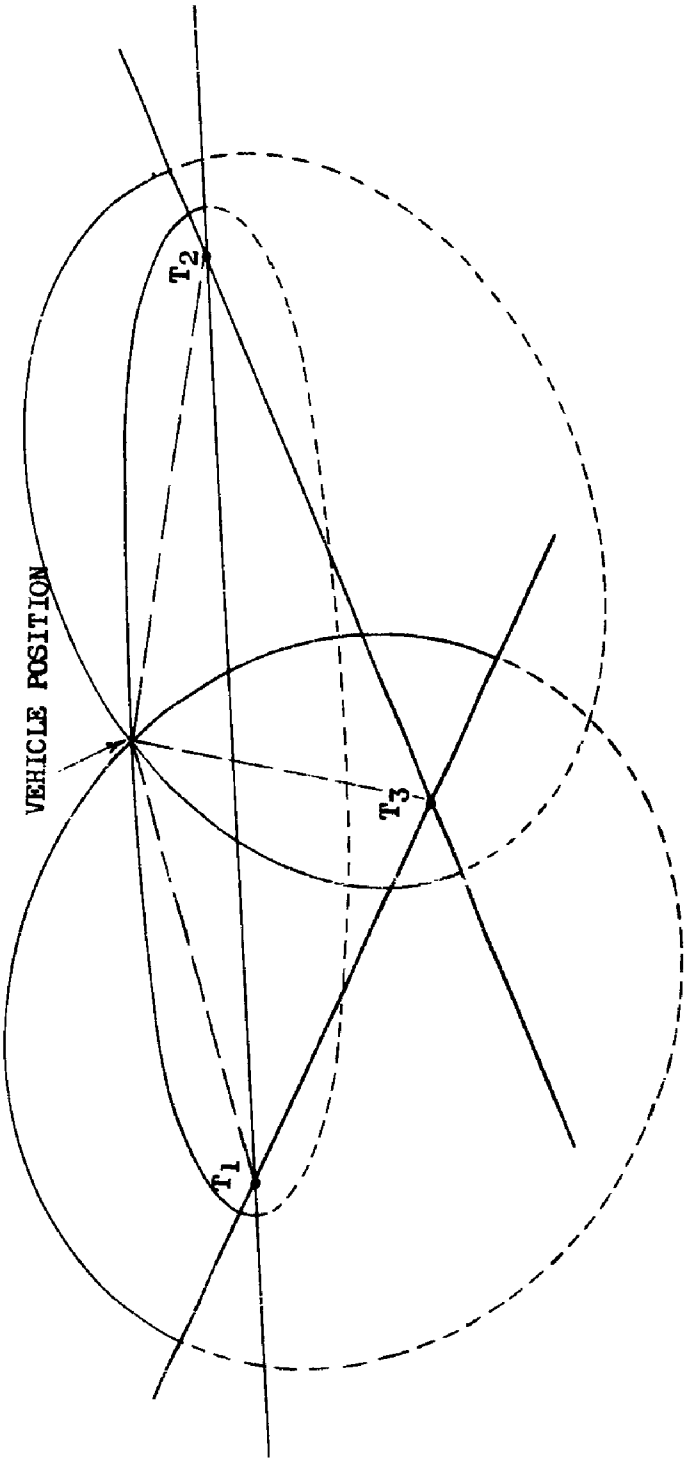

Figure 2. Three Range Sum Ellipses

1.3 STUDY METHODS

Since the primary objective of the study was to evaluate the performance of tracking systems, analytical techniques were employed to simulate, with the aid of a high-speed digital computer, the tracking characteristics of the systems. In the simulation program the tracking system geometry was represented in a geocentric coordinate system. The location of each tracking station was depicted in this coordinate system, as well as spacecraft position and velocity data. Thus, the computer program simulated the situation which a real tracking system would have encountered in tracking the spacecraft from horizon to horizon. In addition, the program included provisions for calculating the partial derivatives of the spacecraft position and velocity with respect to tracking system parameters, such as station longitude and latitude, slant range, and radial distance of the station from the earth's center of mass. The partial derivatives were then combined with estimates of probable errors in the tracking system parameters. In combining the probable errors from the various sources, mathematical methods were employed which accounted for the presence (or absence) of correlation in the errors. In this manner, the tracker simulation program computed the probable errors in spacecraft position and velocity that would result if these errors had been present in a real system.

The tracking systems of the study involve several special problem areas in common. These include the problems of establishing the accuracy with which: 1) coordinates can be determined for each tracking station, 2) corrections can be made for tropospheric and ionospheric propagation effects on the system measurements, and 3) "clocks" can be synchronized at the several stations. Surveys of classified and unclassified literature relating to these common problems were made. Also discussions were held with specialists to determine the current and near future state of the art in these subject areas. Detailed studies were undertaken in the areas of tropospheric propagation and in satellite methods of surveying the tracking system. These studies were pursued in rather considerable detail because of their special importance in relation to the performance of long baseline tracking systems. Detailed description of the work performed in this study is contained in the following sections of this report.

SECTION II

THE GEOMETRICAL TRACKING MODEL

2.1 TRACKING MODEL INTRODUCTION

The tracking analysis is based on a model of the earth, its atmosphere, and on selected spacecraft trajectories. The model chosen for this study is the result of an effort to represent as realistically as possible the tracking parameters which go into the error analysis without including refinements which would be cumbersome mathematically while contributing nothing essential to the final results.

The physical model includes the International Spheroid and circular equatorail orbits. Although a spherical earth model would suffice for the present analysis, future advantage to this approach is foreseen in its use as a subroutine in programs involving non-equatorial orbits. Data from a lunar trajectory, available in Convair-Astronautics files, was also used in the physical model.

A new and simple atmospheric model using a spherical earth, was developed to replace the flat-earth model for expressing range errors due to atmospheric effects as a function of elevation angle.

The details of these model features and the coordinate systems employed are explained on the following pages. Concluding the section is a short discussion on the limitations of long baseline tracking systems in providing coverage for low-altitude satellites.

A glossary of symbols for Sections II and III is presented in paragraph 2.7.

2.2 COORDINATE SYSTEMS AND ROTATION MATRICES

The computer program used in the analysis of tracking system performance employs several sets of coordinate systems. These coordinate systems are all right-handed orthogonal systems with their origin at the earth's center of mass. One system is associated with position and motion of the spacecraft. A second system, rotating with the earth, is associated with each station of the tracking complex. The third system, also rotating with the earth, is oriented with two axes in the plane of the equator and one aligned with the earth's axis of rotation. Each of these coordinate systems is illustrated in Figure 3. The more precise description of the directions defined by the axes of these coordinate systems are as follows: 1) X'', Y'', Z'' are coordinates which rotate in such a way that Z'' is through the missile, X'' in the plane of $\bar{r}$ and $\bar{v}$, and Y'' is perpendicular to X'' and Z'' so as to form a right handed system. 2) X_n', Y_n', Z_n' are coordinates which are fixed with respect to the rotating earth.

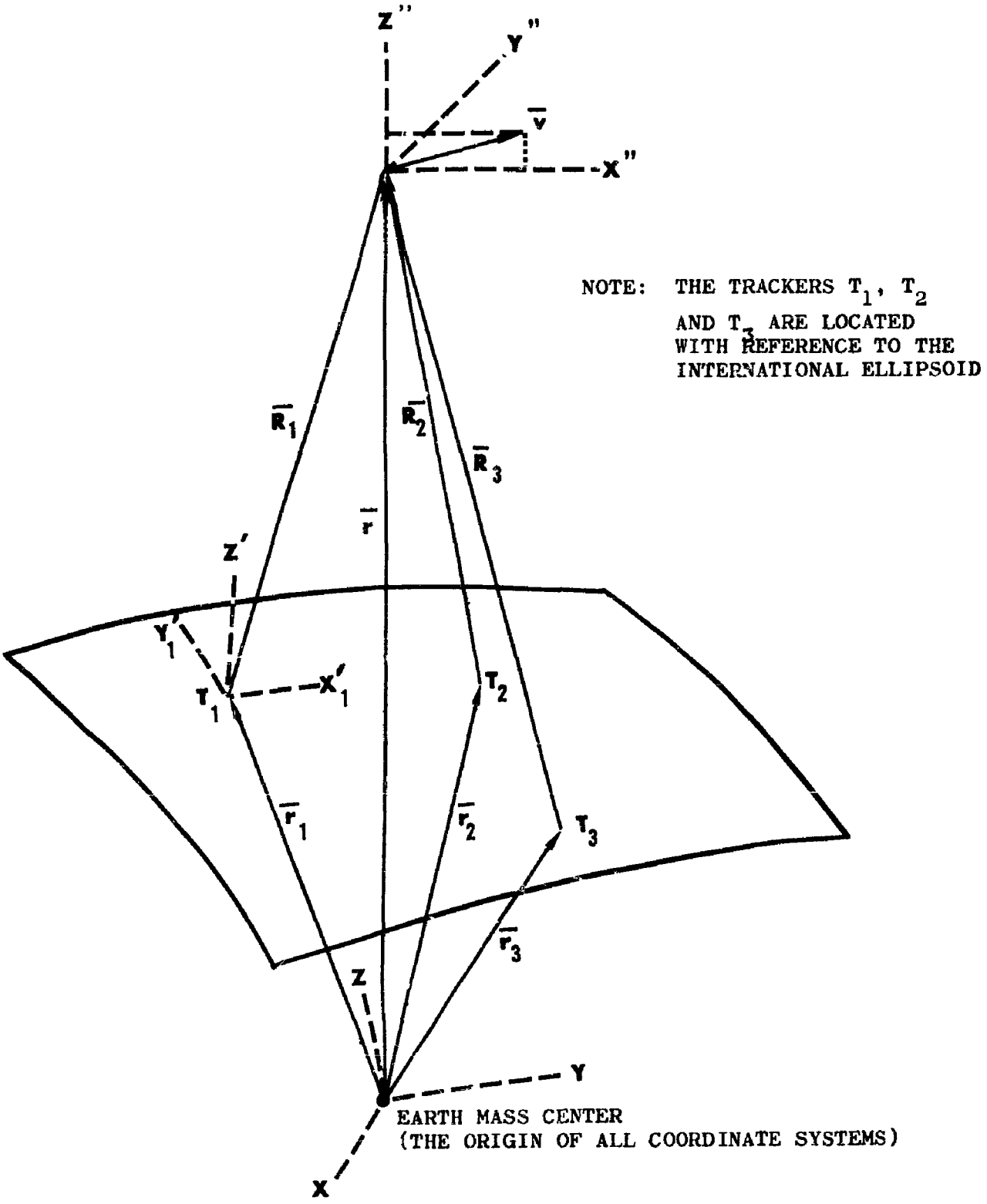

Figure 3. Coordinate Systems Employed in Tracker Analysis

Z_n' is in the direction of the normal to the spheroid at station n, and X_n' is in the direction of east and Y_n' in the direction of north at station n, and 3) X, Y, Z are coordinates which are fixed with respect to the rotating earth. X is through the point on the spheroid having zero latitude and zero longitude, Z is the axis of rotation of the earth, and Y is normal to X and Z so as to form a right handed system.

All geometrical computations in the computer program were performed in X, Y, and Z coordinates. Several short subroutines were provided to rotate the vector position and velocity of the spacecraft into this system. (These coordinate transformations are required because the available file of spacecraft trajectory programs are expressed in several different coordinate systems.) For the present treatment, however, it will be understood that trajectory data is given in X_4', Y_4', and Z_4' coordinates. Five three-by-three rotation matrices will be employed in all:

$$M_5 = \left[\bar{1}_{X''} \; \bar{1}_{Y''} \; \bar{1}_{Z''}\right]^* \quad \text{and} \quad M_n = \left[\bar{1}_{X_n'} \; \bar{1}_{Y_n'} \; \bar{1}_{Z_n'}\right] \quad n = 1, 2, 3, 4$$

M_1, M_2, and M_3 are used in internal computations, M_4 rotates $\bar{r}'$ and $\bar{v}'$ into $\bar{r}$ and $\bar{v}$, and M_5 rotates $\bar{r}$ and $\bar{v}$ into $\bar{r}''$ and $\bar{v}''$.

2.3 THE OBLATE EARTH

The International Spheroid was chosen as the geometrical surface of reference for use in this study. Trackers are located by latitude and longitude coordinates on the spheroid and by a vertical coordinate, h, along the perpendicular to the spheroid. Figure 4 illustrates the coordinates involved.

The following relationships provide a means of computing the required functions of either ϕ_i or ϕ_i' given one or the other.

$$\sin\phi = \frac{\sin\phi'}{\left(\sin^2\phi' + \frac{b^4}{a^4}\cos^2\phi'\right)^{1/2}}$$

$$\cos\phi = \frac{\cos\phi'}{\left(\cos^2\phi' + \frac{a^4}{b^4}\sin^2\phi'\right)^{1/2}}$$

*Denotes matrix transpose

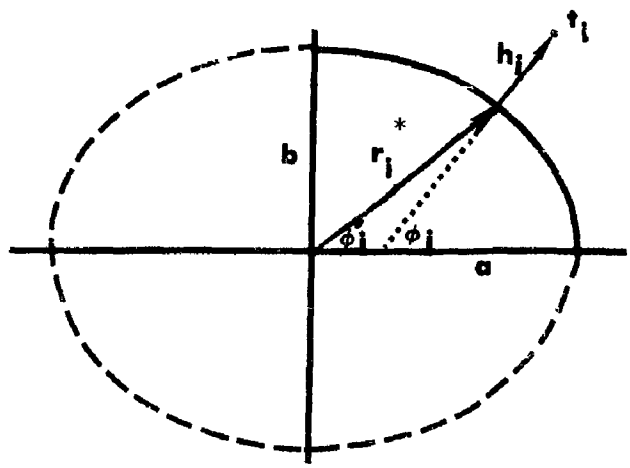

Figure 4. Oblate Earth

$$\sin \phi' = \frac{\sin \phi}{\left(\sin^2 \phi + \frac{a^4}{b^4} \cos^2 \phi\right)^{1/2}}$$

$$\cos \phi' = \frac{\cos \phi}{\left(\cos^2 \phi + \frac{b^4}{a^4} \sin^2 \phi\right)^{1/2}}$$

The equatorial radius, a, is 20,926,428 feet, and the polar radius, b, is 20,855,969 feet. Using the center of mass of the spheroid as an origin, the vector position of tracker i is

$$\bar{r}_i \begin{bmatrix} X_i \\ Y_i \\ Z_i \end{bmatrix} \begin{bmatrix} r_i^* \cos \phi' \cos \lambda + h_i \cos \phi \cos \lambda \\ -r_i^* \cos \phi' \sin \lambda - h_i \cos \phi \sin \lambda \\ r_i^* \sin \phi' + h_i \sin \phi \end{bmatrix}$$

Given target position, $\overline{r}'$, then,

$$\overline{r} = \begin{bmatrix} X \\ Y \\ Z \end{bmatrix} = M_4 \overline{r}' = M_4 \begin{bmatrix} X' \\ Y' \\ Z' \end{bmatrix} .$$

The range vector $\overline{R}_i$ is

$$\overline{R}_i = \overline{r} - \overline{r}_i = \begin{bmatrix} X - X_i \\ Y - Y_i \\ Z - Z_i \end{bmatrix}$$

2.4 THE ATMOSPHERE

In order to simulate tracking errors, it is necessary to have an atmospheric model (see Figure 5 below) because radio waves passing from a vacuum into and through a medium of index of refraction >1 undergo bending and decrease in velocity of propagation. According to Snell's Law, for $V = V(\rho)$ (a function of ρ alone)

$$\rho \frac{\sin i}{V} \text{ equals a constant}$$

In practice, the effects of atmospheric refraction are taken into account in the range computations, ordinarily using a standard atmosphere.

In a study of tracking errors, however, one is dealing with residual effects after the correction has been made. Consequently, it is not necessary to employ an atmospheric model of greater complexity than that necessary to represent the residual errors.

Although the functional dependence of range errors on elevation angle is seldom taken into account in studies of this nature, its effect is well recognized. A flat-earth model with atmosphere of uniform index of refraction and thickness is generally used with considerable success at Convair-Astronautics. Figure 6 illustrates the flat-earth model.

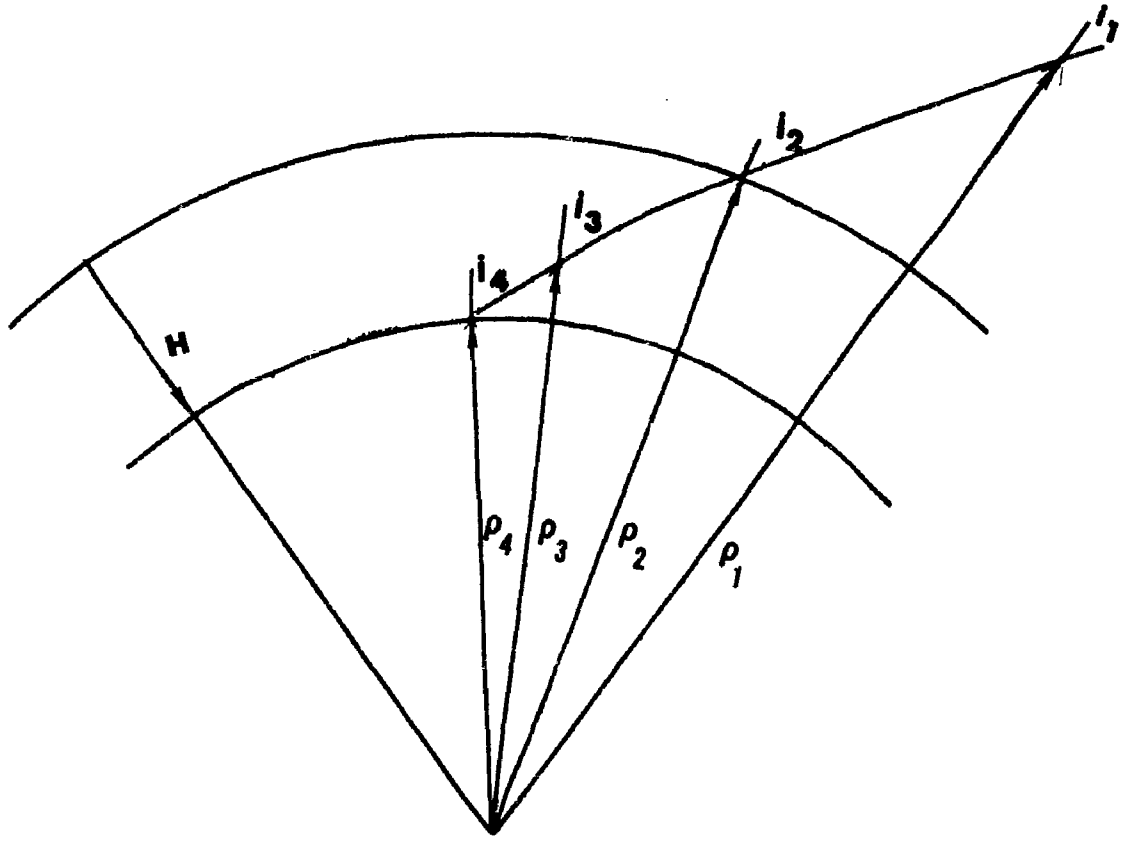

Figure 5. Ray Path Bending

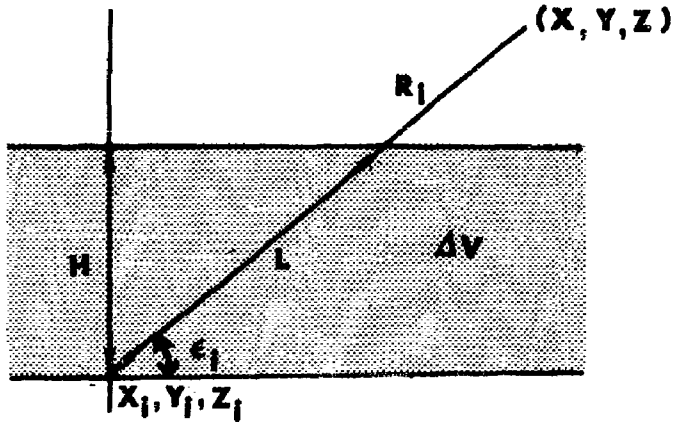

Figure 6. Flat Earth Atmospheric Model

A missile at (X, Y, Z) is observed from tracker i at (X_i, Y_i, Z_i). The electric path from missile to tracker has a portion of its path

$$L_i = H \csc \epsilon_i$$

within the atmosphere where the speed of propagation is $(c - \Delta V)$ and a portion outside the atmosphere where its speed of propagation is c. Ignoring the slight effects of residual bending, the time delay in traversing portion L_i is

$$\Delta t_i \cong \frac{L_i}{c^2} \Delta V$$

and the corresponding interpretational error in R_i is

$$\Delta R_i \cong L_i \frac{\Delta V}{c}$$

For the flat earth model, $\sigma_{R_i}^2$ becomes simply

$$\sigma_{R_i}^2 \cong \sigma_p^2 \csc^2 \epsilon_i$$

where $\sigma_{p_i}^2$ is obtained empirically. $\sigma_{p_i}^2$ is the variance of R_i due to propagation effects for a zenith observation at tracker i. Expression (2-1) behaves well except in the neighborhood of $\epsilon_i = 0$, where it expands rapidly. An expression based on a spherical earth model which behaves well for all values of ϵ_i and which computes easily has been developed. (Figure 7 illustrates the spherical earth model.)

The expression is:

$$L_i = (r_i^2 \sin^2 \epsilon_i + 2 r_i H + H^2)^{1/2} - r_i \sin \epsilon_i$$

$$\Delta R_i \cong L_i \frac{\Delta V}{c}$$

and for the spherical earth model, $\sigma_{R_i}^2$ becomes

$$\sigma_{R_i}^2 = \sigma_{P_i}^2 \left[(A^2 \sin^2 \epsilon_i + 2A + 1)^{1/2} - A \sin \epsilon_i \right]^2$$

where $2A = \frac{\sigma_{h_i}^2}{\sigma_{p_i}^2} - 1.$

The elements $\sigma_{p_i}^2$ and $\sigma_{h_i}^2$ are the variances of R_i due to propagation effects at tracker i for zenith and horizon observations, respectively, and are obtained empirically. As a matter of interest, the value of H corresponding to this treatment is

$$H = \frac{2 r_i \sigma_{p_i}^2}{\sigma_{h_i}^2 - \sigma_{p_i}^2} \cong 2 r_i \frac{\sigma_{p_i}^2}{\sigma_{h_i}^2} .$$

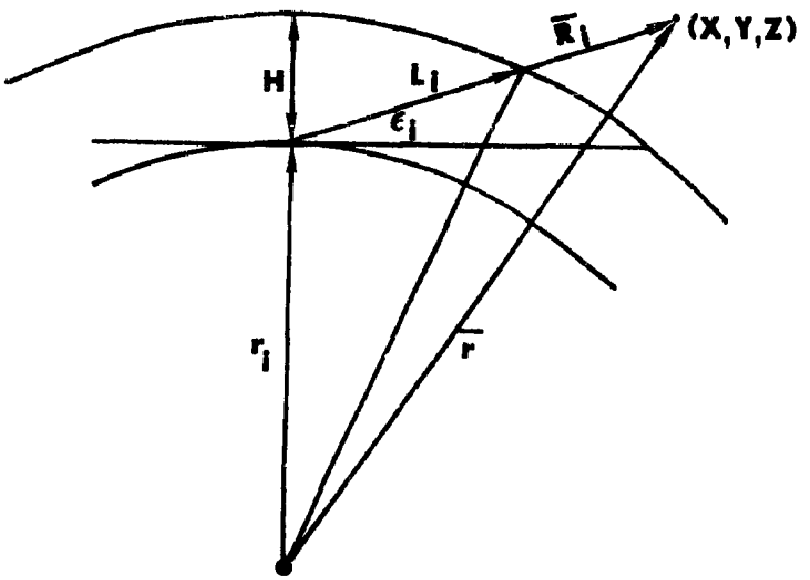

Figure 7. Spherical Earth Atmospheric Model

2.5 TRAJECTORY DATA

Eight equatorial orbits and one lunar trajectory were simulated on the Convair-Astronautics IBM 7090 for analysis of two equilateral tracking complexes.

2.5.1 Equatorial Orbits

The gravitational field of the International Spheroid is:

$$g = \frac{GM}{r^2} \left[1 - C_1 \frac{a^2}{r^2} (3 \sin^2 \phi - 1) + C_2 \frac{a^4}{r^4} \left(\frac{35}{3} \sin^4 \phi - 10 \sin^2 \phi + 1 \right) \right]$$

For an equatorial orbit the latitude, ϕ = O, and

$$g_e = \frac{GM}{r^2}\left[1 + C_1\frac{a^2}{r^2} + C_2\frac{a^4}{r^4}\right]$$

where $C_1 = 0.0016382$

and $C_2 = 0.0000045$.

For a circular orbit, $g_\theta = K'M\omega^2 r$, and

$$\omega^2 = K\frac{a^3}{r^3}\left[1 + C_i\frac{a^2}{r^2} + C_2\frac{a^4}{r^4}\right] \quad \text{rad}^2/\text{sec}^2,$$

where $K = 1.5361686 \times 10^{-6}$.

This equation was used to compute eight circular equatorial orbits at altitudes of 100, 300, 600, 1000, 3000, 6000, 10,000, and 19,324 nautical miles. The magnitude of the orbital velocity was computed:

$$v = r\ (\omega - \Omega)$$

where ω and Ω are the angular velocity of the satellite and tracker complex (rotating with the earth), respectively. The satellite velocity with respect to tracker net is then, v. For 19,324 nautical miles elevation, $\omega = \Omega$, and the satellite remains stationary with respect to the trackers. This is the so-called "24-hour orbit".

In the analysis of tracking satellite orbits the set of trackers were located as shown in Table 1.

Table 1. Location of Trackers in Analysis of Tracking Satellite Orbits

T	λ	ϕ	h
1	0°	9.6506789°	1492.3 feet
2	8.3774642°	- 4.8081969°	0.0 feet
3	- 8.3774642°	- 4.8081969°	0.0 feet

The coordinates were computed so as to give an equilateral configuration of precisely 1000 nautical mile base-line length and so that in the "overhead" case:

$$R_1 = R_2 = R_3$$

$$\epsilon_1 = \epsilon_2 = \epsilon_3$$

and a perpendicular from the satellite to the plane of the tracker triangle goes through the centroid of the triangle and also through the center of the earth. Tracker locations were so chosen to provide a simple spot check on all quantities computed, which, in the overhead case, are rapidly done on a hand calculating machine. They were also chosen to give results which would depend as little as possible on geometrical parameters other than elevation angle and radius of orbit.

2.5.2 Lunar Trajectory

Data were taken from a simulated lunar trajectory in the Convair-Astronautics files, starting from launch at Cape Canaveral on January 23, 1960 and terminating in the vicinity of the moon. Thirty-four points, comprising two complete passes of the vehicle from horizon to horizon, were computed. These points are evenly spaced from t = 0.331 day, (r = 379.30 megafeet) to t = 1.774 days, (r = 1012.14 megafeet).

In order to lend realism to the lunar spacecraft tracking simulation, tracker sites were chosen as shown in Table 2.

Table 2. Location of Tracker Sites for Lunar Spacecraft Tracking Simulation

	λ	ϕ	h
Haiti	72° 20'20"	18° 30'00"	24 feet
Guatemala	91° 30'00"	14° 49'00"	7657 feet
Alabama	85° 46'40"	32° 52'59"	59 feet

These sites make up an equilateral triangle, exactly 1200 nautical miles on a side. In this case, however, the orbital points correspond to fairly unfavorable tracking geometry, in order to simulate the performance of a non-strategically located tracking system in tracking a typical lunar mission. (It is obvious that any three given tracker locations can not be optimum for all future missions, thus this case is considered to be more realistic than an analysis in which the tracking system is shifted around so that the spacecraft is continually in the "overhead" position.)

2.6 LONG BASELINE SYSTEM TRACKING COVERAGE

A characteristic disadvantage of long baseline systems is the limited coverage provided to near-earth spacecraft. The requirement that the spacecraft be in view of all three trackers simultaneously may be stated as follows:

$$\overline{1}_{r_i} \cdot \overline{1}_{R_i} > 0 \qquad i = 1, 2, 3$$

If tracking is limited by other factors, such as tropospheric propagation effects, to elevation angles greater than ϵ_o, then the conditions become:

$$\overline{\uparrow}_{r_i} \cdot \overline{\uparrow}_{R_i} > \sin \epsilon_o \qquad i = 1, 2, 3$$

Figure 8 illustrates the effect of these limitations for equilateral tracker configurations of baseline lengths of 200 to 2000 nautical miles. The height of the satellite below which tracking cannot be provided, is shown as a function of the system elevation angle tracking limit. For example, if tracking below 10 degrees elevation angle is not permitted and the tracking system baselines are 1600 nautical miles, then tracking can be provided for satellities above 300 nautical miles.

Another way of viewing this coverage is shown in Figure 9 for systems tracking down to the local horizontal. The figure presents the percent of the circular orbit path covered for a satellite passing over one of the tracking stations and bisecting the opposite baseline. Here, for example, a 2200 nautical mile baseline system can track 15 percent of the path of a satellite orbiting at an altitude of 1500 nautical miles, or correspondingly, for a duration of 22 minutes. The coverage depicted in these two figures is the maximum coverage that can be provided for equilateral triangular configurations. Less coverage would be provided for satellite or spacecraft passing to one side of the tracking system.

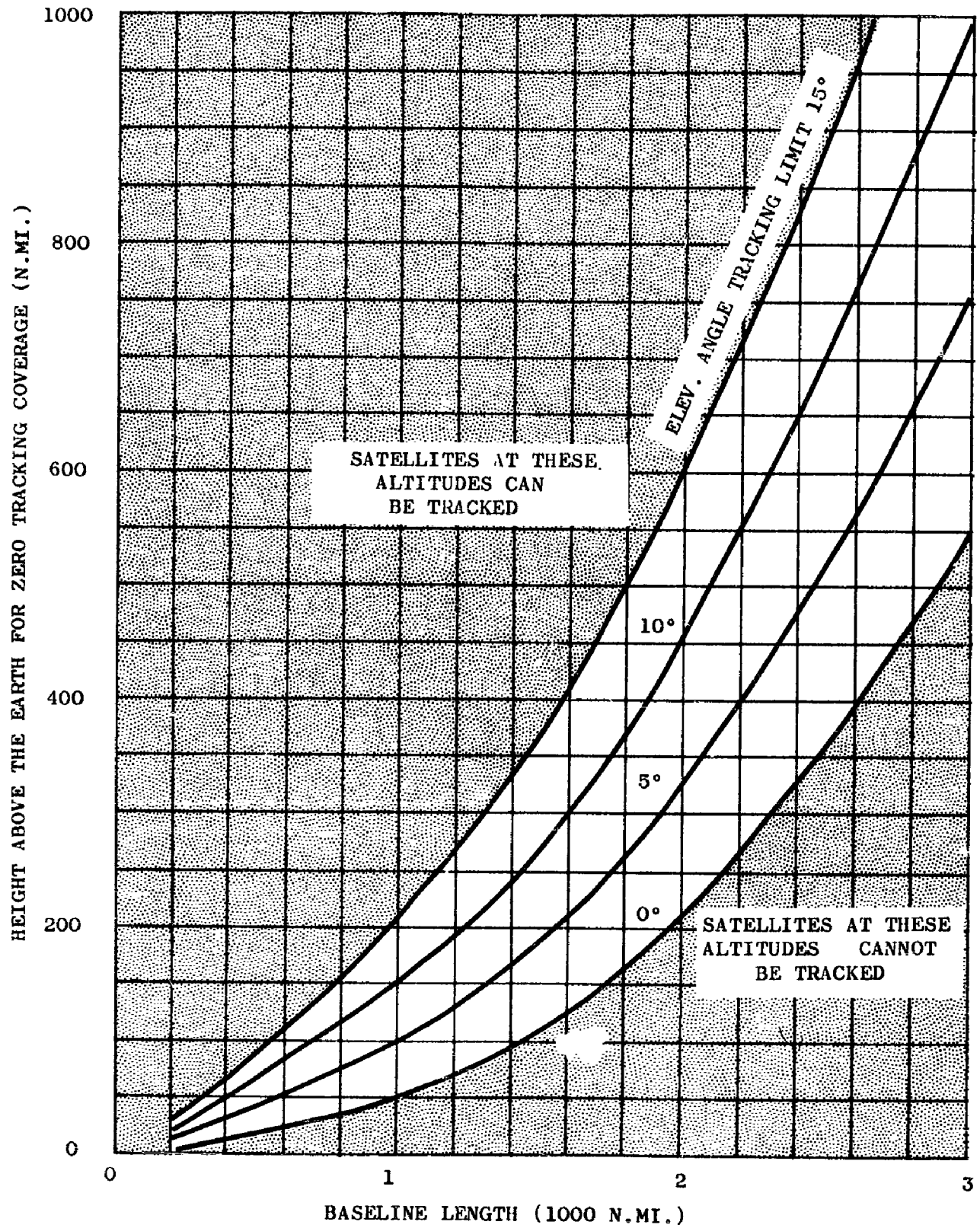

Figure 8. Minimum Orbit Altitude vs. Baseline Length for Various Elevation Angles

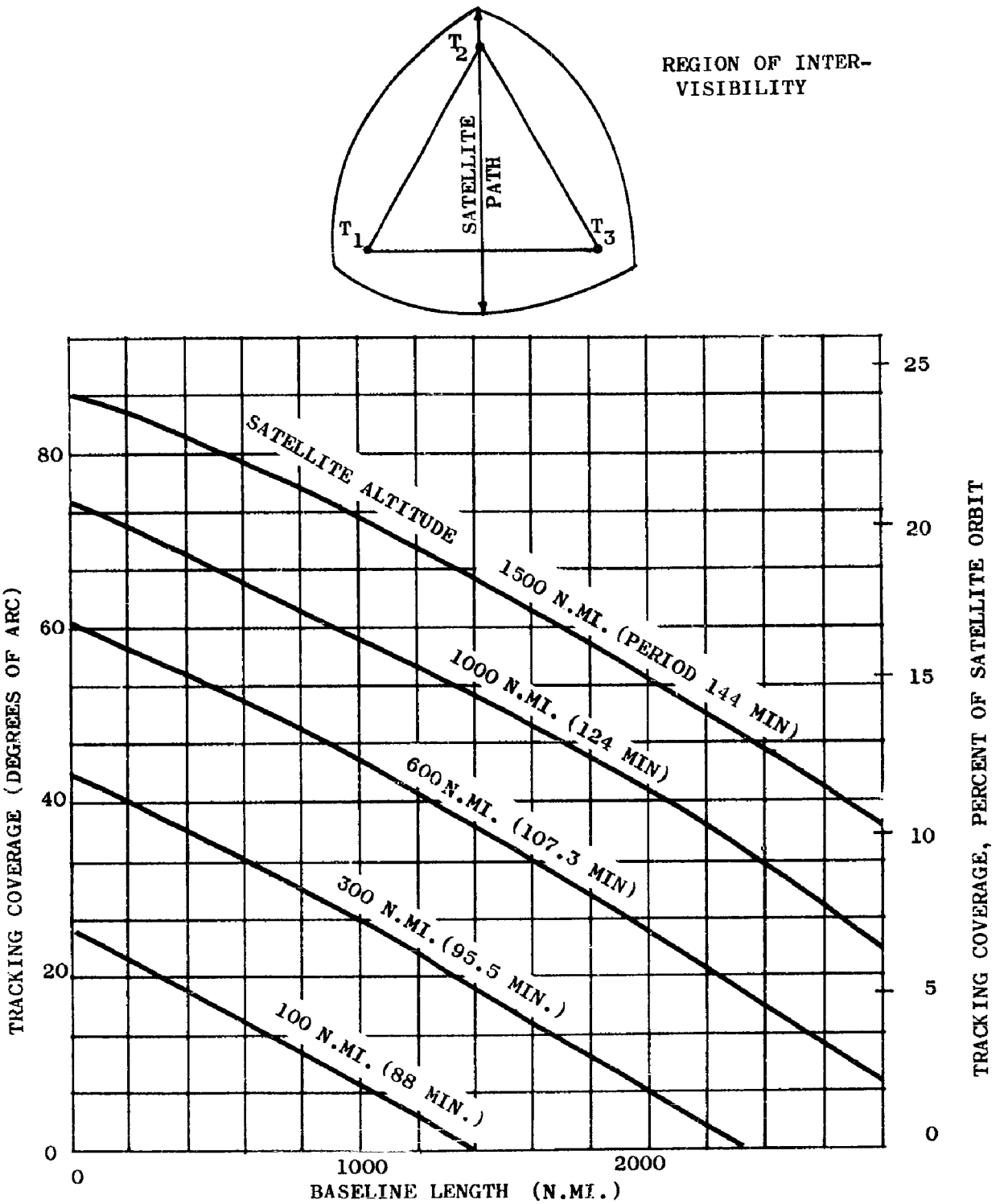

Figure 9. Tracking Coverage for Circular Orbits

2.7 GLOSSARY OF SYMBOLS

a = equatorial radius of earth

b = polar radius of earth

C = velocity of light in vacuum

h_i = height of station i above the reference spheroid

H = model atmosphere thickness

L_i = slant range path in model atmosphere to tracker i

N_i = separation of geoid and spheroid at station i

$\overline{r}_i$ = vector from earth's center of mass to station i

r_i^* = length of vector from the earth's center of mass to a point on the spheroid below station i

$\overline{R}_i$ = vector from station i to missile

$\overline{r}$ = vector from earth's center of mass to missile

$\overline{v}$ = velocity of missile

ϕ_i' = geocentric latitude of station i

ϕ_i = geographic latitude of station i

λ_i = longitude of station i

$\overline{1}_q$ = unit vector in the q direction

T_i = tracker i

ρ = radial distance from center of earth

V = velocity of electromagnetic propagation

ϵ_i = elevation angle of missile at tracker i

ω = angular velocity of missile

Ω = angular velocity of earth

SECTION III

ERROR ANALYSIS

3.1 GENERAL

Errors in spacecraft position and velocity result from errors in the quantities which go into their computation. These errors are usually small enough to be treated as differentials, and, as such, their squares are ignored. Thus, any system error, Δa_i, may be propagated into an error in spacecraft position, $\overline{\Delta r}$, and velocity, $\overline{\Delta v}$, by

$$\overline{\Delta r} = \begin{bmatrix} \Delta x \\ \Delta y \\ \Delta z \end{bmatrix} = \Delta a_i \begin{bmatrix} \frac{\partial x}{\partial a_i} \\ \frac{\partial y}{\partial a_i} \\ \frac{\partial z}{\partial a_i} \end{bmatrix} \qquad \overline{\Delta v} = \begin{bmatrix} \Delta \dot{x} \\ \Delta \dot{y} \\ \Delta \dot{z} \end{bmatrix} = \Delta a_i \begin{bmatrix} \frac{\partial \dot{x}}{\partial a_i} \\ \frac{\partial \dot{y}}{\partial a_i} \\ \frac{\partial z}{\partial a_i} \end{bmatrix}$$

The partial derivatives are a measure of the sensitivity of tracking errors to errors in a_i and usually become very large for certain portions of a trajectory, ordinarily near the plane of the tracker triangle.

This section contains a discussion of the system errors, the geometrical partial derivatives and their formation, and the statistical considerations which are involved in arriving at a meaningful evaluation of tracking precision. Several significant achievements were made in this particular phase of the study. One is the demonstration of equivalence of a broad category of range, range sum, and range difference hybrid tracking systems insofar as their errors are concerned. This advance eliminates the need for individual analysis of the enormous number of combinations of R_i, $(R_i + R_j)$, and $(R_i - R_j)$, making it possible to design a tracking net and also leaving the designer relatively free to consider only those hybrids which are advantageous from the standpoint of hardware implementation and operation.

A second important result of the following analysis is the establishment of a proper set of ground rules for handling the correlation of range and range-rate errors. This leads to a far more realistic representation of tracking precision in two important regions - near the horizon, where elevation angles become small, and in deep space, where ranges are large. In both cases the overall tracking accuracy estimated from results of other studies of this subject

(which neglect the effect of correlation) is insufficient to recommend the long baseline system. But in both cases the proper treatment of correlation in range and range-rate errors clearly shows that tracking errors are only a small fraction of those presented in prior reports by other organizations.

A third contribution which shows great promise in the field of tracker design is the development of a new analytic method of optimizing baseline length so as to render maximum tracking precision for particular missions. The procedure is only outlined in the present report and illustrated by a single case study, owing to the fact that it was initiated late in the contract period.

An analysis of a 4-tracker, three range difference system is presented in the latter portion of the section. The model corresponds to the situation in which an uncooperative object is tracked by measurement of arrival time at four ground stations of a pulse or other identification signal emitted at an unknown time from the object itself.

The final part of the section describes the computer simulation of the tracking model and discusses the numerical results of runs made for eight equatorial orbits and one lunar trajectory.

3.2 THE ERROR MODEL

Several reports on tracking errors which have appeared as the result of prior contract awards have been examined in the course of a general survey of the literature on this subject. In all cases which have come to our attention, the errors dealt with were errors in range and range rate, and no consideration was given to the correlation which exists among them. If this assumption were true, deep space guidance from earth-based trackers would be virtually impractical. Entirely erroneous results are likewise obtained at low elevation angles. It may be that the following equation is true:

$$\sigma^2_{R_n} = \sigma^2_o + \left(\sigma^2_f + \sigma^2_c\right) R^2_n + \left(\sigma^2_k + \sigma^2_{k_b}\right) f^2\left(\epsilon_n\right) + \left(\sigma^2_t + \sigma^2_{t_b}\right) \dot{R}^2_n + \sigma^2_{X'_n} \left(\bar{1}_{X'_n} \cdot \bar{1}_{R_n}\right)^2 + \sigma^2_{Y'_n} \left(\bar{1}_{Y'_n} \cdot \bar{1}_{R_n}\right)^2 + \sigma^2_{Z'_n} \left(\bar{1}_{Z'_n} \cdot \bar{1}_{R_n}\right)^2,$$

but $\begin{vmatrix} \sigma^2_X & \sigma_{XY} & \sigma_{XZ} \\ \sigma_{YX} & \sigma^2_Y & \sigma_{YZ} \\ \sigma_{ZX} & \sigma_{ZY} & \sigma^2_Z \end{vmatrix}$ is not equal to

$$\begin{vmatrix} \frac{\partial X}{\partial R_1} & \frac{\partial X}{\partial R_2} & \frac{\partial X}{\partial R_3} \\ \frac{\partial Y}{\partial R_1} & \frac{\partial Y}{\partial R_2} & \frac{\partial Y}{\partial R_3} \\ \frac{\partial Z}{\partial R_1} & \frac{\partial Z}{\partial R_2} & \frac{\partial Z}{\partial R_3} \end{vmatrix} \begin{vmatrix} \sigma^2_{R_1} & 0 & 0 \\ 0 & \sigma^2_{R_2} & 0 \\ 0 & 0 & \sigma^2_{R_3} \end{vmatrix} \begin{vmatrix} \frac{\partial X}{\partial R_1} & \frac{\partial Y}{\partial R_1} & \frac{\partial Z}{\partial R_1} \\ \frac{\partial X}{\partial R_2} & \frac{\partial Y}{\partial R_2} & \frac{\partial Z}{\partial R_2} \\ \frac{\partial X}{\partial R_3} & \frac{\partial Y}{\partial R_3} & \frac{\partial Z}{\partial R_3} \end{vmatrix}$$

as is generally assumed.

In the study, rather than deal with three range errors and three range-rate errors as though they were uncorrelated, 27 individual system errors are considered. They are, at trackers 1, 2, and 3, respectively:

a. timing	Δt_1,	Δt_2,	Δt_3
b. timing	Δt_b,	Δt_b,	Δt_b
c. propagation	Δk_1,	Δk_2,	Δk_3
d. propagation	Δk_b,	Δk_b,	Δk_b
e. frequency	Δf_1,	Δf_2,	Δf_3
f. velocity of light	Δc,	Δc,	Δc
g. zero set	ΔS_1,	ΔS_2,	ΔS_3
h. east tracker coordinate	$\Delta X_1'$,	$\Delta X_2'$,	$\Delta X_3'$
i. east tracker coordinate	$\Delta X_b'$,	$\Delta X_b'$,	$\Delta X_b'$
j. north tracker coordinate	$\Delta Y_1'$,	$\Delta Y_2'$,	$\Delta Y_3'$
k. north tracker coordinate	$\Delta Y_b'$,	$\Delta Y_b'$,	$\Delta Y_b'$
l. vertical tracker coordinate	$\Delta Z_1'$,	$\Delta Z_2'$,	$\Delta Z_3'$
m. vertical tracker coordinate	$\Delta Z_b'$,	$\Delta Z_b'$,	$\Delta Z_b'$

These 27 errors are assumed to be independent and uncorrelated. In practice there are 27 standard deviations involved in the final covariance matrices of position and velocity of the spacecraft. However, the results presented in this report assume that equivalent equipment

and timing are established at each tracker site, that the same methods are employed in making the atmospheric corrections, and that all locations are surveyed independently with the same methods. Under these assumptions the standard deviations of equivalent quantities are equal:

$$\sigma t_i = \sigma t$$

$$\sigma f_i = \sigma f$$

$$\sigma s_i = \sigma s \qquad i = 1, 2, 3$$

$$\sigma k_i = \sigma k$$

$$\sigma X_i' = \sigma X'$$

$$\sigma Y_i' = \sigma Y'$$

$$\sigma Z_i' = \sigma Z'$$

It is for this reason that the typical variance and covariance terms, σX^2 and σXY, as discussed in paragraph 3.7, contain only 14 distinct variances, σa_i^2.

3.3 SYSTEM ERRORS

The factors contributing errors in the radar measurements of tracking systems are depicted in generalized notation in Figure 10. The slant ranges to be measured by the system are denoted by R_1, R_2, and R_3. The tracking system is assumed to measure, via the radar signal, three sets of slant range sums, $R_i + R_j$; for example, $R_1 + R_2$, $R_2 + R_3$, and $R_3 + R_1$. The error model analysis shows that in general the ranging error is composed of contributions from five factors: timing, propagation, frequency, velocity of light, and zero set.

The timing errors, Δt_i, represent the inaccuracy in synchronization of each of the clocks within the system. In addition, there occurs a timing error, Δt_b, of the system with respect to a master clock (not a part of the system). Clock synchronization by radio propagation methods alone is not feasible because of the lack of accurate knowledge of the propagation path and propagation velocity, and, thus of the elapsed time on the path. Radio methods, however, can be used to maintain clock synchronization once it has been established. In the method described by Reder and Winkler, stable clocks at each of two stations are initially synchronized by physically transporting a third stable clock between stations. Radio signals in the VLF band are then used to compare the time rate (frequency) and phase of the station clocks, thus locking the clocks in synchronization. A clock synchronization of a few tenths of a microsecond was achieved.

RANGE ERRORS IN ($R_i + R_j$)

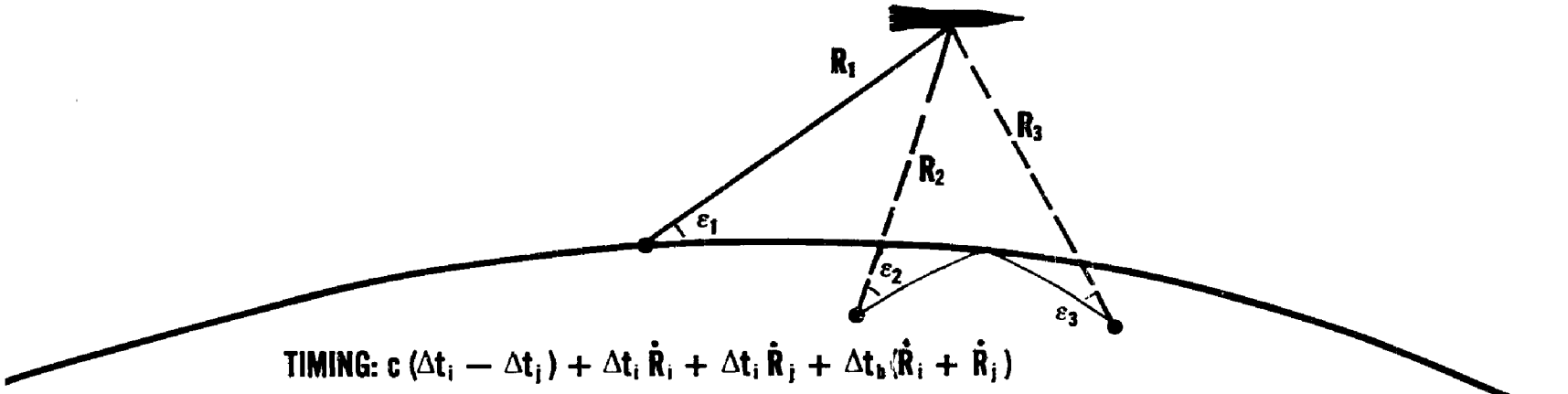

TIMING: $c\,(\Delta t_i - \Delta t_j) + \Delta t_i\,\dot{R}_i + \Delta t_i\,\dot{R}_j + \Delta t_b\,(\dot{R}_i + \dot{R}_j)$

PROPAGATION: $(k_b + k_i)\,f(\varepsilon_i) + (k_b + k_j)\,f(\varepsilon_j)$

VELOCITY OF LIGHT: $\dfrac{\Delta c}{c}\,(R_i + R_j)$

FREQUENCY: $-\dfrac{\Delta f_i}{f_i}\,(R_i + R_j)$

ZERO SET: Δs_i

Figure 10. Factors Contributing Errors to Range Measurements

In the computer simulation the values

$$\sigma t = 1.0 \text{ microsecond}$$

and $$\sigma t_b = 1.0 \text{ millisecond}$$

are used for the uncorrelated and correlated timing errors at each tracker.

A strong disadvantage to range sum or range difference measurements is immediately evident in the term, $C(\Delta t_i - \Delta t_j)$. If the time difference is of the order of one microsecond, a range sum error of almost 1000 feet results. However, it is sometimes possible to devise a clever procedure which nulls the effect of this error on computed values of missile position and velocity. For example, the three measurements

$$(R_1 + R_2), \quad (R_3 + R_1), \text{ and } (R_3 + R_2)$$

may be used to compute R_1 as follows:

$$R_1 = 1/2\ (R_1 + R_2) + 1/2\ (R_3 + R_1) - 1/2\ (R_3 + R_2),$$

Ignoring for the moment errors other than $c(\Delta t_i - \Delta t_j)$, the error ΔR_1 in R_1 is:

$$\Delta R_1 = 1/2\ c\ (\Delta t_1 - \Delta t_2) + 1/2\ c\ (\Delta t_3 - \Delta t_1) - 1/2\ c\ (\Delta t_3 - \Delta t_2), \qquad \Delta R_1 \equiv 0$$

Similarly, ΔR_2 and ΔR_3 may be nulled if all available range sum measurements are combined in the proper order to compute R_2 and R_3.

The second and third terms of the errors in range sum are very small, being proportional only to range-sum rates. However, no ingenious method of double-path cancellation can improve on the range-only measurement, for which i = j and the first term cancels identically. The cancellation is due to the fact that, for a range-only measurement, travel time along path $(R_1 + R_1)$ is taken from a single clock.

The range sum error due to uncertainty in the speed of signal propagation within the atmosphere has already been introduced in paragraph 2.4, Section II. An extension of the discussion is necessary, however, when three range sums are employed to compute missile position. Atmospheric irregularities may vary greatly in extent and configuration and, consequently, introduce a certain degree of error correlation for the three ray paths, R_1, R_2, and R_3. Not a great deal is known as a result of experiment because, ordinarily, atmospheric profiles are run individually: and an experimental study of the correlation coefficient requires simultaneous profiling over a large region. It is possible, however, to make an intelligent estimate, based on what we do know about the atmosphere. Obviously, the correlation coefficient for two range measurements approaches unity as the baseline between the trackers approaches zero length. It approaches a constant as baseline lengths become very large, the constant being

determined by the "goodness-of-fit" of the standard atmosphere employed in correction of the range measurements for refraction effects. In general, it may be said that the propagation error has a component, $k_i f(\epsilon_i)$, which is entirely uncorrelated for i = 1, 2, and 3; and a component, $k_b f(\epsilon_i)$, which is wholly correlated, k_b having the same value whether i is 1, 2, or 3. Referring to the notation of paragraph 2.4, then:

$$\sigma k_i^2 + \sigma k_b^2 = \sigma p_i^2 \quad \text{for } i = 1, 2, 3.$$

For the computer simulation, which uses baselines of 1000-1200 nautical miles, the values:

$$\sigma p_i = 1 \text{ foot}$$

$$\sigma h_i = 30 \text{ feet}$$

$$\sigma k_i^2 = \sigma k_b^2 = \sigma k^2$$

are considered reasonable.

The velocity of light and signal frequency act as scale factors in the sense that the error in range they produce is proportional to the range, itself. A tracking network may be designed to use one frequency from a single oscillator, or three frequencies from individual oscillators at each tracker. In the former case resultant range errors are totally correlated and

$$\frac{\Delta f_i}{f_i} = \frac{\Delta f}{f}; \quad i = 1, 2, 3.$$

In the latter case the error equality does not hold, but in either case the standard deviations of scale factor are assumed to be

$$\sigma f_i = \sigma f \qquad i = 1, 2, 3,$$

on the reasoning that equal equipment must have equal probable errors in output. The velocity of light, however, can have but a single error, and the standard deviation in scale factor is σc. It is quite fortunate that this is so, because at lunar distances range errors due to an error in c may be several hundred feet. If they were uncorrelated they would produce uncertainties in vehicle positon greater than those of all other system errors combined. Total correlation reduces their effect to insignificance. The values used in the computer simulation are:

$$\sigma c = 3 \times 10^{-7}$$

$$\sigma f = 1 \times 10^{-8}$$

The error referred to as "zero set" may be regarded as an error introduced by the equipment calibration at each tracker or may be used to represent any uncorrelated error in range which is independent of both the tracker configuration and the position of the space vehicle relative to it. The value used in the program is

$$\sigma s_1 = \sigma s_2 = \sigma s_3 = \sigma s = 10 \text{ feet.}$$

Figure 11 lists the corresponding errors in range-sum rate ($\dot{R}_i + \dot{R}_j$). Clock synchronization and zero set errors produce no errors in range rate, because in all cases the range-rate errors turn out to be time derivatives of the geometrical quantities involved in the range errors.

3.4 SURVEYING ERRORS

By far, the largest tracking errors are introduced through lack of knowledge of the tracker locations. This will continue to be the state of affairs for some time to come. Even though programs now being developed for the geodetic use of artificial earth satellites are carried through as swiftly and efficiently as possible, there will be a lag of months or perhaps several years before an organized, first-order reduction of satellite data can be concluded. Until this is accomplished one must continue to rely on the methods of classical geodesy.

Latitude and longitude in an isolated spot are obtained from a zenith observation at a known time. The principal lateral error in such a means of location arises from lack of knowledge of the direction of the local vertical with respect to the normal to the spheroid at that point. This deviation of the vertical is a deflection caused by mass anomalies, especially those in the immediate vicinity of the astronomical observation. Lateral errors of many thousands of feet may occur if nothing is known about these mass anomalies. Fortunately, however, several methods are available in the literature for computation of the deflection of the vertical from local gravity anomalies. One which is more easily applied than the others is "A New and Simple Method for Calculating the Deflections of the Vertical from Gravity Anomalies with the Aid of the Bessel Fourier Series" by Chuji Tsuboi, Proc. Japan Acad., 30, (1954), No. 6.

The precision of this computation is limited only by the extent and accuracy of gravity coverage around the station. Provided the above procedures are employed, it is not unreasonable to assume that lateral position on the earth's surface may be obtained with a standard deviation of 100 feet, in areas where gravity coverage is good and the gravity anomalies are not too irregular. The figure:

$$\sigma X' = \sigma Y' = 140 \text{ feet}$$

was used for all tracking simulations.

RANGE RATE ERRORS IN $(\dot{R}_i + \dot{R}_j)$

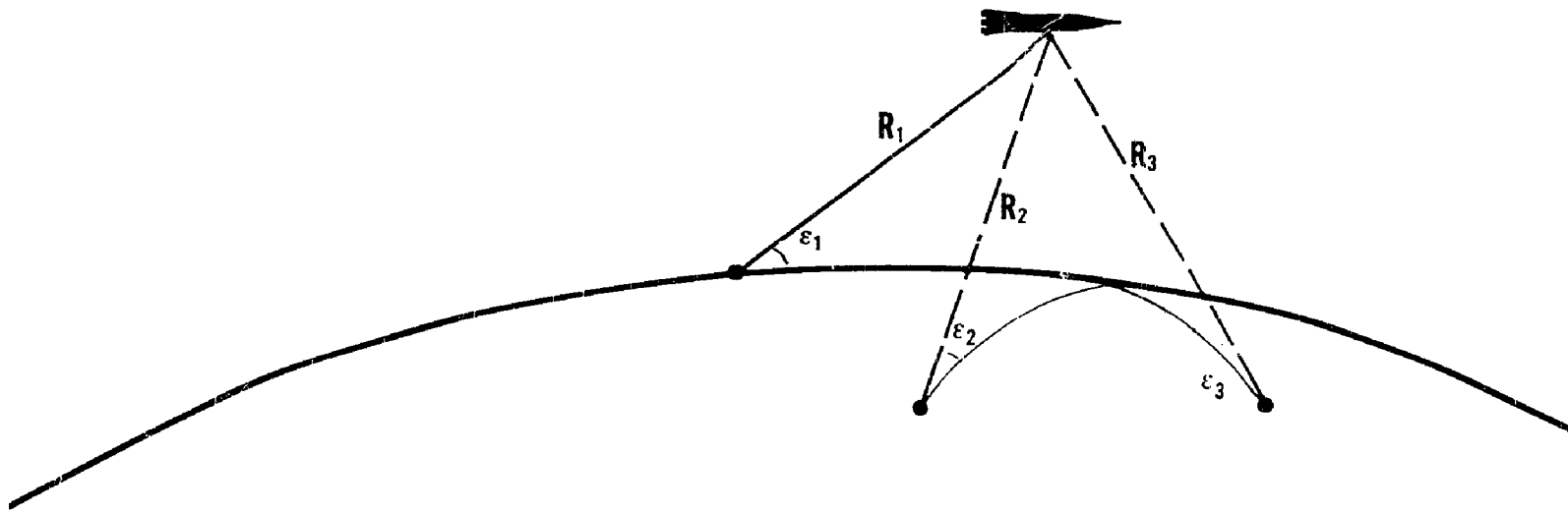

PROPAGATION: $(k_b + k_i)\,\dot{\varepsilon}_i\, f'(\varepsilon_i) + (k_b + k_j)\,\dot{\varepsilon}_j\, f'(\varepsilon_j)$

VELOCITY OF LIGHT: $-\frac{\Delta c}{c}(\dot{R}_i + \dot{R}_j)$

FREQUENCY: $-\frac{\Delta f_i}{f_i}(\dot{R}_i + \dot{R}_j)$

Figure 11. Factors Contributing Errors to Range Rate Measurements

Since the same mass anomalies enter, in differing degree, into the deflection of the vertical of all three trackers, there is a certain amount of correlation among the three errors in lateral location, even though no direct tie may exist in the measurements. In the case where a direct cross-country tie is made between stations A and B, the location errors at starting point A are carried directly to B with an additional error incurred between A and B. Thus, the very important problem of error correlation must be examined from the standpoint of the method of survey used. It is not within the present scope of this study to analyze specific problems of such nature, but (as will be seen in the results of the tracker simulation program) the errors in tracking due to correlated and uncorrelated survey errors are quite different from each other and are an order of magnitude more important than all other sources of error combined. A more detailed analysis of the surveying problem is suggested as the most promising means of improving the accuracy of currently feasible long baseline tracking systems. In the tracking simulation, correlated and uncorrelated lateral errors were arbitrarily set at 100 feet each:

$$\sigma X'_b = \sigma X'_i = \sigma Y'_b = \sigma Y'_i = 100 \text{ feet.}$$

At any one station, therefore,

$$\sigma X'_n = (\sigma X'^2_i + \sigma X'^2_b)^{1/2} = 140 \text{ feet, and}$$

$$\sigma Y'_n = (\sigma Y'^2_i + \sigma Y'^2_b)^{1/2} = 140 \text{ feet.}$$

Uncertainties in the vertical coordinate of a tracker are quite a different matter. Errors in elevation of tracker with respect to the geoid may be neglected, but the distance from geoid to spheroid undulates, due to the same mass anomalies in the earth which cause deflection of the vertical. The variation, however, is much smaller. For widely separated points in the western hemisphere the value,

$$\sigma Z'_i = 25 \text{ feet}$$

is a good approximation.

A relatively large correlated uncertainty,

$$\sigma Z'_i = 200 \text{ feet}$$

is present, almost entirely attributed to doubt as to the exact value which should be used for the equatorial radius of the International Spheroid.

3.5 ERROR MODEL EQUIVALENCE

In formulating error models for specific hybrid tracking systems, it was observed that the same error terms appear as in the pure three-range-only model. This suggested that an equivalence of some sort might exist which would allow the results of the range-only error analysis to be applied to a general hybrid tracking system.

It was found that such a reduction is possible and that the pure three-range-only system is the most accurate member of the family of long baseline systems under consideration in this study. This is demonstrated in the following paragraphs.

Three equations determine the target position:

$$R_1^2 = (X - X_1)^2 + (Y - Y_1)^2 + (Z - Z_1)^2$$

$$R_2^2 = (X - X_2)^2 + (Y - Y_2)^2 + (Z - Z_2)^2$$

$$R_3^2 = (X - X_3)^2 + (Y - Y_3)^2 + (Z - Z_3)^2$$

The solution for X, Y, and Z is given in Appendix I. While it is not necessary to have this solution in order to perform the error analysis, it is necessary to know what equations are to be solved. In the hybrid case the measurements are S_1, S_2, and S_3, which are ranges, or sums and differences of ranges. The general equivalence proof is given in Appendix I for any linear function of R_1, R_2, and R_3; $S_m = S_m (R_1, R_2, R_3)$, but for discussion purposes the case:

$$S_1 = (R_1 + R_2)$$

$$S_2 = (R_1 + R_3) \qquad (3\text{-}1)$$

$$S_3 = (R_1 + R_1)$$

will be used, so as not to confuse the equivalence by generalized notation. Equations (3-1) represent a range sum hybrid which has been suggested for study. Figure 12 illustrates the hybrid system.

A single transmitter, at tracker 1, is employed. Trackers 2 and 3 are receivers only. A signal is initiated at T1, travels ray path R_1 to the missile or spacecraft, and actuates a transponder which starts a new wave front from M. One ray returns to T1 and completes $S_3 = (R_1 + R_1)$. Two other rays travel paths R_2 and R_3, completing $S_2 = (R_1 + R_3)$ and $S_1 = (R_1 + R_2)$.

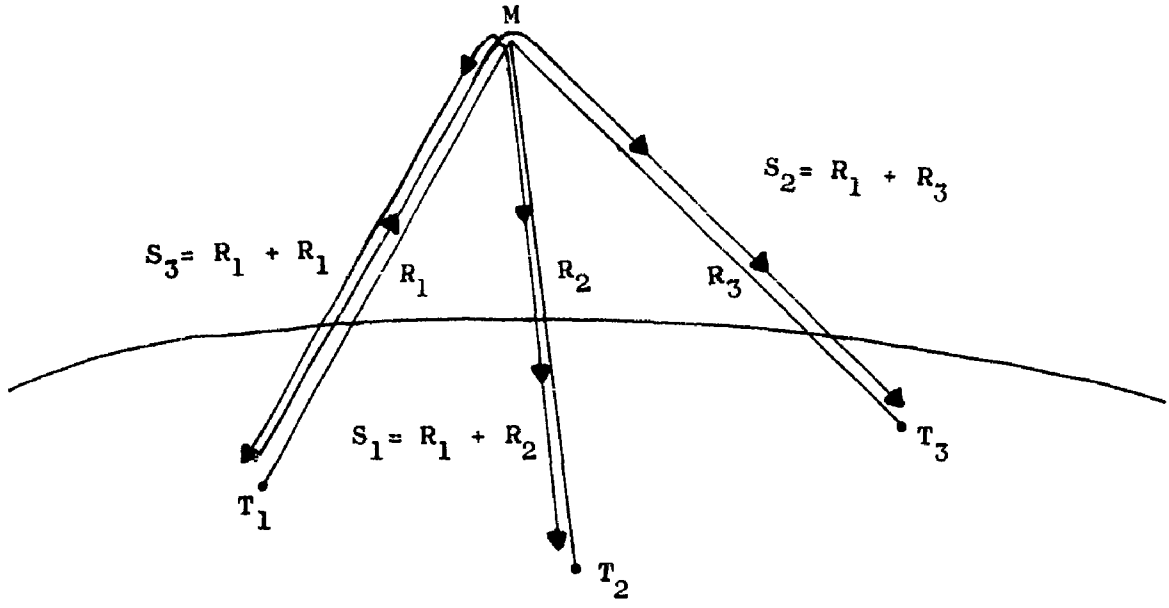

Figure 12. Hybrid Range - Range Sum Mode

The simplest solution for X, Y, Z is obtained by solving first for R_1, R_2, and R_3 and using these in the pure three-range-only solution.

$$R_1 = 1/2\, S_3$$

$$R_2 = S_1 - 1/2\, S_3 \qquad (3\text{-}2)$$

$$R_3 = S_2 - 1/2\, S_3$$

The equivalence is found by direct comparison of the errors in R_1, R_2, and R_3 as found by equations 3-2 with those which would have been present had the pure three-range-only combination been used. By the error model in Figure 12, the range only errors are:

$$\Delta R_i = \Delta t_i \dot{R}_i + \Delta t_b \dot{R}_i + (k_b + k_i) f(\epsilon_i) + \frac{\Delta c}{c} R_i - \frac{\Delta f_i}{f_i} R_i + 1/2\ \Delta S_i .$$

The errors deriving from (3-2) are:

$$\Delta R_1 = \dot{R}_1 (\Delta t_1 + \Delta t_b) + (k_b + k_1) f(\epsilon_1) + \left(\frac{\Delta c}{c} - \frac{\Delta f_1}{f_1}\right) R_1 + 1/2\ \Delta S_1$$

$$\Delta R_2 = c(\Delta t_1 - \Delta t_2) + \dot{R}_2(\Delta t_1 + \Delta t_b) + (k_b + k_2) f(\epsilon_2) + \frac{\Delta c}{c} R_2 - \frac{\Delta f_1}{f_1} R_2 + 1/2\,\Delta S_1$$

$$\Delta R_3 = c(\Delta t_1 - \Delta t_3) + \dot{R}_3(\Delta t_1 + \Delta t_b) + (k_b + k_3) f(\epsilon_3) + \frac{\Delta c}{c} R_3 - \frac{\Delta f_1}{f_1} R_3 + 1/2\,\Delta S_1$$

If the system errors in timing, frequency, and zero set are referenced to tracker 1, $\Delta t_1 = 0$, $\frac{\Delta f_1}{f_1} = \frac{\Delta f}{f}$ and $\Delta S_1 = \Delta S$; and the pure three-range-only errors become:

$$\Delta R_1 = \Delta t_b \dot{R}_1 + (k_b + k_1) f(\epsilon_1) + \frac{\Delta c}{c} R_1 - \frac{\Delta f}{f} R_1 + 1/2\ \Delta S,$$

$$\Delta R_2 = (\Delta t_b + \Delta t_2) \dot{R}_2 + (k_b + k_2) f(\epsilon_2) + \frac{\Delta c}{c} R_2 - \frac{\Delta f}{f} + \frac{\Delta f_2}{f_2} R_3 + 1/2\ (\Delta S + \Delta S_2),$$

$$\Delta R_3 = (\Delta t_b + \Delta t_3) \dot{R}_3 + (k_b + k_3) f(\epsilon_3) + \frac{\Delta c}{c} R_3 - \frac{\Delta f}{f} + \frac{\Delta f_3}{f_3} R_3$$

$$+ 1/2\ (\Delta S + \Delta S_3). \qquad (3\text{-}3)$$

The hybrid errors are then:

$$\Delta R_1 = \Delta t_b \dot{R}_1 + (k_b + k_1) f(\epsilon_1) + \frac{\Delta c}{c} R_1 - \frac{\Delta f}{f} R_1 + 1/2\,\Delta S,$$

$$\Delta R_2 = -c\,\Delta t_2 + \Delta t_b \dot{R}_2 + (k_b + k_2) f(\epsilon_2) + \frac{\Delta c}{c} R_2 - \frac{\Delta f}{f} R_2 + 1/2\,\Delta S,$$

$$\Delta R_3 = -c\,\Delta t_3 + \Delta t_b \dot{R}_3 + (k_b + k_3) f(\epsilon_2) + \frac{\Delta c}{c} R_3 - \frac{\Delta f}{f} R_3 + 1/2\,\Delta S. \qquad (3\text{-}4)$$

In tabular form, the comparison between hybrid errors, equations (3-4), and the pure three-range-only errors, equations (3-3), is as follows:

Table 3. Error Comparison

	ERRORS IN THREE-RANGE-ONLY SYSTEM WHICH DO NOT APPEAR IN HYBRID SYSTEM	ERRORS IN HYBRID SYSTEM WHICH DO NOT APPEAR IN THREE-RANGE-ONLY SYSTEM
R_1	none	none
R_2	$\dot{R}_2\,\Delta t_2 - \frac{\Delta f_2}{f_2} R_2 + 1/2\,\Delta S_2$	$-c\,\Delta t_2$
R_3	$\dot{R}_3\,\Delta t_3 - \frac{\Delta f_2}{f_2} R_3 + 1/2\,\Delta S_3$	$-c\,\Delta t_3$

The terms $-c\Delta t_2$ and $-c\Delta t_3$ which exist for the hybrid only, may be well over 1000 feet. The range-only terms, $\dot{R}_2\Delta t_2$ and $R_3\Delta t_3$, are of the order of a few hundredths of a foot, even for range rates of 25,000 feet per second; the terms $\frac{\Delta f_2}{f_2} R_2$ and $\frac{\Delta f_3}{f_3} R_3$ are of the order of 15 feet at lunar distance for $\frac{\Delta f}{f} = 10^{-8}$; and the terms ΔS_2 and ΔS_3 are of the order of

10 feet. Since these errors are two or more orders of magnitude less than the errors of the hybrid case, it may be concluded that a detailed analysis of the hybrid would simply demonstrate its inferiority.

A similar model comparison for errors in range rate shows that the pure three-range-only system contains errors $\frac{\Delta f_2}{f_2}\dot{R}_2$ in $\dot{R}_2$ and $\frac{\Delta f_3}{f_3}\dot{R}_3$ in $\dot{R}_3$ which do not appear in the hybrid. However, these are only of the order of 0.01 foot per second. The very slight superiority of the hybrid in measuring range rate does not imply that it measures missile velocity with greater accuracy, because the system cannot obtain a good measurement of velocity without a good knowledge of position.

The demonstration that tracking errors due to errors in station location are identical for the three-range-only case and for all possible range sum and range difference systems involving no more than three trackers, is given below. The equation:

$$\Delta X = \frac{\partial X}{\partial X'_1}\Delta X'_1 + \frac{\partial X}{\partial X'_2}\Delta X'_2 + \frac{\partial X}{\partial X'_3}\Delta X'_3$$
$$+ \frac{\partial X}{\partial Y'_1}\Delta Y'_1 + \frac{\partial X}{\partial Y'_2}\Delta Y'_2 + \frac{\partial X}{\partial Y'_3}\Delta Y'_3$$
$$+ \frac{\partial X}{\partial Z'_1}\Delta Z'_1 + \frac{\partial X}{\partial Z'_2}\Delta Z'_2 + \frac{\partial X}{\partial Z'_3}\Delta Z'_3$$

gives the error in the X coordinate of the target due to the three components of error in tracker location at each of three trackers. Similar expressions can be written for ΔY and ΔZ.

Using the notation in Appendix I,

$$\overline{\Delta r} = P_\lambda \begin{bmatrix} \Delta X'_1 \\ \Delta X'_2 \\ \Delta X'_3 \end{bmatrix} + P_\phi \begin{bmatrix} \Delta Y'_1 \\ \Delta Y'_2 \\ \Delta Y'_3 \end{bmatrix} + P_r \begin{bmatrix} \Delta Z'_1 \\ \Delta Z'_2 \\ \Delta Z'_3 \end{bmatrix} .$$

Since P_λ , P_ϕ , and P_r contain no terms involving hybrid range sums but, instead, have terms in $\bar{R}_1$, $\bar{R}_2$, $\bar{R}_3$, it is evident that the analysis of tracking errors due to uncertainties in tracker location for hybrid systems measuring range sums or differences is exactly the same as for the range-only case.

3.6 THE GEOMETRICAL PARTIAL DERIVATIVES

If $X(R_1, R_2, R_3)$ is a function of three variables, R_1, R_2, and R_3, and if these are functions of i other variables, a_i, then:

$$\frac{\partial X}{\partial a_i} = \frac{\partial X}{\partial R_1}\frac{\partial R_1}{\partial a_i} + \frac{\partial X}{\partial R_2}\frac{\partial R_2}{\partial a_i} + \frac{\partial X}{\partial R_3}\frac{\partial R_3}{\partial a_i} \tag{3-5}$$

Similarly, if $\dot{X}$ $(R_1, R_2, R_3, \dot{R}_1, \dot{R}_2, \dot{R}_3)$ is a function of R_1, R_2, R_3, $\dot{R}_1$, $\dot{R}_2$, and $\dot{R}_3$, and if these are functions of the same i other variables, a_i, then

$$\frac{\partial \dot{X}}{\partial a_i} = \frac{\partial \dot{X}}{\partial R_1}\frac{\partial R_1}{\partial a_i} + \frac{\partial \dot{X}}{\partial R_2}\frac{\partial R_2}{\partial a_i} + \frac{\partial \dot{X}}{\partial R_3}\frac{\partial R_3}{\partial a_i} + \frac{\partial \dot{X}}{\partial \dot{R}_1}\frac{\partial \dot{R}_1}{\partial a_i} + \frac{\partial \dot{X}}{\partial \dot{R}_2}\frac{\partial \dot{R}_2}{\partial a_i} + \frac{\partial \dot{X}}{\partial \dot{R}_3}\frac{\partial \dot{R}_3}{\partial a_i} \tag{3-6}$$

In expressions (3-5) and (3-6), X may be replaced by Y or Z and $\dot{X}$ by $\dot{Y}$ or $\dot{Z}$ to obtain the corresponding partial derivatives. The variables a_i are the 27 quantities whose errors are listed in paragraph 3.2.

A complete list of the partial derivatives used in the analysis appears in Appendix I. Their use in forming the covariance matrices of position and velocity of the spacecraft is developed in the remaining portions of Section III.

3.7 STATISTICAL CONSIDERATIONS

The 27 errors, Δa_i, considered in this study are treated as uncorrelated. If this is the case, the variance of a position or velocity parameter P is:

$$\sigma_P^2 = \sum_i \left(\frac{\partial p}{\partial a_i}\right)^2 \sigma a_i^2 \quad , \tag{3-7}$$

and the covariance of two parameters, P and Q, is

$$\sigma_{PQ} = \sum_i \left(\frac{\partial P}{\partial a_i}\right)\left(\frac{\partial Q}{\partial a_i}\right) \sigma a_i^2 \quad . \tag{3-8}$$

The coordinates X, Y, Z, $\dot{X}$, $\dot{Y}$, or $\dot{Z}$ may assume the positions of P and Q in these expressions. Typical variance and covariance terms, for P = X and Q = Y, are expanded in Figures 13 and 14. Although the assumptions of equal equipment and methods of tracker

location allow the expression for σx^2 to be factored into thirteen terms in σa_i^2, it should be noted that σx^2 is the sum of 27 terms, $\left(\frac{\partial X}{\partial a_i}\right)^2 \sigma a_i^2$. Similarly the expression for σXY is the sum of 27 terms, $\left(\frac{\partial X}{\partial a_i}\right)\left(\frac{\partial Y}{\partial a_i}\right)\sigma a_i^2$.

In the computer simulation both covariance matrices

$$M_{\bar{r}} = \begin{bmatrix} \sigma X^2 & \sigma YX & \sigma ZX \\ \sigma XY & \sigma Y^2 & \sigma ZY \\ \sigma XZ & \sigma YZ & \sigma Z^2 \end{bmatrix} \quad \text{and} \quad M_{\dot{\bar{r}}} = \begin{bmatrix} \sigma \dot{X}^2 & \sigma \dot{Y}\dot{X} & \sigma \dot{Z}\dot{X} \\ \sigma \dot{X}\dot{Y} & \sigma \dot{Y}^2 & \sigma \dot{Z}\dot{Y} \\ \sigma \dot{X}\dot{Z} & \sigma \dot{Y}\dot{Z} & \sigma \dot{Z}^2 \end{bmatrix}$$

are formed by a relatively small number of matrix operations and not by the enormous number of scalar operations which equations (3-7) and (3-8) might imply.

The importance of correlation in range errors, ΔR_1, ΔR_2, and ΔR_3 may be illustrated by a consideration of the term in σX^2 which expresses the effect of uncertainty in signal frequency. The pure three-range-only model uses three transmitters, and, as in Figure 13:

$$\sigma X_f^2 = \sigma f^2 \left[R_1^2 \left(\frac{\partial X}{\partial R_1}\right)^2 + R_2^2 \left(\frac{\partial X}{\partial R_2}\right)^2 + R_3^2 \left(\frac{\partial X}{\partial R_3}\right)^2 \right] \tag{3-9}$$

(three uncorrelated frequency errors).

Had a means been devised for using a single transmitter, or should the three frequencies be related in such a way that they are all equal but subject to a common error, Δf, the frequency terms in σX^2 would have been:

$$\sigma X_f^2 = \sigma f^2 \left[R_1 \left(\frac{\partial X}{\partial R_1}\right) + R_2 \left(\frac{\partial X}{\partial R_2}\right) + R_3 \left(\frac{\partial X}{\partial R_3}\right) \right]^2 \tag{3-10}$$

The great difference between these two terms is simply illustrated by an "overhead" case, with an equilateral tracker net and the spacecraft directly over the centroid of the tracker triangle, (see Figure 15).

$$
\begin{aligned}
\sigma_X^2 = \sigma_t^2 \Bigg[& R_1^2 \left(\frac{\partial X}{\partial R_1}\right)^2 + R_2^2 \left(\frac{\partial X}{\partial R_2}\right)^2 + R_3^2 \left(\frac{\partial X}{\partial R_3}\right)^2 \Bigg] + \sigma_{t_b}^2 \Bigg[R_1 \left(\frac{\partial X}{\partial R_1}\right) + R_2 \left(\frac{\partial X}{\partial R_2}\right) + R_3 \left(\frac{\partial X}{\partial R_3}\right) \Bigg]^2 \\
& + \sigma_k^2 \Bigg[f^2(\epsilon_1) \left(\frac{\partial X}{\partial R_1}\right)^2 + f^2(\epsilon_2) \left(\frac{\partial X}{\partial R_2}\right)^2 + f^2(\epsilon_3) \left(\frac{\partial X}{\partial R_3}\right)^2 \Bigg] \\
& + \sigma_{k_b}^2 \Bigg[f(\epsilon_1) \left(\frac{\partial X}{\partial R_1}\right) + f(\epsilon_2) \left(\frac{\partial X}{\partial R_2}\right) + f(\epsilon_3) \left(\frac{\partial X}{\partial R_3}\right) \Bigg]^2 \\
& + \sigma_c^2 \Bigg[R_1 \left(\frac{\partial X}{\partial R_1}\right) + R_2 \left(\frac{\partial X}{\partial R_2}\right) + R_3 \left(\frac{\partial X}{\partial R_3}\right) \Bigg]^2 + \sigma_f^2 \Bigg[R_1^2 \left(\frac{\partial X}{\partial R_1}\right)^2 + R_2^2 \left(\frac{\partial X}{\partial R_2}\right)^2 + R_3^2 \left(\frac{\partial X}{\partial R_3}\right)^2 \Bigg] \\
& + \sigma_s^2 \Bigg[\left(\frac{\partial X}{\partial R_1}\right)^2 + \left(\frac{\partial X}{\partial R_2}\right)^2 + \left(\frac{\partial X}{\partial R_3}\right)^2 \Bigg] \\
& + \sigma_{X'}^2 \Bigg[\left(\frac{\partial X}{\partial X_1'}\right)^2 + \left(\frac{\partial X}{\partial X_2'}\right)^2 + \left(\frac{\partial X}{\partial X_3'}\right)^2 \Bigg] + \sigma_{X_b'}^2 \Bigg[\left(\frac{\partial X}{\partial X_1'}\right) + \left(\frac{\partial X}{\partial X_2'}\right) + \left(\frac{\partial X}{\partial X_3'}\right) \Bigg]^2 \\
& + \sigma_{Y'}^2 \Bigg[\left(\frac{\partial X}{\partial Y_1'}\right)^2 + \left(\frac{\partial X}{\partial Y_2'}\right)^2 + \left(\frac{\partial X}{\partial Y_3'}\right)^2 \Bigg] + \sigma_{Y_b'}^2 \Bigg[\left(\frac{\partial X}{\partial Y_1'}\right) + \left(\frac{\partial X}{\partial Y_2'}\right) + \left(\frac{\partial X}{\partial Y_3'}\right) \Bigg]^2 \\
& + \sigma_{Z'}^2 \Bigg[\left(\frac{\partial X}{\partial Z_1'}\right)^2 + \left(\frac{\partial X}{\partial Z_2'}\right)^2 + \left(\frac{\partial X}{\partial Z_3'}\right)^2 \Bigg] + \sigma_{Z_b'}^2 \Bigg[\left(\frac{\partial X}{\partial Z_1'}\right) + \left(\frac{\partial X}{\partial Z_2'}\right) + \left(\frac{\partial X}{\partial Z_3'}\right) \Bigg]^2
\end{aligned}
$$

Figure 13. Diagonal Term in Range-only Covariance Matrix (Position)

$$\sigma_{xy} = \sigma_t^2 \left[\dot{R}_1^2 \left(\frac{\partial X}{\partial R_1}\right)\left(\frac{\partial Y}{\partial R_1}\right) + \dot{R}_2^2 \left(\frac{\partial X}{\partial R_2}\right)\left(\frac{\partial Y}{\partial R_2}\right) + \dot{R}_3^2 \left(\frac{\partial X}{\partial R_3}\right)\left(\frac{\partial Y}{\partial R_3}\right) \right]$$

$$+ \sigma_{t_b}^2 \left[\dot{R}_1 \left(\frac{\partial X}{\partial R_1}\right) + \dot{R}_2 \left(\frac{\partial X}{\partial R_2}\right) + \dot{R}_3 \left(\frac{\partial X}{\partial R_3}\right) \right] \left[\dot{R}_1 \left(\frac{\partial Y}{\partial R_1}\right) + \dot{R}_2 \left(\frac{\partial Y}{\partial R_2}\right) + \dot{R}_3 \left(\frac{\partial Y}{\partial R_3}\right) \right.$$

$$+ \sigma_k^2 \left[f^2(\epsilon_1) \left(\frac{\partial X}{\partial R_1}\right)\left(\frac{\partial Y}{\partial R_1}\right) + f^2(\epsilon_2) \left(\frac{\partial X}{\partial R_2}\right)\left(\frac{\partial Y}{\partial R_2}\right) + f^2(\epsilon_3) \left(\frac{\partial X}{\partial R_3}\right)\left(\frac{\partial Y}{\partial R_3}\right) \right]$$

$$+ \sigma_{k_b}^2 \left[f(\epsilon_1) \left(\frac{\partial X}{\partial R_1}\right) + f(\epsilon_2) \left(\frac{\partial X}{\partial R_2}\right) + f(\epsilon_3) \left(\frac{\partial X}{\partial R_3}\right) \right] \left[f(\epsilon_1) \left(\frac{\partial Y}{\partial R_1}\right) + f(\epsilon_2) \left(\frac{\partial Y}{\partial R_2}\right) \right.$$

$$+ \sigma_c^2 \left[R_1 \left(\frac{\partial X}{\partial R_1}\right) + R_2 \left(\frac{\partial X}{\partial R_2}\right) + R_3 \left(\frac{\partial X}{\partial R_3}\right) \right] \left[R_1 \left(\frac{\partial Y}{\partial R_1}\right) + R_2 \left(\frac{\partial Y}{\partial R_2}\right) + R_3 \left(\frac{\partial Y}{\partial R_3}\right) \right.$$

$$+ \sigma_f^2 \left[R_1^2 \left(\frac{\partial X}{\partial R_1}\right)\left(\frac{\partial Y}{\partial R_1}\right) + R_2^2 \left(\frac{\partial X}{\partial R_2}\right)\left(\frac{\partial Y}{\partial R_2}\right) + R_3^2 \left(\frac{\partial X}{\partial R_3}\right)\left(\frac{\partial Y}{\partial R_3}\right) \right]$$

$$+ \sigma_s^2 \left[\left(\frac{\partial X}{\partial R_1}\right)\left(\frac{\partial Y}{\partial R_1}\right) + \left(\frac{\partial X}{\partial R_2}\right)\left(\frac{\partial Y}{\partial R_2}\right) + \left(\frac{\partial X}{\partial R_3}\right)\left(\frac{\partial Y}{\partial R_3}\right) \right]$$

$$+ \sigma_{X'}^2 \left[\left(\frac{\partial X}{\partial X'_1}\right)\left(\frac{\partial Y}{\partial X'_1}\right) + \left(\frac{\partial X}{\partial X'_2}\right)\left(\frac{\partial Y}{\partial X'_2}\right) + \left(\frac{\partial X}{\partial X'_3}\right)\left(\frac{\partial Y}{\partial Y'_3}\right) \right]$$

$$+ \sigma_{X'_b}^2 \left[\left(\frac{\partial X}{\partial X'_1}\right) + \left(\frac{\partial X}{\partial X'_2}\right) + \left(\frac{\partial X}{\partial X'_3}\right) \right] \left[\left(\frac{\partial X}{\partial X'_1}\right) + \left(\frac{\partial Y}{\partial X'_2}\right) + \left(\frac{\partial Y}{\partial X'_3}\right) \right]$$

$$+ \sigma_{Y'}^2 \left[\left(\frac{\partial X}{\partial Y'_1}\right)\left(\frac{\partial Y}{\partial Y'_1}\right) + \left(\frac{\partial X}{\partial Y'_2}\right)\left(\frac{\partial Y}{\partial Y'_2}\right) + \left(\frac{\partial X}{\partial Y'_3}\right)\left(\frac{\partial Y}{\partial Y'_3}\right) \right]$$

$$+ \sigma_{Y'_b}^2 \left[\left(\frac{\partial X}{\partial Y'_1}\right) + \left(\frac{\partial X}{\partial Y'_2}\right) + \left(\frac{\partial X}{\partial Y'_3}\right) \right] \left[\left(\frac{\partial Y}{\partial Y'_1}\right) + \left(\frac{\partial Y}{\partial Y'_2}\right) + \left(\frac{\partial Y}{\partial Y'_3}\right) \right]$$

$$+ \sigma_{Z'}^2 \left[\left(\frac{\partial X}{\partial Z'_1}\right)\left(\frac{\partial Y}{\partial Z'_1}\right) + \left(\frac{\partial X}{\partial Z'_2}\right)\left(\frac{\partial Y}{\partial Z'_2}\right) + \left(\frac{\partial X}{\partial Z'_3}\right)\left(\frac{\partial Y}{\partial Z'_3}\right) \right]$$

$$+ \sigma_{Z'_b}^2 \left[\left(\frac{\partial X}{\partial Z'_1}\right) + \left(\frac{\partial X}{\partial Z'_2}\right) + \left(\frac{\partial X}{\partial Z'_3}\right) \right] \left[\left(\frac{\partial Y}{\partial Z'_1}\right) + \left(\frac{\partial Y}{\partial Z'_2}\right) + \left(\frac{\partial Y}{\partial Z'_3}\right) \right]$$

Figure 14. Off-Diagonal Term in Range-only Covariance

$$\sigma_{xy} = \sigma_t^2 \left[\dot{R}_1^2 \left(\frac{\partial X}{\partial R_1}\right)\left(\frac{\partial Y}{\partial R_1}\right) + \dot{R}_2^2 \left(\frac{\partial X}{\partial R_2}\right)\left(\frac{\partial Y}{\partial R_2}\right) + \dot{R}_3^2 \left(\frac{\partial X}{\partial R_3}\right)\left(\frac{\partial Y}{\partial R_3}\right) \right]$$

$$+ \sigma_{t_b}^2 \left[\dot{R}_1 \left(\frac{\partial X}{\partial R_1}\right) + \dot{R}_2 \left(\frac{\partial X}{\partial R_2}\right) + \dot{R}_3 \left(\frac{\partial X}{\partial R_3}\right) \right] \left[\dot{R}_1 \left(\frac{\partial Y}{\partial R_1}\right) + \dot{R}_2 \left(\frac{\partial Y}{\partial R_2}\right) + \dot{R}_3 \left(\frac{\partial Y}{\partial R_3}\right) \right]$$

$$+ \sigma_k^2 \left[f^2(\epsilon_1) \left(\frac{\partial X}{\partial R_1}\right)\left(\frac{\partial Y}{\partial R_1}\right) + f^2(\epsilon_2) \left(\frac{\partial X}{\partial R_2}\right)\left(\frac{\partial Y}{\partial R_2}\right) + f^2(\epsilon_3) \left(\frac{\partial X}{\partial R_3}\right)\left(\frac{\partial Y}{\partial R_3}\right) \right]$$

$$+ \sigma_{k_b}^2 \left[f(\epsilon_1) \left(\frac{\partial X}{\partial R_1}\right) + f(\epsilon_2) \left(\frac{\partial X}{\partial R_2}\right) + f(\epsilon_3) \left(\frac{\partial X}{\partial R_3}\right) \right] \left[f(\epsilon_1) \left(\frac{\partial Y}{\partial R_1}\right) + f(\epsilon_2) \left(\frac{\partial Y}{\partial R_2}\right) + f(\epsilon_3) \left(\frac{\partial Y}{\partial R_3}\right) \right]$$

$$+ \sigma_c^2 \left[R_1 \left(\frac{\partial X}{\partial R_1}\right) + R_2 \left(\frac{\partial X}{\partial R_2}\right) + R_3 \left(\frac{\partial X}{\partial R_3}\right) \right] \left[R_1 \left(\frac{\partial Y}{\partial R_1}\right) + R_2 \left(\frac{\partial Y}{\partial R_2}\right) + R_3 \left(\frac{\partial Y}{\partial R_3}\right) \right]$$

$$+ \sigma_f^2 \left[R_1^2 \left(\frac{\partial X}{\partial R_1}\right)\left(\frac{\partial Y}{\partial R_1}\right) + R_2^2 \left(\frac{\partial X}{\partial R_2}\right)\left(\frac{\partial Y}{\partial R_2}\right) + R_3^2 \left(\frac{\partial X}{\partial R_3}\right)\left(\frac{\partial Y}{\partial R_3}\right) \right]$$

$$+ \sigma_s^2 \left[\left(\frac{\partial X}{\partial R_1}\right)\left(\frac{\partial Y}{\partial R_1}\right) + \left(\frac{\partial X}{\partial R_2}\right)\left(\frac{\partial Y}{\partial R_2}\right) + \left(\frac{\partial X}{\partial R_3}\right)\left(\frac{\partial Y}{\partial R_3}\right) \right]$$

$$+ \sigma_{X'}^2 \left[\left(\frac{\partial X}{\partial X'_1}\right)\left(\frac{\partial Y}{\partial X'_1}\right) + \left(\frac{\partial X}{\partial X'_2}\right)\left(\frac{\partial Y}{\partial X'_2}\right) + \left(\frac{\partial X}{\partial X'_3}\right)\left(\frac{\partial Y}{\partial Y'_3}\right) \right]$$

$$+ \sigma_{X'_b}^2 \left[\left(\frac{\partial X}{\partial X'_1}\right) + \left(\frac{\partial X}{\partial X'_2}\right) + \left(\frac{\partial X}{\partial X'_3}\right) \right] \left[\left(\frac{\partial X}{\partial X'_1}\right) + \left(\frac{\partial Y}{\partial X'_2}\right) + \left(\frac{\partial Y}{\partial X'_3}\right) \right]$$

$$+ \sigma_{Y'}^2 \left[\left(\frac{\partial X}{\partial Y'_1}\right)\left(\frac{\partial Y}{\partial Y'_1}\right) + \left(\frac{\partial X}{\partial Y'_2}\right)\left(\frac{\partial Y}{\partial Y'_2}\right) + \left(\frac{\partial X}{\partial Y'_3}\right)\left(\frac{\partial Y}{\partial Y'_3}\right) \right]$$

$$+ \sigma_{Y'_b}^2 \left[\left(\frac{\partial X}{\partial Y'_1}\right) + \left(\frac{\partial X}{\partial Y'_2}\right) + \left(\frac{\partial X}{\partial Y'_3}\right) \right] \left[\left(\frac{\partial Y}{\partial Y'_1}\right) + \left(\frac{\partial Y}{\partial Y'_2}\right) + \left(\frac{\partial Y}{\partial Y'_3}\right) \right]$$

$$+ \sigma_{Z'}^2 \left[\left(\frac{\partial X}{\partial Z'_1}\right)\left(\frac{\partial Y}{\partial Z'_1}\right) + \left(\frac{\partial X}{\partial Z'_2}\right)\left(\frac{\partial Y}{\partial Z'_2}\right) + \left(\frac{\partial X}{\partial Z'_3}\right)\left(\frac{\partial Y}{\partial Z'_3}\right) \right]$$

$$+ \sigma_{Z'_b}^2 \left[\left(\frac{\partial X}{\partial Z'_1}\right) + \left(\frac{\partial X}{\partial Z'_2}\right) + \left(\frac{\partial X}{\partial Z'_3}\right) \right] \left[\left(\frac{\partial Y}{\partial Z'_1}\right) + \left(\frac{\partial Y}{\partial Z'_2}\right) + \left(\frac{\partial Y}{\partial Z'_3}\right) \right]$$

Figure 14. Off-Diagonal Term in Range-only Covariance Matrix

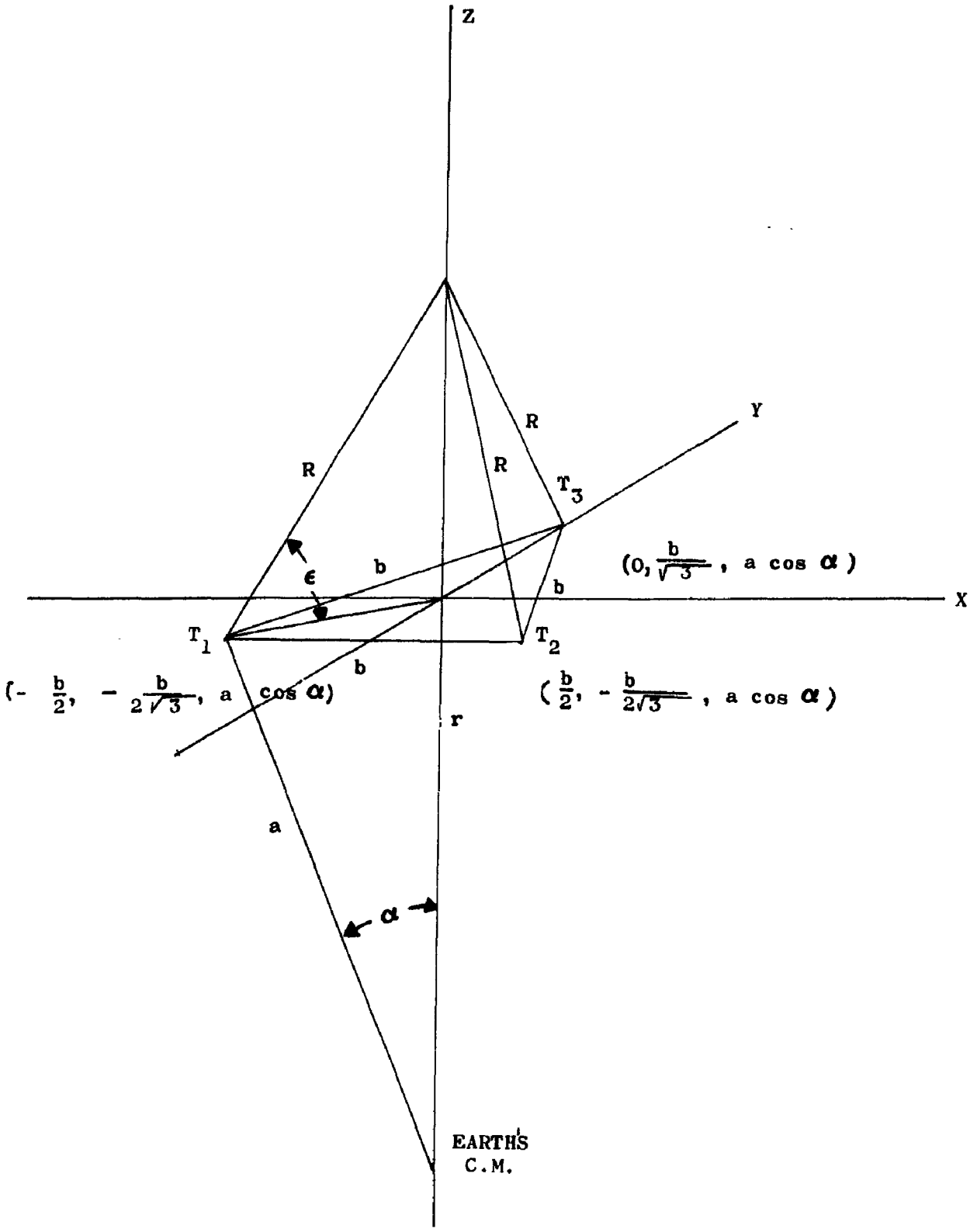

Figure 15. Geometry of the Overhead Case

The necessary partial derivatives are

$$\begin{bmatrix} \frac{\partial X}{\partial R_1} & \frac{\partial X}{\partial R_2} & \frac{\partial X}{\partial R_3} \\ \frac{\partial Y}{\partial R_1} & \frac{\partial Y}{\partial R_2} & \frac{\partial Y}{\partial R_3} \\ \frac{\partial Z}{\partial R_1} & \frac{\partial Z}{\partial R_2} & \frac{\partial Z}{\partial R_3} \end{bmatrix} = \begin{bmatrix} \frac{R}{b} & -\frac{R}{b} & 0 \\ \frac{\sqrt{3}}{3}\frac{R}{b} & \frac{\sqrt{3}}{3}\frac{R}{b} & -\frac{2\sqrt{3}}{3}\frac{R}{b} \\ \frac{R}{(9R^2 - 3b^2)^{1/2}} & \frac{R}{(9R^2 - 3b^2)^{1/2}} & \frac{R}{(9R^2 - 3b^2)^{1/2}} \end{bmatrix}.$$

Substituting the partial derivatives from (3-11) in (3-9) and (3-10), (3-11)

$$\sigma X^2 = 0, \quad \sigma Y^2 = 0, \text{ and } \sigma Z^2 = \sigma f^2 R^2$$

for the case of three correlated frequency errors; or

$$\sigma X^2 = 2\sigma f^2 \frac{R^4}{b^2}, \quad \sigma Y^2 = 2\sigma f^2 \frac{R^4}{b^2} \text{ and } \sigma Z^2 = \frac{1}{3}\sigma f^2 R^2$$

for the case of three uncorrelated frequency errors.

Using the values $\sigma f = 10^{-8}$, $R = 1.5 \times 10^9$ feet (lunar distance), and $b = 6 \times 10^6$ feet (1000 nautical mile baseline), the results are

$\sigma X = 0$
$\sigma Y = 0$
$\sigma Z = 15$ feet

(3 correlated frequency errors)

$\sigma X = 5300$ feet
$\sigma Y = 5300$ feet
$\sigma Z = 5$ feet

(3 uncorrelated frequency errors)

The comparison is even more striking if one makes the mistake of treating the error $\frac{\Delta c}{c}$ as uncorrelated for the three range measurements. In this case the results are as follows:

Correct treatment:

$\sigma X = 0$

$\sigma Y = 0$ ($\frac{\Delta c}{c}$ equal for R_1, R_2, and R_3)

$\sigma Z = 450$ feet.

Erroneous treatment:

$\sigma X = 160,000$ feet

$\sigma Y = 160,000$ feet (ignoring correlation in range errors)

$\sigma Z = 150$ feet.

The preceding results demonstrate the importance of a clear understanding of the nature of equipment errors, of the uncertainties in the physical constants involved in tracking, and, by extension, of the errors in tracker location. Especially important is a knowledge of the degree to which these errors are correlated. The latter subject may become highly involved in the case of any three specific tracker sites, but the mastery of it is absolutely essential to a correct evaluation of the corresponding precision of tracking which may be expected.

3.8 BASELINE OPTIMIZATION

It has not been possible during the term of the present contract to advance the study of baseline optimization to the degree desired. To do so will require functional expressions of the degree of correlation of system errors at trackers 1, 2, and 3 in terms of baseline length. Once these relationships are generated, the optimization problem is quite simple. Following is an example of a routine carried out for minimization of the cross-range components, σX and σY, of uncertainty in target position for the "overhead case", $R_1 = R_2 = R_3 = R$. Figure 15 and the partial derivatives in formula 3-11 apply to this case. Considering only σo, σf, σk, σk_b, and σc, the expression for σx^2 in Figure 13 reduces to:

$$\sigma X^2 = \left[\left(\frac{\partial X}{\partial R_1}\right) + \left(\frac{\partial X}{\partial R_2}\right) + \left(\frac{\partial X}{\partial R_3}\right) \right]^2 \left[\sigma k_b^2 \sec^2 \epsilon + \sigma c^2 R^2 \right]$$

$$+ \left[\left(\frac{\partial X}{\partial R_1}\right)^2 + \left(\frac{\partial X}{\partial R_2}\right)^2 + \left(\frac{\partial X}{\partial R_3}\right)^2 \right] \left[\sigma o^2 + \sigma f^2 R^2 + \sigma k^2 \sec^2 \epsilon \right]$$

Substituting for the partial derivatives,

$$\sigma X^2 = 2 \frac{R^2}{b^2} \left[\sigma o^2 + \sigma f^2 R^2 + \sigma k^2 \sec^2 \epsilon \right] = \sigma Y^2 . \qquad (3\text{-}12)$$

Similarly,

$$\sigma Z^2 = \frac{R^2}{3R^2 - b^2} \left[\sigma o^2 + \left(\sigma f^2 + 3 \sigma c^2 \right) R^2 + \left(\sigma k^2 = 3 \sigma k_b^2 \right) \sec^2 \epsilon \right] \qquad (3\text{-}13)$$

where $R^2 = a^2 + r^2 - 2ar \cos \alpha$ (3-14)

and $\sec^2 \epsilon = \dfrac{a^2 + r^2 - 2ar \cos \alpha}{r^2 \sin^2 \alpha}$. (3-15)

Several criteria may be used for error minimization. The two considered here are

(a) $\dfrac{\partial \sigma X^2}{\partial \alpha} = 0 = \dfrac{\partial \sigma Y^2}{\partial \alpha}$

(b) $\sigma X^2 = \sigma Y^2 = \sigma Z^2$.

Both conditions (a) and (b) may be met by substituting equations (3-14) and (3-15) in (3-12) and (3-13), then performing the indicated operations:

(a) $\dfrac{\partial \sigma X^2}{\partial \alpha} = 0$

(b) $\sigma X^2 - \sigma Z^2 = 0$.

The solution of each of these equations requires a short iterative process, but this represents no difficulty on a digital computer.

Figure 16 is a graphical illustration of the solutions for (a) and (b) above in terms of baseline length, σX or σY, and σZ. For spacecraft altitudes in the vicinity of H = 650 nautical

miles there is little to favor one criterion over the other, but for H > 650 nautical miles, condition (a) gives the minimum S.E.P. and for H <650 nautical miles, condition (b) gives the minimum S.E.P. In the latter case,

$$S.E.P. = \sigma X = \sigma Z$$

because the confidence region is spherical.

The foregoing analysis is not intended to represent more than an introduction to the study of baseline optimization since surveying errors have not been included, and these are the most important for long baseline systems. For shorter baseline systems, the need for more accurate surveying is more than offset by the fact that correlation in survey errors for the three trackers increases rapidly with decreasing baseline lengths, and other system errors, such as in relative timing, assume greater importance. The present study has not been directed in such a way as to reveal what baseline and what instrumentation provides best tracking under present state-of-the-art conditions, but an extension of the foregoing methods will certainly throw a great deal of light on the subject.

3.9 IMPROVEMENT COEFFICIENTS

In systems design there is a continual effort to improve performance, and the question may come down to how well a given system might perform if D dollars were spent on reduction of the system uncertainties in the most efficient manner. The answer to this question depends on the definition of performance, but performance will normally be rated in terms of certain quantities to be found in the covariance matrices of missile position and velocity at a particular phase of a mission, for instance, immediately prior to an anticipated guidance maneuver. In principle, it makes little difference to the systems analyst what the critical quantities are. It may be that the measurement of Z is the controlling factor (as in a soft landing), or the CEP (as in an impact problem), or the SEP (as in rendezvous). The criterion selected may be any arbitrary function of the elements of the two covariance matrices without changing the essence of the solution. The following treatment assumes that X is the critical quantity and, consequently, that σX is the measure of performance.

One may write an expression for $\Delta\sigma X$ in terms of i changes in system uncertainties $\Delta\sigma a_i$.

$$\Delta\sigma X = \sum_{j=1}^{j=i} \frac{\partial\sigma X}{\partial\sigma a_j} \frac{\partial\sigma a_j}{\partial Da_j} \Delta Da_j ,$$

where Da_j is the number of dollars spent in reducing the uncertainty in a_j. The restriction must hold that

$$\sum_{j=1}^{j=1} Da_j = D \qquad (3\text{-}1C)$$

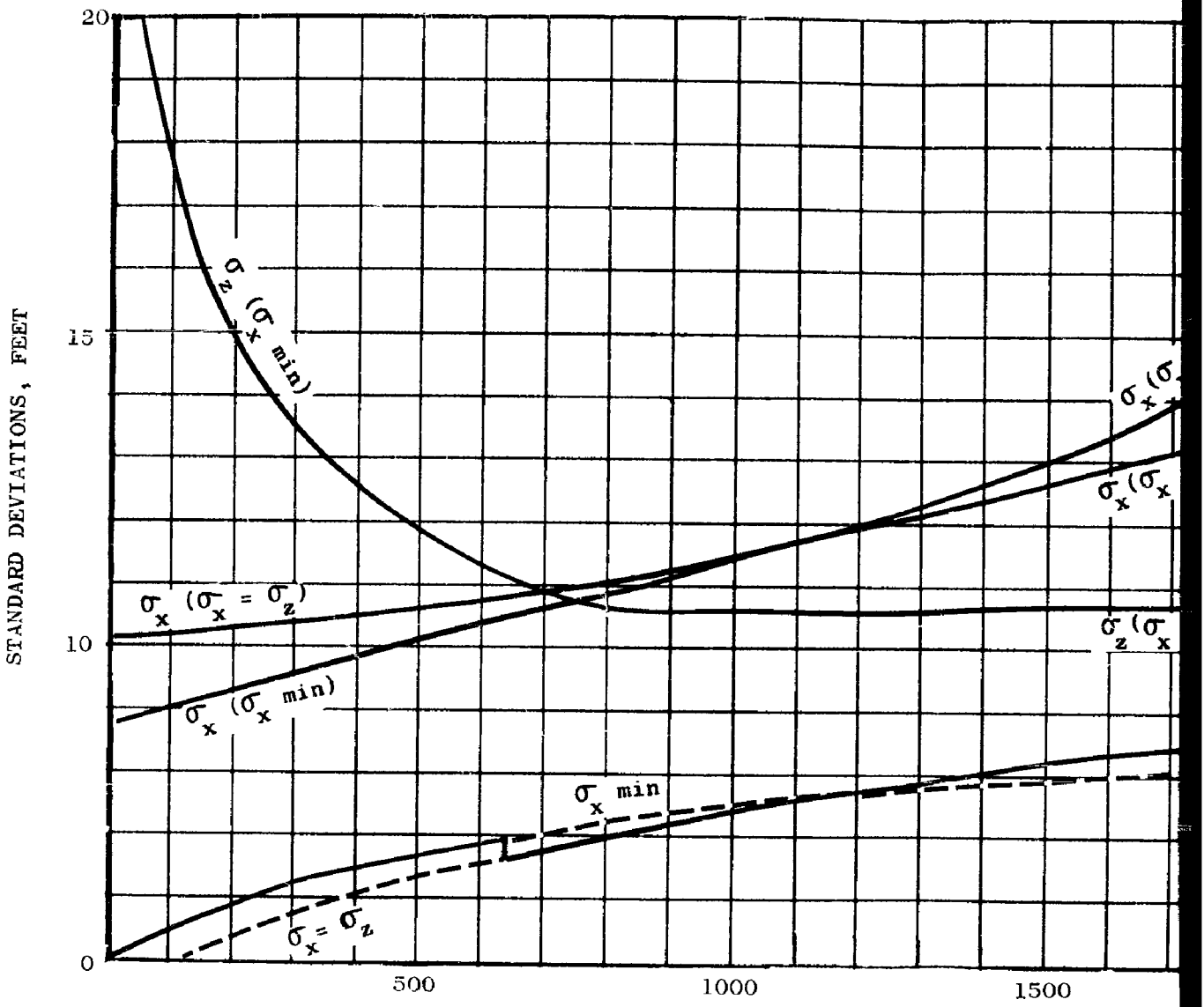

1

Figure 16. Baseline Optimizatio

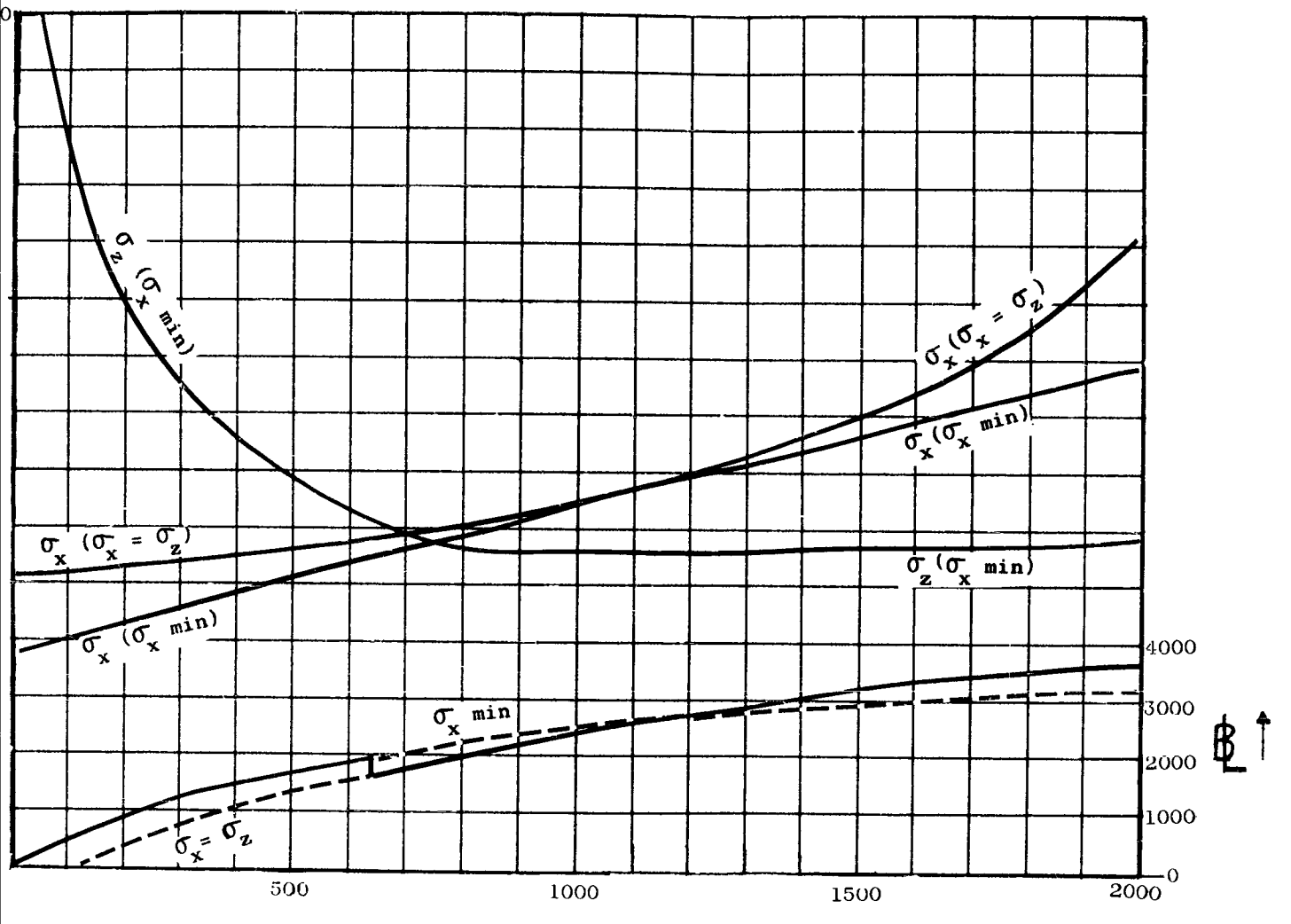

Figure 16. Baseline Optimization

The partial derivatives, $\frac{\partial \sigma a_j}{\partial Da_j}$, are generally available in graphical form or may be generated. An example is $a_j = \frac{\Delta f}{f}$, the beat frequency at each transmitter, divided by the signal frequency. In this case $\sigma a_j = \sigma f$, and the hardware designer should be able to supply at least a curve which defines $\frac{\partial \sigma f}{\partial D_f}$, the improvement possible in oscillator calibration as a function of the dollars spent in doing so. For the sake of the present discussion, let us assume that all partial derivatives $\frac{\partial \sigma a_j}{\partial Da_j}$ are obtained in this way and expressed as truncated power series in Da_j.

The partial derivatives $\frac{\partial \sigma X}{\partial \sigma a_j}$ are part of the computer simulation output. In the case above:

$$\frac{\partial \sigma X}{\partial \sigma f} = \frac{\partial f}{\partial X}\left[R_1^2\left(\frac{\partial X}{\partial R_1}\right)^2 + R_2^2\left(\frac{\partial X}{\partial R_2}\right)^2 + R_3^2\left(\frac{\partial X}{\partial R_3}\right)^2\right],$$

which can also be written as a truncated power series in D_f. These are the quantities referred to as improvement coefficients.

The condition that D dollars be spent in the most efficient manner possible may be stated:

$$\frac{\partial \Delta \sigma X}{\partial \Delta Da_j} = 0 \qquad \frac{\partial^2 \Delta \sigma X}{\partial \Delta Da_j 2} > 0$$

This expression, including (3-16), gives i equations in i unknowns, Da_j, which are then solved for Da_j, the number of dollars to be spent in improving σa_j.

If the foregoing procedure has been used periodically throughout the development of a system, it will continually optimize hardware design in terms of dollar value. If it is applied late in the design period, it will show where money has been used inefficiently. In the latter case, the optimization would have to be rerun with:

$$\Delta Da_k = 0$$

for those components, a_k, on which development had been carried beyond the point of maximum return. Figure 17 illustrates the improvement coefficients as a function of geocentric angle.

3.10 PROGRAM OUTPUT

A general flow chart of the over-all computer program is illustrated in Figure 18. The starting point in this program is the selection of tracking station (locations) and the spacecraft trajectory to be tracked by the system. The program computes the partial derivatives of spacecraft position and velocity with respect to the tracking station coordinates. These partial derivatives then are combined with estimates of the probable errors in station location (survey errors) and errors in the radio measurements of the tracking system. The result of combining these error estimates with the partial derivatives is a set of covariance matrices which represent the confidence regions for spacecraft position and velocity.

This set of matrices is then used in a subroutine to form a set of improvement coefficients which describe the sensitivity of the confidence regions to reductions in the system errors.

The covariance matrix output is also used in a subroutine to form station relocation improvement coefficients which provide a measure of the effects on the tracking system performance of relocating one or more tracking stations.

Many figures of merit may be used to measure the reliability of a given tracker complex for some point on a given trajectory. For a specific mission, it is desirable to choose a special figure of merit which best evaluates the expectancy of successful performance. Generally speaking, errors in some of the components of position or velocity are less important than the others. For example, the problem of soft impact on a planet requires more accurate knowledge of the component of position along the trajectory immediately prior to the terminal guidance maneuver than of the two cross-trajectory components. However, since the mission objectives of this study are very general, the program output has been made rather general. It is as follows:

a) Covariance matrix: The covariance matrix representation is used to describe a confidence region for the terminal points of the vector position and velocity of the missile.

$$M_{\bar{r}} = \begin{bmatrix} \sigma X^2 & \sigma YX & \sigma ZX \\ \sigma XY & \sigma Y^2 & \sigma ZY \\ \sigma XZ & \sigma YZ & \sigma Z^2 \end{bmatrix} \qquad M_{\dot{\bar{r}}} = \begin{bmatrix} \sigma \dot{X}^2 & \sigma \dot{Y}\dot{X} & \sigma \dot{Z}\dot{X} \\ \sigma \dot{X}\dot{Y} & \sigma \dot{Y}^2 & \sigma \dot{Z}\dot{Y} \\ \sigma \dot{X}\dot{Z} & \sigma \dot{Y}\dot{Z} & \sigma \dot{Z}^2 \end{bmatrix}$$

where:

$$\sigma X^2 = \sum_i \left(\frac{\partial X}{\partial ai}\right)^2 \sigma^2_{ai} \qquad \sigma XY = \sum_i \left(\frac{\partial X}{\partial ai}\right)\left(\frac{\partial Y}{\partial ai}\right) \sigma^2_{ai} \; ;$$

etc.

Since it is customary to speak of "errors" or "probable errors" in X, Y, Z, $\dot{X}$, $\dot{Y}$, $\dot{Z}$, rather than their variances, a more convenient expression of tracking accuracy is output in the form,

$$V_{\bar{r}} = \begin{bmatrix} \sigma X \\ \sigma Y \\ \sigma Z \end{bmatrix} \qquad V_{\dot{\bar{r}}} = \begin{bmatrix} \sigma \dot{X} \\ \sigma \dot{Y} \\ \sigma \dot{Z} \end{bmatrix}$$

where the six elements are standard deviations in the components of missile position and velocity.

A third figure of merit is the quantity

$$C_{\bar{r}} = \left(\sigma X^2 + \sigma Y^2 + \sigma Z^2 \right)^{1/2}$$

and

$$C_{\dot{\bar{r}}} = \left(\sigma \dot{X}^2 + \sigma \dot{Y}^2 + \sigma \dot{Z}^2 \right)^{1/2}.$$

The values of these are invariant with respect to coordinate rotation and, hence, hold also for the eigenvalues of the covariance matrix. The two values are intimately related to the S. E. P. and have been called simply the "probable error" in position and velocity. If

$\sigma X = \sigma Y = \sigma Z$ or $\sigma \dot{X} = \sigma \dot{Y} = \sigma \dot{Z}$, the relationship is

$$(\text{S. E. P.})_{\bar{r}} = \frac{C_{\bar{r}}}{\sqrt{3}}$$

$$(\text{S. E. P.})_{\dot{\bar{r}}} = \frac{C_{\dot{\bar{r}}}}{\sqrt{3}}.$$

Therefore, these are also part of the numerical output.

A fourth figure of merit is the description of the ellipsoidal confidence region in terms of its semi-axes. When the covariance matrix is rotated into an orientation such that its off-diagonal terms are all zero, the diagonal terms are referred to as eigenvalues.

The square roots of these,

$$\sigma X_E, \quad \sigma Y_E, \quad \sigma Z_E, \quad \text{or} \quad \sigma \dot{X}_E, \quad \sigma \dot{Y}_E, \quad \sigma \dot{Z}_E,$$

are the semi-axes of the ellipsoidal confidence region of position and velocity, respectively.

The elongation of the ellipsoid along one or two of its axes is considered to be a poor characteristic, since the S. E. P. is generally only slightly less than the longest axis of the confidence region.

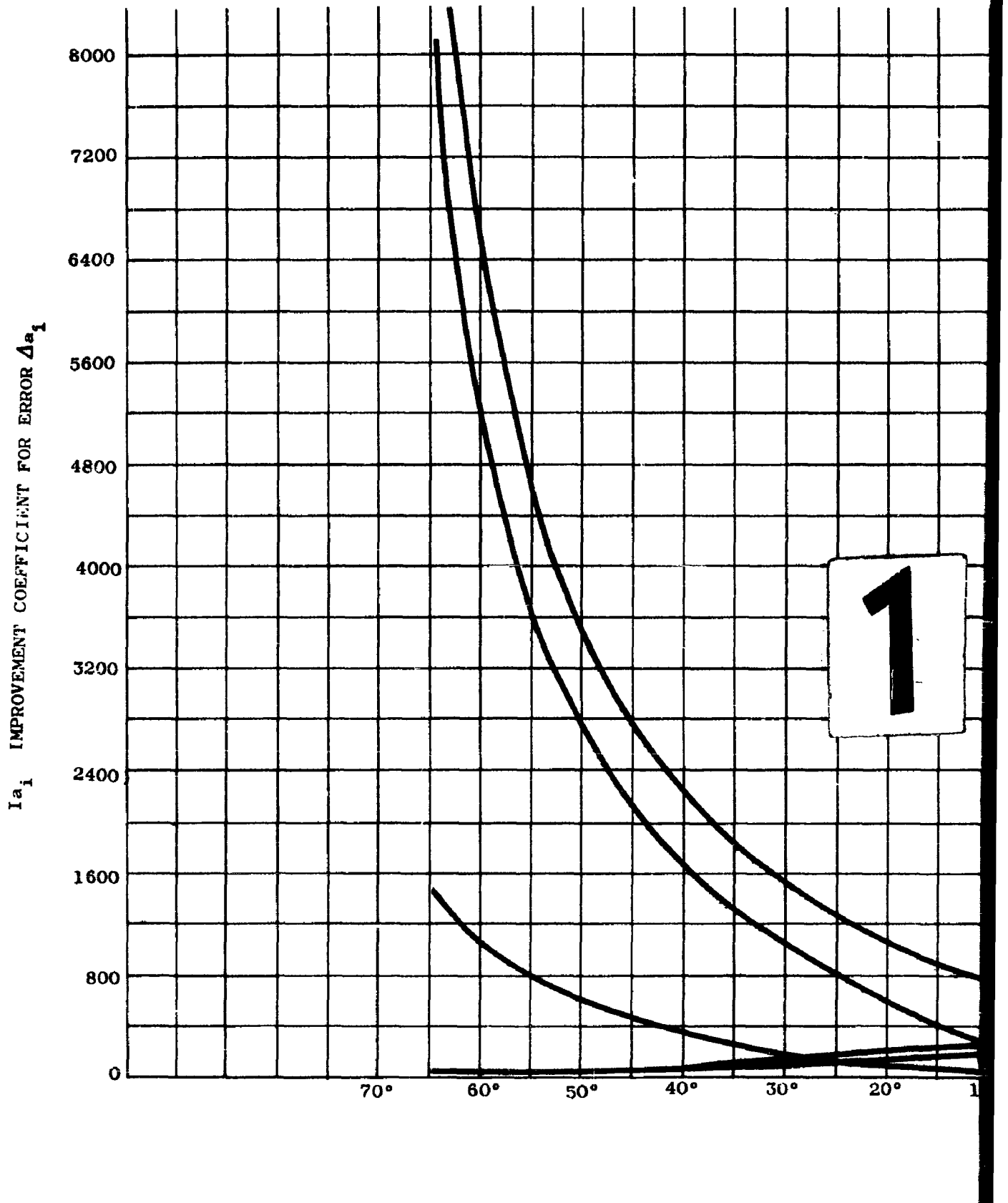
$I a_i$ IMPROVEMENT COEFFICIENT FOR ERROR Δa_1
8000
7200
6400
5600
4800
4000
3200
2400
1600
800
0
70°
60°
50°
40°
30°
20°
1

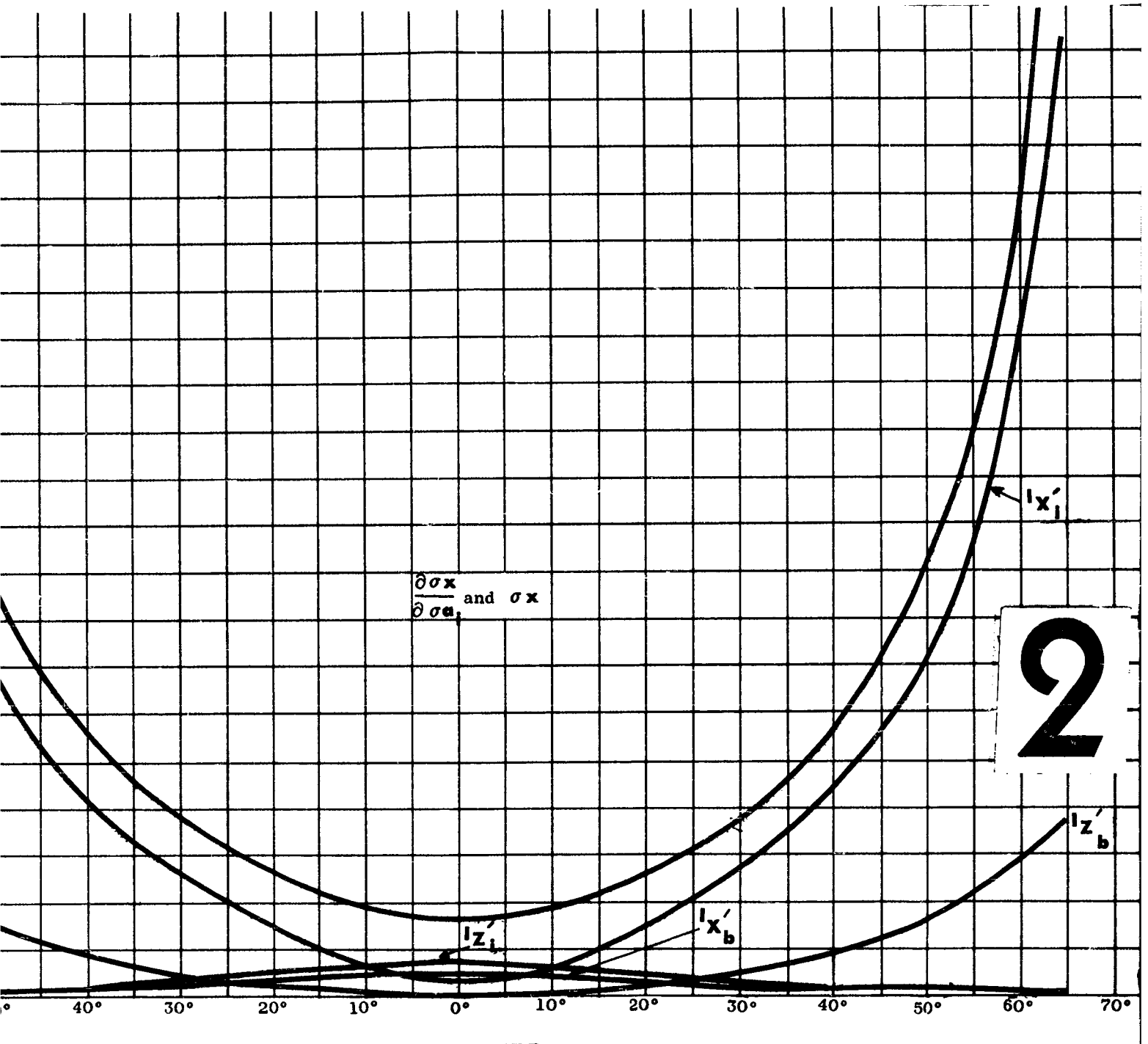

Figure 17. Improvement Coefficients vs. Geocentric Angle for

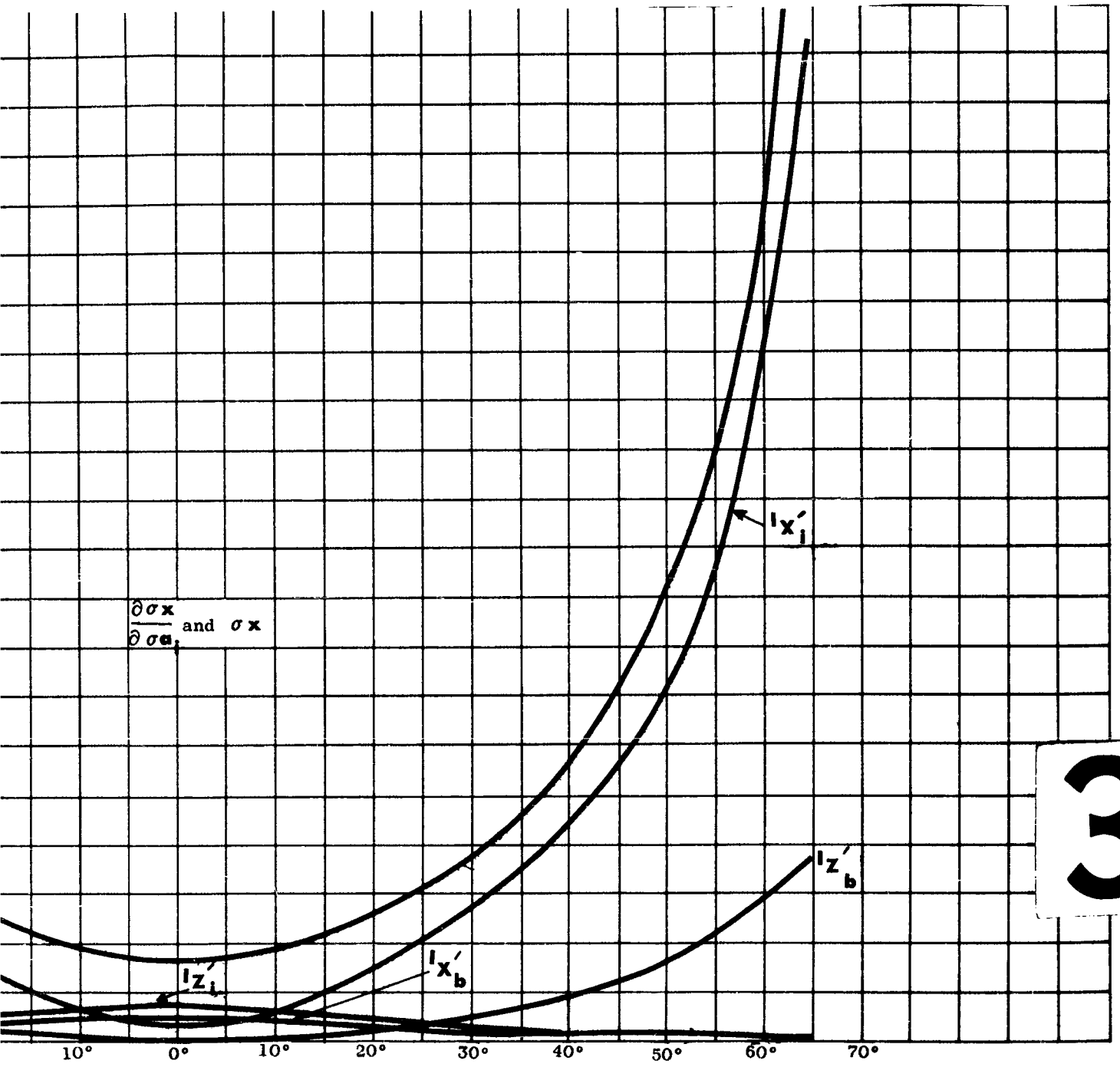

Figure 17. Improvement Coefficients vs. Geocentric Angle for a 10,000 N. MI. Orbit

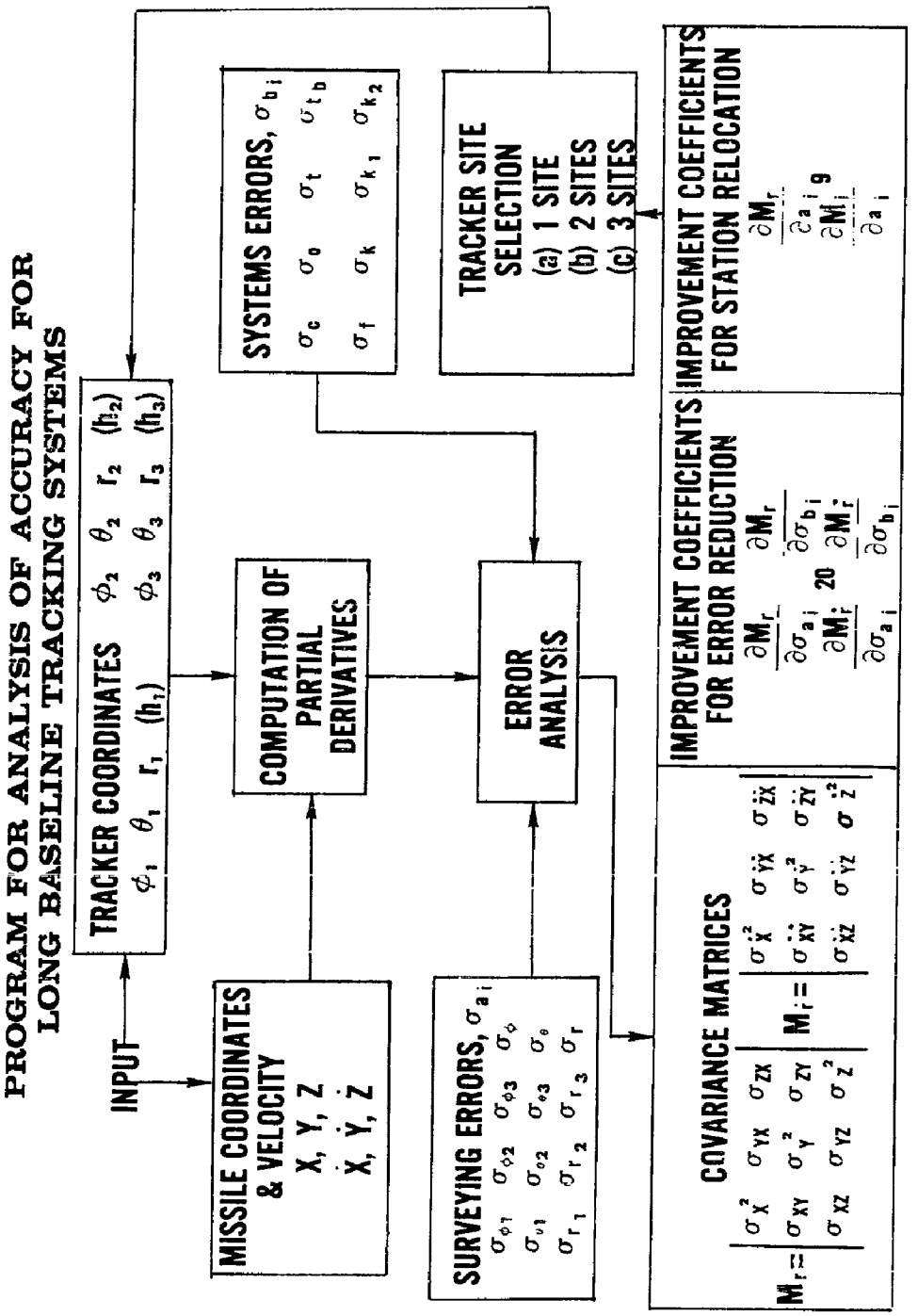

Figure 18. Program for Analysis of Accuracy for Long-Baseline Tracking Systems

The fifth figure of merit used is the radius of the sphere of equal volume:

$$(R.S.E.V.)_{\bar{r}} = \left(\sigma\dot{X}_E\ \sigma\dot{Y}_E\ \sigma\dot{Z}_E\right)^{1/3}$$

$$(R.S.E.V.)_{\dot{\bar{r}}} = \left(\sigma\dot{X}_E\ \sigma\dot{Y}_E\ \sigma\dot{Z}_E\right)^{1/3}$$

These quantities, however, tend to give an optimistic error value if there is great dissimilarity among the eigenvalues, even though for:

$$\sigma X_E = \sigma Y_E = \sigma Z_E \quad \text{or} \quad \sigma\dot{X}_E = \sigma\dot{Y}_E = \sigma\dot{Z}_E$$

the R.S.E.V. is equal to the S.E.P.

Frequently the situation arises in which a particular tracking system fails to meet accuracy specifications or in which it would be highly desirable to increase safety factors. For this purpose a set of "improvement coefficients"

$$I_{\bar{r}_{ai}} = \frac{\sigma ai}{100}\begin{vmatrix} \frac{\partial\sigma X}{\partial\sigma ai} \\ \frac{\partial\sigma Y}{\partial\sigma ai} \\ \frac{\partial\sigma Z}{\partial\sigma ai} \end{vmatrix} \qquad I_{\dot{\bar{r}}_{ai}} = \frac{\sigma ai}{100}\begin{vmatrix} \frac{\partial\sigma X}{\partial\sigma ai} \\ \frac{\partial\sigma Y}{\partial\sigma ai} \\ \frac{\partial\sigma Z}{\partial\sigma ai} \end{vmatrix}$$

are computed for all measurements, a_i. The elements are the changes of standard deviation in X, Y, Z, $\dot{X}$, $\dot{Y}$, and $\dot{Z}$ corresponding to a 1 percent- change in σai. These coefficients are useful in pointing out ways and means of increasing tracking precision, as demonstrated in paragraph 3.9.

The program output can be summarized as follows:

r - The radial distance to the spacecraft from the earth's mass center, in millions of feet.

v - The spacecraft velocity magnitude, feet/second.

R_1, R_2, R_3 - The distance from the spacecraft to tracking station 1, 2, and 3, millions of feet.

ϵ_1, ϵ_2, ϵ_3 - The line-of-sight elevation angle to the spacecraft from tracking station 1, 2, and 3; in degrees of arc above local horizontal.

σ_X, σ_Y, σ_Z - The standard deviation in spacecraft position in the coordinate directions X, Y, and Z, feet.

$\sigma_{\dot{X}}$, $\sigma_{\dot{Y}}$, $\sigma_{\dot{Z}}$ - The standard deviation in spacecraft velocity in the coordinate directions X, Y, and Z, feet/second.

E_X, E_Y, E_Z - The semi-major and two semi-minor axes of the ellipsoid of probable error of spacecraft position. The X, Y, and Z directions are not specified, feet.

$E_{\dot{X}}$, $E_{\dot{Y}}$, $E_{\dot{Z}}$ - The semi-major and the two semi-minor axes of the ellipsoid of probable error of spacecraft velocity. The X, Y, and Z directions are not specified, feet/second.

$C_p/\sqrt{3} = \frac{1}{\sqrt{3}} \sqrt{\sigma_X^2 + \sigma_Y^2 + \sigma_Z^2}$ - radius of the equivalent spherical error of spacecraft position, feet.

$C_r/\sqrt{3} = \frac{1}{\sqrt{3}} \sqrt{\sigma_X^2 + \sigma_Y^2 + \sigma_Z^2}$ - radius of the equivalent spherical error of spacecraft velocity, feet.

R.S.E.V. $= (E_X E_Y E_Z)^{1/3}$ - radius of the sphere of volume equal to that of the confidence region, feet

3.11 THREE RANGE DIFFERENCES

A system which measures only the arrival times of the same phase at four stations and computes three range differences was examined. A station at sea level with zero latitude and longitude was added to the equatorial complex already described. Standard deviations in X, Y, and Z were formed for the same equatorial orbits used in the three range system. The input standard deviations, coordinate systems, units, etc. are the same as assumed for the three range system. Details of the computations are described in Appendix I. The results of this examination are included in paragraph 3.12.

This system, in theory, could be employed to track passively a transmitting but uncooperative vehicle traveling over the complex. However, as the graphs indicate, the distance to the target formed this way is very poor, at the present state-of-the-art in the area of time-synchronization. For positions of the vehicle nearly over the central station, the direction can be determined to 0.4 milliradian for ranges to 10.000 nautical miles.

Improvement in the synchronization of clocks over long distances (1000 nautical miles will reduce the errors somewhat, but it is not until the time error between stations is of the order of 10^{-9} seconds that the system approaches the accuracy of the range-only measuring system (whose clocks are synchronized to 10^{-6} seconds). The degree of improvement is illustrated in Figure 19, which presents the standard deviation in X, Y, and Z as functions of the timing accuracy.

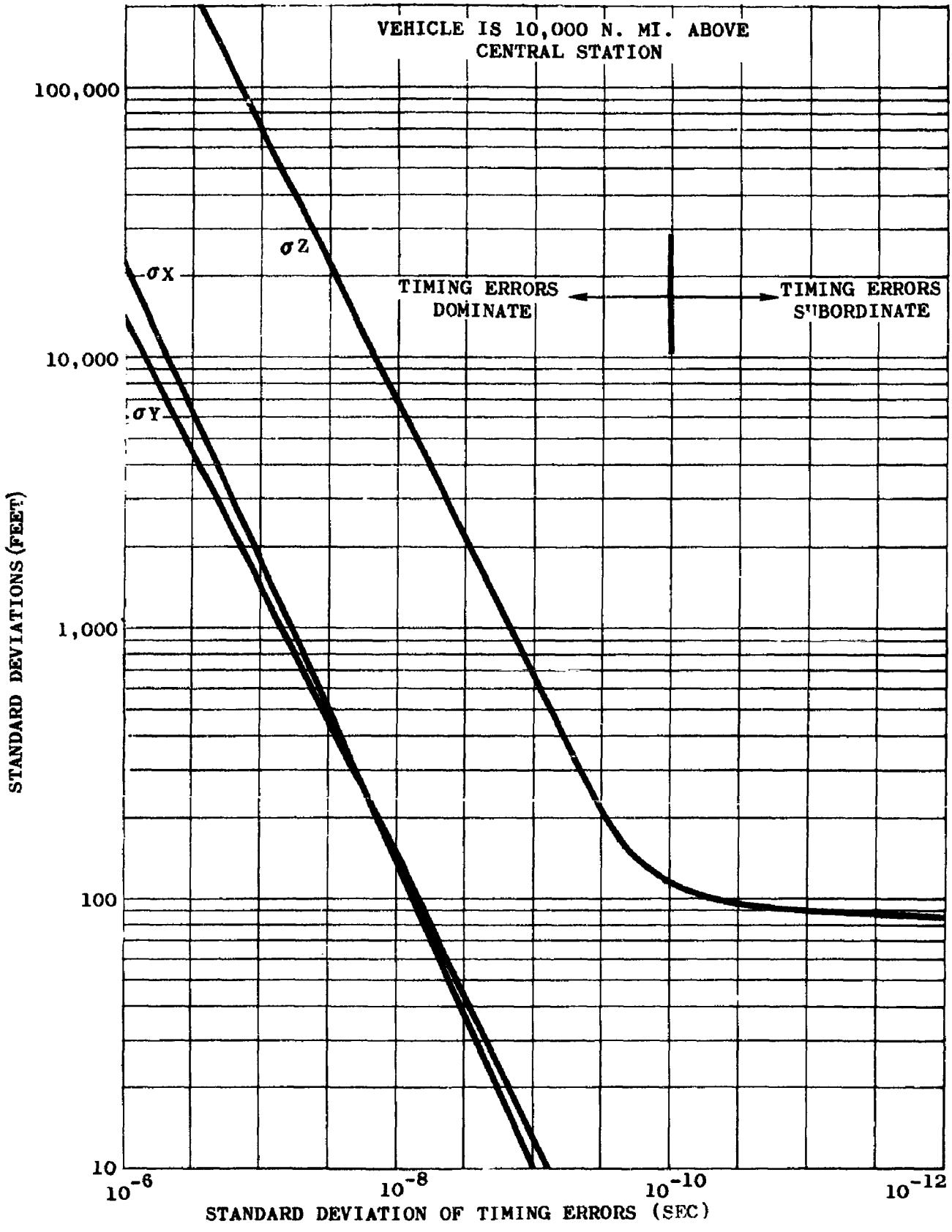

Figure 19. Tracking System Improvement vs. Time-Synchronization Errors

3.12 Tracker System Simulation Results

Using the analytical techniques previously discussed and the digital computer program, a tracking system employing three range-only measurements and a tracking system employing three range-difference measurements were simulated. The results of these simulations are presented in Figures 20 through 37.

The first five figures depict the results of using a three-range-only tracking system for measuring the position and velocity of a spacecraft on a typical lunar trajectory with launch from Cape Canaveral. For the chosen trajectory and tracker location, the spacecraft was visible for two intervals in the transition from the earth to the moon. The first two figures depict the errors in position and velocity with realistic values for the surveying errors. The third figure depicts the spacecraft position and velocity errors for the same tracker configuration but for which the surveying errors have been reduced to zero. The remaining two figures of the first five depict composite root-sum-square errors for the lunar spacecraft. These results represent the ultimate which can be obtained with this type of system by improving the surveying techniques.

The next ten figures depict the same general results for a three range-only tracking system in measuring the position and velocity of earth satellites. The first six of these ten figures reflect typical surveying errors. The remaining four figures assume the surveying errors have been reduced to zero. In these satellite figures the circular orbiting satellite yields position errors which are symmetrical about the centroid of the tracking triangle. However, the velocity errors are not symmetrical about this central point because of the vector nature of the satellite velocity.

The remaining three figures depict the results of a tracking system which measures three range differences. The position errors to be obtained with this type of system are extremely large in the Z component. This reflects, principally, the errors of time-synchronization among the tracking stations. A value of one microsecond was assumed.

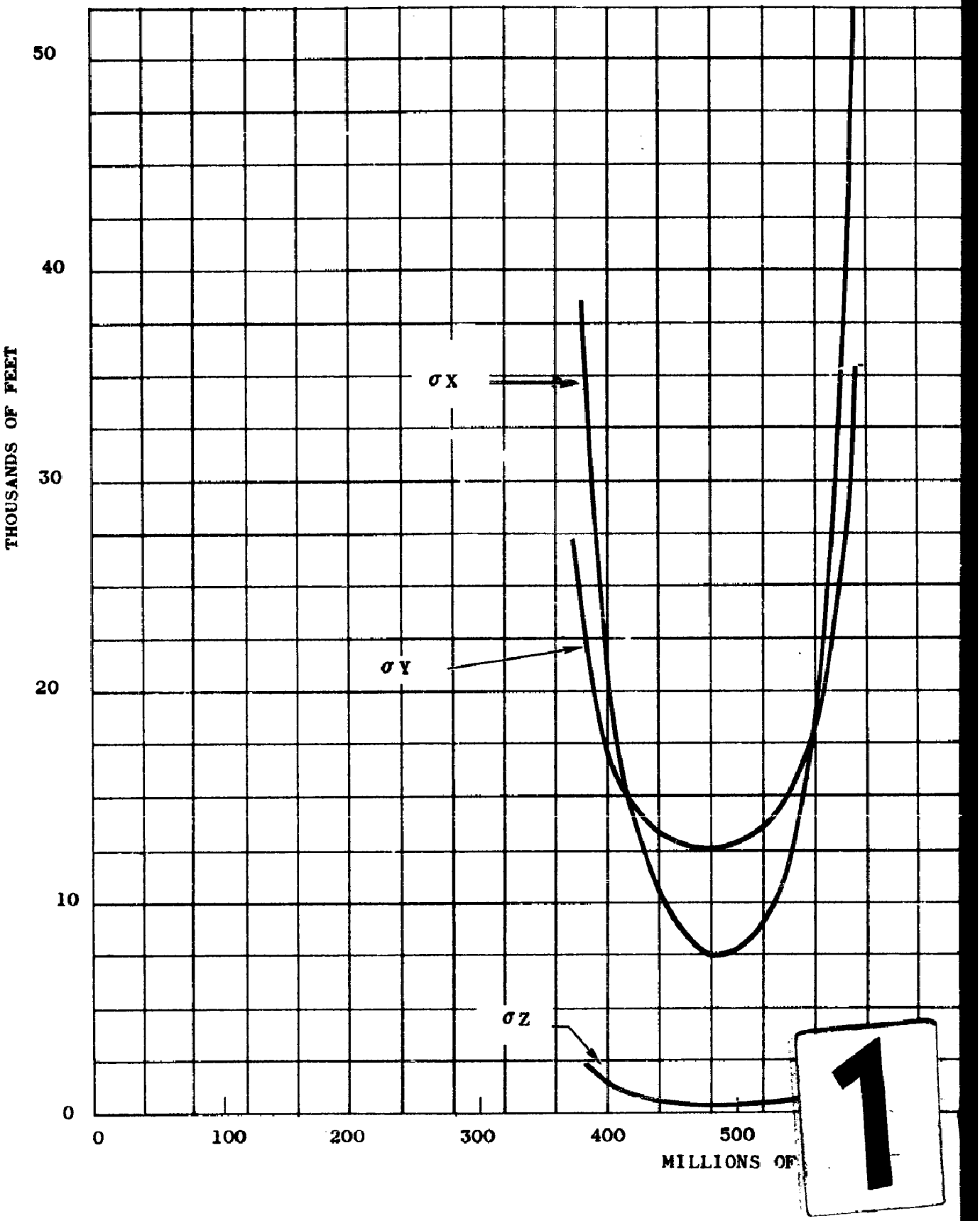
50
40
30
20
10
0
THOUSANDS OF FEET
σ X
σ Y
σ Z
0
100
200
300
400
500
MILLIONS OF
1

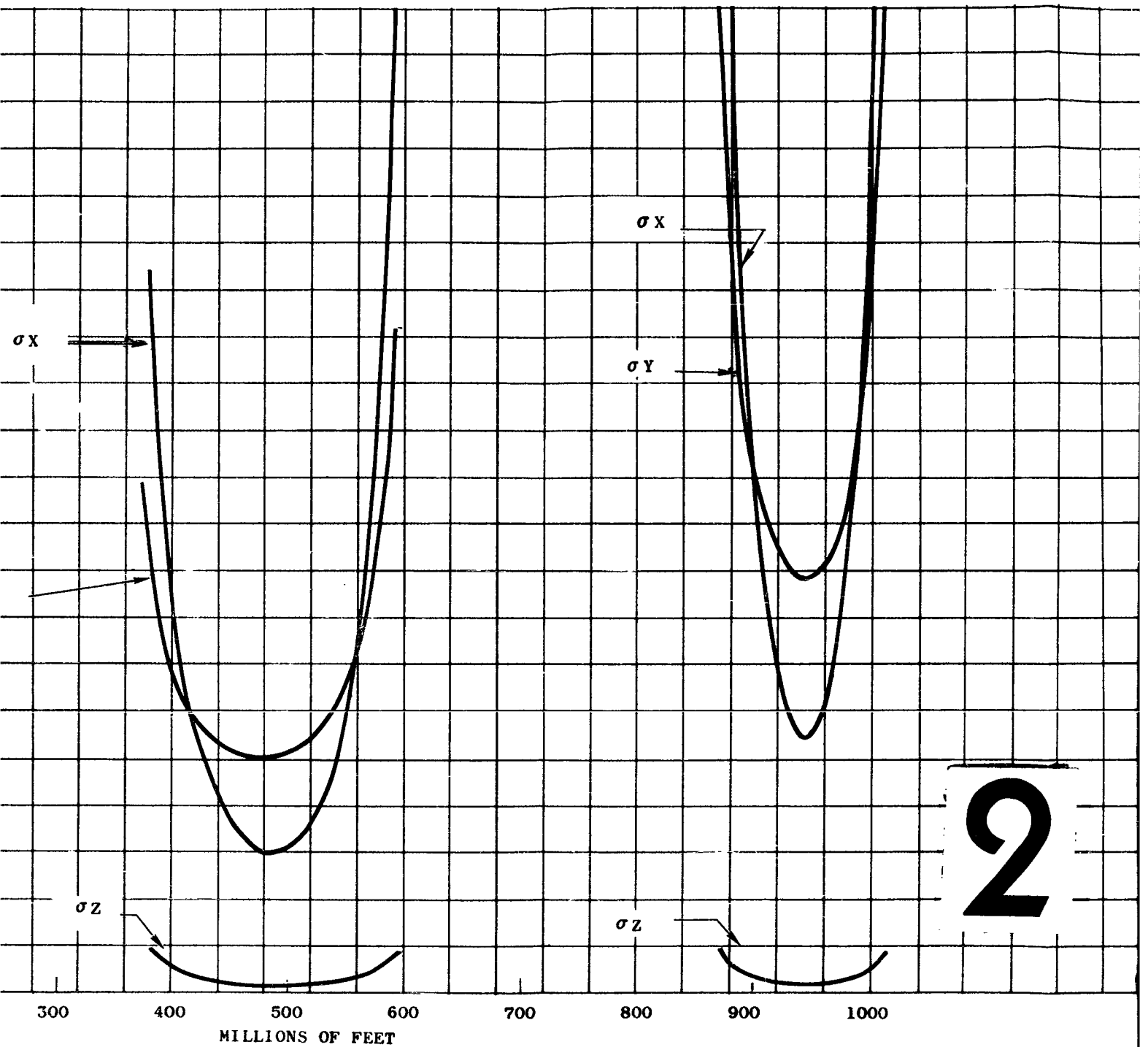

Figure 20. Standard Deviation in Positio
Spacecraft for Two Horizon-t

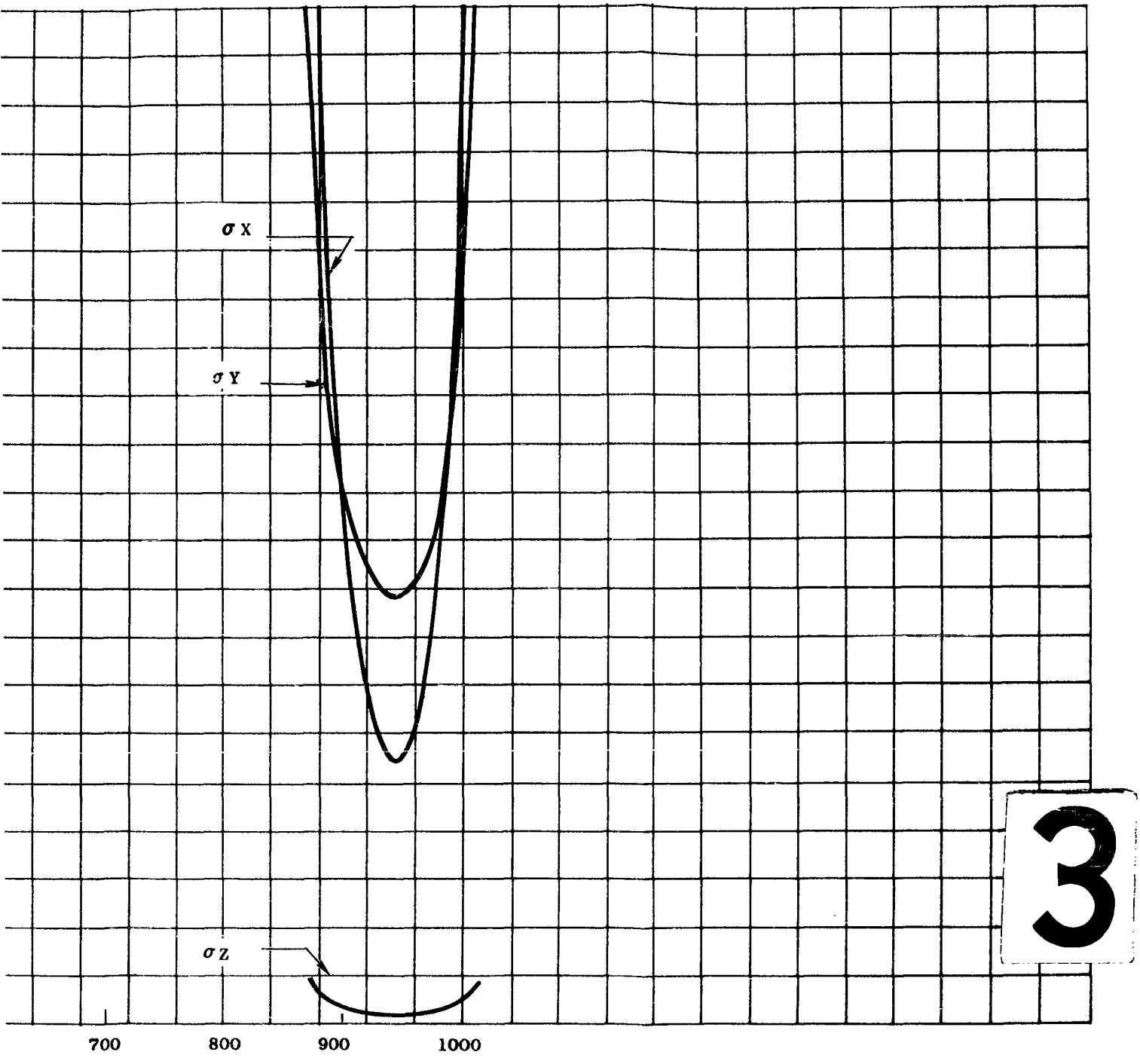

Figure 20. Standard Deviation in Position vs. Radial Distance to a Lunar Spacecraft for Two Horizon-to-Horizon Passes

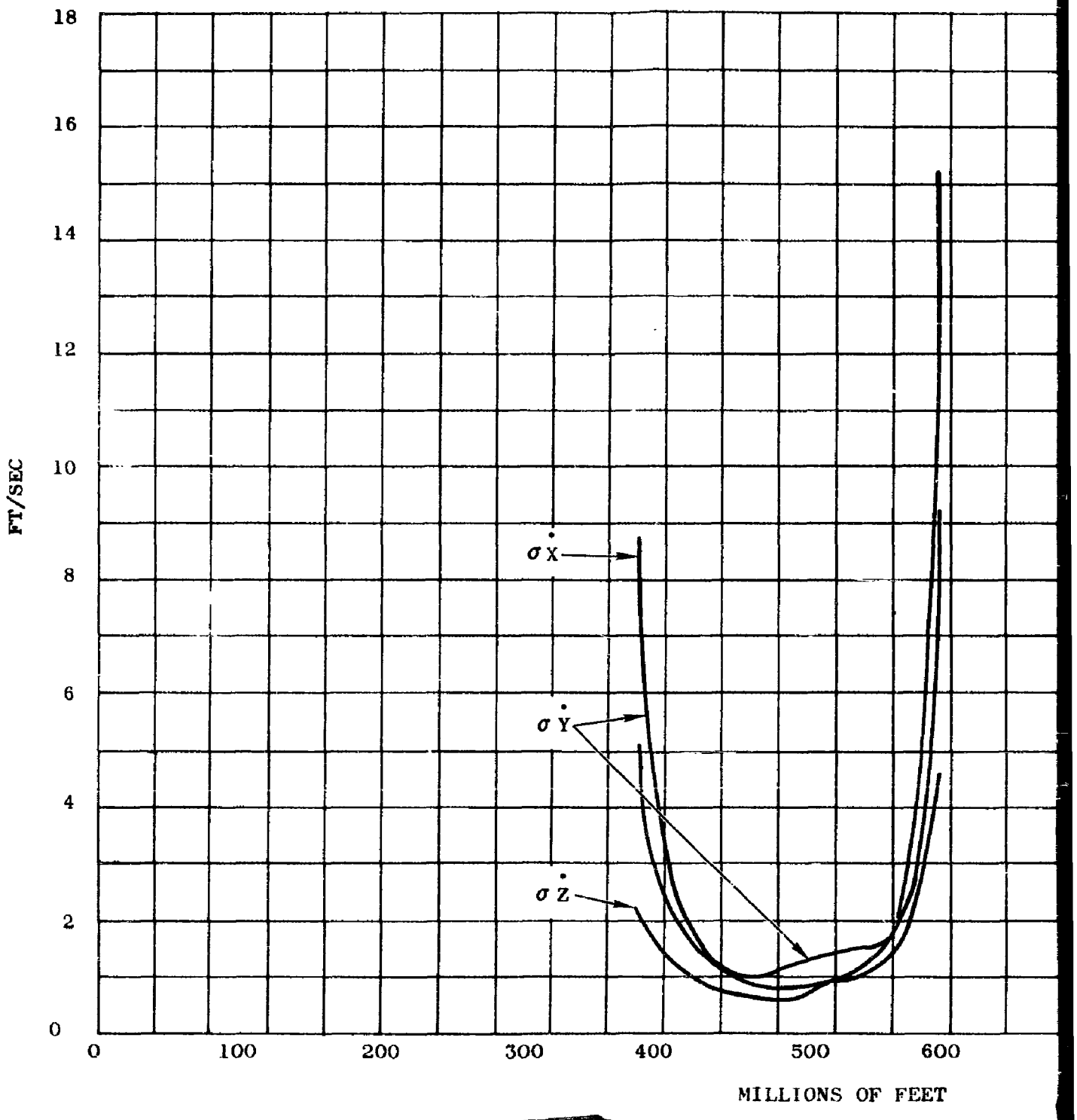

Figure 21. Standard
Spacecraf

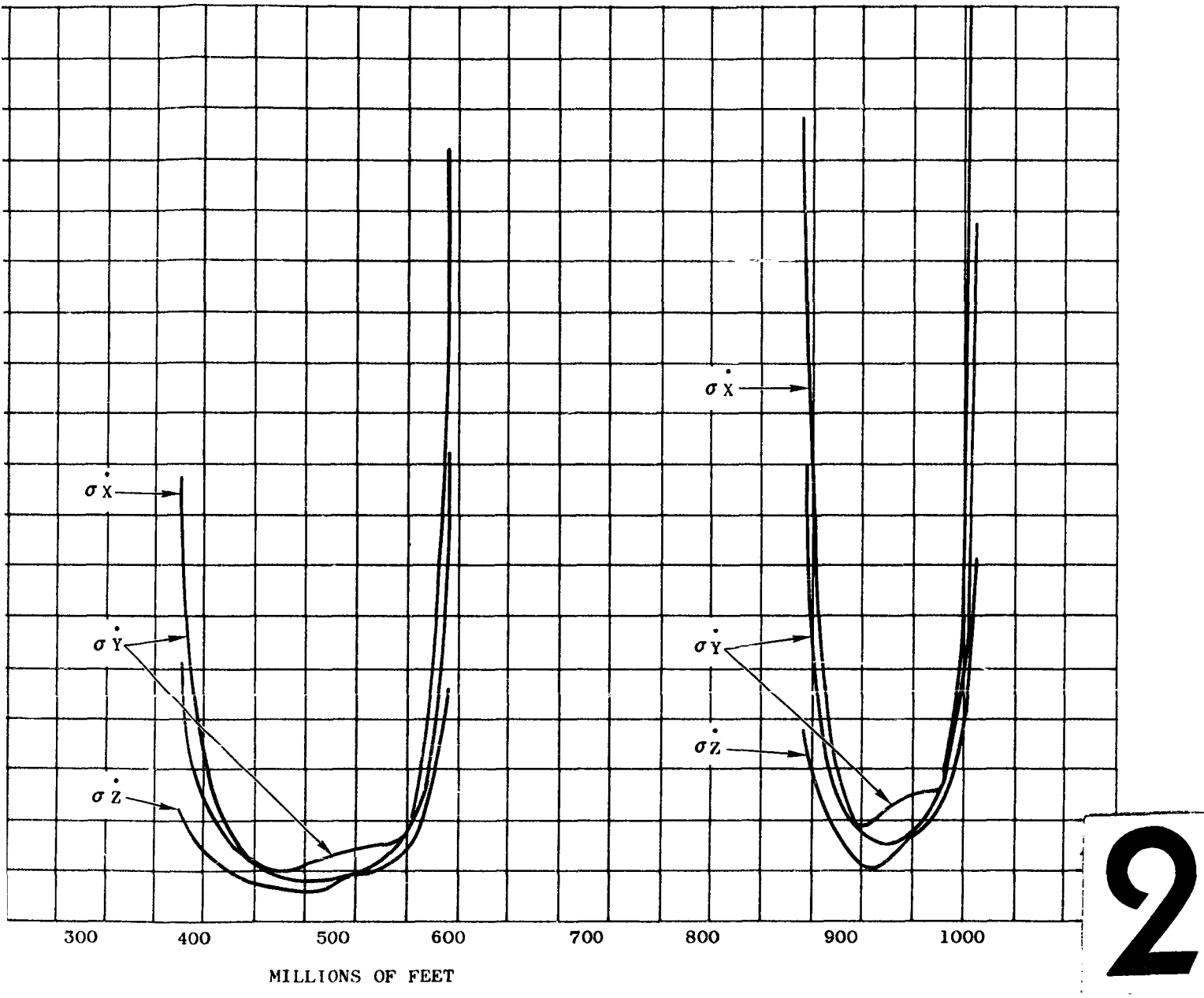

2

Figure 21. Standard Deviation in Velocity vs. Radial Distance to a Lunar Spacecraft for Two Horizon-to-Horizon Passes

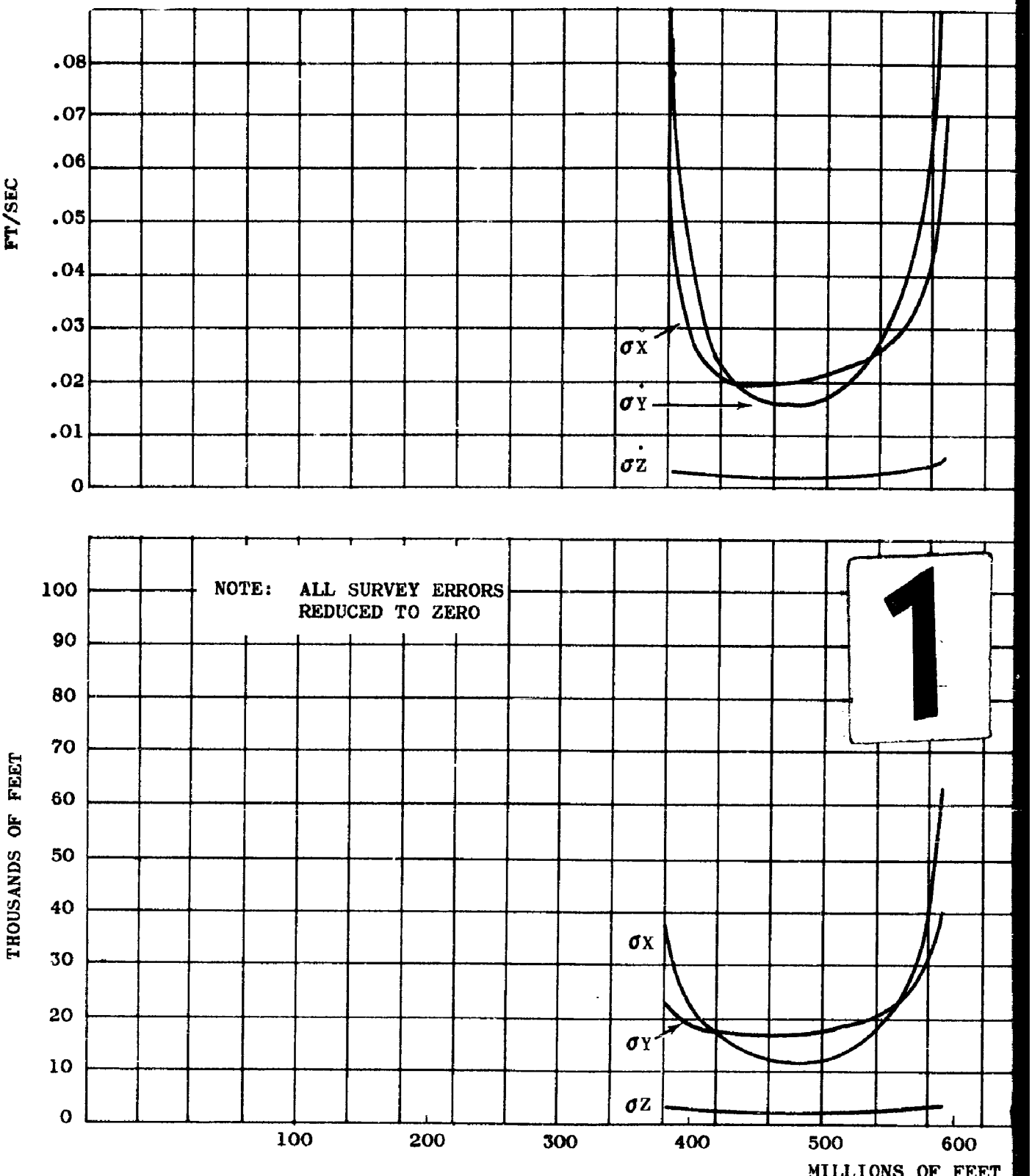

Figure 22. Standard Dev
Spaced

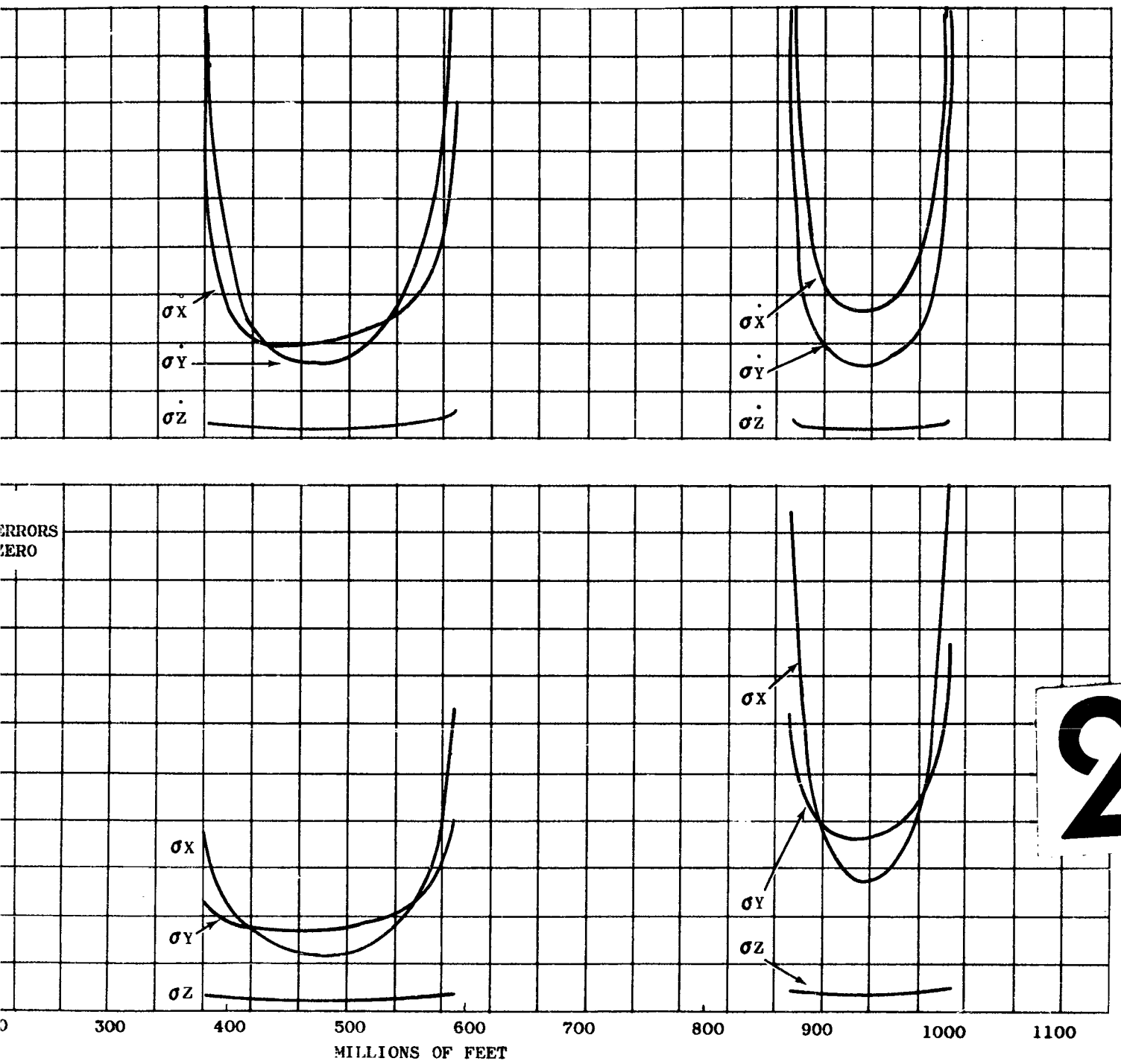

Figure 22. Standard Deviation (Position and Velocity) vs. Radial Distance to a Lunar Spacecraft for Two Horizon-to-Horizon Passes

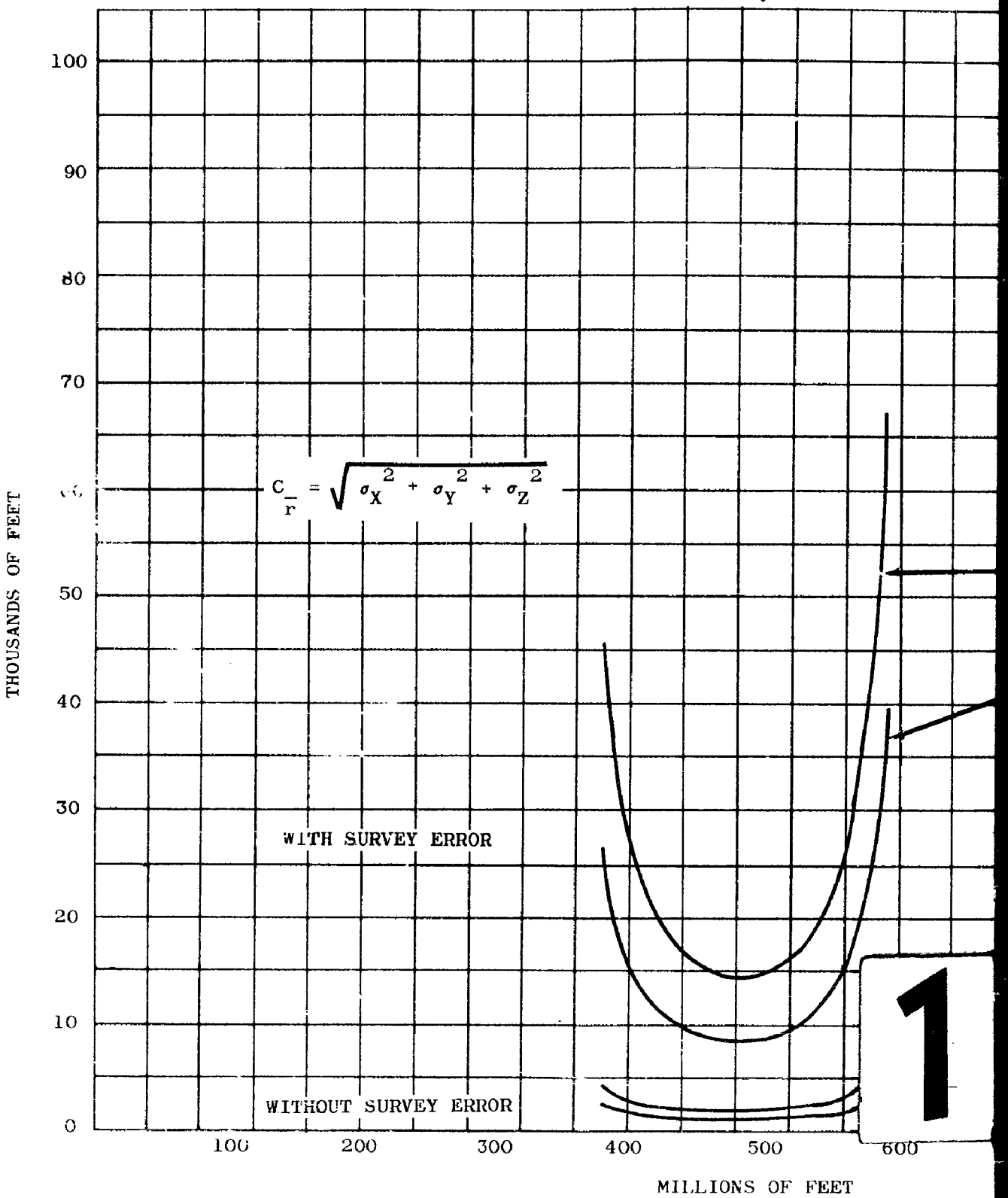

Figure 23. Composite Root-Sum
Spacecraft fo

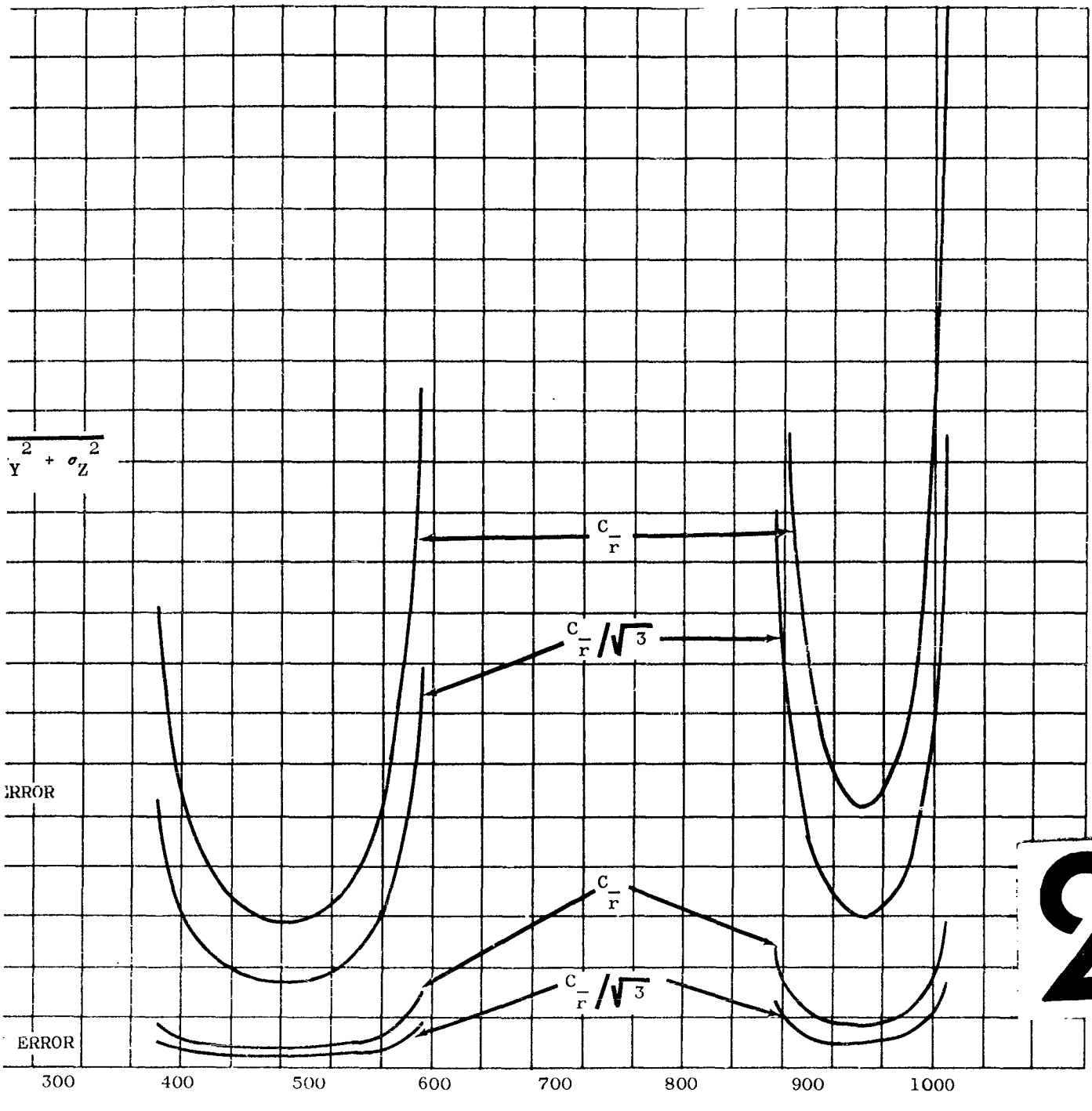

Figure 23. Composite Root-Sum-Square Position Error vs. Radial Distance to a Lunar Spacecraft for Two Horizon-to-Horizon Passes

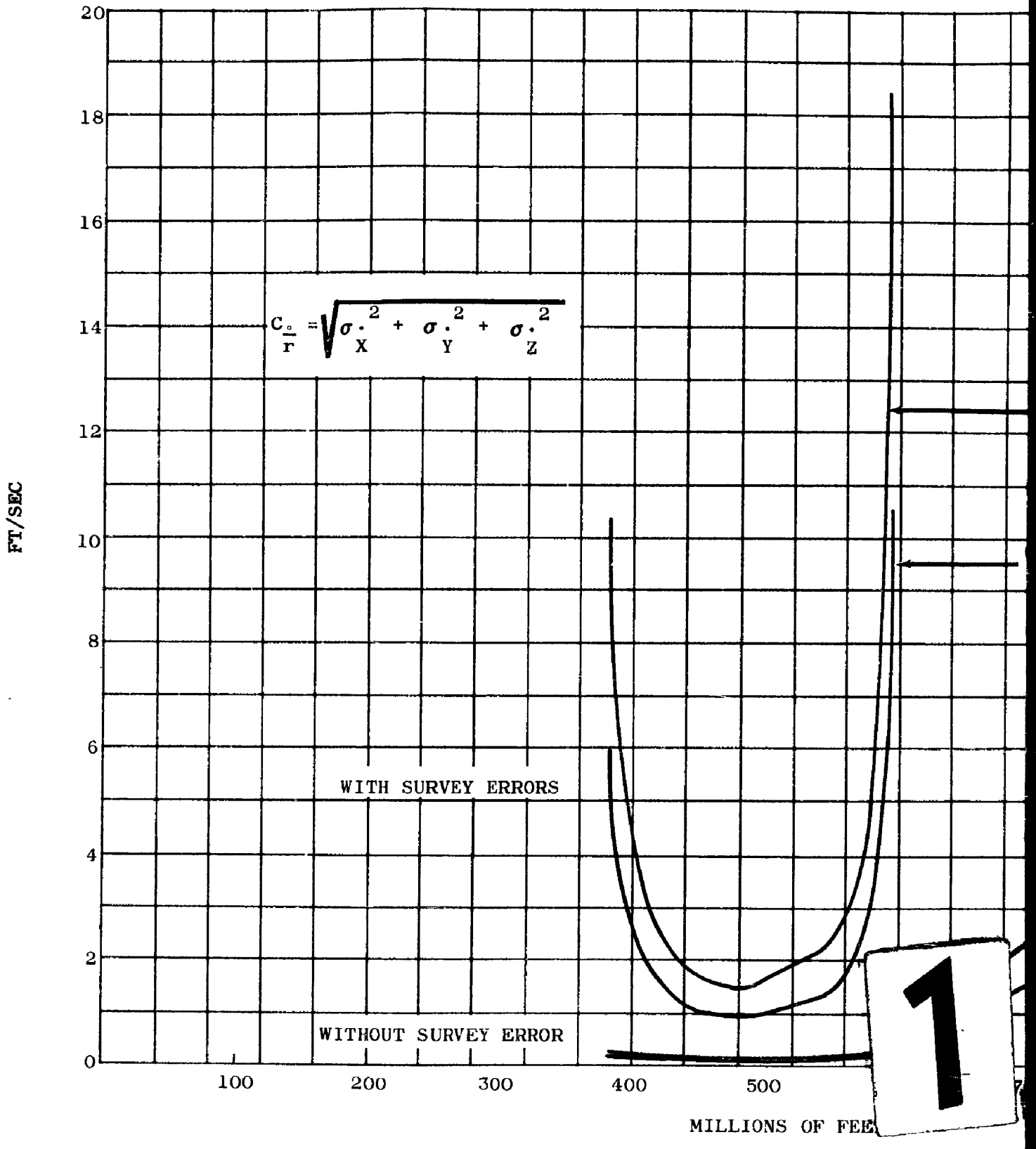

Figure 24. Composite Root-Sum-Square V
Spacecraft for Two Ho

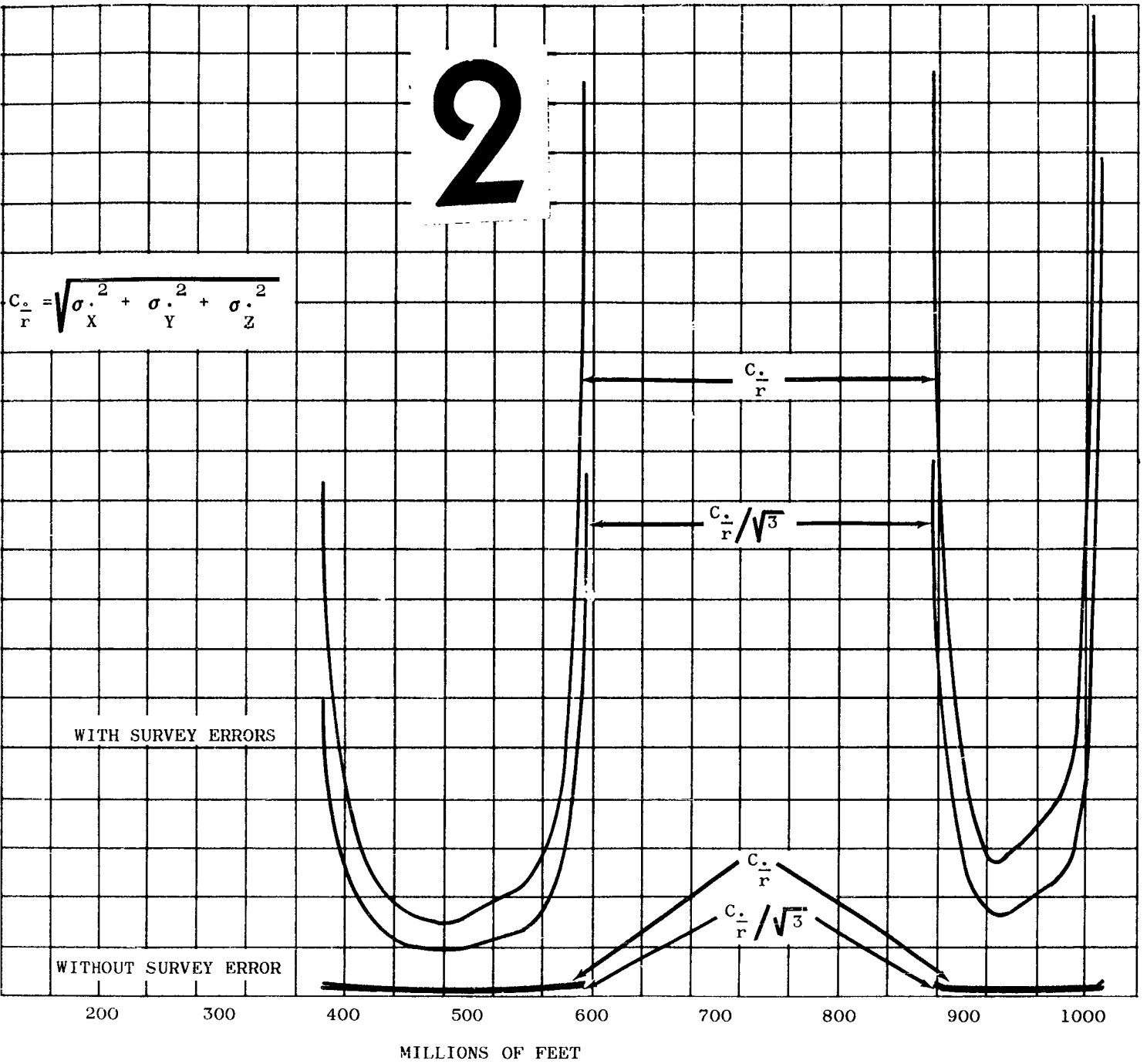

Figure 24. Composite Root-Sum-Square Velocity Error vs. Radial Distance to a Lunar Spacecraft for Two Horizon-to-Horizon Passes

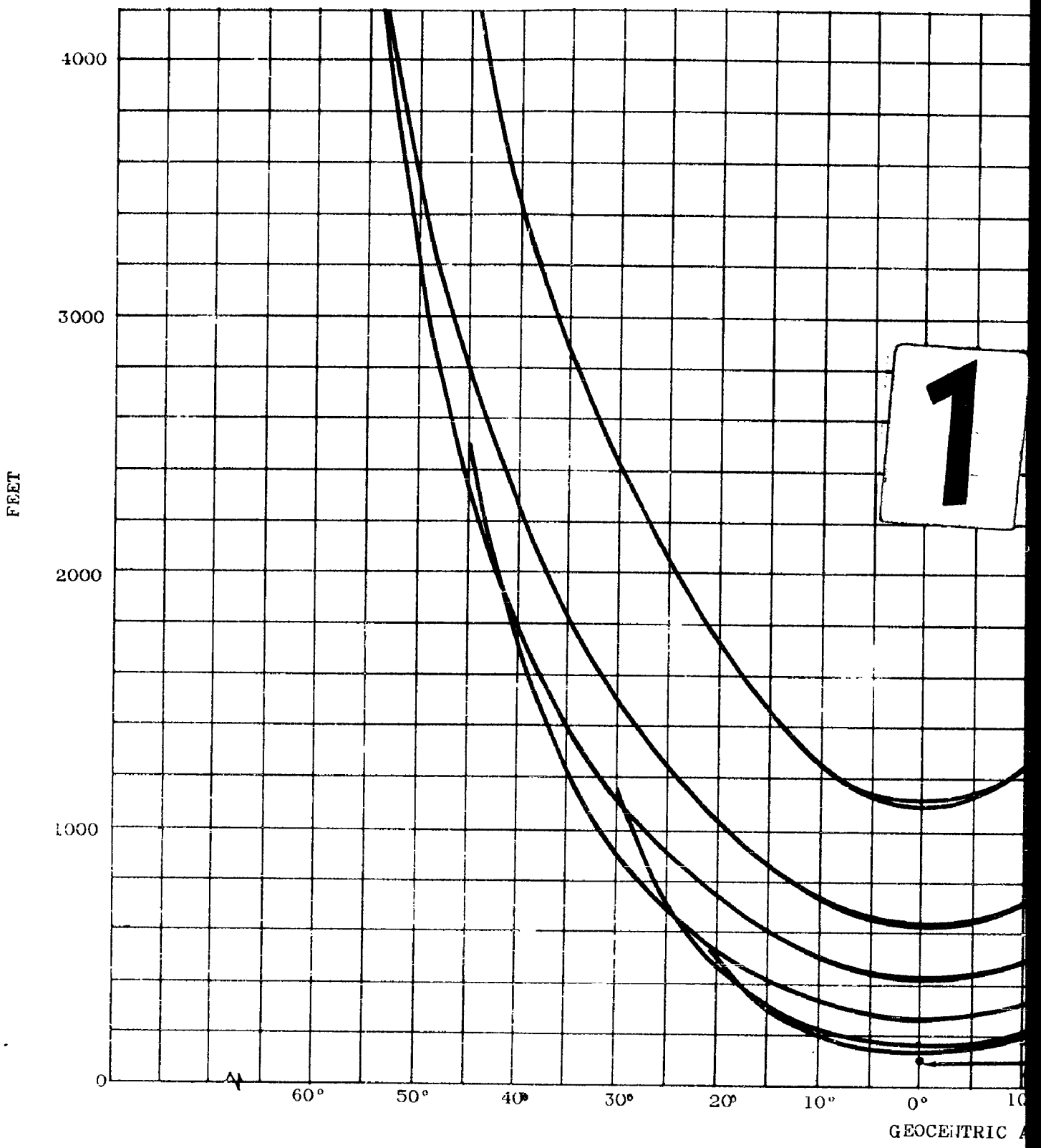
4000
3000
2000
1000
0
FEET
60°
50°
40°
30°
20°
10°
0°
GEOCENTRIC
1

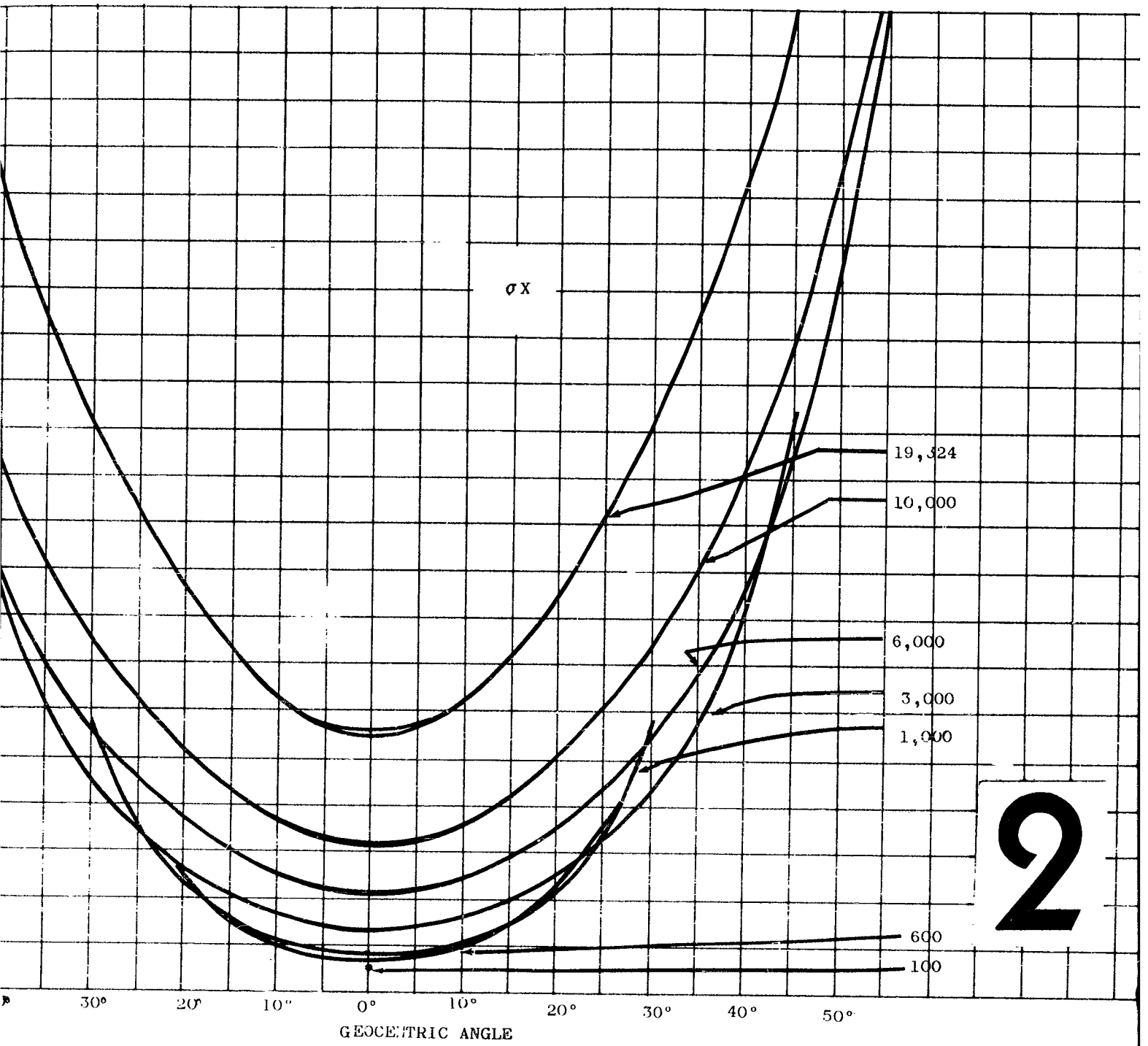

Figure 25. Standard Deviation in X Coordinate of S
Geocentric Orbit Angle

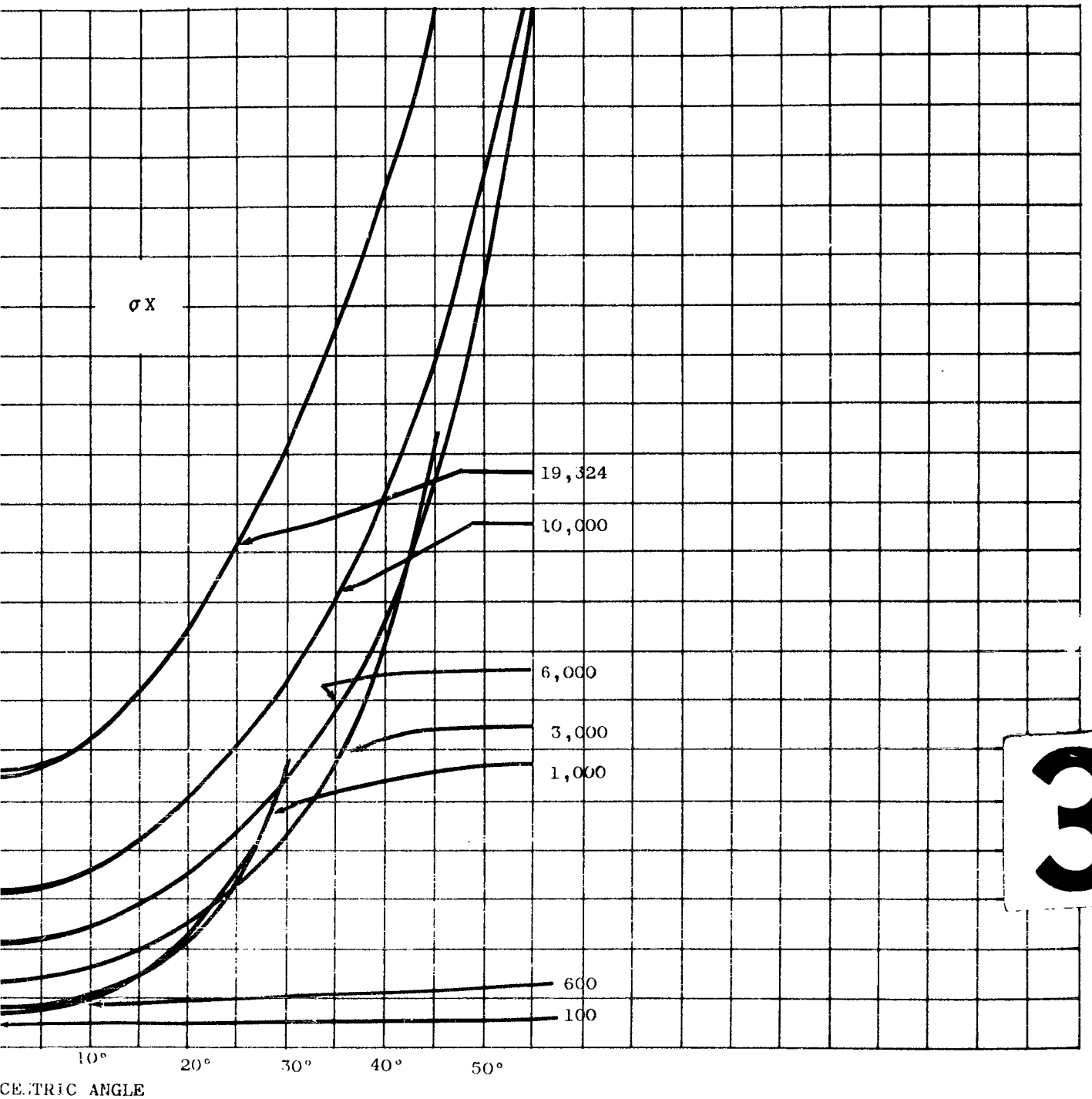

Figure 25. Standard Deviation in X Coordinate of Satellite Position vs. Geocentric Orbit Angle

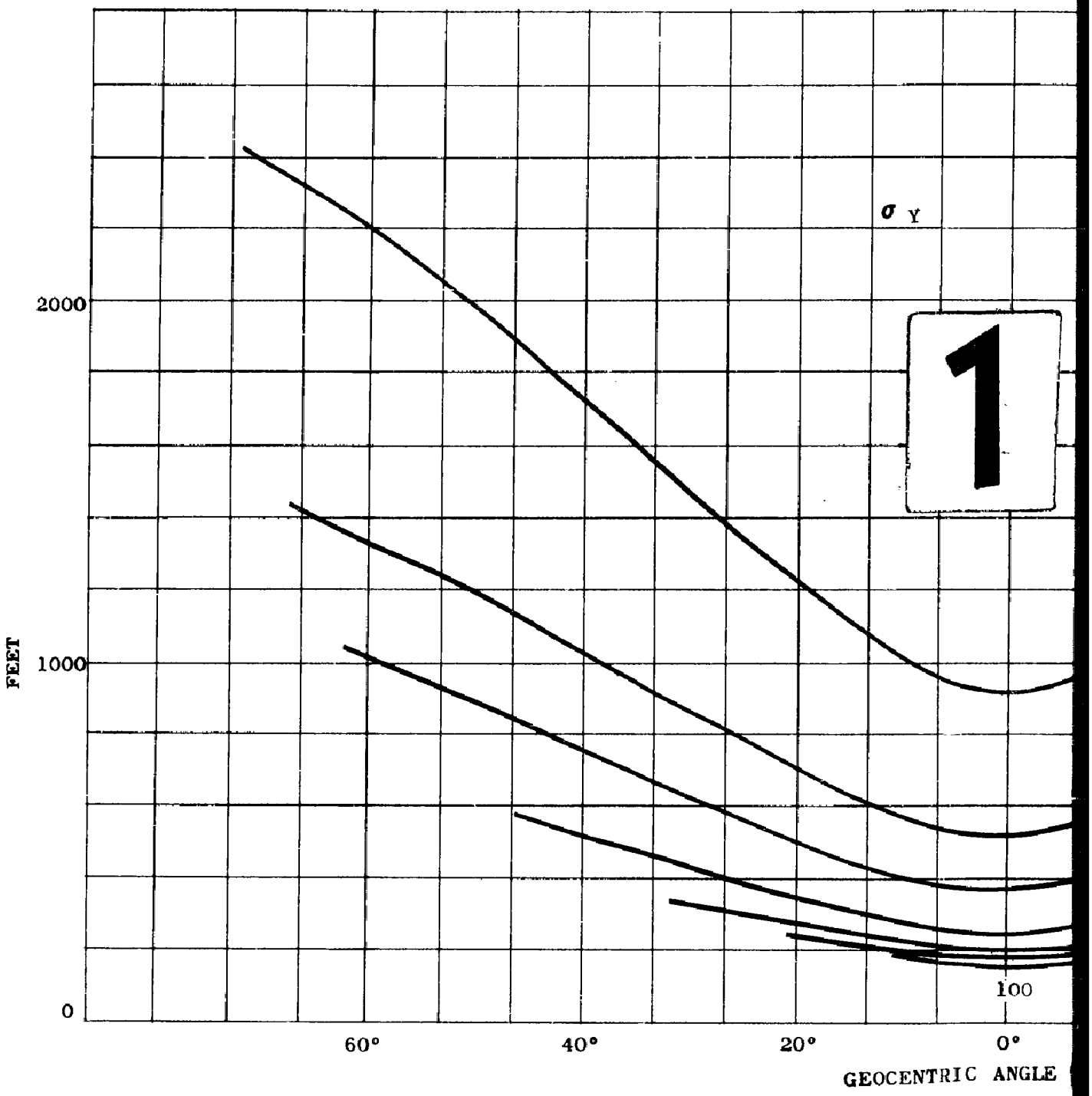
σ_Y
2000
1000
0
FEET
1
100
60°
40°
20°
0°
GEOCENTRIC ANGLE

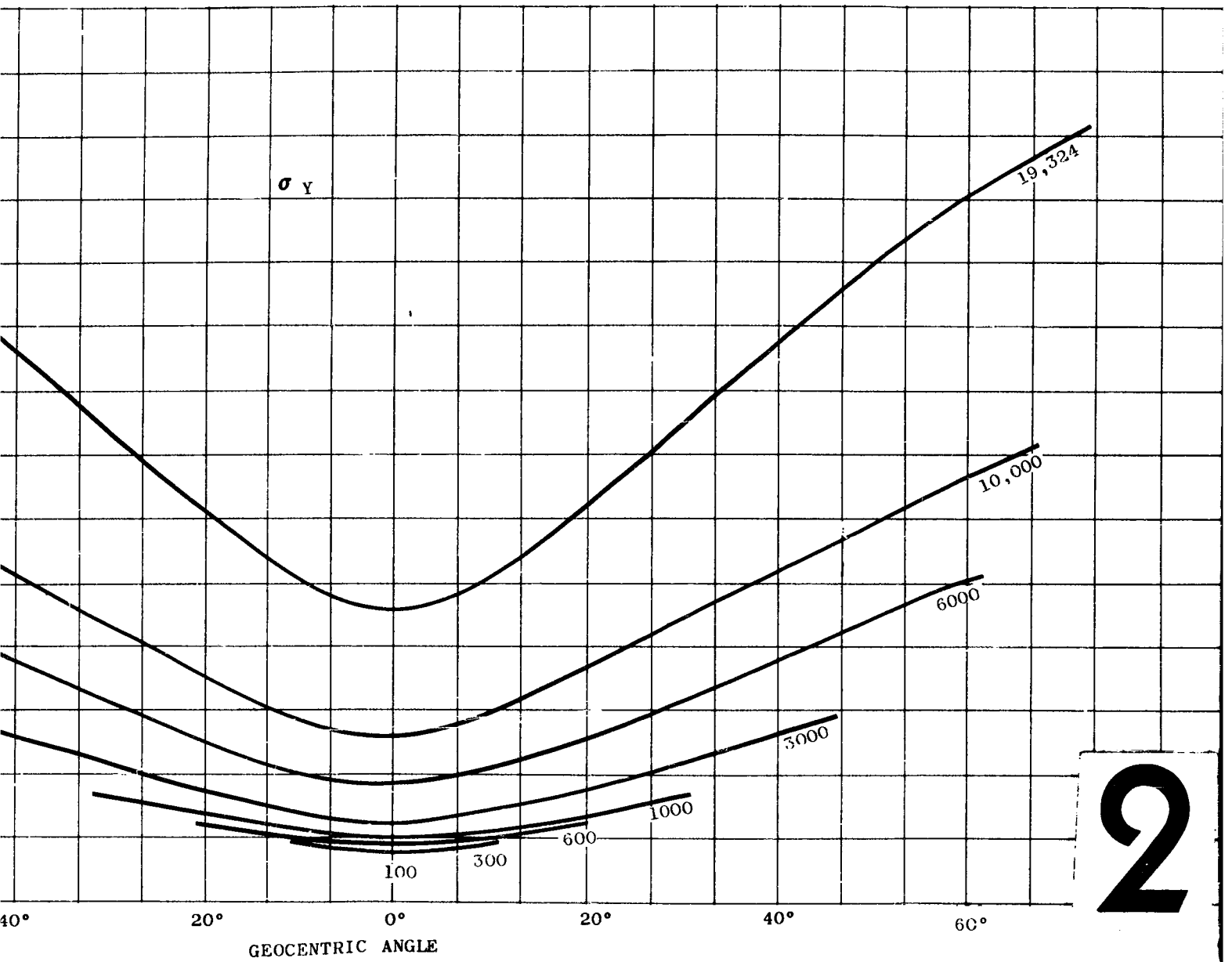

Figure 26. Standard Deviation in Y Coordinate of Satellite Positio
Geocentric Orbit Angle

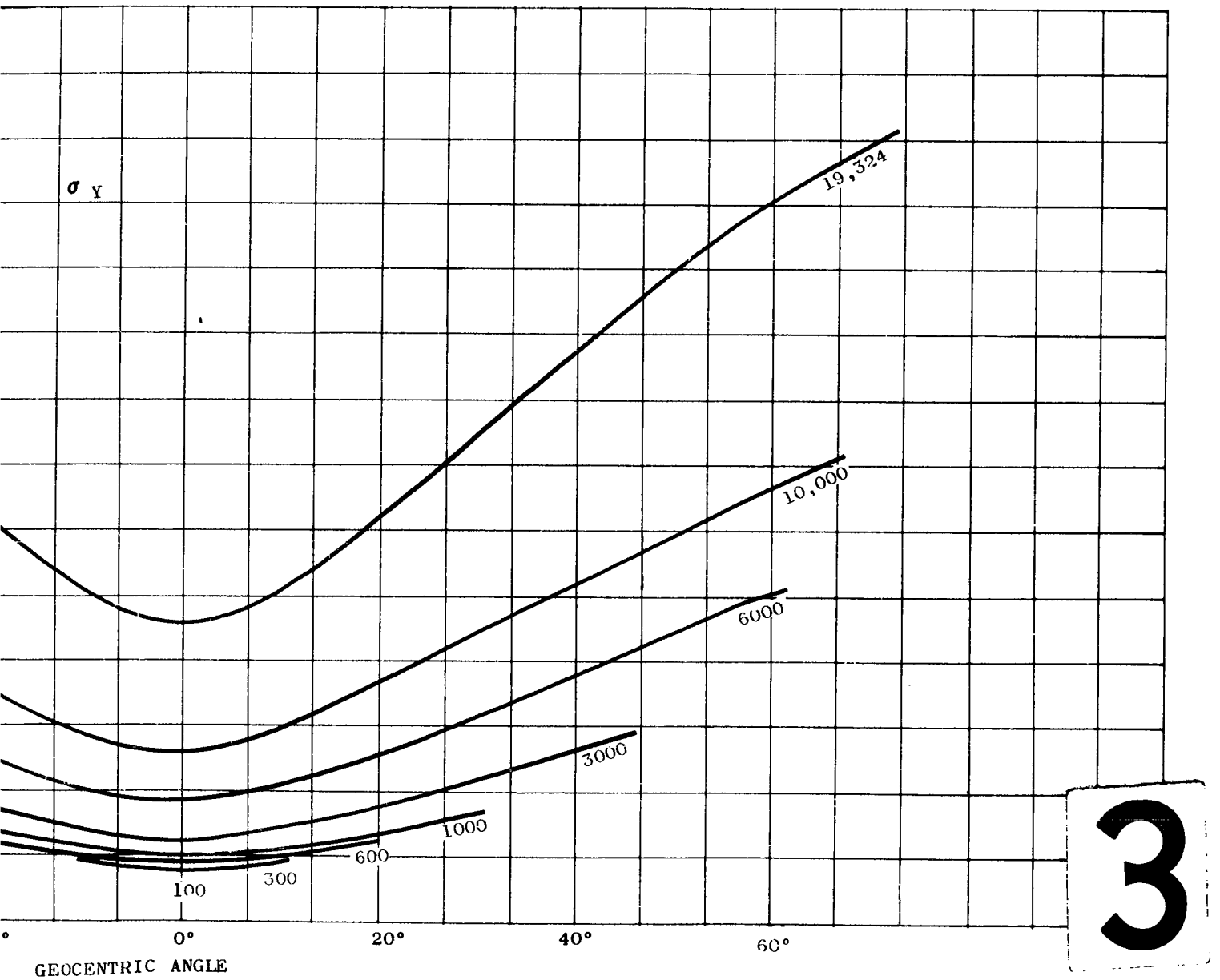

Figure 26. Standard Deviation in Y Coordinate of Satellite Position vs. Geocentric Orbit Angle

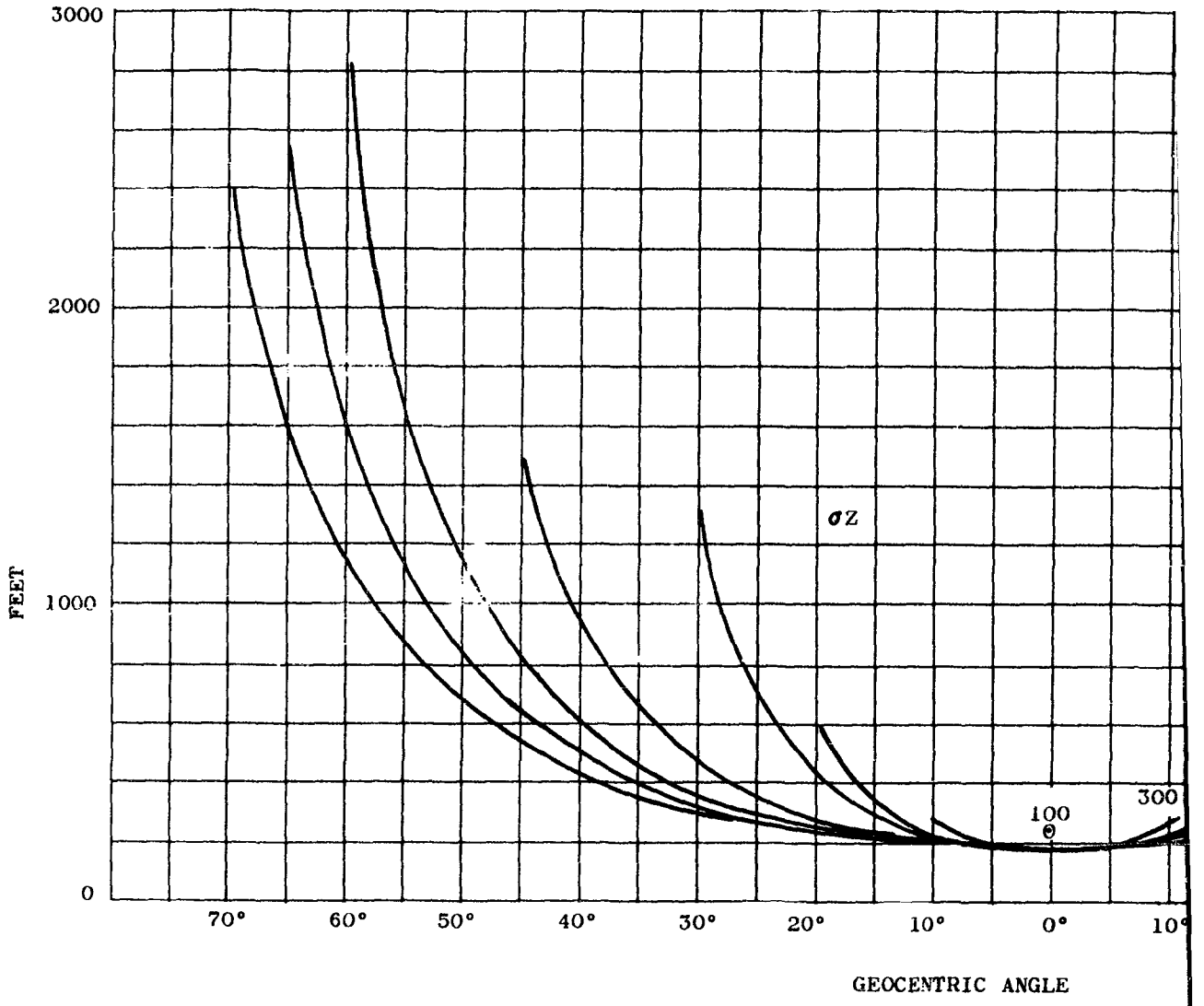
3000
2000
1000
0
FEET
σz
100
300
70°
60°
50°
40°
30°
20°
10°
0°
10°
GEOCENTRIC ANGLE

Figure 1

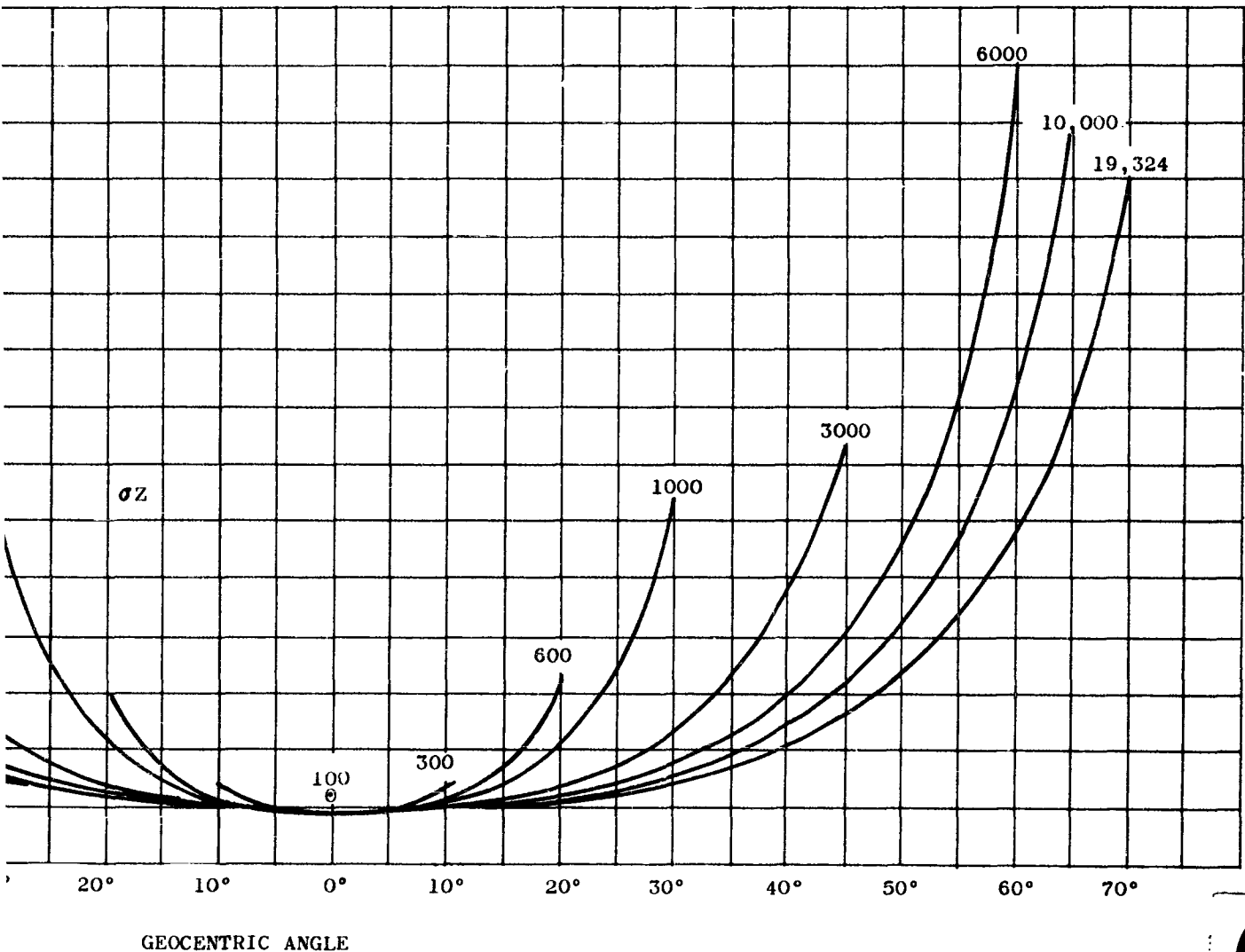

Figure 27. Standard Deviation in Z Coordinate of Satellite Position vs. Geocentric Orbit Angle

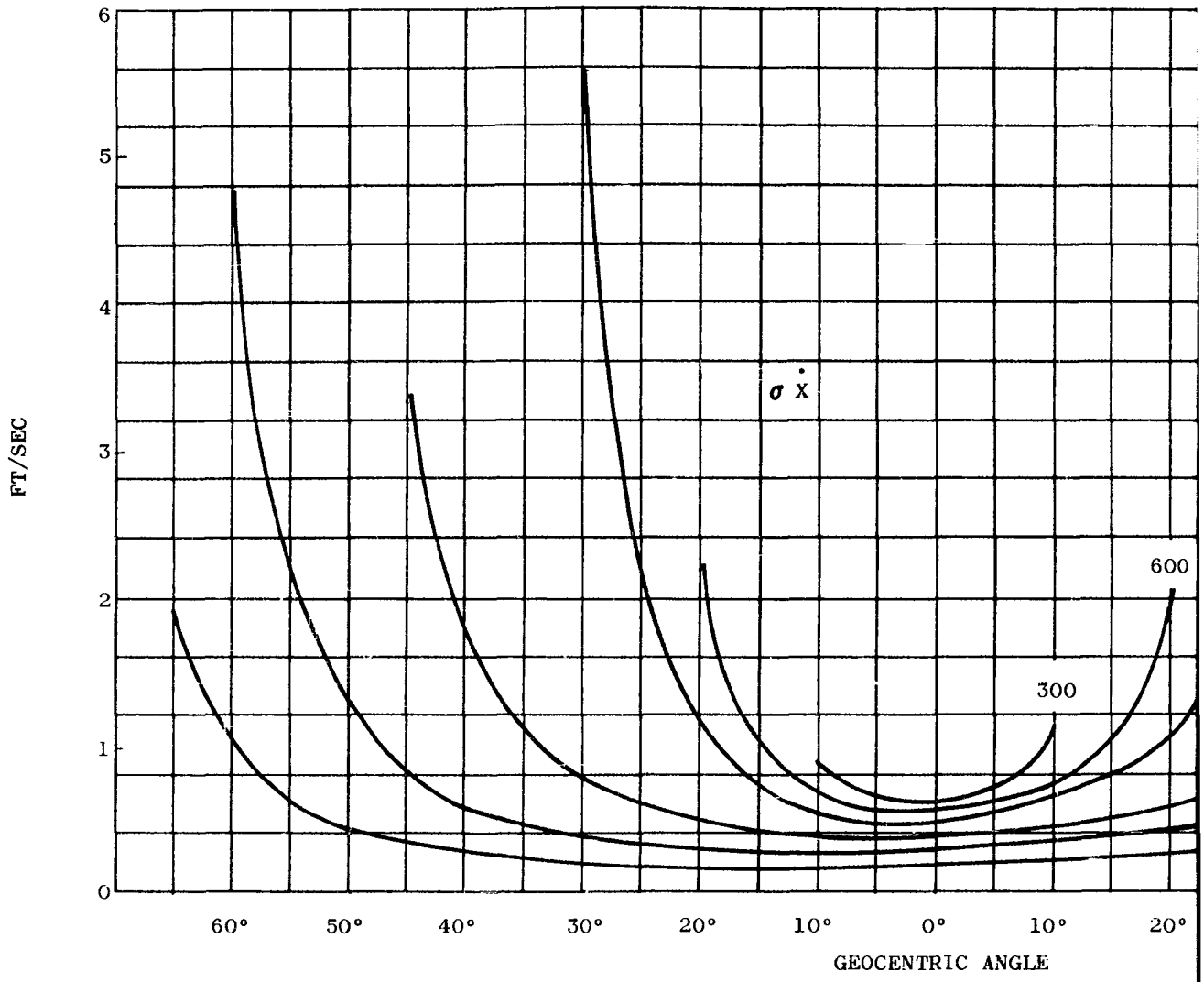

Figure 28. Standard Deviatio
Geoc

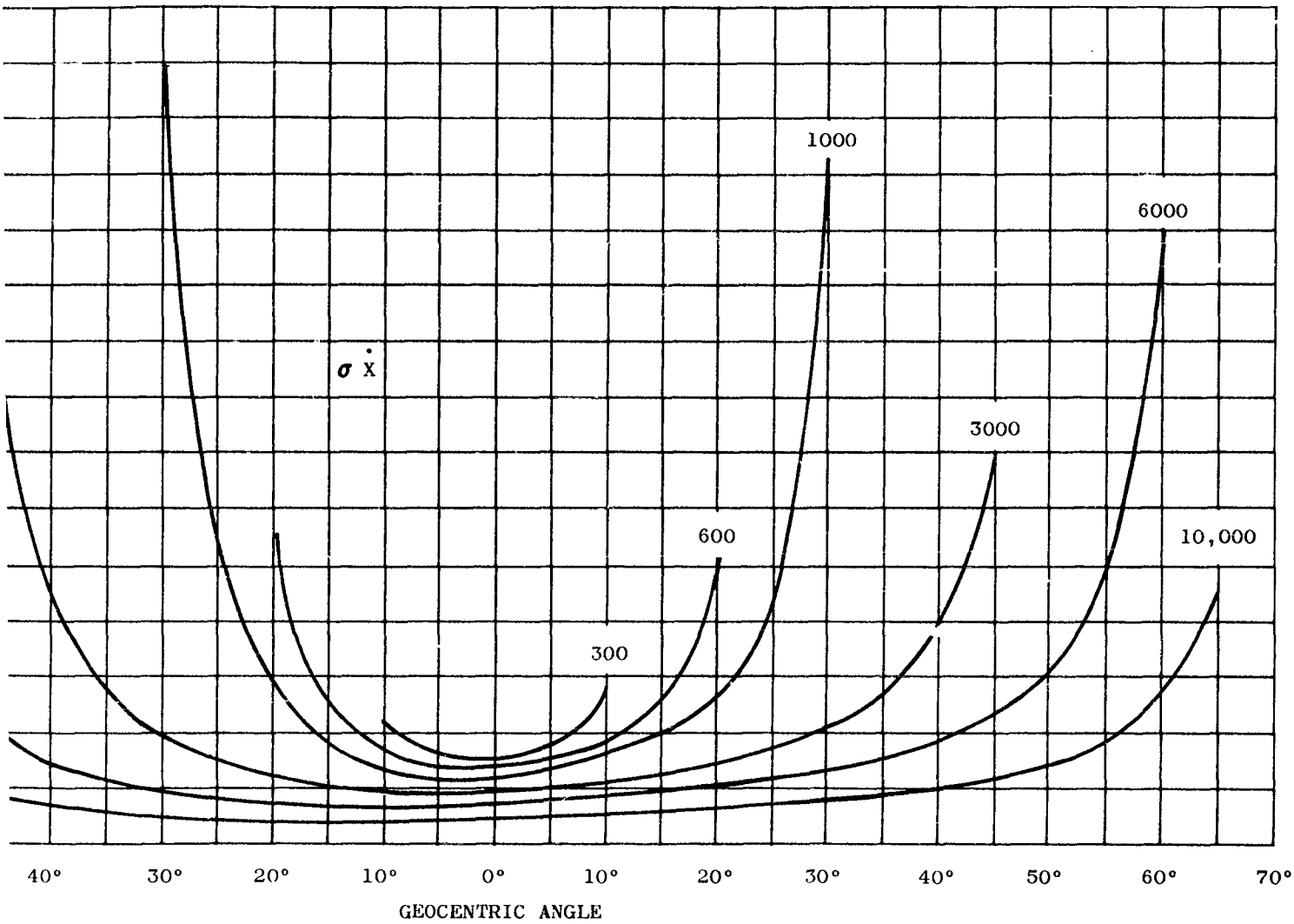

2

Figure 28. Standard Deviation in $\dot{X}$ Component of Satellite Velocity vs. Geocentric Orbit Angle

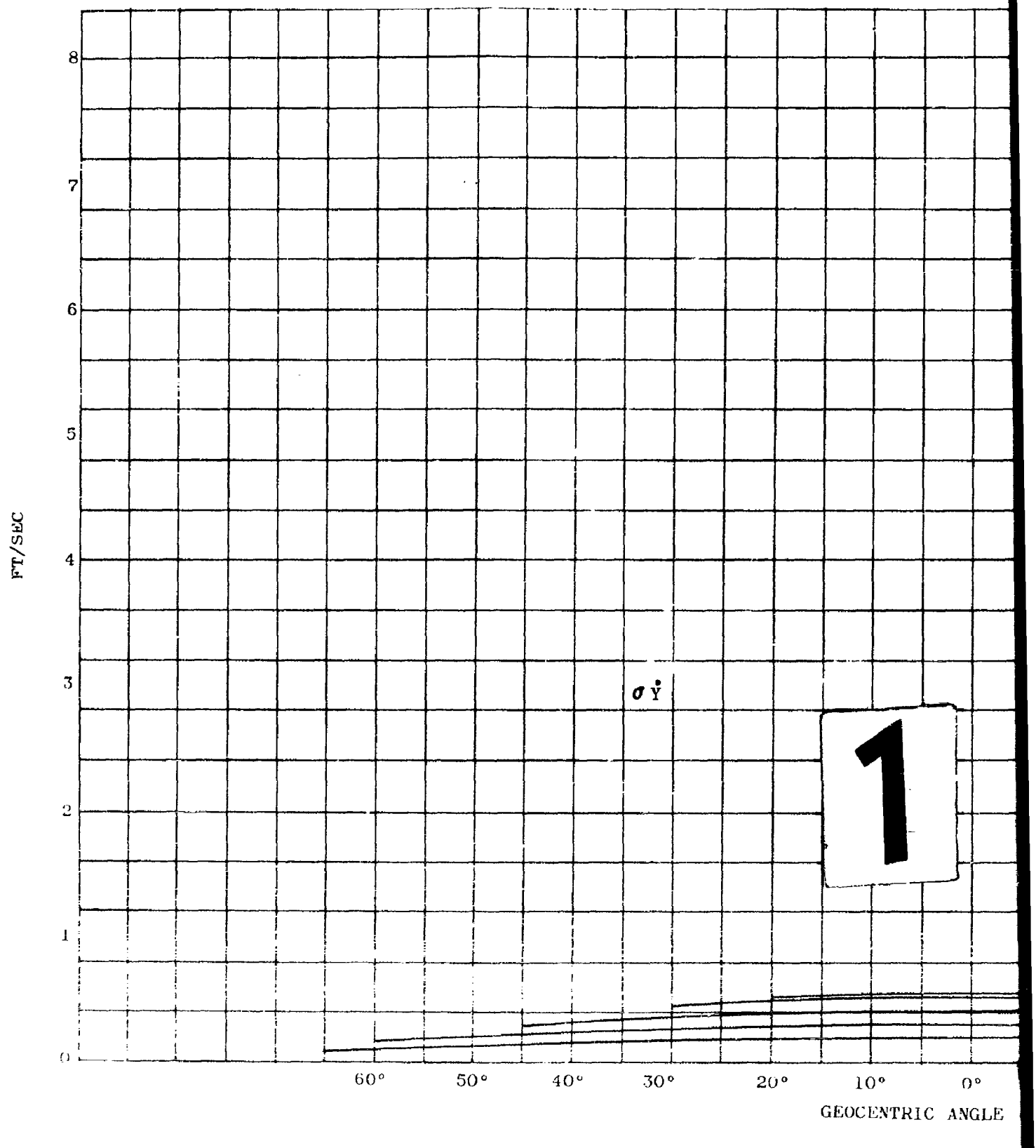
FT/SEC
8
7
6
5
4
3
2
1
0
$\sigma_{\dot{Y}}$
1
60°
50°
40°
30°
20°
10°
0°
GEOCENTRIC ANGLE

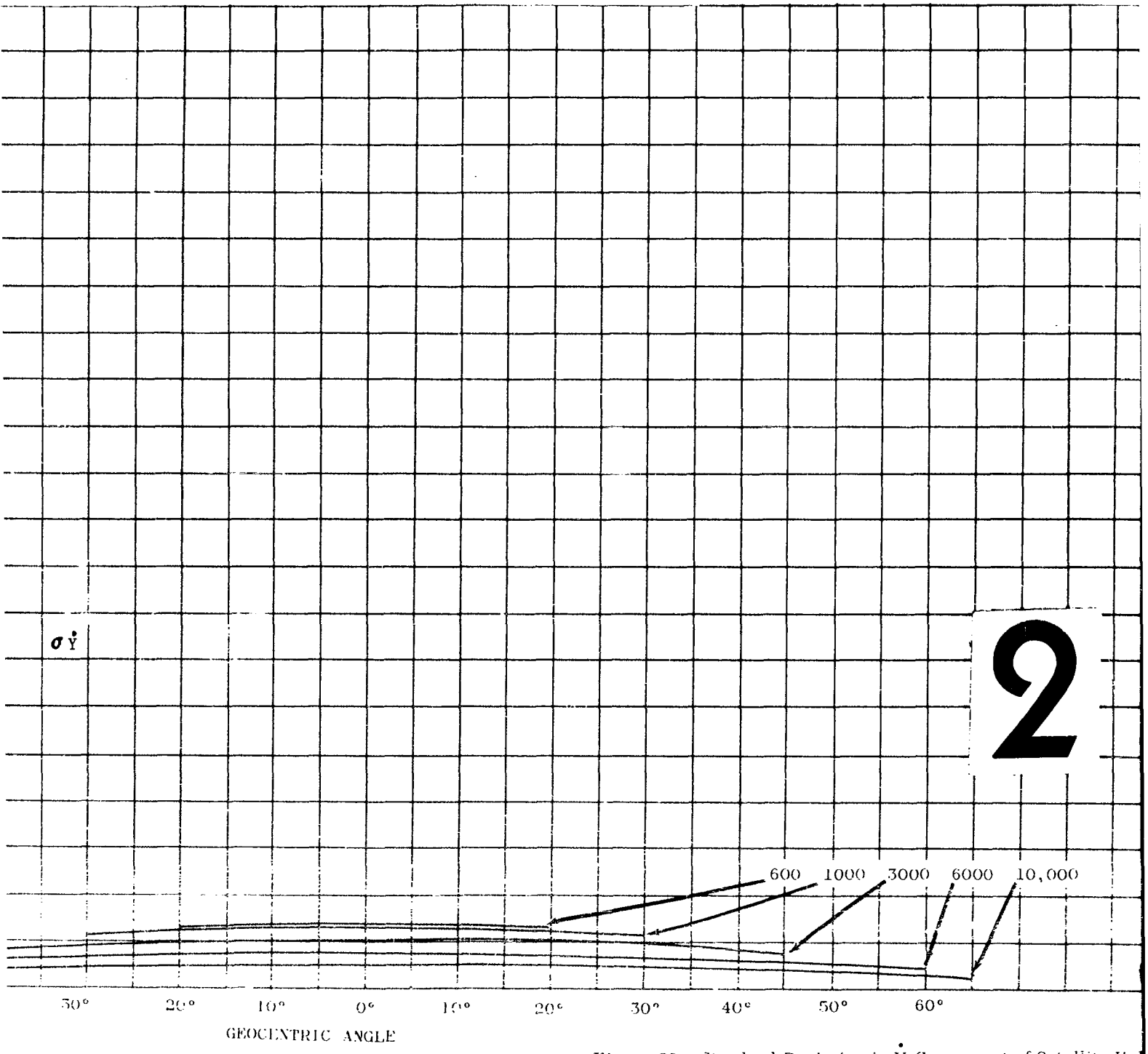

Figure 29. Standard Deviation in $\dot{Y}$ Component of Satellite Vel
Geocentric Orbit Angle

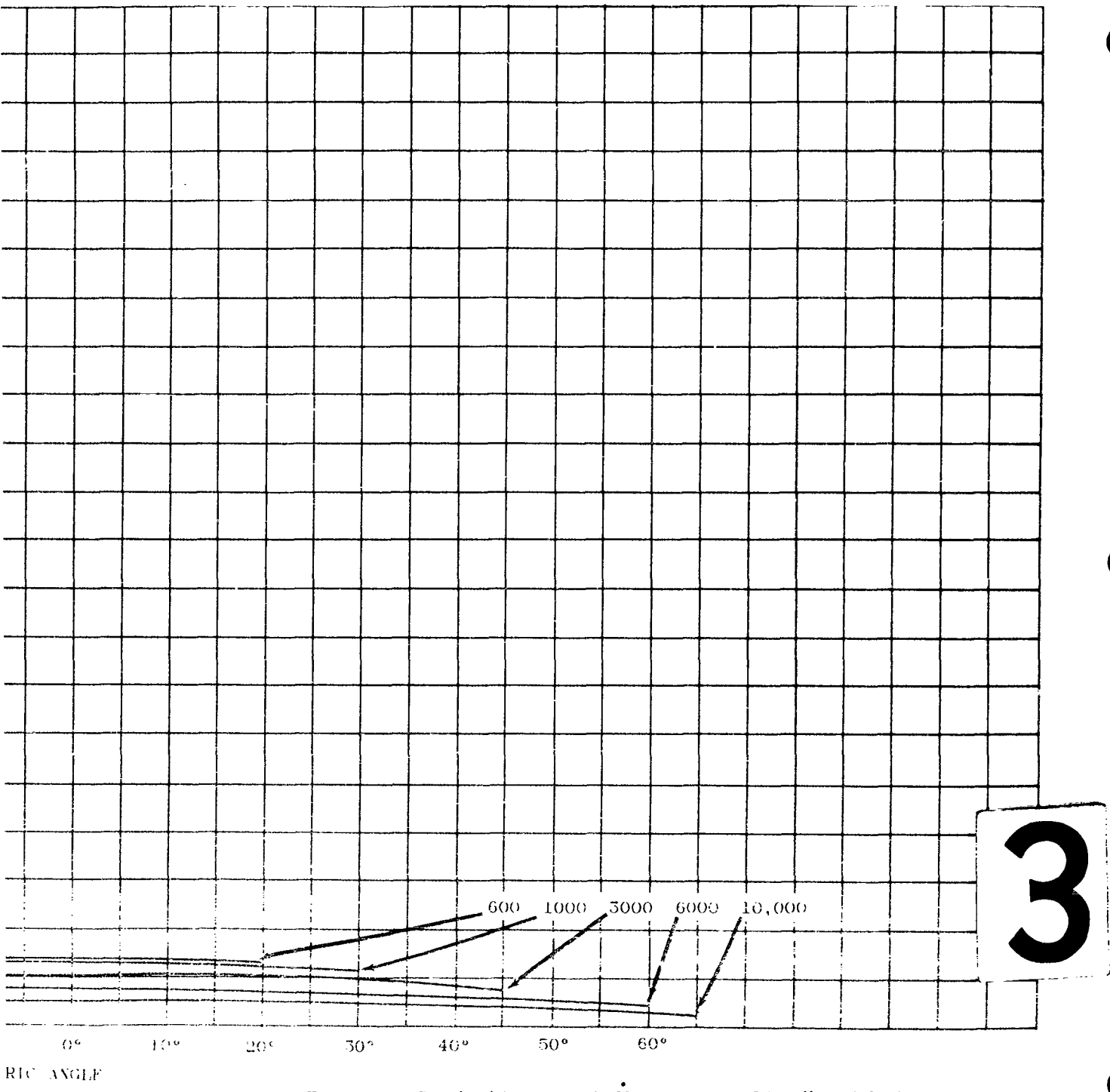

Figure 29. Standard Deviation in $\dot{Y}$ Component of Satellite Velocity vs. Geocentric Orbit Angle

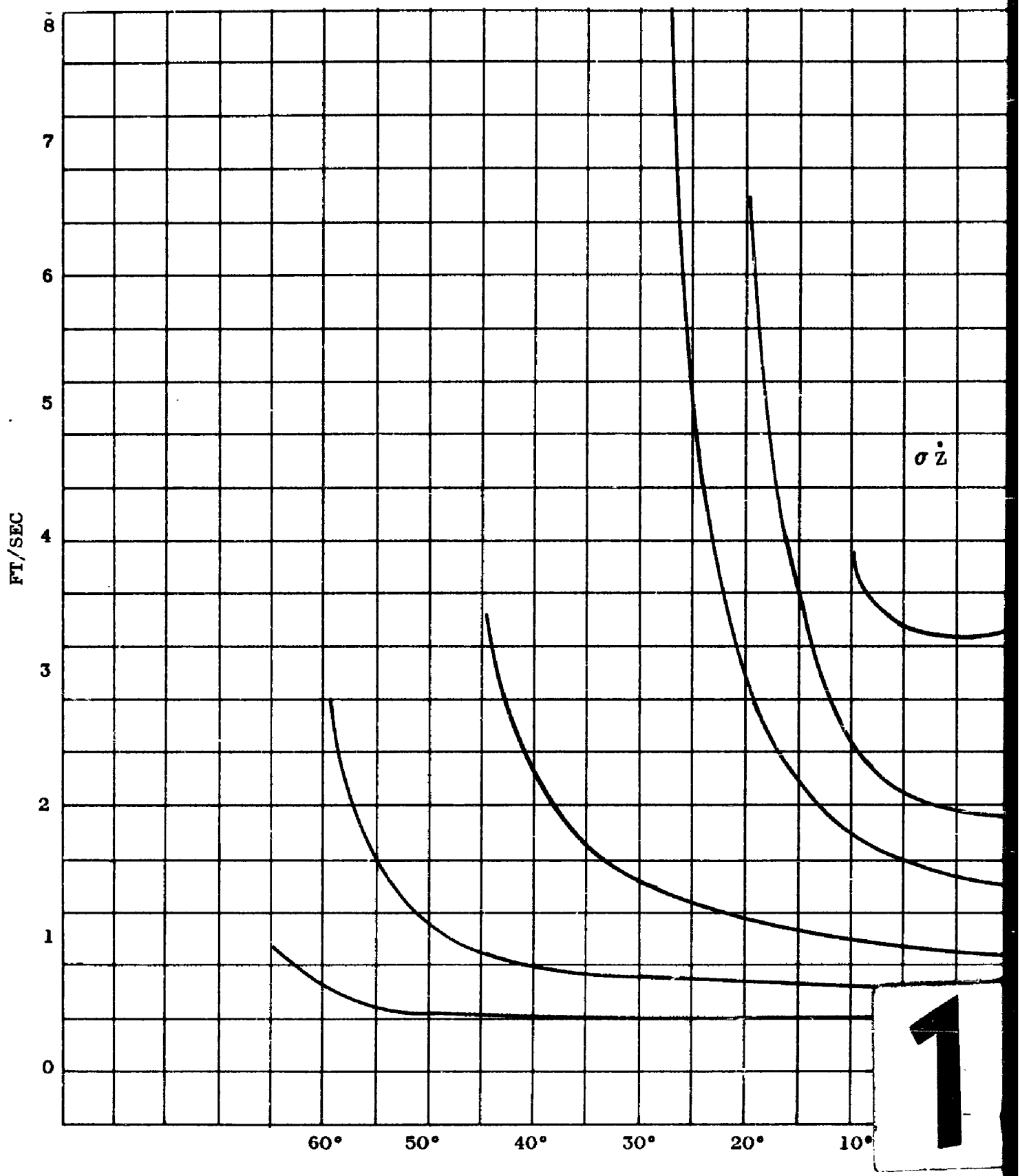
FT/SEC
8
7
6
5
4
3
2
1
0
60°
50°
40°
30°
20°
10°
$\sigma \dot{z}$
1

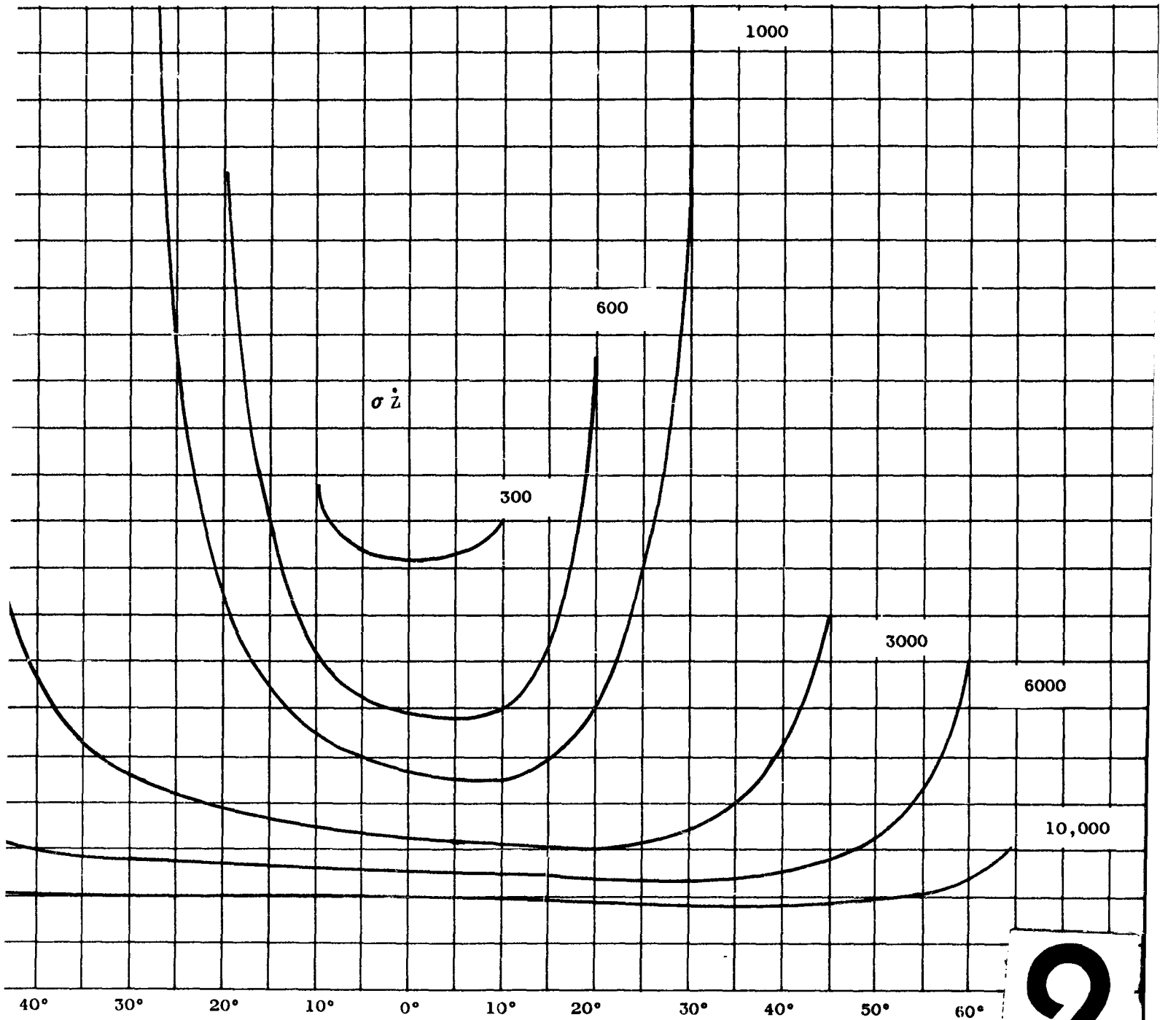

Figure 30. Standard Deviation in Z
Geocentric

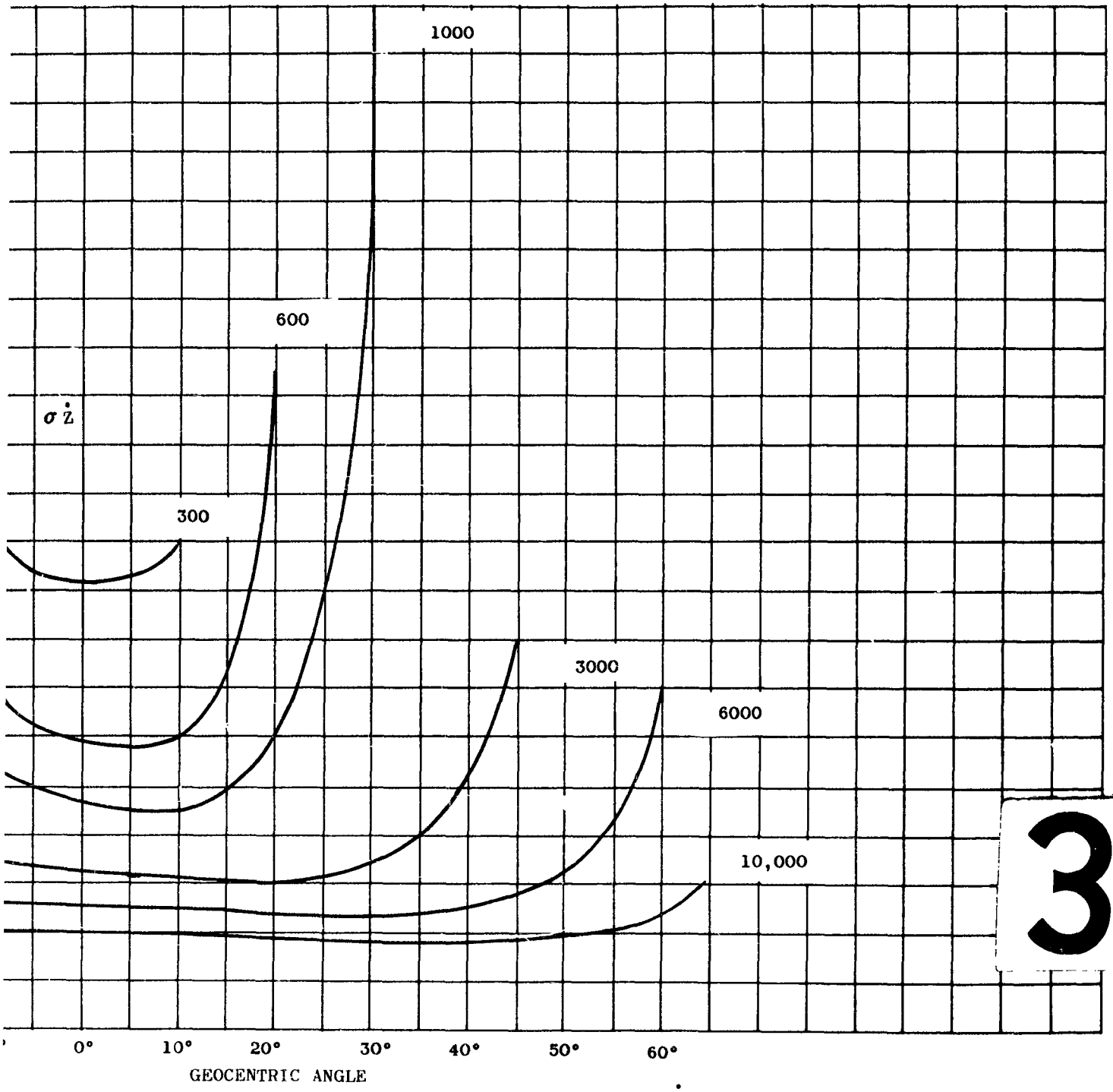

Figure 30. Standard Deviation in $\dot{Z}$ Component of Satellite Velocity vs. Geocentric Orbit Angle

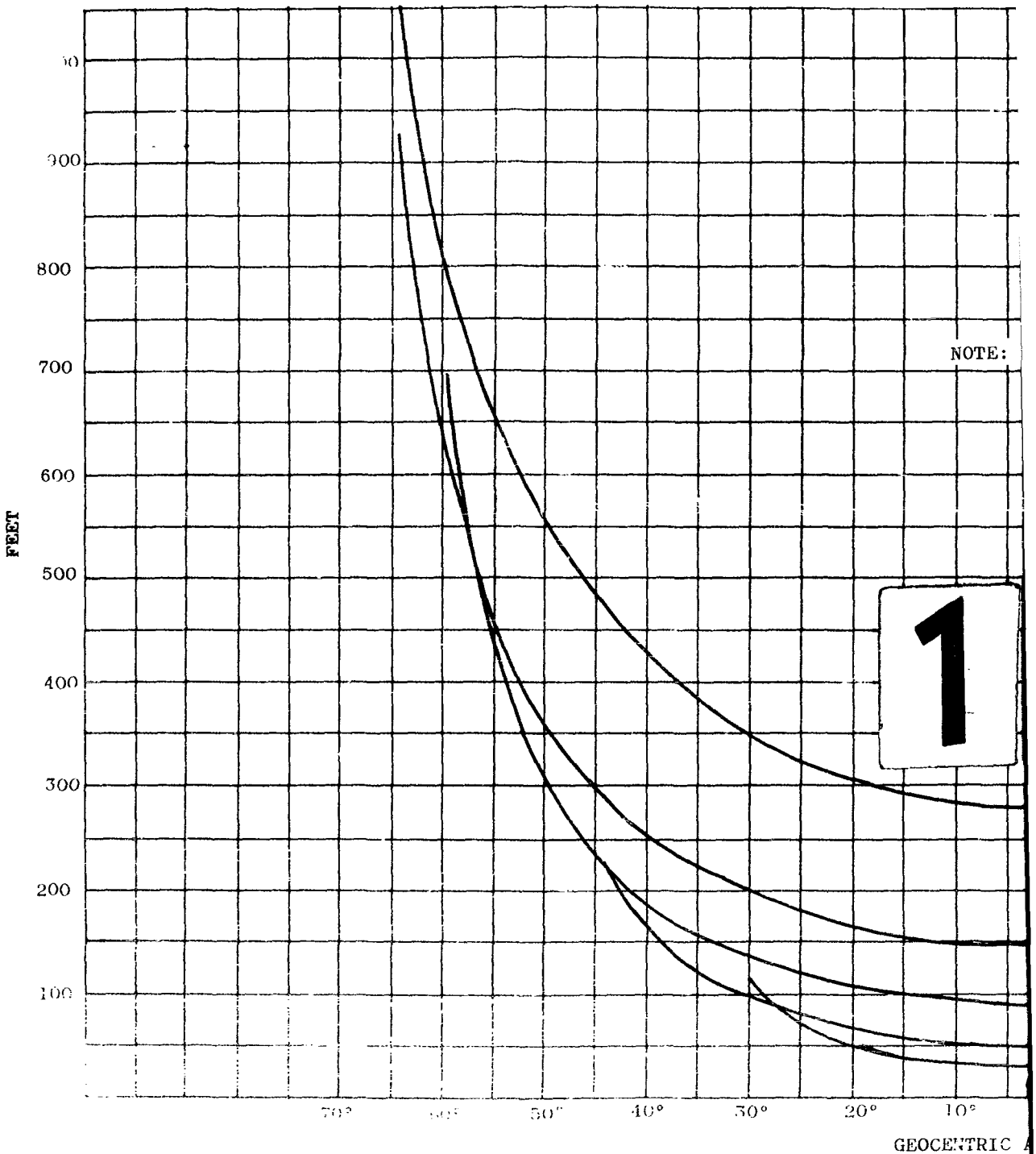
900
800
700
600
500
400
300
200
100
FEET
70°
50°
40°
30°
20°
10°
GEOCENTRIC
NOTE:
1

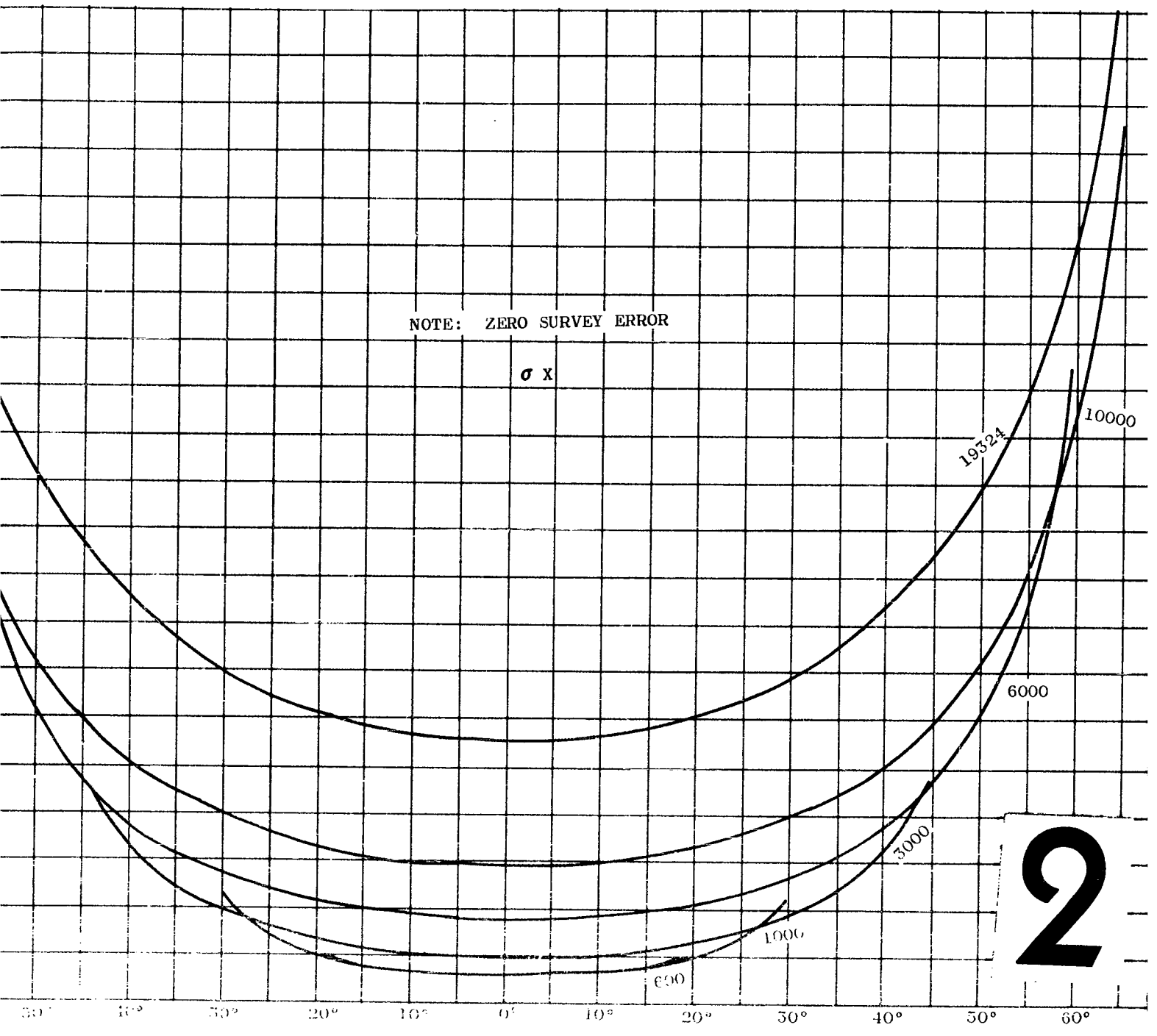

Figure 31. Standard Deviation in X Coordinate of Sa
Geocentric Orbit Angle (Zero Survey

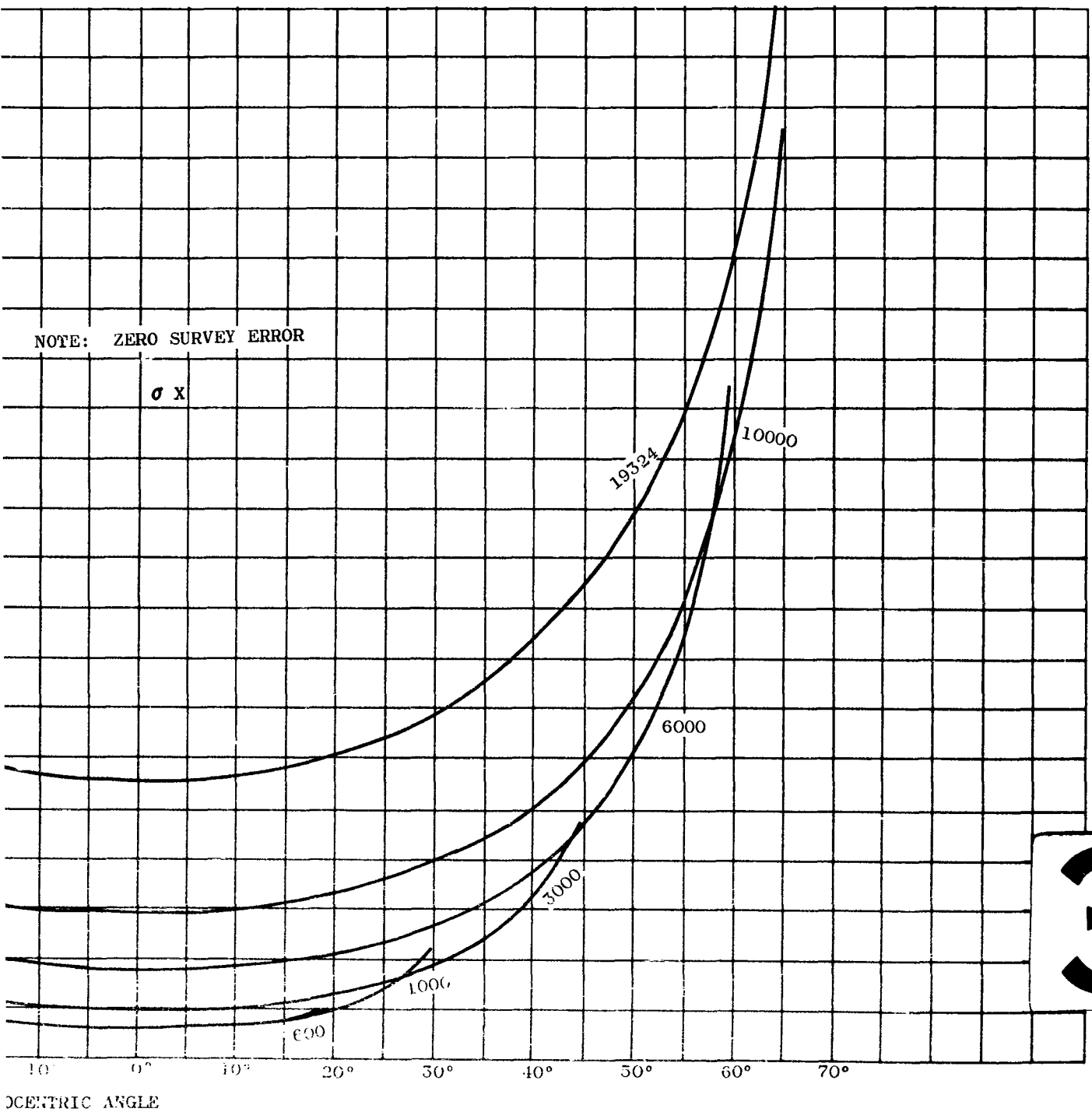

Figure 31. Standard Deviation in X Coordinate of Satellite Position vs. Geocentric Orbit Angle (Zero Survey Error)

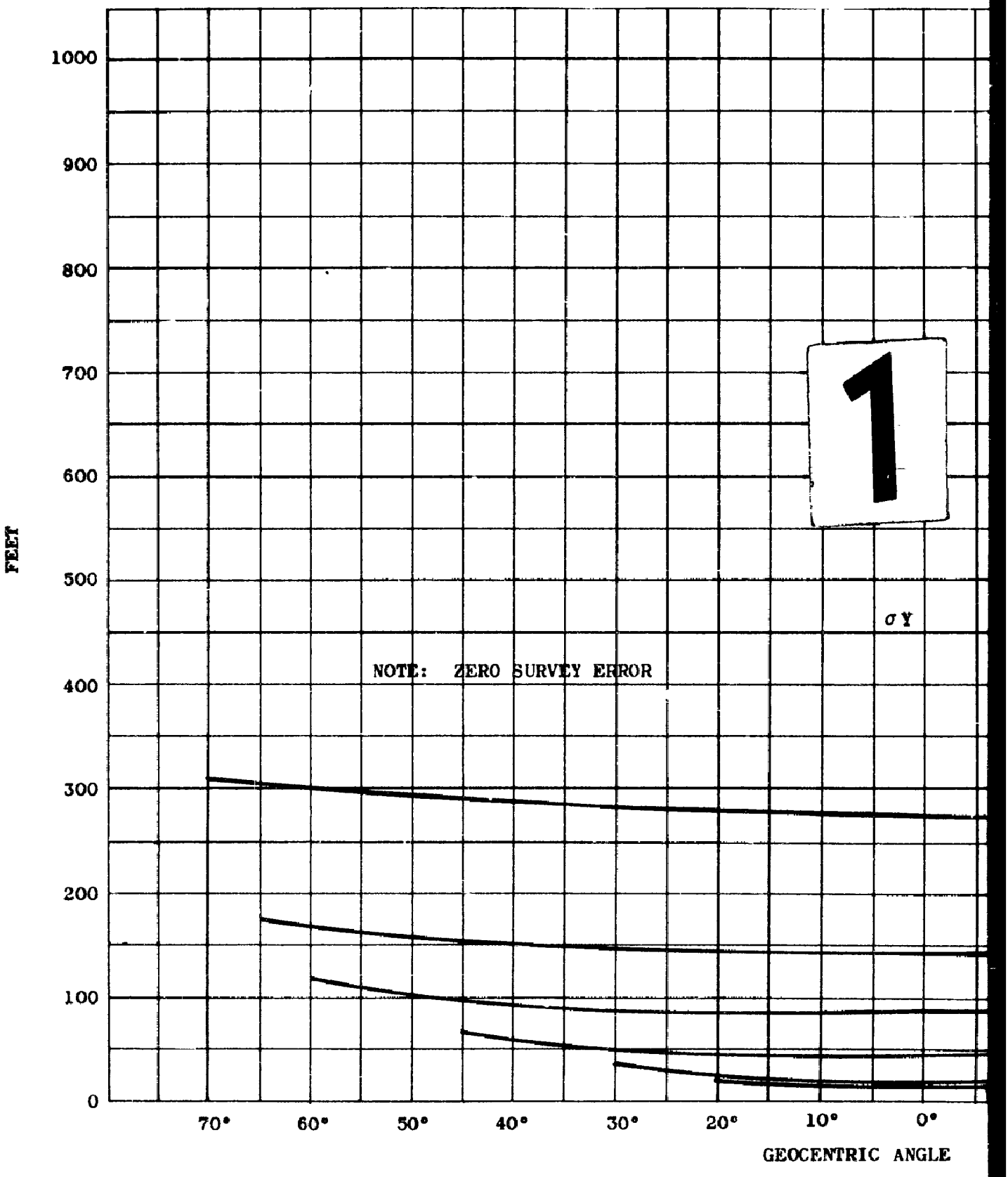
1000
900
800
700
600
500
400
300
200
100
0
FEET
1
σ Y
NOTE: ZERO SURVEY ERROR
70°
60°
50°
40°
30°
20°
10°
0°
GEOCENTRIC ANGLE

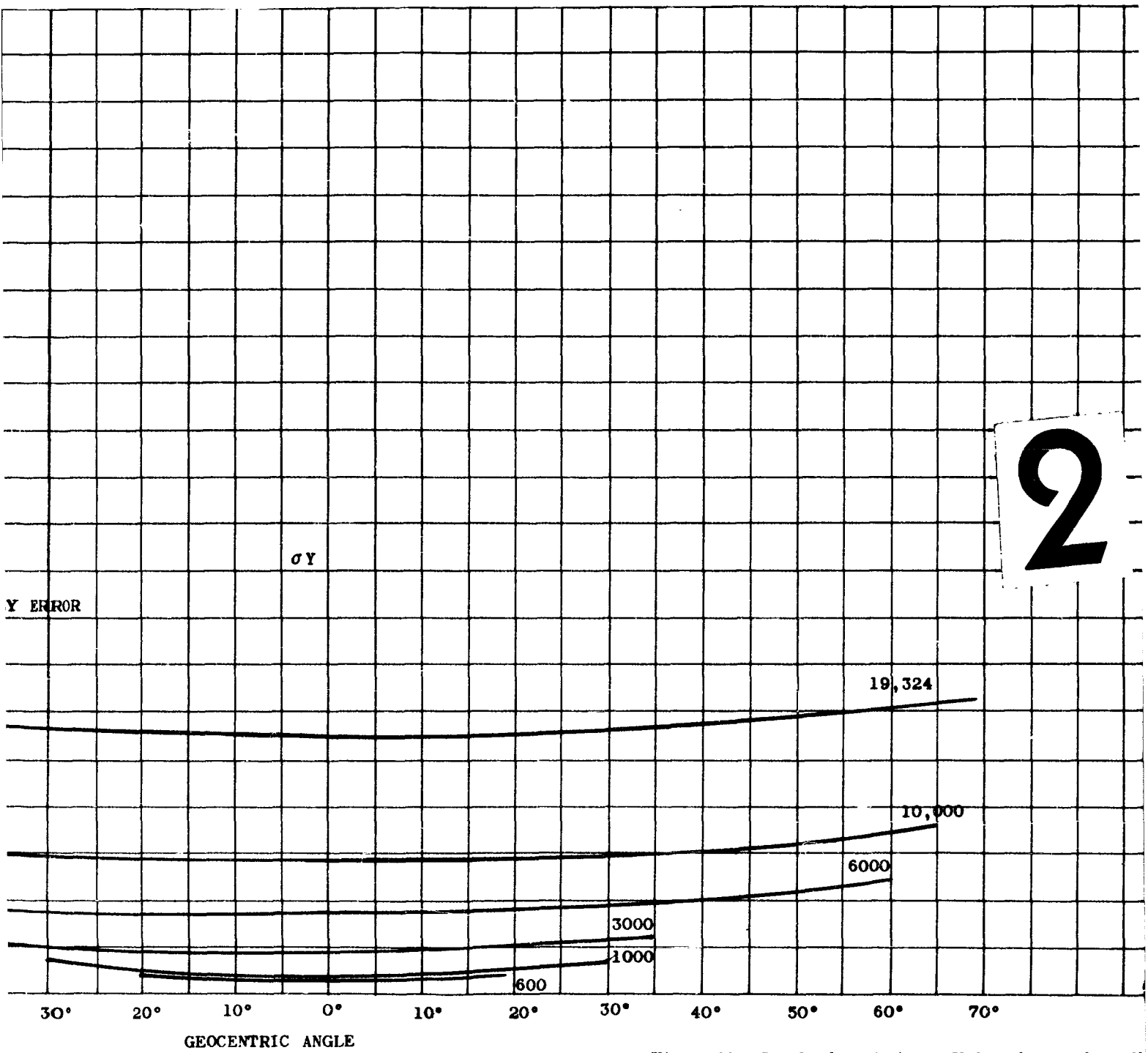

Figure 32. Standard Deviation in Y Coordinate of Satell
Geocentric Orbit Angle (Zero Survey Err

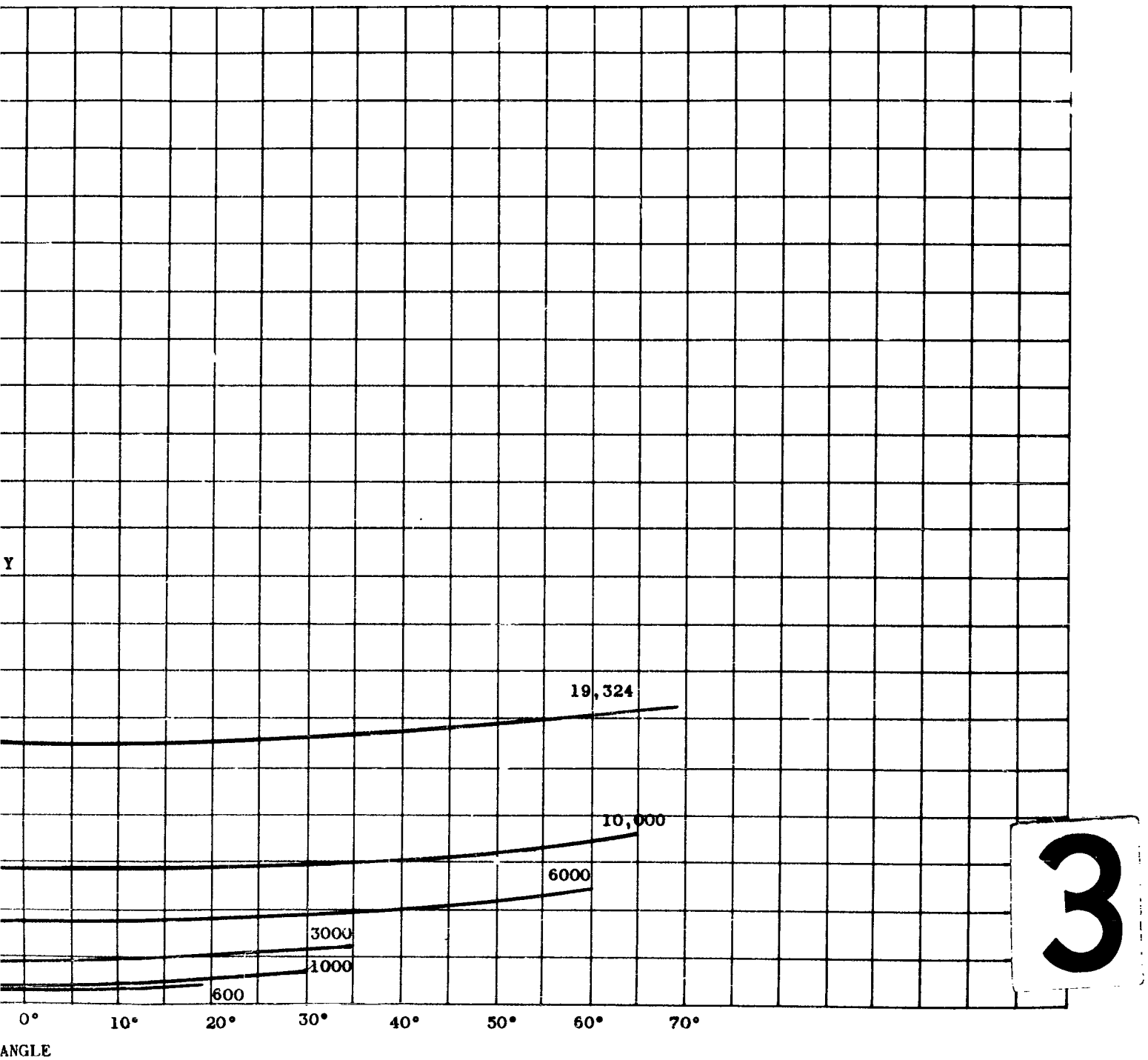

Figure 32. Standard Deviation in Y Coordinate of Satellite Position vs. Geocentric Orbit Angle (Zero Survey Error)

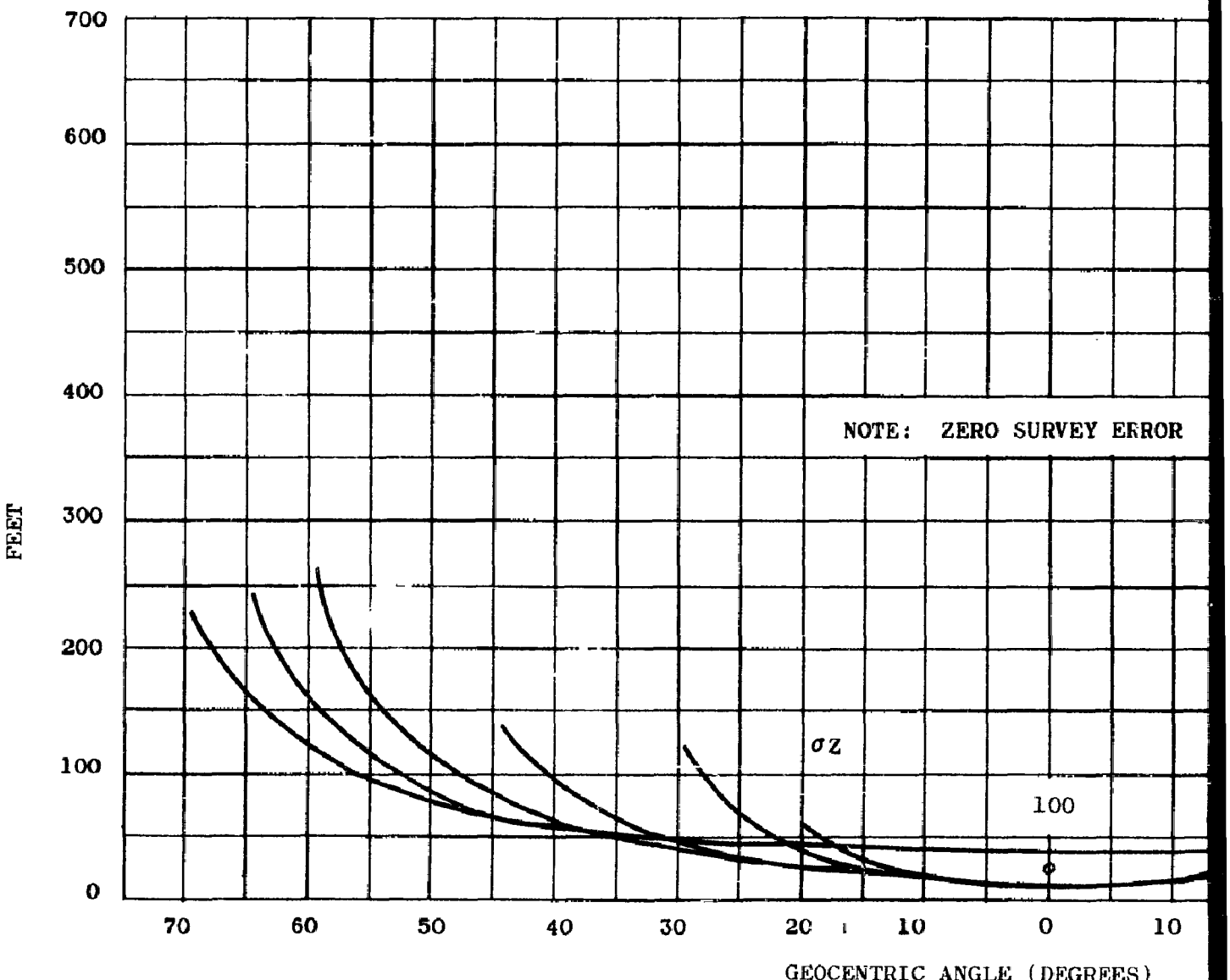

Figure 33. Sta

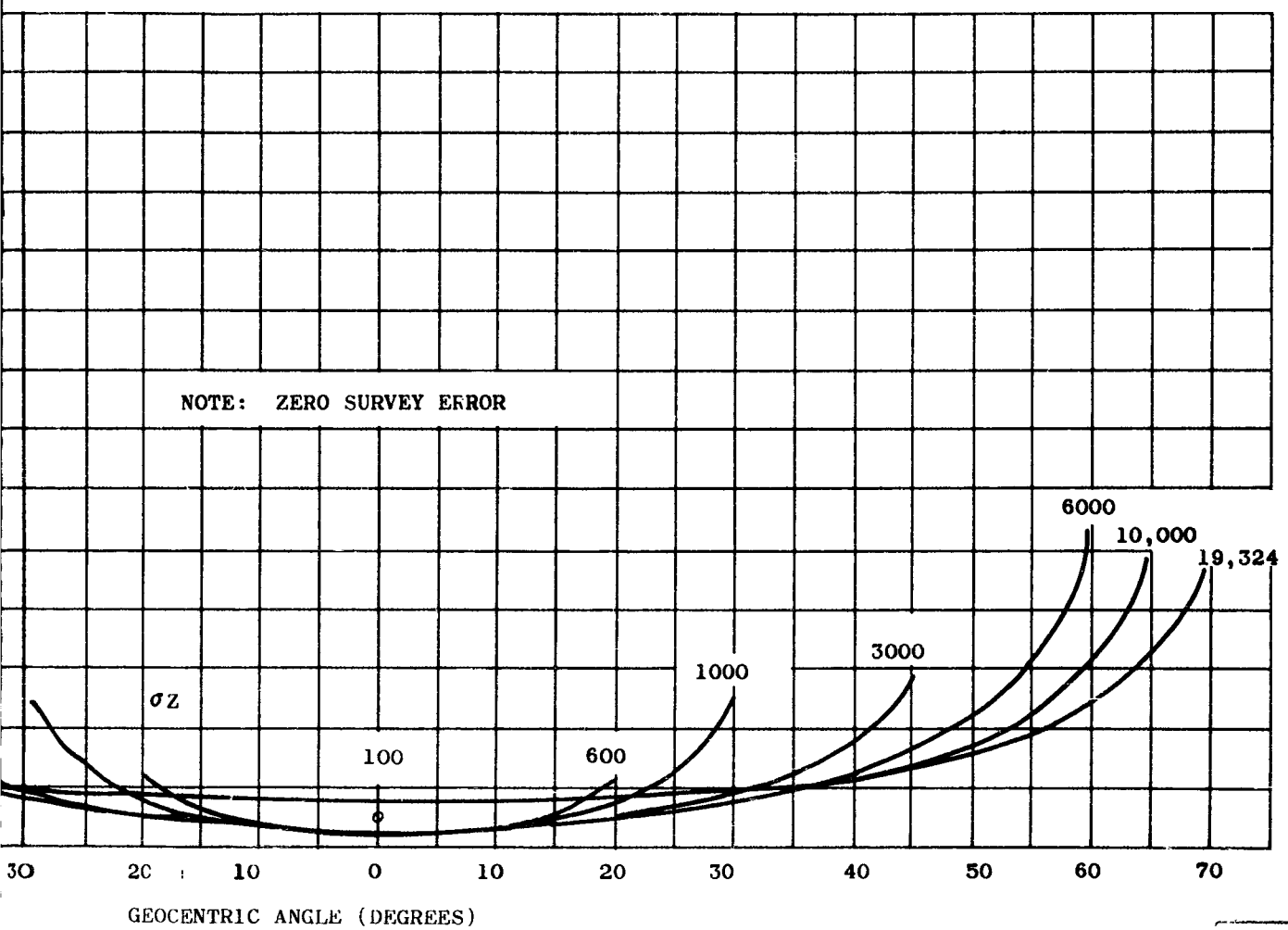

Figure 33. Standard Deviation in Z Coordinate of Satellite Position vs. Geocentric Orbit Angle (Zero Survey Error)

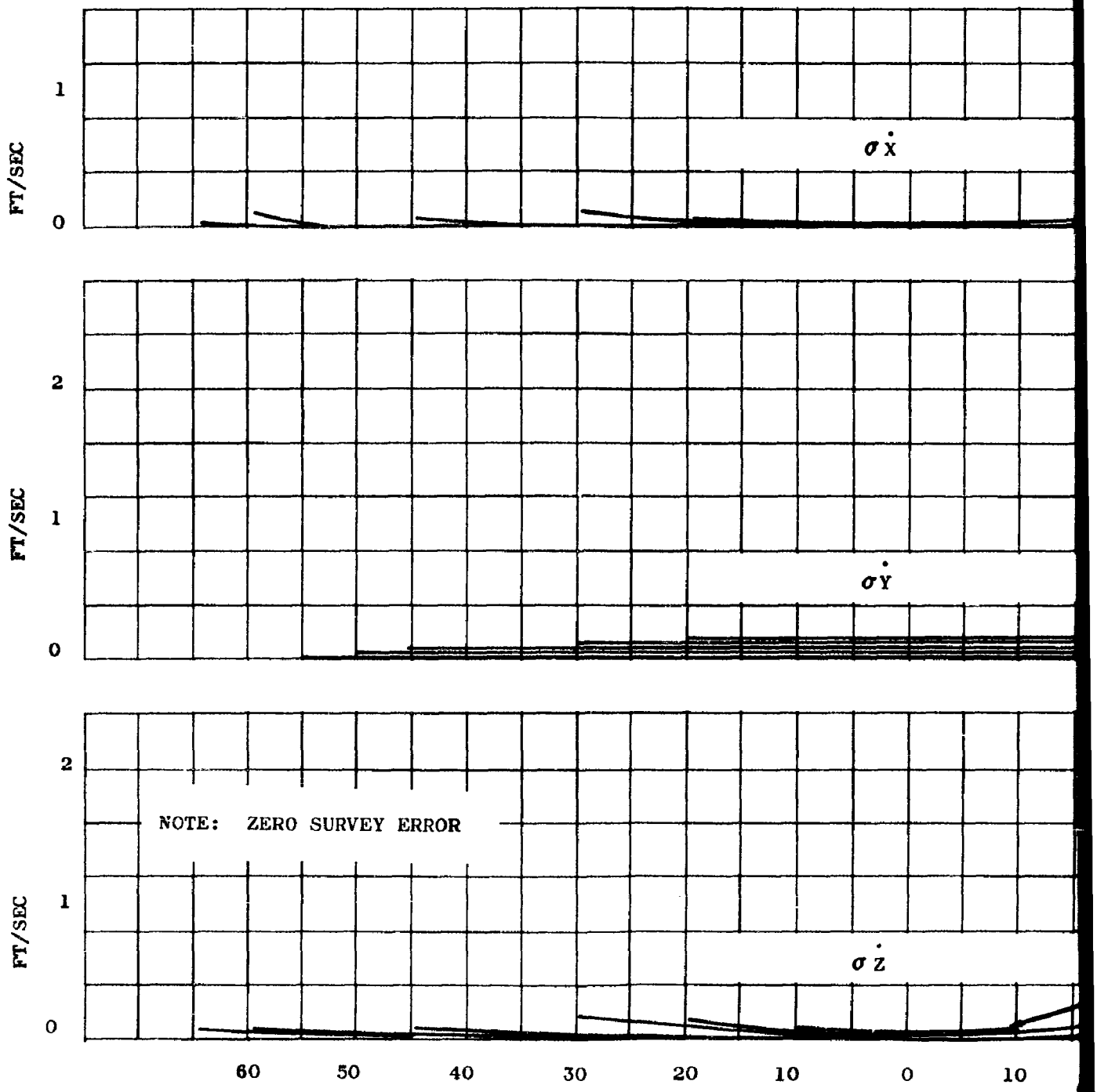

Figure 34. Standard
Ge

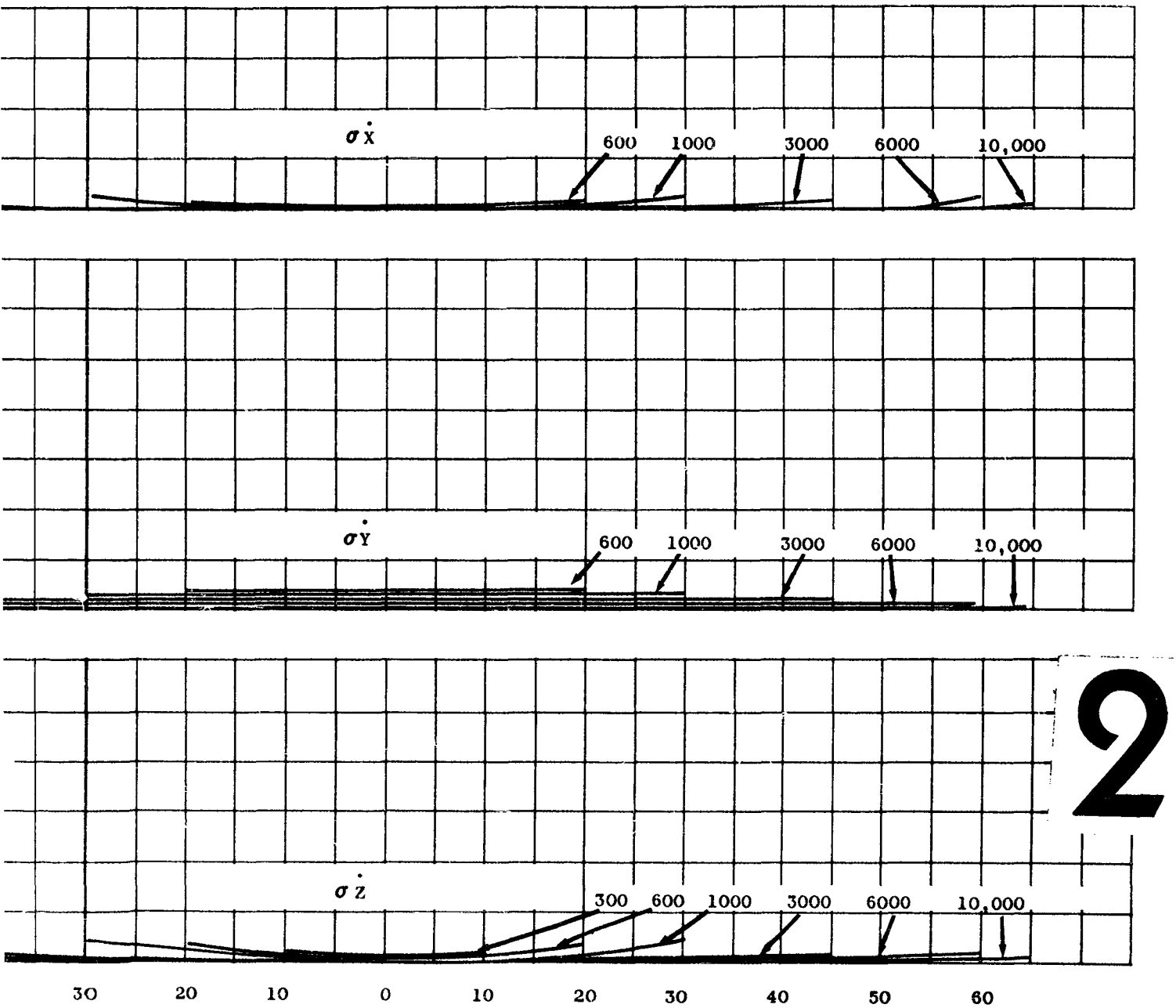

Figure 34. Standard Deviation in $\dot{X}$, $\dot{Y}$, and $\dot{Z}$ Components of Satellite Velocity vs. Geocentric Orbit Angle (Zero Survey Error)

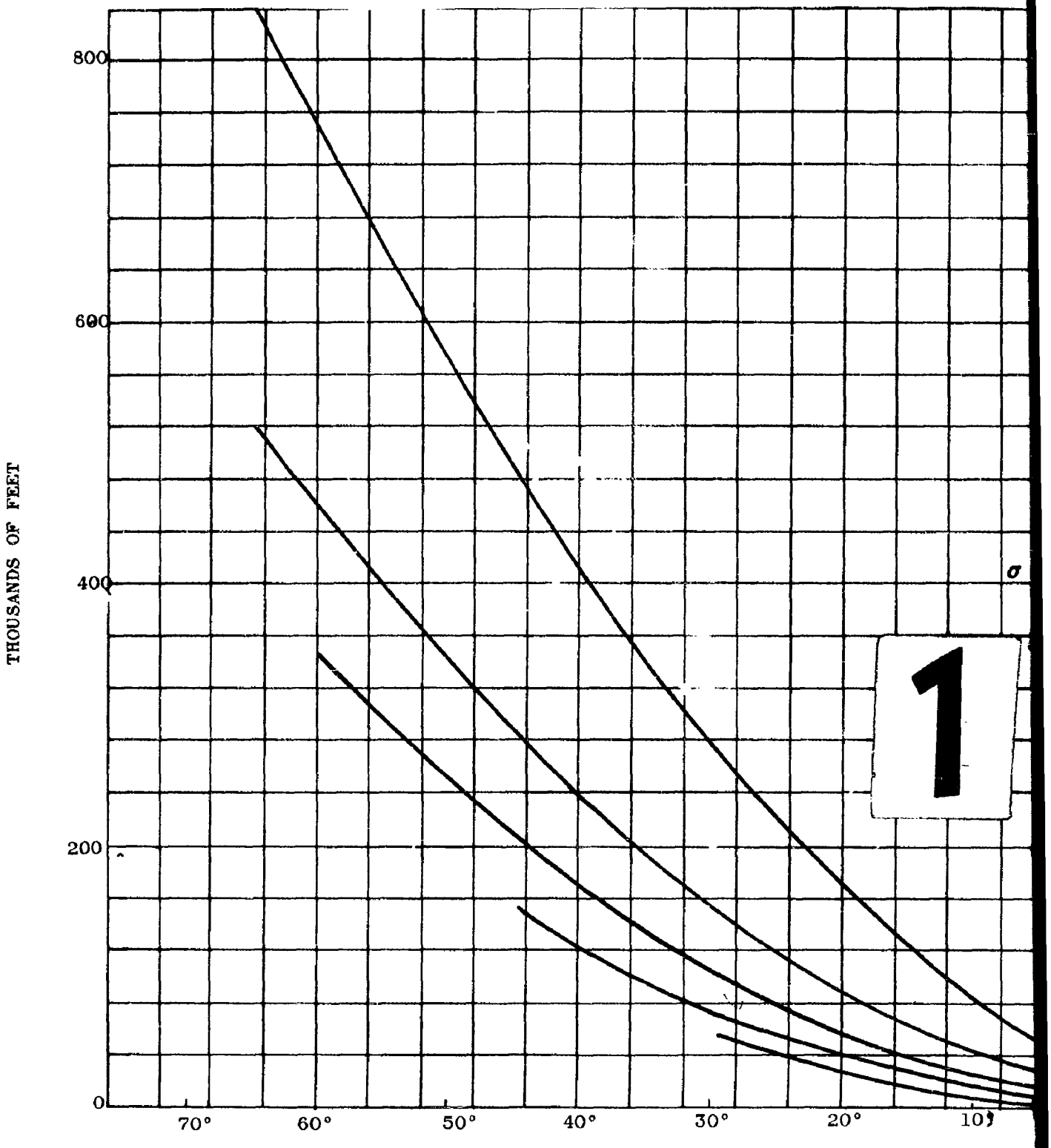
THOUSANDS OF FEET
800
600
400
200
0
70°
60°
50°
40°
30°
20°
σ
1

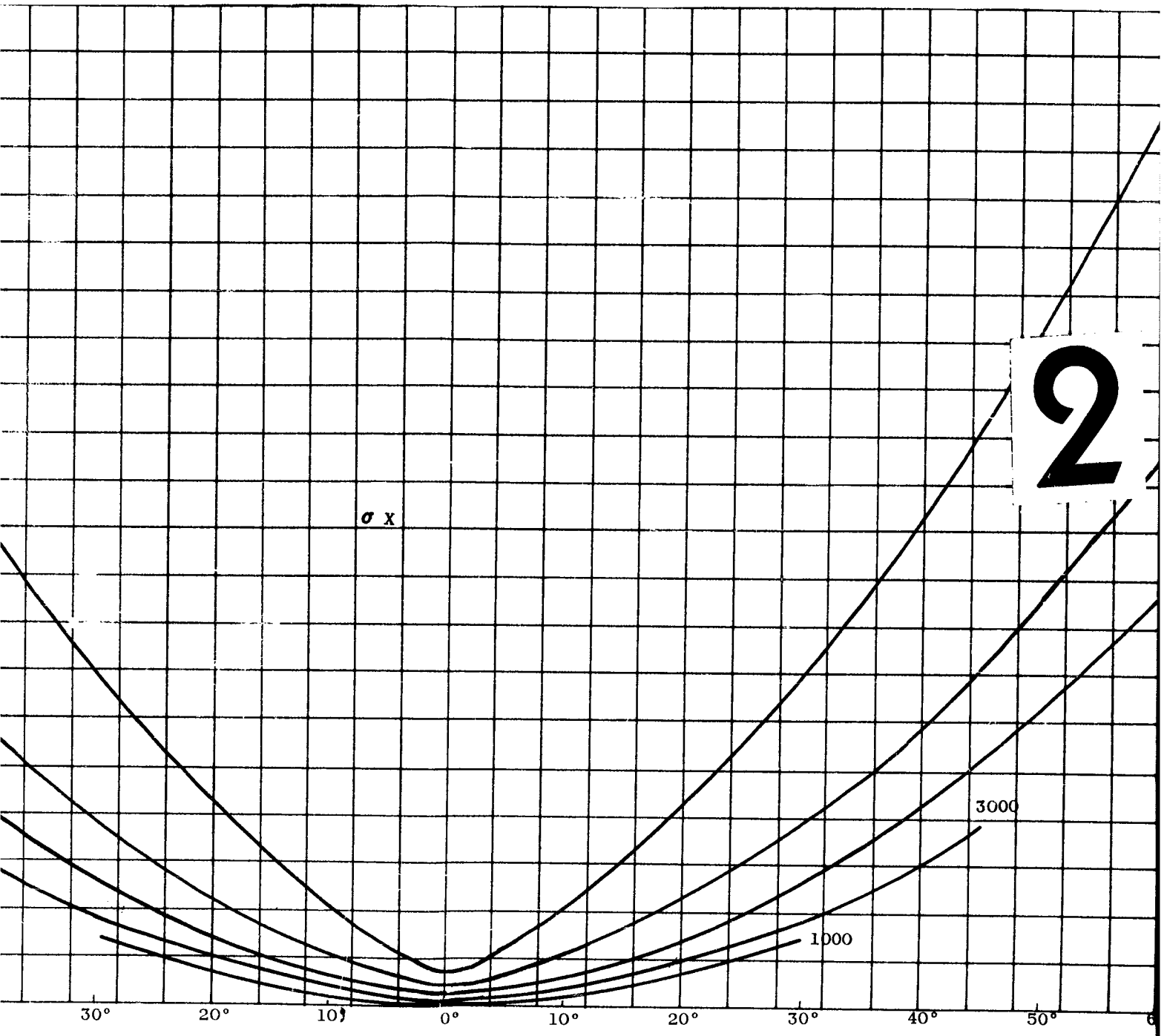

Figure 35. Standard Deviation in X Coordinate of Satellite Positi
Difference Measurements vs. Geocentric Orbit Angle for Se

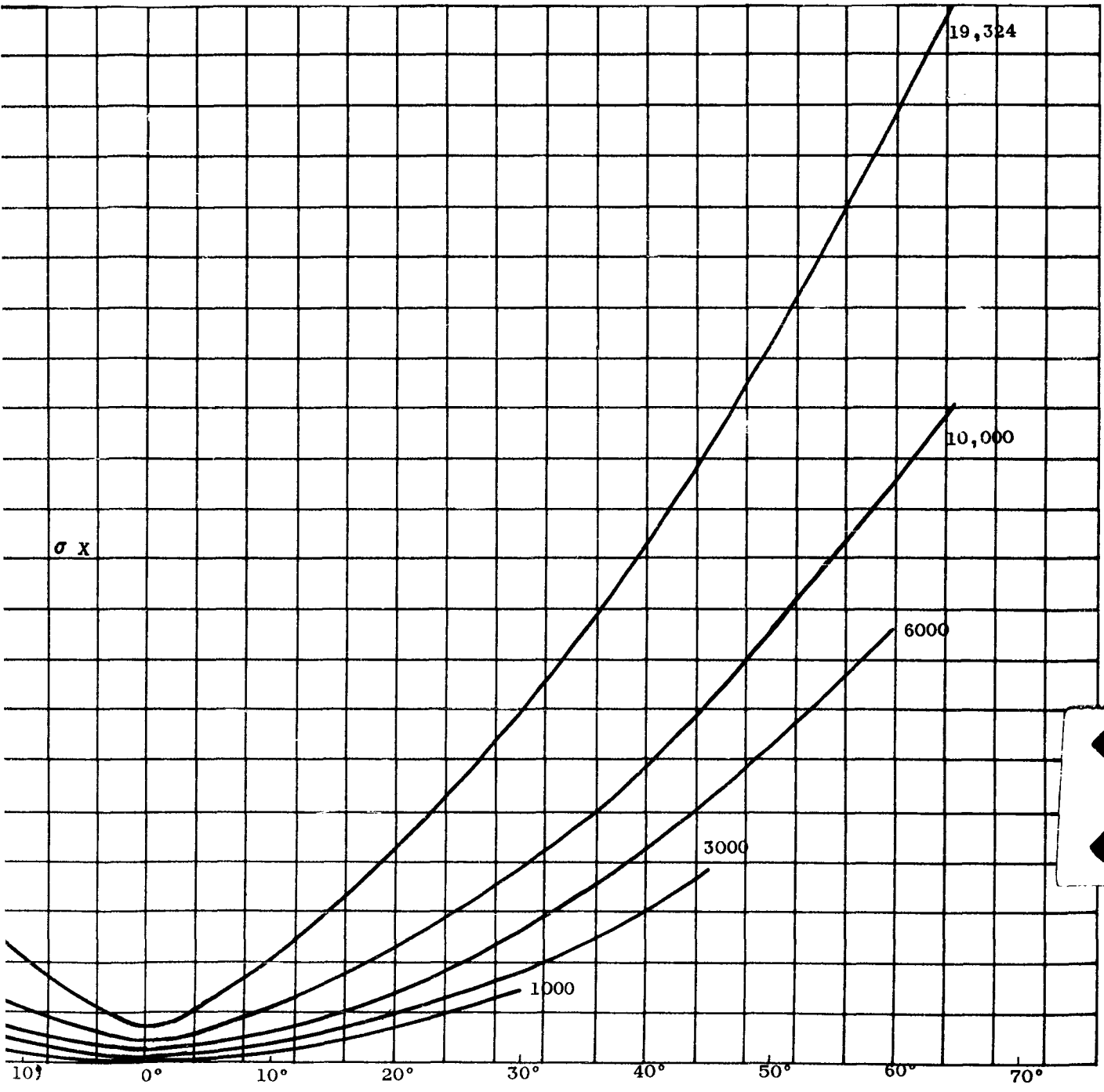

Figure 35. Standard Deviation in X Coordinate of Satellite Position for Three Range Difference Measurements vs. Geocentric Orbit Angle for Several Altitudes

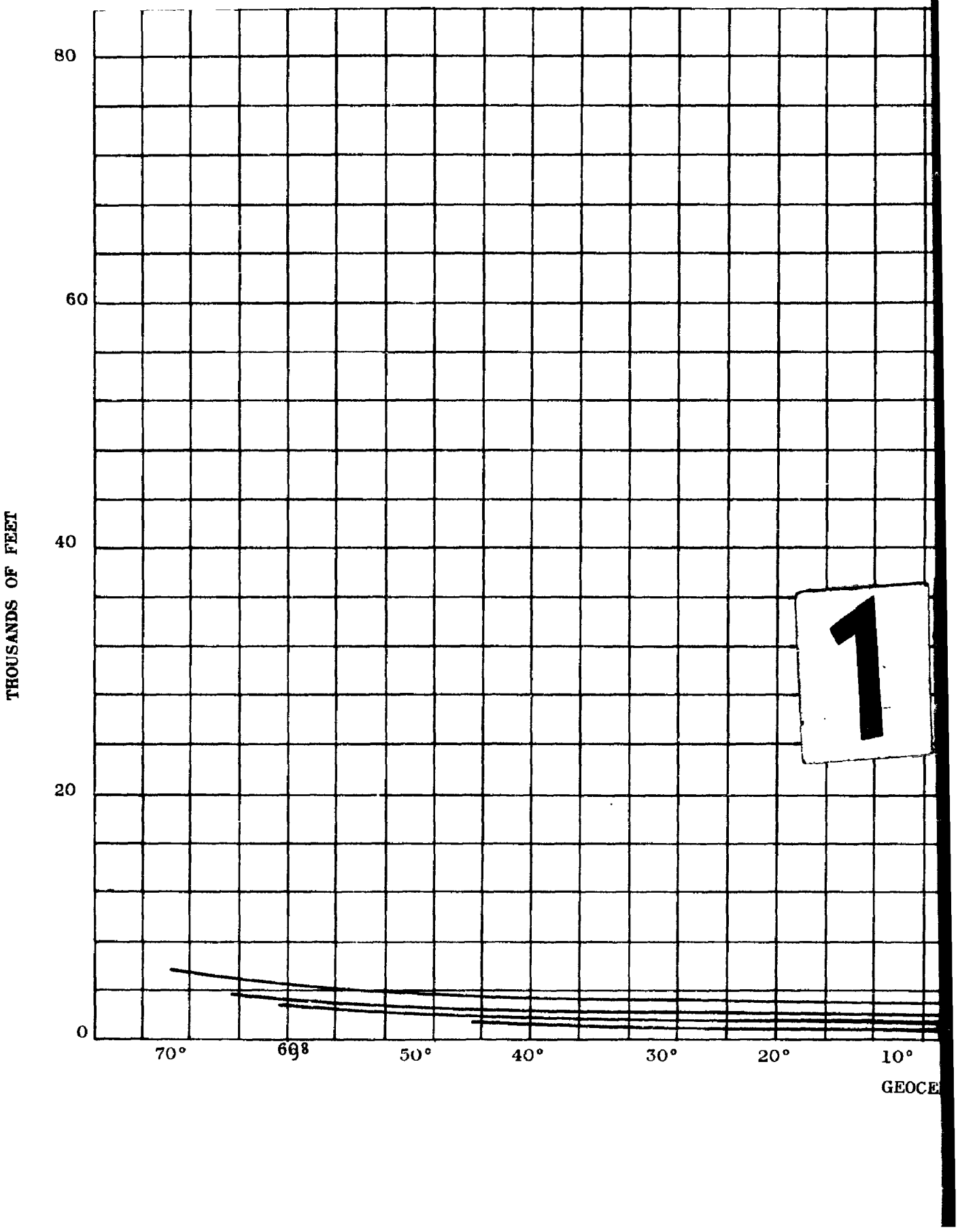
80
60
40
20
0
THOUSANDS OF FEET
70°
60°
50°
40°
30°
20°
10°
GEOCE

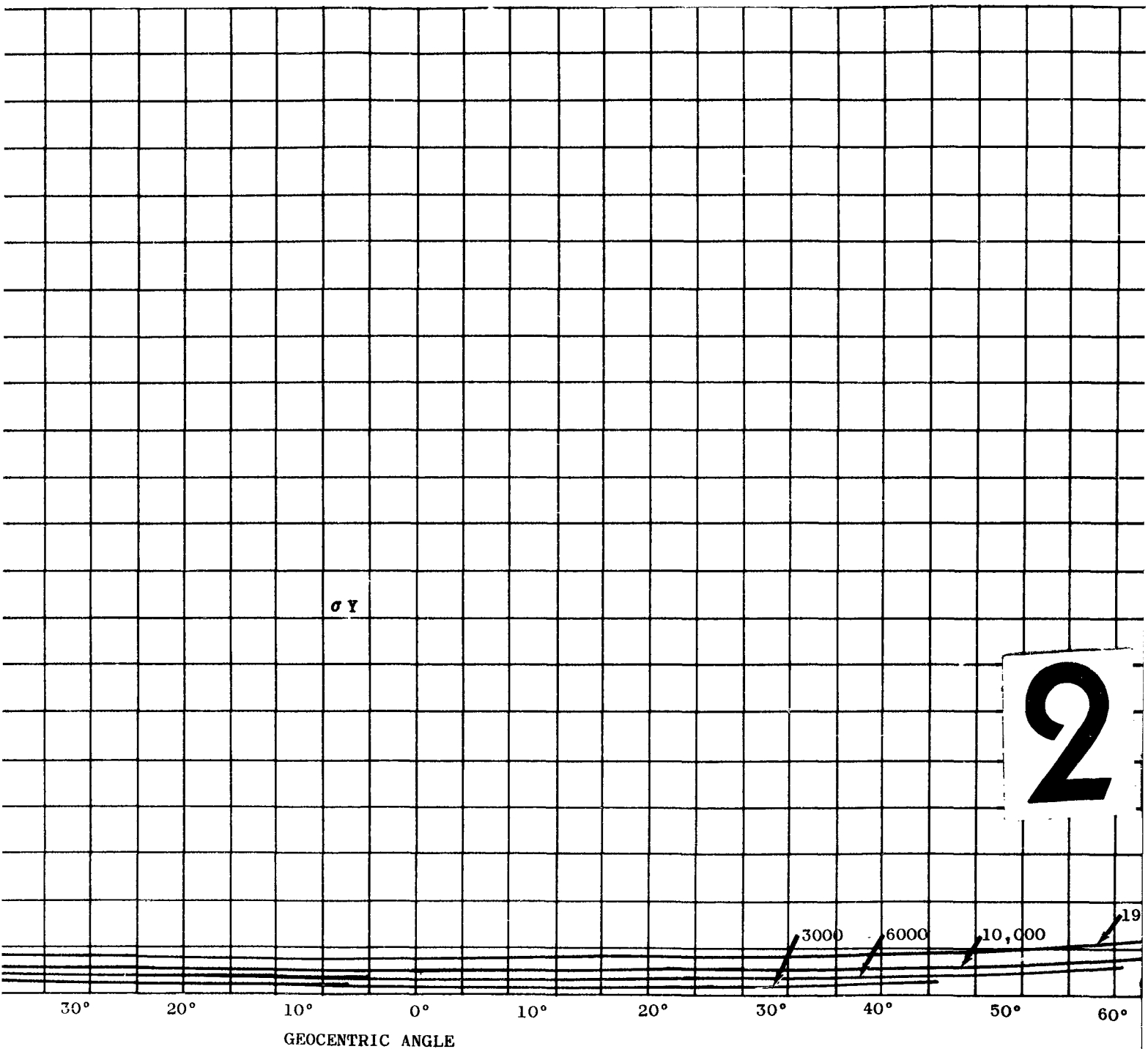

Figure 36. Standard Deviation in Y Coordinate of Satellite Positio
Difference Measurements vs. Geocentric Orbit Angle for Sev

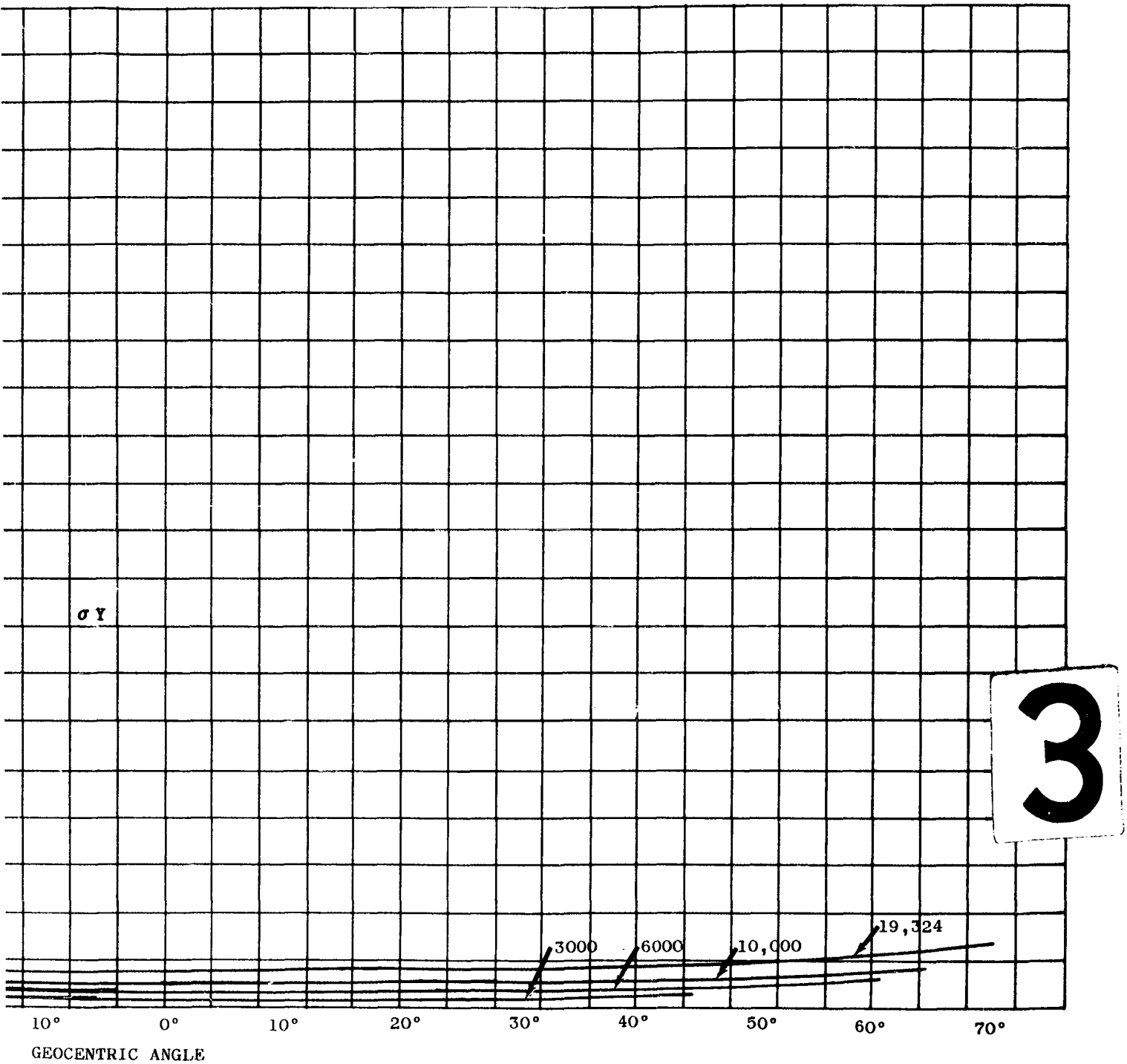

Figure 36. Standard Deviation in Y Coordinate of Satellite Position for Three Range Difference Measurements vs. Geocentric Orbit Angle for Several Altitudes

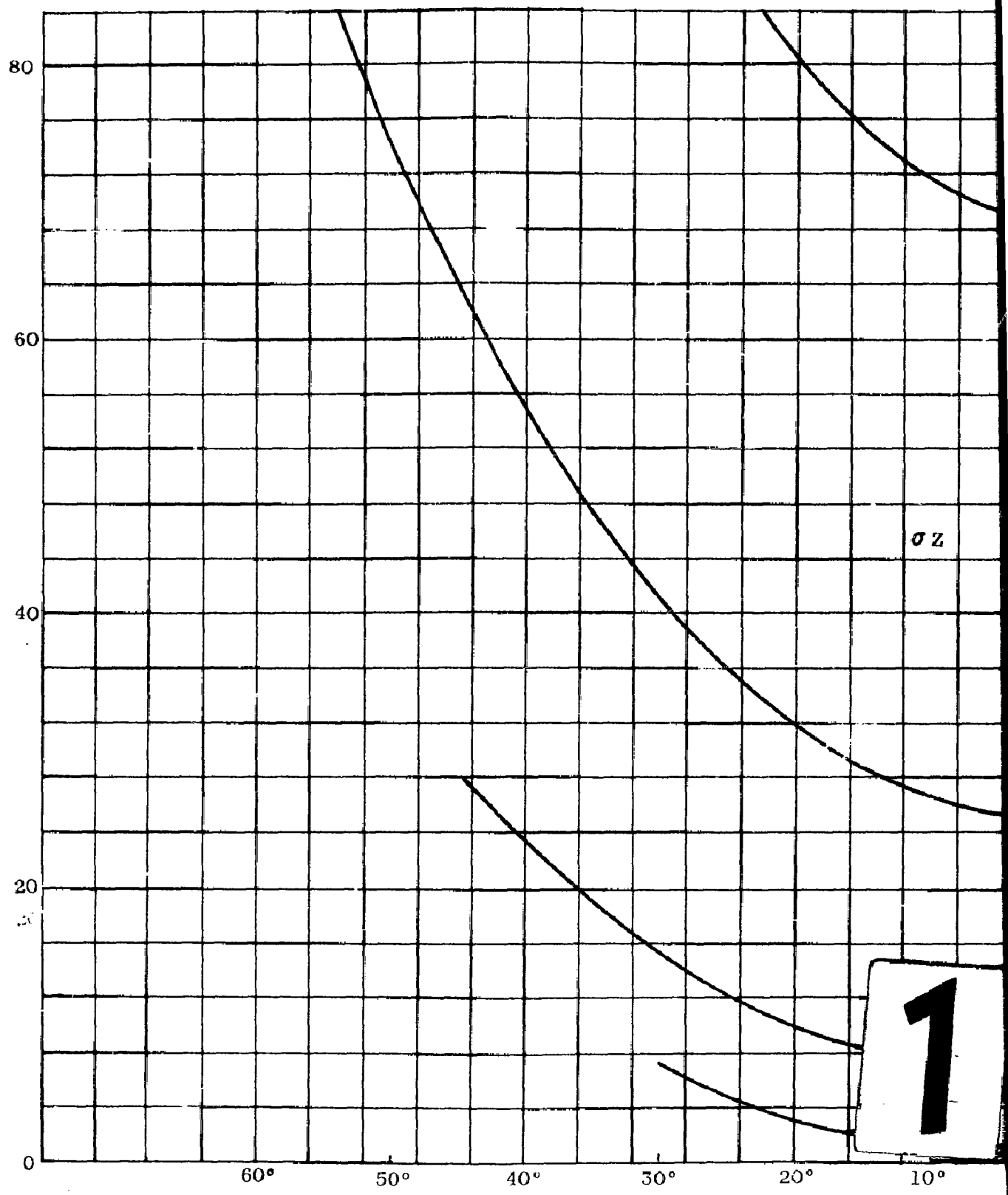
80
60
40
20
0
THOUSANDS OF FEET
σ z
60°
50°
40°
30°
20°
10°

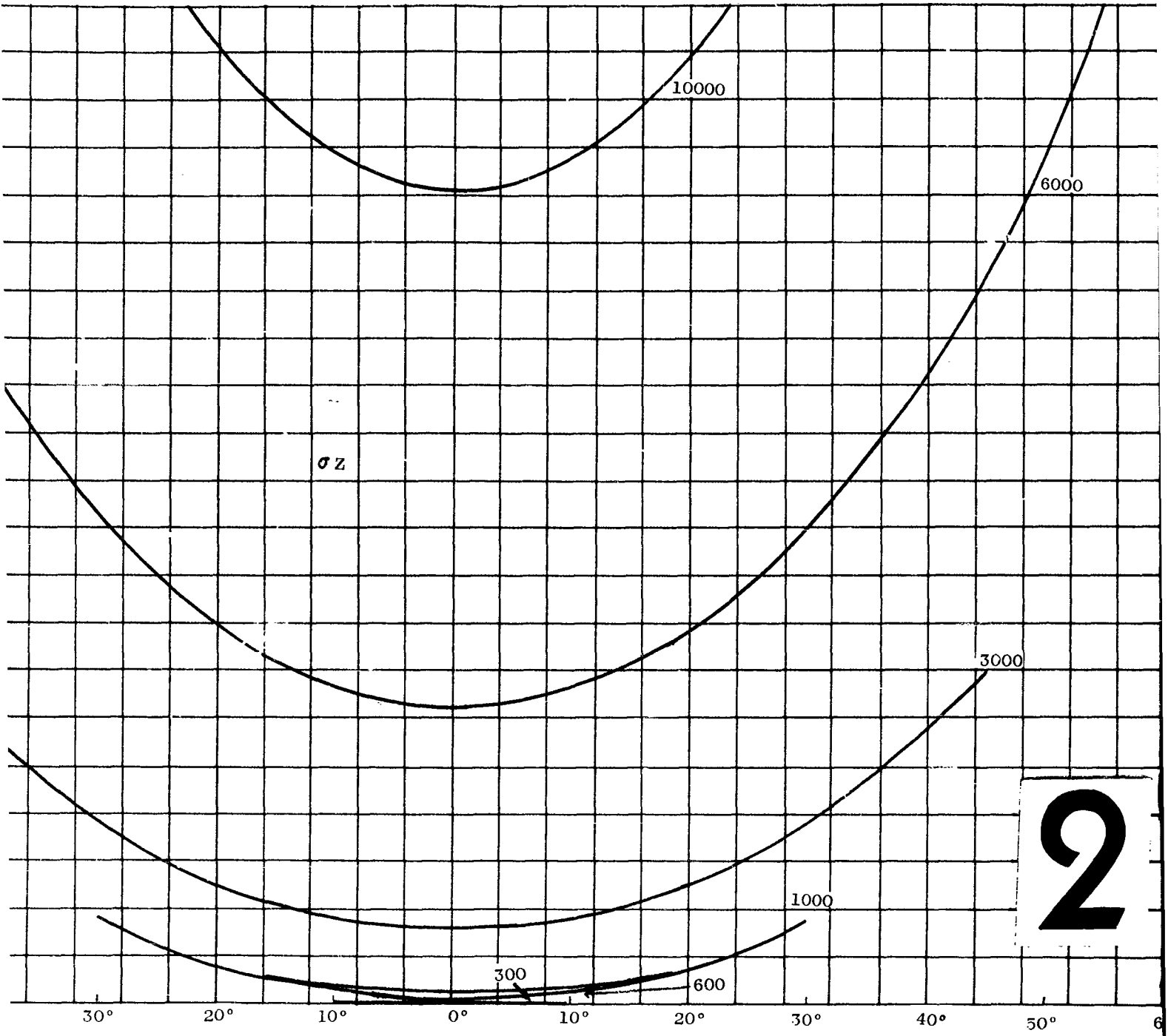

Figure 37. Standard Deviation in Z Coordinate of Satellite Posi
Difference Measurements vs. Geocentric Orbit Angle for S

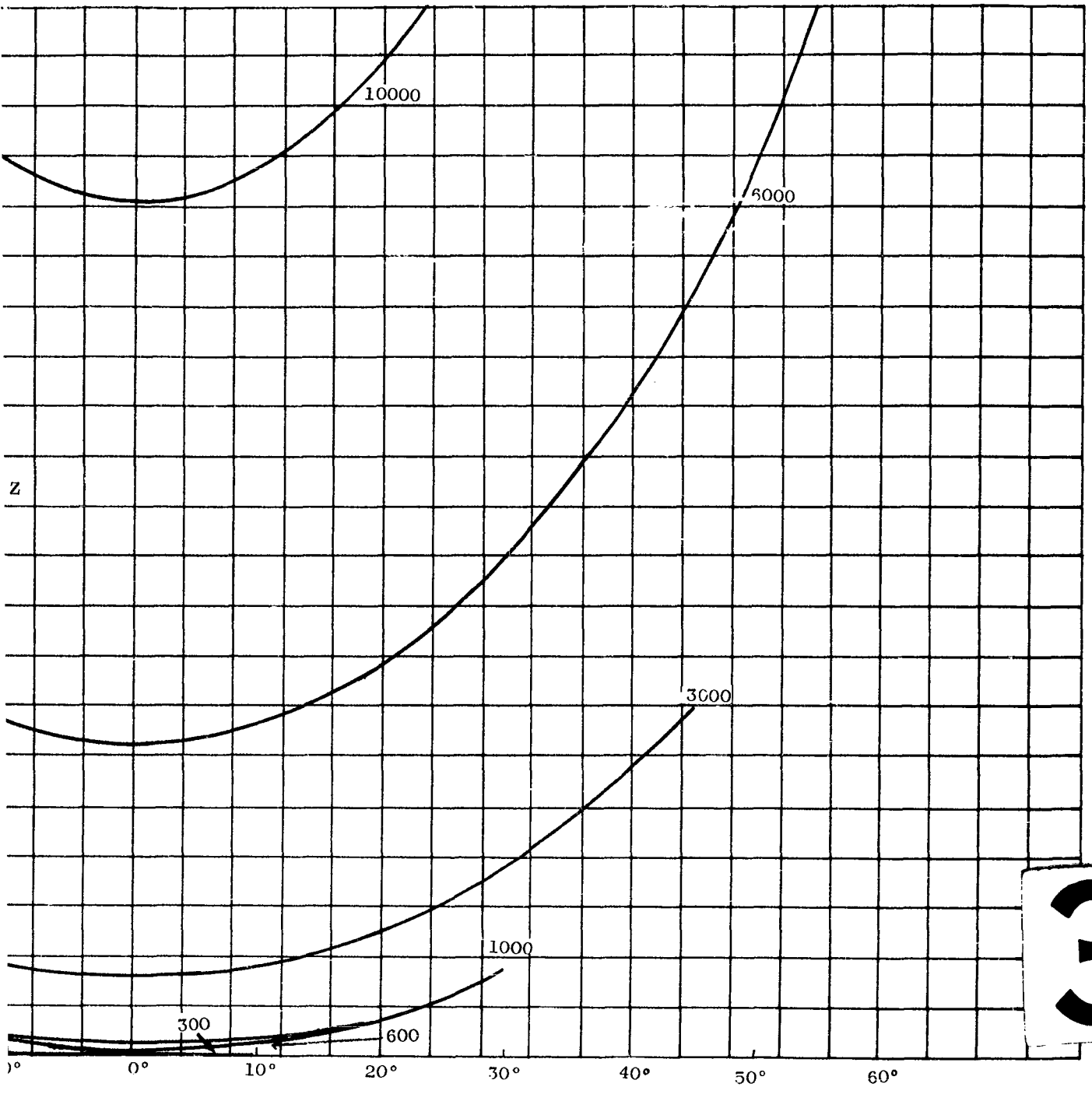

Figure 37. Standard Deviation in Z Coordinate of Satellite Position for Three Range Difference Measurements vs. Geocentric Orbit Angle for Several Altitudes

SECTION IV

SURVEYING OF THE TRACKING SYSTEM WITH AN EARTH SATELLITE

4.1 THE SURVEYING PROBLEM

One of the most critical problems associated with any precision tracking system is that of establishing the accurate location of the tracking system complex in some specified coordinate system. Determination of the location requires a geodetic survey with an accuracy commensurate with the accuracy requirements of the trajectory measurement system.

Using classical geodetic techniques, the best accuracies attainable over line-of-sight distances are of the order one part error in 400,000 of the distance measured. Over land and water areas, such as the island chain southeast of Cape Canaveral, the highest accuracies attainable are approximately one part error in 100,000. (At distances of 1,000 nautical miles the accuracies would amount to approximately one part error in 20,000.) In the case of remote island areas such as Ascension Island, the error in location would be approximately 300 feet. This degree of error would require an extensive gravity survey to determine the deflection of the local vertical. Since survey accuracies of approximately one part error in 10^6 are necessary to meet the stringent requirements for some of the operational systems, it is clear that classical geodetic techniques cannot furnish the accuracies required for the location of precision tracking systems.

The "new" geodetic survey must be an "absolute" survey, in the sense that the vector position of the tracking system with respect to the earth's center of mass must be determined. This is required because the earth's gravitational field is the dominant field affecting orbiting vehicles. Thus, it is necessary to accurately locate the tracking system in the earth's gravitational field to facilitate accurate trajectory determination and prediction.

The survey problem has several phases which can be considered somewhat independently. These phases include the selection and determination of a common coordinate system that can be established accurately at each station. Such a system may consist of spatial directions determined from star field observations. Another phase of the problem is that of determining the vector position of each tracking station relative to the earth's center of mass and thereby the baseline lengths. These phases are discussed in the following paragraphs.

As suggested by Convair-Astronautics as early as 1953 and by several authors (Reference II-1, -3, -4, and -6 in Bibliography), a technique based on astronomical reference systems, in combination with electronic and optical measurements of artificial satellites, is best suited to surveying long baseline systems. The fixed star system is the most stable absolute reference

system in nature. Artificial satellites photographed with the fixed star background can be utilized to obtain terrestrial data, including the tracking site coordinates on the earth with respect to the fixed star coordinate system.

In this method, the vector position of an orbiting vehicle is determined with respect to an individual tracking station. The position is obtained from range measurements of the tracking system, in combination with angle data obtained by photographing a light flash on the vehicle against the background of stars. The locus of a set of these vectors describes the vehicle's orbit with respect to the individual tracking station. In general, the orbit will not be a conic section, because the gravitational field of the earth is not a pure central force field but has superposed on it effects resulting from the earth's oblateness and from gravity anomalies (non-uniform distribution of mass within the earth). Taking such effects into account, the orbit of the vehicle can be determined by using numerical integration techniques: Cowell's method, Encke's method, or by semi-analytical methods that describe the deviation or departure (as in Encke's method) of the actual orbit from some assumed reference conic section.

A method for determination of the earth's mass center from the orbit observations is described in the following paragraphs. In essence, the actual orbit is reduced to a two-body (conic section) datum orbit. This is done by determining the deviations and subtracting them from the actual orbit. (The deviations are obtained from the perturbing acceleration by the methods indicated in the prior paragraph.) This materially reduces the complexity of the mathematics required for the determination of the earth's center of mass by reducing the problem to one for which there is an analytical solution.

4.2 DETERMINATION OF A DATUM ORBIT

Because of the earth's gravitational attraction and the convenience of describing the motion of a spacecraft in simple mathematical expressions, the earth's mass center is the natural origin of any flight-path geometry. Therefore, any method of spacecraft tracking has to refer all position data to the center of the earth's mass. Since tracking is accomplished from stations on the surface of the earth, it is necessary to know the location vector of the earth's mass center with respect to each of the tracking stations.

The orbit of a satellite in the vicinity of the earth is influenced by several factors, but the earth's gravity is the primary agent in prescribing the orbit. All other influences, such as the gravitational effects of the sun, the moon, and the planets, are of perturbing nature and are fairly small. The gravitational field of the earth is fairly well known, from gravimetric and geodetic measurements as well as from astronomic observations. An approximate expression (third and higher order terms have been omitted) for the earth's gravitational field is:

$$\bar{g} = -\bar{e}_r \frac{k}{r^2}\left[1 + \frac{n}{r^2}\left(1 - 3\sin^2\Theta\right)\right] - \bar{e}_\Theta \frac{6kn}{r^4}\sin\Theta\cos\Theta$$

From this equation we can see that a body moving in this field experiences a large acceleration, on which is superimposed a small acceleration. The large acceleration is the Newtonian component of the earth's gravity. (A Newtonian force field is generated by spherical shaped homogeneous or concentric homogeneous masses, and the magnitude of the force is inversely proportional to the square of the distance from the sphere's center. Since the earth has an ellipsoidal shape, its gravity field is non-Newtonian, but can be considered as being composed of a Newtonian field and a rather small perturbing field.)

Satellites moving in a Newtonian field obey Keplers laws, i.e. follow elliptical orbits. Slight deviations in the earth's mass distribution alter its field from the Newtonian and, therefore, cause slight deviations from the Keplerian orbit. A theoretical investigation of orbital characteristics in the earth's non-Newtonian field has been made in Appendix II. Differential equations describing the perturbation from Keplerian orbits have been derived (equations II-52, II-53, and II-54). Solutions of this set of equations can be utilized to find an unperturbed (datum) orbit from the perturbed, nonelliptical orbit. With sufficient data describing the datum orbit the center of the earth's mass can be computed.

Suppose both range and direction data are obtained from a single station to five points of an orbit. If the elapsed time between successive observations is determined, sufficient information is available to solve the sets of equations II-52 to II-54, Appendix II. Figure 38 illustrates the situation. Point B is an earth station and S_1, S_2 ... are orbital points at which photogrammetric observations have been made. From these observations the vectors $r_1 \bar{e}_{s_1}$, $r_2 \bar{e}_{s_2}$,... are known with respect to our astronomical coordinate vectors, $\bar{e}_a$, $\bar{e}_b$, $\bar{e}_c$. Since the orbit is a three dimensional curve, the five points S_1 ... S_5 will not lie in a plane. If the perturbing vector, $\overline{\Delta S}_i$, is subtracted from each of the vectors $r_1 \bar{e}_{s_1}$, $r_2 \bar{e}_{s_2}$,..., a new set of five points, S'_i (i = 1, 2, 3, 4, 5, ...), is obtained which describe an unperturbed ellipse, the datum orbit. The earth's mass center is the focal point of this ellipse.

Finding solutions of the perturbing vector,

$$\overline{\Delta S}_i = \bar{e}_{r_i} \Delta r_i + \bar{e}_{\theta_i} \Delta p_i + \bar{e}_{\phi_i} \Delta q_i \qquad (4\text{-}1)$$

is the first step in the process. The components Δr_i, Δp_i, Δq_i are solutions of the set of simultaneous differential equations (II-52 to II-54 in Appendix II) which can be written in terms of t_i, the time elapsed between the first and ith observation, and the parameters p, ϵ, χ_{0A} and α of the unperturbed ellipse. That is,

$$\Delta r_i = \Delta r\ (t_i,\ p,\ \epsilon,\ \chi_{0A},\ \alpha)$$

$$\Delta p_i = \Delta p\ (t_i,\ p,\ \epsilon,\ \chi_{0A},\ \alpha)$$

$$\Delta q_i = \Delta q_i\ (t_i,\ p,\ \epsilon,\ \chi_{0A},\ \alpha)$$

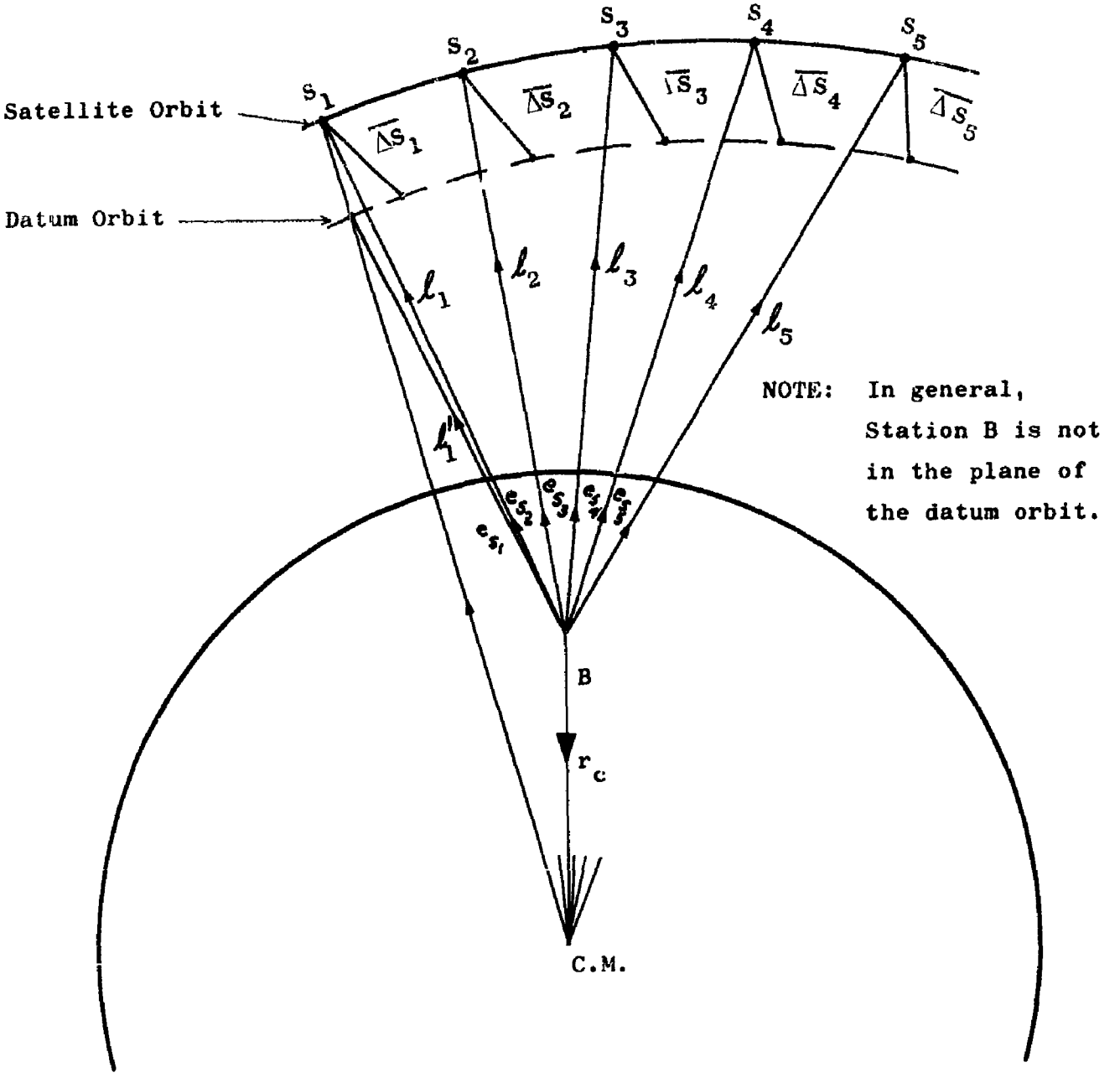

Figure 38. Orbit Points of a Satellite at Station B

Where:

p is the semi latus rectum.

ϵ is the eccentricity.

χ_{0A} is the true anomaly angle of perigee, and

α is the inclination angle of the plane containing the ellipse.

Since the four parameters of the ellipse are not known, a convergent iteration process may be applied, using the five observed points $S_1 \ldots S_5$ to obtain an ellipse which best fits these points. This method yields a set of elliptical parameters, p_1, ϵ_1, χ_{0A_1} and α_i, from which a set of five perturbing vectors,

$$\overline{\Delta S}_{i_1} = \bar{e}_{r i1} \Delta r_{i1} + \bar{e}_{\theta i1} \Delta p_{i1} + \bar{e}_{\phi i1} \Delta q_{i1};$$

and a set of five new points defined by

$$\overline{S}_{i_1} = r_i \bar{e}_{si} - \overline{\Delta S}_{i1}, \quad i = 1,2,3,4,5$$

may be computed. These five new points can be used as new inputs for a first iteration in finding a more refined second set of parameters, p_2, ϵ_2, χ_{0A2} and α_2. In this fashion, refined values of the ellipse parameters are obtained, provided that the method is convergent with a reasonable number of iterations, V. The criterion for convergence is given by

$$\lim_{V \to \infty} (p_{V+1} - p_V) \longrightarrow 0$$

$$\lim_{V \to \infty} (\epsilon_{V+1} - \epsilon_V) \longrightarrow 0$$

$$\lim_{V \to \infty} (\chi_{V+1} - \chi_V) \longrightarrow 0$$

$$\lim_{V \to \infty} (\alpha_{V+1} - \alpha_V) \longrightarrow 0$$

If reasonable convergence is found after V = N steps, then the set of vectors,

$$\overline{S}_{iN} = r_i \bar{e}_{si} - \overline{\Delta S}_{iN}, \quad i = 1,2,3,4,5$$

will define five points which are points of an unperturbed ellipse.

In applying the iteration process it is necessary to select a criterion for choosing a best fit to the five (or more) data points. Several methods are possible, but for purposes of discussion, we will employ the method of least squares. The best fitting plane of the datum orbit can be described by a unit normal vector, $\bar{n}_V$, and a magnitude, N, along the normal vector.

The distance of the point $S_i^{(v)}$ from that plane is denoted by $d_i^{(v)}$, defined by the equation:

$$d_i^{(v)} = (\bar{S}_{iv} \cdot \bar{n}_v) - N, \quad i = 1,2,3,4,5$$

In order to find the three unknowns, namely the two direction cosines of the unit normal vector, $\bar{n}_v$, and the magnitude, N, the following expression must be minimized:

$$\Delta^2 = \sum_{i=1}^{5} \left[d_i^{(v)}\right]^2 \longrightarrow \text{Minimum}$$

Consequently, three equations are obtained by writing the partial differential of the above equation with respect to the three unknowns and setting each expression equal to zero. We shall not proceed in writing down all the equations but only indicate that a linear equation in three unknowns results. Solutions of this equation yield the directions and magnitude of the vector, $N\bar{n}_v$, which defines a plane, $p^{(v)}$, containing the ellipse of the Vth approach. The projection on the datum plane of the five reduced datum points $S_i^{(v)} \ldots (\bar{S}_{iv})$ finally defines the points of the ellipse, of which the parameters p_v, ϵ_v, and χ_{0A_v}, can be obtained. The inclination angle, α_v, of plane $p^{(v)}$, is given by the expression:

$$\alpha_v = \frac{\pi}{2} - \arccos\ (\bar{n}_v \cdot \bar{e}_p),$$

where $\bar{e}_p$ is the unit vector pointing towards the celestial north pole. The unit vector $\bar{e}_p$ can be expressed with respect to the astronomical coordinate systems, $\bar{e}_a$, $\bar{e}_b$, $\bar{e}_c$, with an accuracy of at least 0.1 sec of arc deviation, which is sufficient in connection with the perturbation problem.

So far, determination of the coefficients, Δr_i, Δp_i, and Δq_i of equation 4-1 have been described. Now we must consider how the unit vectors $\bar{e}_{r_i}$, $\bar{e}_{\theta i}$ and $\bar{e}_{\phi i}$ can be expressed. Fortunately they can be represented by using data obtained with conventional geodetic methods. For purposes of computing the correction vector we can use the local geocentric unit vector, $\bar{u}$, which can be obtained by reduction of plumb line observations and represented with respect to the astronomical coordinate system. Errors due to local anomalies of the order of 15 sec of arc can be expected. This error can be ignored as far as the perturbation problem is concerned. Furthermore, for the earth's radius, R, we may use the distance based on the figure of the international spheroid. The error introduced by R is expected to be in the order of $\pm$ 100 meters and can also be ignored. The value for R can be obtained from:

$$R = 6378388\ (1 - 0.003367 \sin^2 \phi' + 0.0000071 \sin^2 2\phi') + H_B,$$

where ϕ' is the geographic latitude and H_B, the altitude of the station above the international spheroid. Thus, the unit vector $\bar{e}_{r_i}$ can be obtained from

$$\bar{e}_{ri} = \frac{R\bar{u} + r_i\bar{e}_{si}}{|R\bar{u} + r_i e_{si}|}$$

To justify the assumption made in using inaccurate figures in R and $\bar{u}$, we must investigate the errors to be expected. Under the assumption of 15 sec of arc lateral error and 100 meters radial error, the maximum lateral deviation of the unit vector, $\bar{e}_{r_i}$, is less than 15 sec of arc under the most unfavorable configuration. This corresponds to a lateral deviation of 7.3 mm (0.29 inch) for $\Delta r_i = 1000$ meters (3300 feet). The result indicates that the assumption made by introducing less accurate figures on R and $\bar{u}$ is tolerable.

By means of the unit vectors, $\bar{e}_r$, and $\bar{e}_p$, the remaining unit vectors, $\bar{e}_{\phi i}$, and $\bar{e}_{\theta i}$, can be obtained from the vector equations:

$$\bar{e}_{\phi i} = \frac{\bar{e}_{ri} \times \bar{e}_p}{|\bar{e}_{ri} \times \bar{e}_\phi|}$$

and

$$\bar{e}_{\theta i} = \bar{e}_{\phi i} \times \bar{e}_{ri} = \frac{\bar{e}_p - \bar{e}_r\,(\bar{e}_p \cdot \bar{e}_{ri})}{|\bar{e}_{ri} \times \bar{e}_\phi|}$$

The unit vector, $\bar{e}_p$, has already been introduced, it being a vector parallel to the earth's rotational axis. Both vectors are therefore represented with respect to the astronomical coordinate system at the tracking station.

4.3 LOCATION OF THE FOCI OF THE ELLIPSE

Applying the techniques described above will obtain a set of five points, S_{in} (i = 1, 2, ...5), of the reduced orbit. The reduced orbit points, S_{in} are points of the desired ellipse whose focal point is the earth's mass center. Since it is known that five points lying in a plane define an ellipse, the center of mass of the earth may be determined, using the five data points obtained by the method described in the prior section. To facilitate the solution, the data is referred to a coordinate system as indicated in Figure 39. Point S'_{in} shall be the origin of the coordinate system with the ξ axis passing through point S'_5. The η axis is perpendicular to the ξ axis. In this coordinate system the equation of the ellipse can be expressed as follows:

$$\xi^2 + A\eta^2 + B\xi_\eta + C\xi + D\eta = 0 \qquad (4\text{-}2)$$

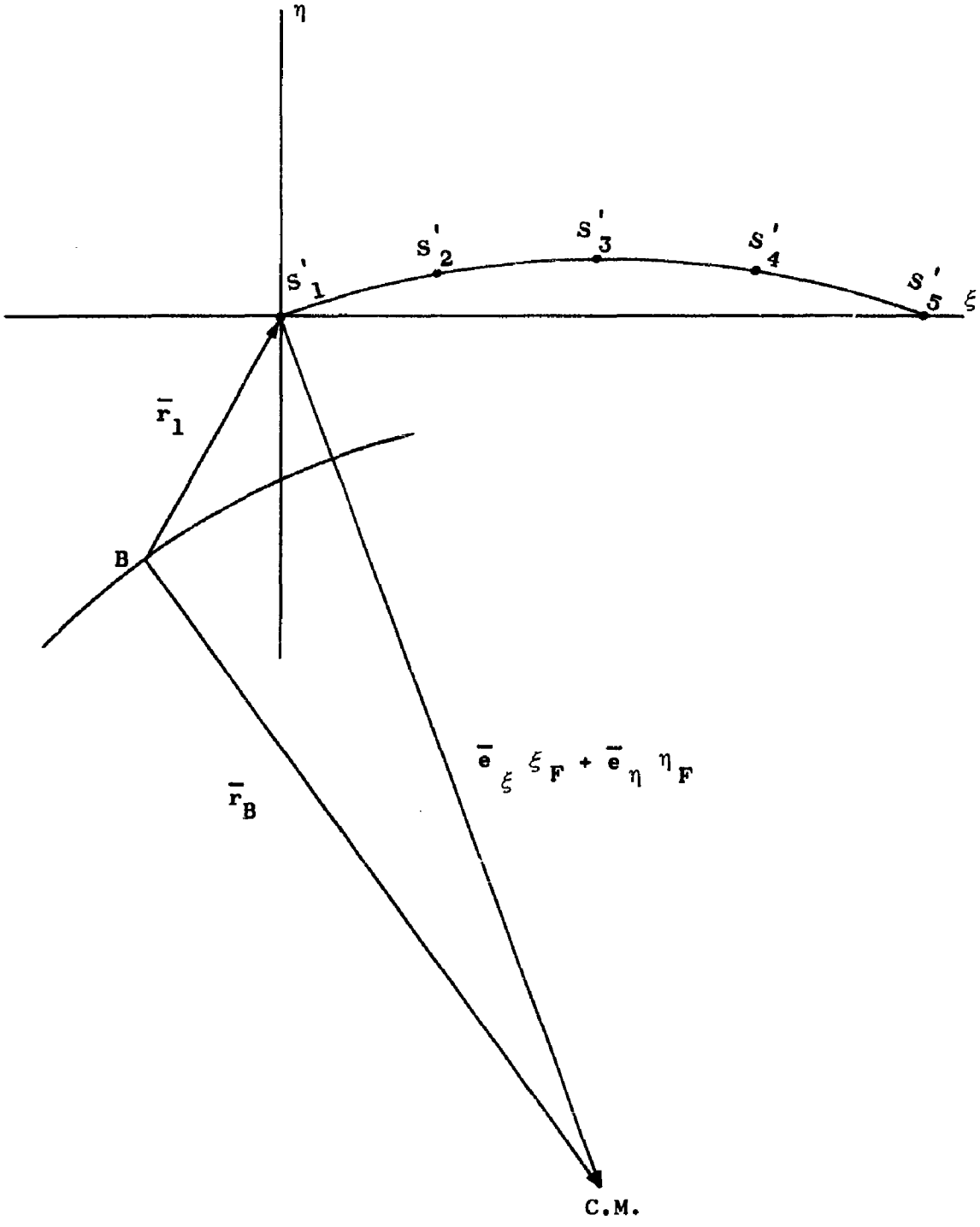

Figure 39. Earth Radius Determination at Station B

The components of the five points S'_{1N} to S'_{5N} in that coordinate system are:

$$S'_{1N}\ (\xi_1, = 0,\ \eta = 0);\ S'_{5N}\ (\xi = \left|\bar{S}_{5N} - \bar{S}_{1N}\right|,\ \eta = 0)$$

$$S'_{iN}\left(\xi_i = \frac{(\bar{S}_{iN} - \bar{S}_{i1}) \cdot (\bar{S}_{5N} - \bar{S}_{1N})}{\left|\bar{S}_{5N} - \bar{S}_{1N}\right|},\quad i = 2,3,4\right.$$

$$\left.\eta_i = \sqrt{(\bar{S}_{iN} - \bar{S}_{1N})^2 - \frac{(\bar{S}_{iN} - \bar{S}_{1N}) \cdot (\bar{S}_{5N} - \bar{S}_{1N})}{\left|\bar{S}_{5N} - \bar{S}_{1N}\right|}}\right) \qquad (4\text{-}3)$$

Hence, the coefficients A, B, C, and D of equation 4-2 may be obtained by introducing the values of ξ_i and η_i as defined by equation 4-3 and solving the resulting set of four linear equations.

From the values of the four coefficients, A, B, C, and D, the magnitude of the components of the ellipse focal points may be computed as follows:

$$\xi_F = -\frac{2AC - DB}{4A - B^2} \pm \frac{1}{\sqrt{2}} \sqrt{\frac{AC^2 + D^2 + BCD}{4A - B^2}}\ \sqrt{(A^2 - 2A + 1 + B^2)^{1/2} + A - 1}$$

$$\eta_F = -\frac{2D - CB}{4A - B^2} \pm \frac{1}{\sqrt{2}} \sqrt{\frac{AC^2 + D^2 + BCD}{4A - B^2}}\ \sqrt{(A^2 - 2A + 1 + B^2)^{1/2} - A + 1}$$

These components are defined along the unit vectors:

$$\bar{e}_\xi = \frac{\bar{S}_{5N} - \bar{S}_{1N}}{\left|\bar{S}_{5N} - \bar{S}_{1N}\right|},\qquad \bar{e}_\eta = \frac{\bar{S}_{5N} - \bar{S}_{1N}}{\left|\bar{S}_{5N} - \bar{S}_{1N}\right|} \times \bar{\eta}_N$$

where $\bar{\eta}_N$ is the unit vector normal to the datum plane.

The center of mass of the earth can finally be expressed with respect to station B in the astronomical coordinate system as follows:

$$\bar{r}_B = \bar{r}_1 + \bar{e}_\xi\ \xi_F + \bar{e}_\eta\ \eta_F,$$

where $\bar{r}_1$ is the vector from station B to the reduced datum point, S_1.

The magnitude of vector $\bar{r}_B$ is the distance of B from the earth's center of mass.

So far only five orbit points have been considered in carrying out the computation. This has been done in order to exhibit the basic principles involved in the method. Actually, more than five points will be necessary to obtain high accuracy. But the computation must be performed with five points out of whatever number of points are chosen. The number of solutions obtained for the vector of the center of the earth mass is of the order:

$$\frac{N(N-1)\ (N-2)\ (N-3)\ (N-4)}{120}$$

This is the number of possible combinations of N observed points, taken five at a time. The average vector of all solutions will be the most probable vector of the earth's mass center.

SECTION V

TROPOSPHERIC PROPAGATION EFFECTS

5.1 INTRODUCTION

This section deals with the contribution to the over-all system range errors by that portion of the atmosphere known as the troposphere. In long-range precision tracking of objects in space, one of the sources of error is the uncontrollable (and sometimes unknown) variation in the value of the propagation velocity which causes ray paths to be retarded and to bend. This results in a difference between apparent distance (as measured by radar or other electromagnetic techniques) and actual or true distance.

Corrections for the variations in propagation constant have been the subject of study by many investigators (see Bibliography, part III, for references cited). In general, corrections for the effect of tropospheric refractions have been based on determining the index of refraction as a function of altitude, h. In most work the index of refraction, η is replaced by the refractivity, N, defined as equal to $(\eta - 1) \times 10^6$. The value of N is usually determined by measurements of meteorological data (barometric pressure, relative humidity, temperature, etc.), either at ground level or as a function of altitude, utilizing information from radiosonde balloons, airborne instruments, etc.

Knowing the value of the refractivity at each altitude, it is possible, using any one of several mathematical techniques, to calculate the range correction at each incremental altitude and to sum up these various range corrections to get the total range error for a given refractivity profile. The range error will, of course, be a function of elevation angle, increasing as the ray path approaches the horizontal.

Changing meteorological conditions on different days, in different climates, and at different seasons of the year cause the refractivity index and the range error to vary significantly. The values of the refractivity index can change over a range of approximately 200 to 400 N-units at the surface, resulting in a variation in range error of 20 to 25 percent at a typical tracking angle of 45 degrees.

The Tropospheric Range Aberration Study was conducted with the following objectives:

a. to determine the magnitude of the Tropospheric Range Aberration (TRA), *

* Note: See Glossary at the end of Appendix III for listing of all special terms used.

b. to determine a reasonable method of providing corrections for these aberrations, considering the accuracy obtainable from various corrective systems and the cost of the hardware required to implement these systems,

c. to determine the magnitude of the residual errors for the system chosen,

d. to decide whether the techniques selected are adequate to obtain the results desired in the over-all tracking system.

5.2 SURVEY OF APPLICABLE LITERATURE

In order to avoid needless duplication of effort during this study, an extensive survey of the related literature was undertaken. The literature reviewed is listed in part III of the Bibliography (Section VII) and is presented to serve as a ready reference source to others investigating aspects of this problem beyond that considered in this study. The objectives of the literature search were two-fold: 1) to determine which investigations by other organizations were directly applicable to the current problem, and 2) to determine the extent to which other investigations had already attained solutions to the problem.

The following preliminary conclusions were drawn from the literature survey:

a. A real-time correction as a function of elevation angle is mandatory.

b. A real-time correction as a function of weather information (either the total profile or surface values of refractivity) is a desirable feature for a solution of this problem.

c. No work had yet been done by other investigators which was directly applicable to simple real-time correction computations (all previous results required either tabular or graphical look-up or extensive calculations of integrals).

d. The probability looked promising that a usable relationship could be found between total range aberration and parameters that are available from the ground.

5.3 CALCULATION OF MAGNITUDE OF TROPOSPHERIC RANGE CORRECTION

Saastad and Forbes (Reference III-62) have derived by ray-tracing methods an equation which was considered most useful for calculating the tropospheric range aberration for this study. This equation assumes a knowledge of the value of refractivity in increments of altitude above the station and assumes that the atmosphere is composed approximately of spherically stratified layers.

The equation was chosen over the mathematical techniques of other investigators, primarily, because it does not involve calculation of the local angle of elevation in each layer of the atmosphere, determination of the total bending, etc., and thereby avoids much of the complexity of other solutions. One result is that this equation ignores the contribution of range

error caused by the path which the ray pursues through the troposphere. This contribution is very, very small in comparison with the range error contributed by the delay is passing through the troposphere (due to the index of refraction being greater than unity).

Should it be desired to apply these techniques to precision tracking of targets within the atmosphere (below 100,000 feet), it would be necessary to recalculate the values, taking into account the error due to the curvature of the path, since this error would then become a larger percentage of the total range.

To implement the investigation, the following equation for the incremental range error was set up on the IBM 7090 digital computer:

$$\Delta TRA_j = \rho_0 \left[\frac{\eta_{j+1} + \eta_j - 2}{2\eta_j} \right] \left[\left(\frac{\rho_{j+1}^2}{\rho_0^2} \eta_j^2 - \eta_0^2 \cos^2 \epsilon_0 \right)^{1/2} - \left(\frac{\rho_j^2}{\rho_0^2} \eta_j^2 - \eta_0^2 \cos^2 \epsilon_0 \right)^{1/2} \right]$$

where:

TRA_j = incremental tropospheric range error for the jth altitude increment (feet),

η_j = index of refraction at bottom of jth altitude increment,

ρ_0 = mean radius of earth (feet),

ρ_j = geocentric altitude at bottom of jth altitude increment (feet),

ϵ_0 = elevation angle of the ray path at the surface.

This equation was solved for 89 altitude increments from sea level to 200,000 feet. The program was arranged to accept the following variables as input:

a. a reference, or "mean," profile of refractivity vs. altitude, based on any chosen value of surface refractivity,

b. ray path elevation angles,

c. a set of perturbation values, chosen so as to introduce super-refraction layers, ducts, etc., into the mean profile.

The program then summed the incremental range errors, starting from the highest increment, so that the total error was obtained for any site altitude down to sea level. A limitation of this calculation is that it does not include a test for potential "trapping" of the rays. (Trapping of radio waves is a phenomenon which occurs at low ray path elevation angles whenever the initial gradient of refractivity is greater than some critical value; this value depends on the initial elevation angle.) It was assumed in the study that the initial elevation angle of the tracker would never be less than a few degrees above the horizon, since due to finite beam-width of the antenna, multipath problems, etc., zero-angle tracking is not practical. Thus, the probability of a ray being captured by a duct is remote. Furthermore, it was felt that the presence of ducts would not invalidate the result of this study, since, under ducting conditions, should the gradient actually be high enough to trap a ray, no return would be obtained from the target; therefore, no erroneous data would be reported by the tracking system.

5.4 ANALYSIS OF REFERENCE PROFILES AND ARTIFICIAL PROFILE PERTURBATIONS

5.4.1 Reference Profiles

R. R. Bean and others working at the Central Radio Propagation Laboratories (CRPL) at the Bureau of Standards have worked extensively in the field of devising suitable reference profiles to describe mean values of radio refractivity as a function of altitude. Admittedly, there is no such thing as a true reference profile, since a mathematically expressed profile would give results which differ from atmospheric conditions of any actual day. However, the various "standard" and "reference" profiles serve a very useful purpose in determining the effects of the atmosphere through mathematical calculations. At CRPL two types of reference profiles have been emphasized. They are: 1) the CRPL Reference Atmosphere - 1958, and 2) the CRPL Exponential Radio Refractive Atmosphere.

5.4.1.1 CRPL Reference Atmosphere - 1958. The CRPL Reference Atmosphere - 1958 is the closer approximation of the two CRPL profiles, yielding a better relationship to actual atmospheric conditions and altitude. However, it is not as straight-forward to handle mathematically as the exponential profile. The 1958 reference atmosphere is composed of three segments. It assumes that at 9 kilometers the refractivity will always lie within ± 4 N-units of the value N = 105 and describes the atmosphere above that altitude by a simple exponential decay to zero at infinite altitudes. At low altitudes this profile assumes that the refractivity decays in a linear fashion to 1 kilometer, with the amount of decay being determined by an exponential function based on a surface refractivity. At intermediate altitudes (between 1 kilometer and 9 kilometers) the CRPL reference atmosphere decays on an exponential, appropriately chosen to join the low-altitude segment to the value of N = 105 at 9 kilometers.

5.4.1.2 CRPL Exponential Radio Refractive Atmosphere. The CRPL Exponential Radio Refractive Atmosphere assumes a single exponential decay of refractivity with altitude. For certain calculations this single exponential is an easier expression to handle mathematically than the Reference Atmosphere. However, for extreme values of surface refractivity this simple exponential decay results in values of refractivity at the higher altitudes which depart significantly from values which are encountered in the actual atmosphere.

5.4.2 Perturbations

Part of the "unreal" aspect of any reference atmosphere is the fact that the existence of ducts, super-refractive layers, and other deviations of the atmosphere from smooth mathematical curves is not taken into account. Bean and Thayer (Reference III-27) give a classification of various types of N-profiles, in terms of the characteristics of the profile. Table 4 is a reprint of a table from the Bean and Thayer report. Illustrations of each of these actual types of different profiles for a single station are given in Appendix III.

In order to investigate the effect of ducts, refractive layers, and other perturbations, the equation for calculating actual range as given in paragraph 5.3 was set up on an IBM 7090 computer. The values for η in this equation were taken from the expressions for tropospheric profiles given in Table 4. The two CRPL reference profiles were programed into the computer in such a way that perturbations equivalent to those observed in the literature could be added to the reference profiles. The objectives of this work, then, were to:

a. determine the tropospheric range aberration (TRA) for each of the available profiles,

b. determine (by suitable modification of the profile) how this TRA was affected by perturbations,

c. determine to what extent the TRA could be minimized by locating the trackers at high, dry sites,

d. investigate the degree of agreement between the available reference profiles of refractivity, and

e. investigate the correlation between TRA and the accompanying surface refractivity (N_s), Δ N (the change in refractitivy in the first kilometer), and the grad-N (the initial gradient in the refractivity-versus-altitude curve).

Reference profiles based on an N_s value of 330 N-units were used in the perturbation analysis. The value of 330 N-units was chosen since it is considered to be the world-wide mean value of sea-level refractivity, N_0.

5.4.3 Results of Range Calculation on Artificial Profiles

The tropospheric range aberration for an elevation angle of 45 degrees is plotted in Figure 40 for each of the artificial atmospheres tested. Points 3, 2, 4, 5 and 6 (through which a smooth line has been drawn) were the CRPL-1958 reference atmospheres, based upon different values of surface refractivity. This line demonstrates the correlation between N_s and TRA in an unperturbed atmosphere. Points 26, 25, 24, and 23 are the various typical atmospheres described by Buck, Shipper & Kline (Reference III-34). The close adherence of the line joining these four points to the line joining the CRPL reference profile indicates the good agreement between the two sources of data. Point 21 is the Millman (Reference III-55) profile

Table 4. Classification of N-Profiles by Type*

CATEGORY	N_s	INITIAL N GRADIENT (N units/meter)	PROFILE CHARACTERISTICS
1. Superrefraction Modified Ground Layer (MGL)	Usually Very High	$-0.130 > \frac{dn}{dh} > -0.150$	No elevated ducts
2. Linear Maximum (MAX)	Near Yearly Maximum	> -0.100	Monotonic decrease of N with height
3. Linear Minimum (LIN)	Near Yearly Minimum	> -0.045**	Monotonic decrease of N with height
4. Elevated Ducts (ED)	As Observed	> -0.130	Base of ducting layer within 2 kilometers of the surface with a gradient < -0.157
5. Surface Duct (DUCT)	Very High	< -0.157	Surface layer at least 50 meters thick, no elevated ducts
6. Combined Profile (COMB)	As Observed	$-0.130 > \frac{dn}{dh} > -0.150$	At least one elevated duct within the first 3 kilometers above the surface

* Reference III-27, Appendix III

** With the exception of Truk, Caroline Islands, where the initial gradient is 0.75 N units per meter

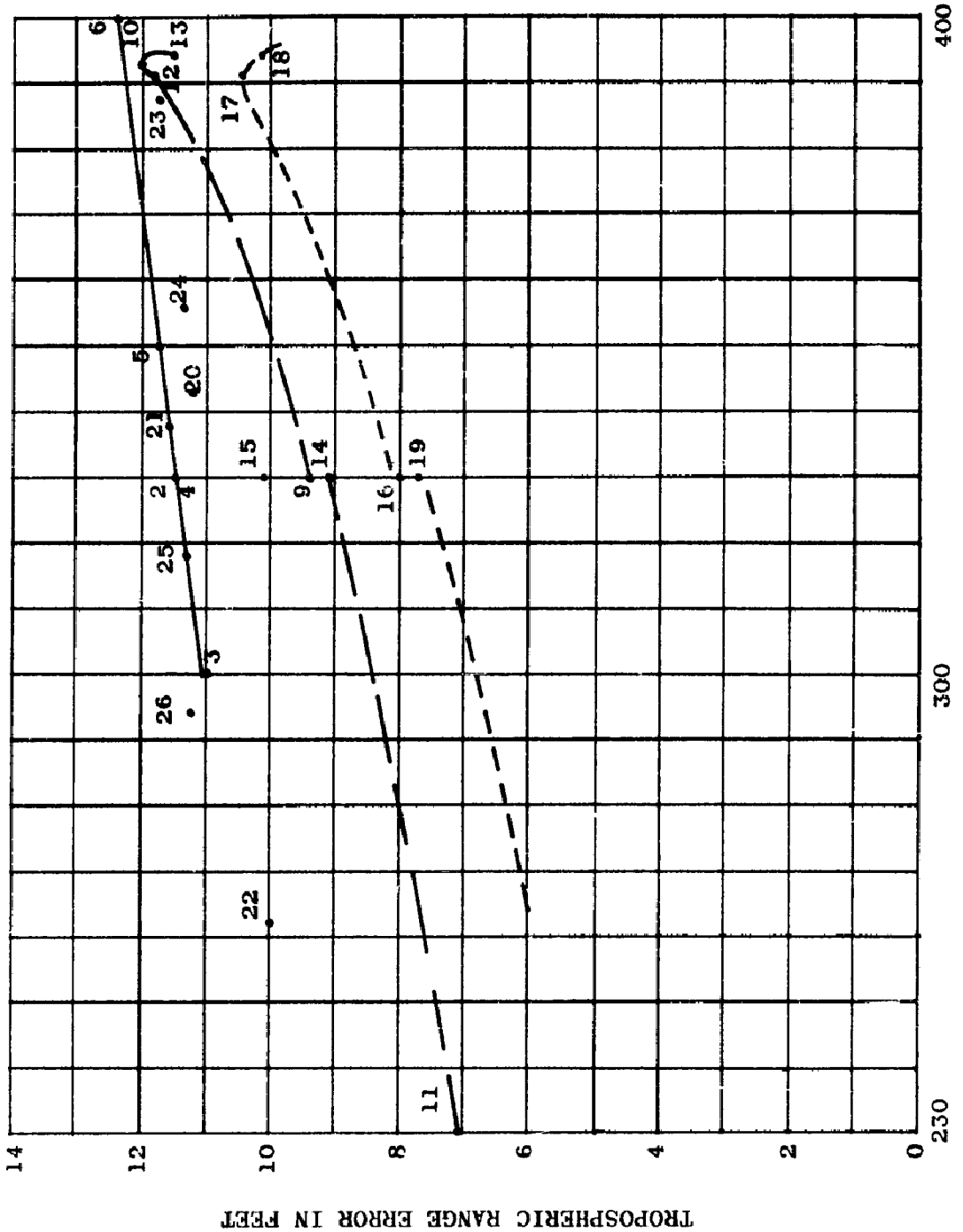

Figure 40. TRA Calculated vs. N_S for Artificial Profiles

describing a typical wet day, and point 22 is the Millman profile for a dry day. Here again the points lie within a reasonable distance of the extrapolation of the CRPL reference atmosphere curve.

The various perturbations of the CRPL reference atmosphere are described by points numbered 11, 14, 9, 12, 10 and 13 through which a long-dashed curve has been drawn. The perturbations on the CRPL exponential reference profile are described by points 19, 16, 17 and 18 (connected on the graph by a short-dashed curve). It is immediately apparent that the sets of data describing the artificially perturbed atmosphere are not in very close agreement with the data obtained from the unmodified reference profile or the average profile described by Buck and Millman.

The values used to inject the perturbations were taken from the available literature and are considered to be typical of the super-refractive ground layers, surface ducts, elevated ducts, and combined gradients actually found in nature in low altitudes. However, examination of the complete profiles resulting from the application of these artificial perturbations disclosed that, at altitudes of 9 kilometers and up, the perturbed data departed seriously from physical realism. The departure, in general, was such that the total area enclosed by the refractivity-versus-altitude curve was reduced. This, in turn, reduced the calculated values of the total tropospheric range aberration (TRA). Plotting these points thereby increased the scatter of the data (note that all artificially perturbed points plot appreciably below the remaining group of points) and resulted in concealing the correlation between TRA and surface refractivity, N_S.

5.4.4 Preliminary Conclusions

At this stage in the investigation several preliminary conclusions were evident:

a. A more accurate description of perturbed profiles would be necessary in order to determine the true spread of data.

b. For relatively low-accuracy tracking systems which do not track below 20 degrees elevation angle, it would be possible to make a fixed correction for tropospheric range aberration which would result in relatively small residual error.

c. For precision high-accuracy range trackers or for systems which are required to track at low elevation angles, i.e., a few degrees from the horizon, the variations in TRA from profile to profile become much more significant and would require additional correction beyond that supplied by a fixed correction.

d. A suitable means of determining the correction for the more accurate tracking systems would be to use a least-squares-fit for a straight-line function relating TRA to surface refractivity. Before a least-squares-fit could be determined, however, it would be necessary to obtain more accurate descriptions of the various types of perturbed profiles.

5.5 ACTUAL PROFILE DATA

When the significance of the preliminary conclusions was realized, efforts were initiated to obtain more realistic expressions for perturbed atmospheres. Convair was fortunate in obtaining data ideally suited to this purpose, through the courtesy of Bradford R. Bean, Chief of the Radio Meteorology Section of the National Bureau of Standards, Boulder Laboratories.

These NBS data are in the form of decks of punched cards describing actual profiles-of-refractivity versus altitude for each of the six classes of perturbed atmospheres. The profile data were taken from weather station records at thirteen widely-separated sites and include one profile of each type for each station (except that no sample of combined gradients was available for Ely, Nevada). Table 5 gives definitions for the six different types of profiles obtained for each station.

Table 5 identifies the various weather stations which were used to supply the profiles-of-refractivity versus altitude. It can be seen that a wide range of geographical conditions is included within this list. Fairbanks, Alaska at 64.5 degrees N is typical of an arctic climate; Truk Island at 7.28 degrees N is typical of an equatorial climate in a maritime air mass; Santa Maria, California and Miami, Florida are typical of coastal stations; while Denver, Colorado and Ely, Nevada are typical of stations in mountainous regions.

The characteristics of the six types of refractivity profiles as measured at Truk Island are plotted in Figure 41. In the lower left corner of the figure are two lines representing the slopes of refractivity which define the difference between super-refractive profiles (slopes greater than 100 N-units per kilometer but less than 157 N-units per kilometer) and ducting profiles (slopes greater than 157 N-units per kilometer).

Using the 77 profiles from the 13 different weather stations, the IBM 7090 computer was employed to calculate the values of total range aberration at 0, 10, 15, 45 and 90 degrees. The resulting TRA values are presented in Table 6, quoted to four significant figures. The associated values of surface refractivity, initial gradient of refractivity, change in refractivity in the first kilometer, altitude of the station and ratio of TRA_0 to TRA_{90} are also contained in the table. Subsequent calculations at 1.0, 2.0, 5.0, 30 and 60 degrees allowed calculations of additional error values.

The wide range in values of the ratio of TRA_0 to TRA_{90} (the ratio of horizontal range error to the zenith range error) should be noted. It is seen that this ratio changes over a 2-to-1 range. It is obvious, therefore, that any relationship, such as the cosecant function of elevation angle, cannot hope to give the right answer when the angle function is multiplied solely by the value of the zenith error. (See further discussion of this point in Appendix III.) It should be recognized that the values of TRA_0 through TRA90 shown in the table are the accurately calculated values obtained by means of integrating the total profile with the IBM 7090 computer. These are not the suggested corrections, which will be introduced later in the report.

Table 5. List of Meteorological Stations Used for Actual N(h) Profiles

STATION NO.	STATION NAME	APPROXIMATE LOCATION		APPROXIMATE ELEVATION (ft)
99999	Truk Island Caroline Is.	7.28°N,	151.51°E	3
12839	Miami, Fla.	25.45°N,	80.15°W	13
14764	Portland, Me.	43.41°N,	70.18°W	66
24240	Tatoosh Island Cape Flattery, Wash.	42.38°N,	124.72°W	98
23236	Santa Maria, Calif.	35.46°N,	120.25°W	233
13742	Washington, D.C.	38.55°N,	77.0°W	289
26411	Fairbanks, Alaska	64.50°N,	147.50°W	433
14834	Joliet, Ill.	41.32°N,	88.05°W	587
13983	Columbia, Mo.	38.58°N,	92.20°W	780
12921	San Antonio, Texas	29.25°N,	98.30°W	797
24011	Bismarck, N.D.	46.50°N,	100.48°W	1657
23062	Denver, Colo.	39.45°N,	105.00°W	5378
23152	Ely, Nevada	39.15°N,	114.53°W	6260

MODIFIED GROUND LAYER PROFILES

Station Number	N_S N-Units	Grad N N-Units/Km	ΔN N-Units/Km	H_S (ft)	Ratio TRA_0/TRA_{90}
99,999	388.5	142.0	62.5	3.28	50.27
12,839	376.5	150.0	59.0	13.12	49.73
14,764	357.5	143.0	80.5	65.62	49.43
24,240	336.5	133.0	68.5	98.43	45.93
22,236	340.0	112.0	51.5	232.95	44.86
13,742	344.0	143.0	48.0	288.70	46.59
26,411	313.1	132.0	47.1	433.00	44.84
14,834	390.5	130.0	77.5	587.0	50.63
13,983	367.0	110.0	56.5	780.90	47.55
12,921	366.0	135.0	65.0	797.0	49.34
24,011	322.5	131.0	58.5	1657.0	46.48
23,062	266.0	135.0	44.0	5378.0	44.74
23,154	280.0	130.0	38.5	6260.0	44.31

MAXIMUM SURFACE PROFILES

99,999	400.0	102.0	70.0	3.28	47.67
12,839	391.5	30.0	59.5	13.10	43.28
14,764	375.0	74.0	75.0	65.60	43.96
42,240	343.0	42.0	46.5	98.40	41.30
23,236	343.0	23.0	51.0	233.00	40.91
13,742	391.0	87.0	67.5	288.70	46.50
26,411	343.5	47.0	48.0	443.00	41.73
14,834	390.0	80.0	85.5	587.00	
13,983	383.0	42.0	73.0	780.90	
12,921	377.5	67.0	53.5	797.00	

Table 6. Summary of 77 Profiles Evaluated

ΔN N-Units/Km	Hs (ft)	Ratio TRA_0/TRA_{90}	TRA_0 (ft)	TRA_{10} (ft)	TRA_{15} (ft)	TRA_{45} (ft)	TRA_{90} (ft)
62.5	3.28	50.27	441.93	49.20	33.52	12.41	8.790
59.0	13.12	49.73	427.69	48.02	32.76	12.14	8.600
80.5	65.62	49.43	413.37	46.68	31.85	11.81	8.362
68.5	98.43	45.93	370.47	45.02	30.72	11.39	8.065
51.5	232.95	44.86	376.78	46.94	32.01	11.86	8.398
48.0	288.70	46.59	386.59	46.38	31.62	11.72	8.296
47.1	433.00	44.84	345.78	43.06	29.38	10.89	7.710
77.5	587.0	50.63	427.78	47.28	32.22	11.93	8.448
56.5	780.90	47.55	396.88	46.64	31.82	11.79	8.347
65.0	797.0	49.34	407.89	46.23	31.52	11.67	8.266
58.5	1657.0	46.48	354.89	46.64	29.09	10.78	7.635
44.0	5378.0	44.74	291.67	36.39	24.83	9.20	6.518
38.5	6260.0	44.31	302.56	38.90	26.00	9.64	6.826
70.0	3.28	47.67	420.72	49.40	36.66	12.46	8.824
59.5	13.10	43.28	382.21	49.40	33.67	12.47	8.830
75.0	65.60	43.96	382.83	48.62	33.17	12.30	8.708
46.5	98.40	41.30	340.95	46.10	31.45	11.66	8.255
51.0	233.00	40.91	339.48	46.37	31.618	11.71	8.292
67.5	288.70	46.50	397.59	47.86	32.614	12.08	8.550
48.0	443.00	41.73	342.38	45.86	31.27	11.59	8.204
85.5	587.00	47.60	404.84	47.59	32.43	12.01	8.505
73.0	780.90	43.75	376.49	48.09	32.79	12.15	8.604
53.5	797.00	44.30	373.53	47.19	32.15	11.91	8.431

MAXIMUM SURFACE PROFILES (Continued)

Station Number	N_S N-Units	Grad N N-Units/Km	ΔN N-Units/Km	H_S (ft)	Ratio TRA_0/TRA_{90}
24,011	350.5	60.0	44.0	1657.00	43.01
23,062	289.5	30.0	39.0	5378.00	40.70
23,154	280.0	52.0	42.5	6260.00	41.21
SURFACE DUCT PROFILES					
99,999	402.50	330.0	72.50	3.28	31.51
12,839	379.50	205.0	65.00	13.10	39.54
14,764	347.50	322.0	67.50	65.60	28.33
24,240	337.00	253.0	70.00	98.40	24.96
23,236	337.00	140.0	48.30	233.00	35.16
13,742	336.00	378.0	65.00	288.70	29.55
26,411	305.00	135.0	34.00	443.00	34.73
14,834	337.00	228.0	54.00	387.00	34.20
13,983	365.00	355.0	74.50	780.90	32.03
12,921	375.50	155.0	61.00	797.00	44.01
24,011	341.50	485.0	82.50	1657.00	28.63
23,062	254.00	165.0	45.50	5378.00	34.81
23,154	267.00	247.0	49.00	6260.00	28.34
COMBINED GRADIENT PROFILES					
99,999	393.50	142.0	64.00	3.28	50.62
12,839	358.50	125.0	55.00	13.12	46.02
14,764	342.00	132.0	45.50	65.62	45.33
24,240	323.00	132.0	57.00	98.43	44.96
23,236	330.00	100.0	79.00	232.95	
13,742	370.50	139.0	73.50	288.70	
26,411	307.00	130.0	34.50	443.00	

2

Table 6. Summary of 77 Profiles Evaluated (Continued)

ΔN N-Units/Km	H_s (ft)	Ratio TRA_0/TRA_{90}	TRA_0 (ft)	TRA_{10} (ft)	TRA_{15} (ft)	TRA_{45} (ft)	TRA_{90} (ft)
44.0	1657.00	43.01	348.21	45.28	30.87	11.43	8.096
39.0	5378.00	40.70	282.20	38.74	26.42	9.79	6.933
42.5	6260.00	41.21	273.07	37.01	25.25	9.36	6.626
72.50	3.28	31.51	274.67	48.78	33.24	12.13	8.715
65.00	13.10	39.54	332.53	47.02	32.06	11.88	8.408
67.50	65.60	28.33	227.79	44.91	30.63	11.35	8.038
70.00	98.40	24.96	202.43	45.19	30.86	11.45	8.108
48.30	233.00	35.16	296.55	47.13	32.14	11.91	8.434
65.00	288.70	29.55	236.47	44.65	30.475	11.30	8.000
34.00	443.00	34.73	274.79	44.14	30.13	11.17	7.911
54.00	387.00	34.20	274.53	44.81	30.57	11.33	8.025
74.50	780.90	32.03	269.31	46.95	32.03	11.87	8.408
61.00	797.00	44.01	370.24	47.06	32.07	11.88	8.412
82.50	1657.00	28.63	225.33	43.92	29.97	11.11	7.869
45.50	5378.00	34.81	227.94	36.44	24.90	9.248	6.547
49.00	6260.00	28.34	185.28	36.46	24.89	9.233	6.535
64.00	3.28	50.62	443.04	48.97	33.37	12.36	8.751
55.00	13.12	46.02	386.05	46.82	31.95	11.85	8.388
45.50	65.62	45.33	371.11	45.72	31.19	11.56	8.185
57.00	98.43	44.96	350.97	43.60	29.74	11.02	7.805
79.00	232.95	44.27	351.81	44.31	30.26	11.22	7.946
73.50	288.70	49.28	415.28	47.12	32.12	11.90	8.425
34.50	443.00	43.69	350.63	44.74	30.55	11.33	8.024

COMBINED GRADIENT PROFILES (Continued)

Station Number	N_S N-Units	Grad N N-Units/Km	ΔN N-Units/Km	H_S (ft)	Ratio TRA_0/TRA_{90}
14,834	340.00	140.0	59.50	587.00	45.56
13,983	346.00	140.0	55.50	780.90	45.66
12,921	359.00	136.0	44.00	797.00	47.01
24,011	318.00	143.0	47.50	1657.00	46.46
23,062	286.00	133.0	56.00	5378.00	47.21
LINEAR MINIMUM PROFILES					
99,999	383.60	82.0	64.0	3.28	44.57
12,839	333.60	28.0	38.60	13.10	39.41
14,764	315.00	39.0	39.00	65.60	39.82
24,240	315.00	38.50	38.50	98.40	40.44
23,236	323.50	41.50	41.50	233.00	40.33
13,742	297.50	29.50	29.50	288.70	38.87
26,411	291.00	33.50	33.50	443.00	38.84
14,834	309.50	36.00	36.00	587.00	39.57
13,983	309.50	35.50	35.50	780.90	39.81
12,921	301.50	31.50	36.50	797.00	39.11
24,011	295.00	35.00	35.00	1657.00	39.75
23,062	237.00	23.00	23.00	5378.00	37.30
23,154	249.50	30.50	30.50	6260.00	39.19
ELEVATED DUCT PROFILES					
99,999	373.50	117.00	51.50	3.28	
12,839	360.00	62.00	54.00	13.10	
14,764	345.00	64.00	56.00	65.60	
24,240	326.00	40.00	51.00	98.40	
23,236	339.50	50.00	73.50	233.00	39.19

Table 6. Summary of 77 Profiles Evaluated (Continued)

ΔN N-Units/Km	H_s (ft)	Ratio TRA_0/TRA_{90}	TRA_0 (ft)	TRA_{10} (ft)	TRA_{15} (ft)	TRA_{45} (ft)	TRA_{90} (ft)
59.50	587.00	45.56	347.37	42.55	29.04	10.77	7.623
55.50	780.90	45.66	392.22	47.57	32.59	12.13	8.589
44.00	797.00	47.01	389.43	46.32	31.58	11.70	8.283
47.50	1657.00	46.46	358.11	43.01	29.35	10.88	7.707
56.00	5378.00	47.21	324.47	38.29	26.15	9.70	6.872
64.0	3.28	44.57	394.36	49.48	33.73	12.49	8.847
38.60	13.10	39.41	329.19	46.56	31.79	11.79	8.352
39.00	65.60	39.82	316.25	44.31	30.24	11.21	7.941
38.50	98.40	40.44	315.38	43.55	29.71	11.01	7.797
41.50	233.00	40.33	326.68	45.20	30.85	11.44	8.099
29.50	288.70	38.87	300.30	43.13	29.43	10.91	7.724
33.50	443.00	38.84	295.86	42.50	29.01	10.75	7.616
36.00	587.00	39.57	312.10	44.01	30.03	11.14	7.885
35.50	780.90	39.81	309.47	43.39	29.61	10.97	7.771
36.50	797.00	39.11	305.16	43.53	29.71	11.02	7.802
35.00	1657.00	39.75	292.57	41.08	28.03	10.39	7.359
23.00	5378.00	37.30	241.79	36.14	24.68	9.15	6.481
30.50	6260.00	39.19	244.35	34.29	23.74	8.86	6.234
51.50	3.28	46.46	389.16	46.82	31.93	11.83	8.376
54.00	13.10	42.64	359.85	47.07	32.13	11.92	8.438
56.00	65.60	42.17	354.95	47.00	32.07	11.88	8.415
51.00	98.40	41.04	323.32	44.01	30.02	11.12	7.877
73.50	233.00	39.19	347.50	49.14	33.66	12.52	8.865

ELEVATED DUCT PROFILES (Continued)

Station Number	N_s N-Units	Grad N N-Units/Km	ΔN N-Units/Km	H_s (ft)	Ratio TRA_0/TRA_{90}
13,742	350.00	55.00	51.00	288.70	37.32
26,411	328.00	37.00	62.50	443.00	41.64
14,834	320.00	38.00	47.50	587.00	40.09
13,983	307.50	37.00	33.50	780.90	39.76
12,921	335.50	7.00	37.00	797.00	40.31
24,011	314.50	37.00	39.50	1657.00	40.14
23,062	278.00	58.00	64.60	5378.00	41.95
23,154	255.00	46.00	29.50	6260.00	39.39

CRPL REFERENCE PROFILES

330.0	46.10	46.10	0	41.00
300.0	39.0	39.00	0	39.20
350.0	52.0	51.60	0	42.30
400.0	68.0	68.10	0	46.1
295.0	30.0	29.50	0	--
359.4	39.0	39.00	0	--
230.0	27.0	26.40	0	35.29

Table 6. Summary of 77 Profiles Evaluated (Continued)

ΔN Units/Km	H_s (ft)	Ratio TRA_0/TRA_{90}	TRA_0 (ft)	TRA_{10} (ft)	TRA_{15} (ft)	TRA_{45} (ft)	TRA_{90} (ft)
51.00	288.70	37.32	311.11	46.53	31.75	11.77	8.336
62.50	443.00	41.64	330.03	44.27	30.20	11.19	7.924
47.50	587.00	40.09	320.25	44.60	30.43	11.28	7.987
33.50	780.90	39.76	307.59	43.14	29.45	10.92	7.735
37.00	797.00	40.31	326.01	45.11	30.79	11.42	8.086
39.50	1657.00	40.14	316.79	44.07	30.06	11.14	7.891
64.60	5378.00	41.95	272.62	36.30	24.76	9.17	6.497
29.50	6260.00	39.39	253.36	35.86	24.49	9.08	6.43
46.10	0	41.00	334.57	45.61	-	11.52	8.159
39.00	0	39.20	307.62	43.80	-	11.08	7.847
51.60	0	42.30	353.53	46.75	-	11.80	8.356
68.10	0	46.1	406.11	49.39	-	12.44	8.809
29.50	0	--	302.54		-	11.12	7.872
39.00	0	--	359.71		-	12.21	8.643
26.40	0	35.29	248.70		-	99.53	7.046

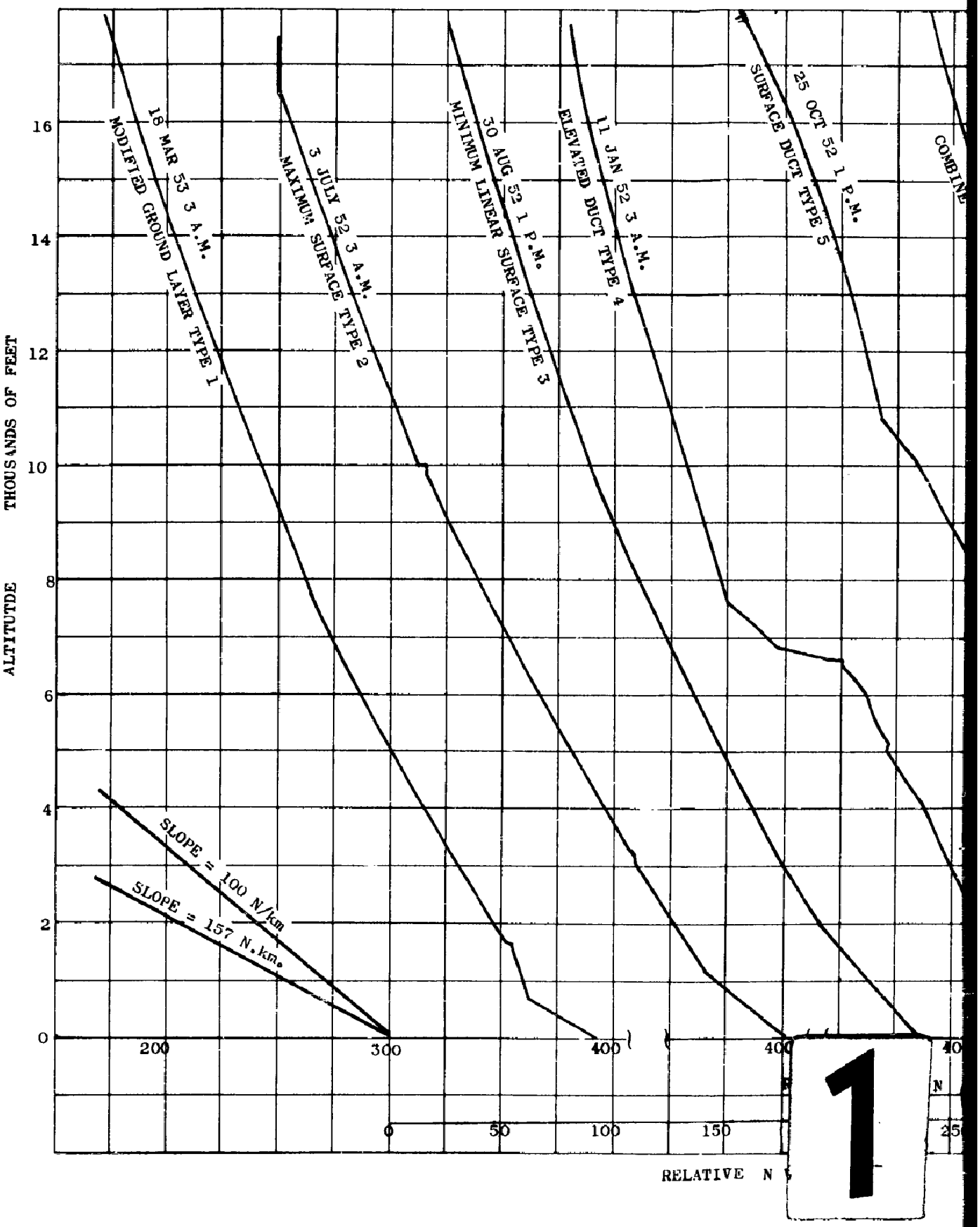
ALTITUTDE THOUSANDS OF FEET
16
14
12
10
8
6
4
2
0
MODIFIED GROUND LAYER TYPE 1
18 MAR 53 3 A.M.
MAXIMUM SURFACE TYPE 2
3 JULY 52 3 A.M.
MINIMUM LINEAR SURFACE TYPE 3
30 AUG 52 1 P.M.
ELEVATED DUCT TYPE 4
11 JAN 52 3 A.M.
SURFACE DUCT TYPE 5
25 OCT 52 1 P.M.
COMBINE
SLOPE = 100 N/km
SLOPE = 157 N.km.
200
300
400
400
0
50
100
150
RELATIVE N
1

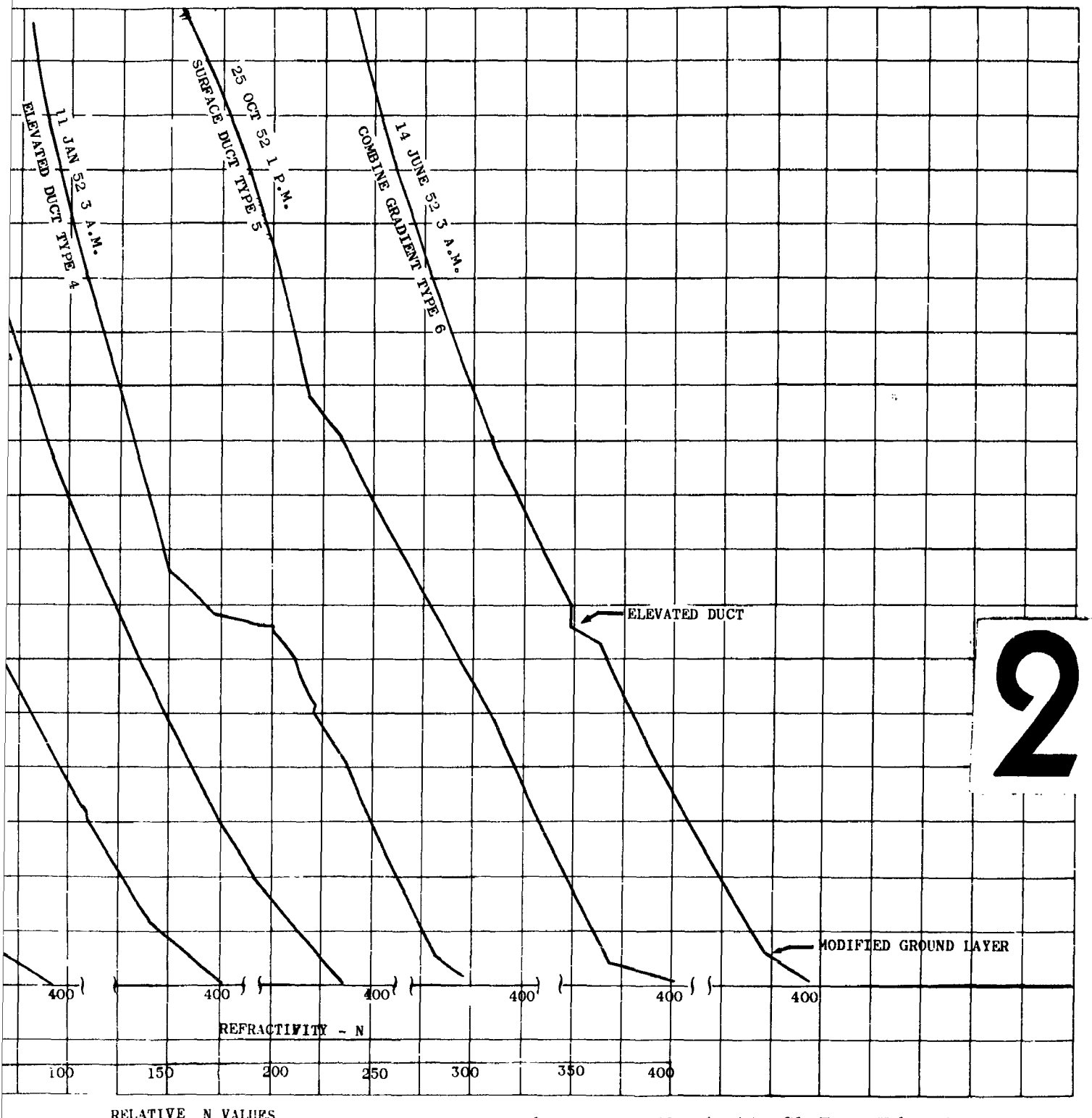

Figure 41. Refractivity vs. Altitude (6 Profile Types Taken at Truk Island, Weather Station No. 99999)

The reduced scatter in this data, as compared to the data calculated from artificially perturbed profiles, should be observed. The range from maximum to minimum tropospheric range aberration at 45 degrees is 8.86 feet to 12.49 feet. This represents a range of approximately ± 17 percent, substantially less than the 38 percent obtained with the artificial data.

5.6 CORRECTIONS AND RESIDUAL ERRORS

5.6.1 Potential Correction Techniques

There are many possible correction techniques available for reduction of tropospheric range aberration effects. The particular technique to be used is determined by the system accuracy required, combined with an appraisal of the expense of collecting and processing the necessary information needed to obtain the required accuracy of correction.

The following parameters are available for use in describing the range correction (at differing rates and degrees of accessibility in a practical sense):

N_S - surface refractivity - available continuously from weather instruments or refractometers

$N_{0.1}$ - refractivity at 0.1 Km above the tracking site - available continuously if tower-mounted instruments are used

N_1 - refractivity at 1.0 Km above the site - available continuously if tethered balloons are used - available periodically from radiosondes

H_S - station altitude above sea level - known

N(h) - profile of refractivity vs altitude - available periodically from radiosondes

FF - form factor of profile; $(FF(N(h)) = \int Ndh)$ - available periodically

ΔN - change in refractivity in first kilometer, $(\Delta N = N_S - N_1)$ - available periodically

Grad N - initial gradient in N(h); Grad $N = 10 (N_S - N_{0.1})$ - available continuously from tower instruments - available periodically from radiosondes

During the preliminary stages of the investigation, it appeared that a real-time correction for variations in refractivity as indicated by accessible surface parameters was not only desirable, but was readily feasible. Table 7 lists eleven different possible combinations of parameters in an approximate order of increasing difficulty of implementing the corrections.

Table 7. Potential Correction Techniques
(Listed in approximate order of expense or difficulty)

TYPE	VARIABLES INVOLVED	TYPE OF CORRECTION	CORRECTION WOULD BE BASED ON:
1	K_0 (a constant)	Fixed and identical for all tracking sites	World-wide mean refractivity value $N_S = 330$
2	$K_1 (H_S)$ Site altitude only	Fixed, but different for each tracker	N_S calculated for each site altitude
3	$K_2 (N_S)$ Site climate	Fixed, but different for each tracker	Average value of refractivity for weather station nearest each Site
4	$K_3 (t, N_S)$ Site climate	Fixed, but value of correction changed at 4- to 12-hour intervals	Average Values of N_S for each time of day and month of year. Data from nearest weather station
5	$K_4 (T, P, R, H)$ Local meteorological conditions	Manually adjustable correction	Calculated values of N_S taken from periodic measurements at each tracker of temperature, pressure and relative humidity
6	$K_5 (F.F.)$ Local meteorological conditions	Manual adjustment	Form factor of profile taken by radiosonde at intervals
7	$k_1 (N_S)$ Local meteorological conditions	Automatic, real-time adjustment	Instantaneous N_S at site using a microwave refractometer (correction referred to a reference profile)
8	$k_2 (N_S) + K_6 (F.F.)$ Local meteorological conditions	Automatic, real-time first-order correction plus manual, periodic, second-order adjustment	Instantaneous N_S at site plus radiosonde profiles taken at intervals

Table 7. Potential Correction Techniques (Continued)
(Listed in approximate order of expense or difficulty)

TYPE	VARIABLES INVOLVED	TYPE OF CORRECTION	CORRECTION WOULD BE BASED ON:
9	$k_3 (N_S) + k_4 (GRAD_n)$ Local meteorological conditions	Automatic, real-time, first- and second-order correction	Instantaneous N_S at site surface plus instantaneous No. 1 read by refractometer on 0.1 Km tower
10	$k_5 (N_S) + k_6 (GRAD_n) + k_7$ (F. F.) local meteorological conditions	Automatic first- and second-order corrections plus manual periodic adjustment for third-order effect	As above, plus added correction for Form Factor of profile derived periodically from radiosonde data
11	$k_7 (N(h))$ Local meteorological conditions	Automatic, full-profile correction	(This would be an idealized theoretical limit, not achievable with present techniques)

It should be noted that any type of correction mechanism must be handles in two parts; one part for determining the correction required at the zenith and the horizon, and the second part for determining the effect of changing elevation angles. Table 7 presents some different methods for determining the zenith and horizon corrections.

Evaluating some of the errors for different methods of correction shows that at 45 degrees:

a. The type 1 correction yields a maximum error of 2.45 feet, or 21.8 percent.

b. The type 2 correction (involving fixed corrections for site altitude, H_s) yields a 0.429-foot error RMS, or 3.8 percent.

c. The type 7 correction (involving real-time surface refractivity) would give an RMS error of 0.378 foot or 3.1 percent.

d. The type 9 correction (including initial gradient of refractivity, Grad N) would give a residual RMS error of 0.361 foot or 2.98 percent.

Time did not permit analysis of the residual errors resulting from combinations involving the Form Factor, as discussed in type 6, 8 and 10 of Table 7.

5.6.2 Residual Errors

Having observed that there is a fair degree of correlation between N_s, H_s, initial gradient, and the total tropospheric range aberration, it was felt that a multiple regression* analysis of effects of TRA upon N_s plus one or more of the parameters mentioned in paragraph 5.6.1 would be profitable. It was expected to show how much of the tropospheric range error can be compensated for, and the relative complexity of the necessary hardware to implement the different correction techniques.

An available computer program was used to determine the various regression coefficients. The data for the 77 profiles was fed into this program to analyze ten different combinations of the desired parameters. The coefficients for the ten possible regression equations as determined by this computer program are given in Table 8.

---

* When a scatter diagram (see for example Figures III-4 and III-5 of Appendix III) shows that some pair of variables (such as TRA and N_s) are connected by a physical law, the use of regression analysis enables the nature of the physical law and the degree of correlation between the two variables to be determined. The solid lines drawn on Figures III-4 and III-5 represent an approximation to the actual physical law connecting in this case surface refractivity with total range aberration. Since the two variables are connected in an irregular manner, the points are scattered above and below the line, rather than falling ideally exactly upon it. Regression analysis provides a systematic technique for estimating the unspecified constants which define the slope, and the axis intercepts of such lines (known as regression lines). The

There are three regression equations shown for each combination of data, since the analysis was carried out for the zenith ray, the horizontal ray, and an intermediate ray at 45 degrees. It should be noted that this table shows the deviations and the probable errors for only that part of the correction which is based upon profile characteristics, i.e., the error due to the function of elevation angle has not been included in this table.

It can be seen that as the number of factors employed in the regression analysis is increased, the accuracy of the results improve. This is illustrated in Table 9. For example, a combination of N_S and H_S gives a sizeable improvement at all tracking angles over a correction based on either H_S or N_S alone. However, the additional factors used in the regression analysis do not improve the high-angle accuracy significantly. For tracking at low elevation angles, it can be seen that the inclusion of a gradient of the N term gives a quite significant improvement.

It is felt that the small increase in accuracy obtained by adding the change in refractivity, ΔN, to the total equation is not justified in comparison to the additional cost of measuring this parameter. Accordingly, it is recommended that corrections for tropospheric range aberration be based on the regression techniques shown as No. 7 in Table 8. This technique involves the use of information on H_S (station altitude), N_S (surface refractivity) and Grad N, (initial gradient of refractivity). The value of Grad N is most reasonably obtained by refractometer measurements taken at both the top and bottom of a tower a few hundred feet high. For the purpose of analysis, it has been assumed that the initial gradient was obtained by measurements at the top and bottom of a tower 100 meters high.

It is recognized that one assumption upon which this regression analysis was based is that the effect of the various parameters upon TRA is cumulative in a linear manner. It is, of course, possible to investigate regression equations in which various powers, cross-products, or other functions of the variables involved are considered. Time did not permit such an analysis, and it was felt unnecessary, in that the low residual error shown by the selected analysis appears to be quite adequate (0.1527 foot out of 11 feet total range aberration at 45 degrees).

---

equation of a sample regression line of y on x is $y' = a + b\,x$, where the regression coefficient, b, and the y - intercept, a, are obtained by mathematical techniques described in standard works on statistical analysis (e. g. Statistics Manual by Edwin L Crow, A. Davis and M. W. Maxfield, Section 6.1).

If the variable in question depends linearly on several factors, it is possible to use a similar technique known as "multiple regression" to obtain the coefficients of an equation connecting the unknown variable with the various possible values of the known parameters. Such an equation would be of the form:

$$y' = a_1 + b_1 x_1 + b_2 x_2 + \ldots + b_k x_k.$$

ϵ	i	A_i Ft.	B_i Ft.	C_i Ft.	D_i Ft.	E_i NUMERIC
0°	1	-12.2995	1.03429	0	0	0
	2	-28.3630	1.17897	-.288777	0	0
	3	-39.4063	1.24814	0	-0.0083089	0
	4	-16.3821	1.08598	-.313435	-0.4103691	0
	5	352.5533	0	0	0	-0.0156675
	6	-0.7315	1.00282	0	0	-0.0008640
	7	-57.587130	1.2601972	-.29377172	0	+0.002162169
	8	-58.0675	1.30668	0	-0.879378	+0.00128141
	9	-38.1414	1.15416	-.313709	+0.357433	+0.00149554
	10	6.9658	0.98029	0	0	-0.00548438
45°	1	3.9197	0.0219649	0	0	0
	2	3.85795	0.0225212	-0.00111025	0	0
	3	3.53372	0.0250101	0	-0.0118626	0
	4	3.57206	.0247401	-0.000521839	-0.0097923	0
	5	11.78435	0	0	0	-0.000428648
	6	6.94167	.0137463	0	0	-0.000225728
	7	6.8249427	.014274744	-0.00060313458	0	
	8	6.67650	.0151516	0	-0.00406704	06

Table 8. Coefficients in the Regression Equations
TRA (ϵ) = $A_i + B_i N_S + G_i$ Grad $N + D_i \Delta N + E_i H$

C_i Ft.	D_i Ft.	E_i NUMERIC	STANDARD DEVIATION (Ft.)	PROBABLE ERROR (Ft.)	PARAMETERS INVOLVED	ACCURA
0	0	0	42.52	28.88	N_S	8
88777	0	0	34.12	23.33	N_S, Grad	4
0	-0.0083089	0	41.55	28.41	N_S ΔN	9
13435	-0.4103691	0	33.90	23.34	N ΔN, Grad	2
0	0	-0.0156675	50.13	34.04	H_S	10
0	0	-0.0008640	42.51	29.06	N_S, H_S	7
0377172	0	+0.0021621694	34.01	23.41	N, Grad, H	3
0	-0.879378	+0.00128141	41.52	28.58	N, ΔN, H	5
13709	+0.357433	+0.00149554	33.85	23.46	N, ΔN, Grad, H	1
0	0	-0.00548438	42.44	29.02	N, e^{H_S}	6
0	0	0	0.3740	0.2534	N_S	9
0111025	0	0	.3610	.2468	N, Grad	8
0	-0.0118626	0	.3513	.2401	N, ΔN	7
00521839	-0.0097923	0	.3490	.2402	N, ΔN, Grad	6
0	0	-0.000428648	.4293	.2916	H_S	10
0	0	-0.000225728	.2273	.1554	N_S, H_S	4
0060313458	0	-0.00021951529	.2212	.1522	N, Grad, H	
0	-0.00406704	-0.000215806	.2234	.1538	N, ΔN, H	

Table 8. Coefficients in the Regression Equations

$TRA(\epsilon) = A_i + B_i N_s + G_i \text{ Grad } N + D_i \Delta N + E_i H_s$

	E_i NUMERIC	STANDARD DEVIATION (Ft.)	PROBABLE ERROR (Ft.)	PARAMETERS INVOLVED	RANKING ACCURACY	RANKING DIFFICULTY
	0	42.52	28.88	N_S	8	2
	0	34.12	23.33	N_S, Grad	4	5
9	0	41.55	28.41	$N_S \Delta N$	9	7
1	0	33.90	23.34	N ΔN, Grad	2	9
	-0.0156675	50.13	34.04	H_S	10	1
	-0.0008640	42.51	29.06	N_S, H_S	7	3
	+0.0021621694	34.01	23.41	N, Grad, H	3	6
	+0.00128141	41.52	28.58	N, ΔN, H	5	8
	+0.00149554	33.85	23.46	N, ΔN, Grad, H	1	10
	-0.00548438	42.44	29.02	N, e^{H_S}	6	4
	0	0.3740	0.2534	N_S	9	2
	0	.3610	.2468	N, Grad	8	5
3	0	.3513	.2401	N, ΔN	7	7
3	0	.3490	.2402	N, ΔN, Grad	6	9
	-0.000428648	.4293	.2916	H_S	10	1
	-0.000225728	.2273	.1554	N_S, H_S	4	3
	-0.00021951529	.2212	.1522	N, Grad, H	2	6
)4	-0.000215806	.2234	.1538	N, ΔN, H	3	8

ϵ	i	A_i Ft.	B_i Ft.	C_i Ft.	D_i Ft.	E_i NUMERIC
45° (Cont.)	9	6.70714	.0149171	-0.000482349	-0.00216536	-0.00021547
	10	5.58353	.0173015	0	0	-0.00047366
90°	1	2.76495	0.01557	0	0	0
	2	2.72141	.0159668	-0.0007827	0	0
	3	2.49212	.01772721	0	-0.00838491	0
	4	2.51902	.0175376	-0.00036619	-0.00693216	0
	5	8.34175	0	0	0	-0.00030414
	6	4.91351	.0097313	0	0	-0.00016049
	7	4.8318364	.010101051	-0.00042202388	0	-0.00015614
	8	4.72861	.0107114	0	-0.00283726	-0.00015357
	9	4.75008	.0105471	-0.000338093	-0.00150431	-0.00015334
	10	3.95474	.0122398	0	0	-0.00033870

Table 8. Coefficients in the Regression Equati

TRA (ϵ) = $A_i + B_i N_S + G_i$ Grad N + $D_i \Delta N + E_i H_S$ (C

C_i Ft.	D_i Ft.	E_i NUMERIC	STANDARD DEVIATION (Ft.)	PROBABLE ERROR (Ft.)	PARAMETERS INVOLVED	AC
-0.000482349	-0.00216536	-0.000215477	.2203	.1527	N, ΔN, Grad, H	
0	0	-0.000473660	.2953	.2019	N, e^{H_S}	
0	0	0	0.2658	0.1805	N_S	
-0.0007827	0	0	.2567	0.1755	N, Grad	
0	-0.00838491	0	.2498	0.17084	N, ΔN	
-0.00036619	-0.00693216	0	.2483	0.1709	N, ΔN, Grad	
0	0	-0.00030414	.3042	0.2066	H_S	
0	0	-0.00016049	.1614	0.1104	N_S, H_S	
-0.00042202388	0	-0.00015614152	.1573	0.1082	N, Grad, H	
0	-0.00283726	-0.00015357	.1588	0.1093	N, ΔN, H	
-0.000338093	-0.00150431	-0.00015334	.1566	0.1086	N, ΔN, Grad, H	
0	0	-0.00033870	.2091	0.1430	N, e^{H_S}	

2

Table 8. Coefficients in the Regression Equations

$TRA(\epsilon) = A_i + B_i N_s + G_i \text{ Grad } N + D_i \Delta N + E_i H_s$ (Continued)

E_i NUMERIC	STANDARD DEVIATION (Ft.)	PROBABLE ERROR (Ft.)	PARAMETERS INVOLVED	RANKING	
				ACCURACY	DIFFICULTY
-0.000215477	.2203	.1527	N, ΔN, Grad, H	1	10
-0.000473660	.2953	.2019	N, e^{H_s}	5	4
0	0.2658	0.1805	N_s	9	2
0	.2567	0.1755	N, Grad	8	5
0	.2498	0.17084	N, ΔN	7	7
0	.2483	0.1709	N, ΔN, Grad	6	9
-0.00030414	.3042	0.2066	H_s	10	1
-0.00016049	.1614	0.1104	N_s, H_s	4	3
-0.00015614152	.1573	0.1082	N, Grad, H	2	6
-0.00015357	.1588	0.1093	N, ΔN, H	3	8
-0.00015334	.1566	0.1086	N, ΔN, Grad, H	1	10
-0.00033870	.2091	0.1430	N, e^{H_s}	5	4

Table 9. Residual Tropospheric Range Aberration After Various Atmospheric Corrections
(1 σ value in feet)

PARAMETERS USED IN CORRECTION	TRACKING ANGLE, "ϵ"		
	90°	45°	0°
H_S	.3042	.4293	50.13
N_S	.2658	.3740	42.52
H_S & N_S	.1614	.2273	42.51
H_S, N_S & ΔN	.1588	.2234	41.52
H_S, N_S & Grad N	.1573	.2212	34.01
H_S, N_S, ΔN & Grad N	.1566	.2203	33.85

5.6.3 Methods of Implementing Correction

5.6.3.1 Digital Computers. As has been mentioned previously, it is possible to utilize a large-scale digital computer to determine the tropospheric range aberration. This calculation may be done on the basis of integrating a known or an assumed profile of refractivity vs. altitude and solving the ray-tracing equation appropriate to the elevation angle in use. If this is to be done on a real-time basis, it requires a very large computer capability. A technique that has been used, therefore, is to pre-calculate the corrections for a large number of profiles and to store the results as a function of elevation angle and profile type. The stored results are then extracted as needed by the tracking computer, using a table look-up technique. Since there are an infinite number of profiles, with an infinite number of perturbations possible on each type of profile, to obtain a good approximation to the proper correction by this technique requires a prohibitive amount of computer storage capacity.

5.6.3.2 Analog Computers. The techniques of performing the range aberration correction which seems most suitable involve the determination of TRA (0) and TRA (90) by regression techniques, and converting these two values into a TRC (ϵ) by utilizing an angle function (as described in paragraph 3.1 of Appendix III). This technique lends itself to utilization of simple, straight-forward analog computer techniques. The constants a, b, c, and e and the values of H_S in the regression equation can be set in on manually adjusted potentiometers since they never change for a given station. The variable inputs to the analog device would then be the value of the elevation angle, the value of surface refractivity and the value of

refractivity at 0.1 kilometer. From the two values of refractivity, N_s and $N_{0.1}$, the initial gradient of N for entry into the regression equation can then be readily determined. Two regression equation solvers are required, one to provide TRA(0) and the other to provide TRA(90). The accuracies required in a correction of this sort are well within the capabilities of straight-forward analog computing devices.

5.6.3.3 Profile Data Acquisition. The usual method of obtaining information on the profile of refractivity vs. altitude is to employ radiosonde balloons or rockets. From the meteorological data obtained from the radiosonde, the refractivity index may be calculated at each data point. The current expression for this conversion is one given by Smith and Weintraub (Reference III-63):

$$N = \frac{77.6}{T} \left(P + 4810 \frac{e_s RH}{T} \right)$$

(The terms used in this equation are identified in the glossary at the end of Appendix III.)

Instead of converting the humidity, temperature, and pressure data acquired by meteorological instruments into a calculated index of refraction, a microwave refractometer (see paragraph 5.6.3.4) can be used and leads to a more direct solution of the problem.

It should be remembered that under the recommended method of performing the correction, it is completely unnecessary to have detailed information about the profile of refractivity at high altitudes. This data would only be useful in case the alternate correction technique employing "form factors" is to be used, or in the event that this work is expanded to utilize periodic form factor information plus instantaneous surface data.

5.6.3.4 Refractometers. The most straight-forward method for obtaining information on surface refractivity and initial gradient of refractivity is by the use of a microwave refractometer. The type developed by C. M. Crain (Reference IV-4) at the University of Texas, or the slightly different type now being used at the National Bureau of Standards at Boulder, Colorado, are both suitable. Reduced to its essentials, the Crain microwave refractometer is a pair of microwave oscillators whose frequencies are determined by electrically identical resonant cavities. One cavity is sealed so that the frequency at which it resonates is not affected by changes in atmospheric conditions. The second cavity is vented to the atmosphere and the pressure, temperature, and relative humidity changes in the atmosphere are reflected by changes in its resonant frequency. The difference between the resonant frequencies of the two oscillators, then, is a direct measure of the refractivity of the sample of air in the vented cavity. Suitable microwave refractometers have been manufactured and sold by the University of Texas (Dr. Straiton); the Aerial Electronics Co., Fairborne, Ohio; and Boulder Scientific Co. at Boulder, Colorado.

5.6.4 Residual Errors

An error analysis was made for the recommended correction technique. The analysis assumed that the regression employing N_S, Grad N, and H_S is used to obtain TRC (0) and TRC (90) and that the Bowers expression is used to convert these two values into the correction at intermediate angles, TRC (ϵ). Table 10 shows the residual error in terms of absolute feet, and in percentage of the actual required correction. The last column of percent error is the root-mean-square value of the magnitudes of the 77 differences between the aberrations (as calculated by profile integration) and the corrections (as calculated by the approximation method described), divided by the aberration for each profile calculated.

Table 10. Residual Range Error (TRRE)
After Recommended Tropospheric Correction

ELEVATION ANGLE "ϵ" (degrees)	TRC MEAN CORRECTION (feet)	TRRE RMS ERROR (feet)	PERCENT ERROR RMS (percent)
0	334.07	33.27	10.80
1	-	38.27	13.75
2	-	12.93	8.38
5	-	3.39	4.52
10	44.52	1.01	2.30
15	30.37	0.61	2.02
30	-	0.36	2.64
45	11.26	0.22	1.93
60	-	0.23	2.64
90	7.97	0.15	1.94

A histogram showing the distribution of the percent errors for each of the 77 profiles at five representative angles is shown in Figure 42. It can be seen that the extreme error is less than eight percent down to an elevation angle of 10 degrees. From Table 10 it was seen that the root-mean-square error is less than 2.4 percent down to the same tracking angle. The tendency toward "skewness" in the data (which is most apparent at low elevation angles) is

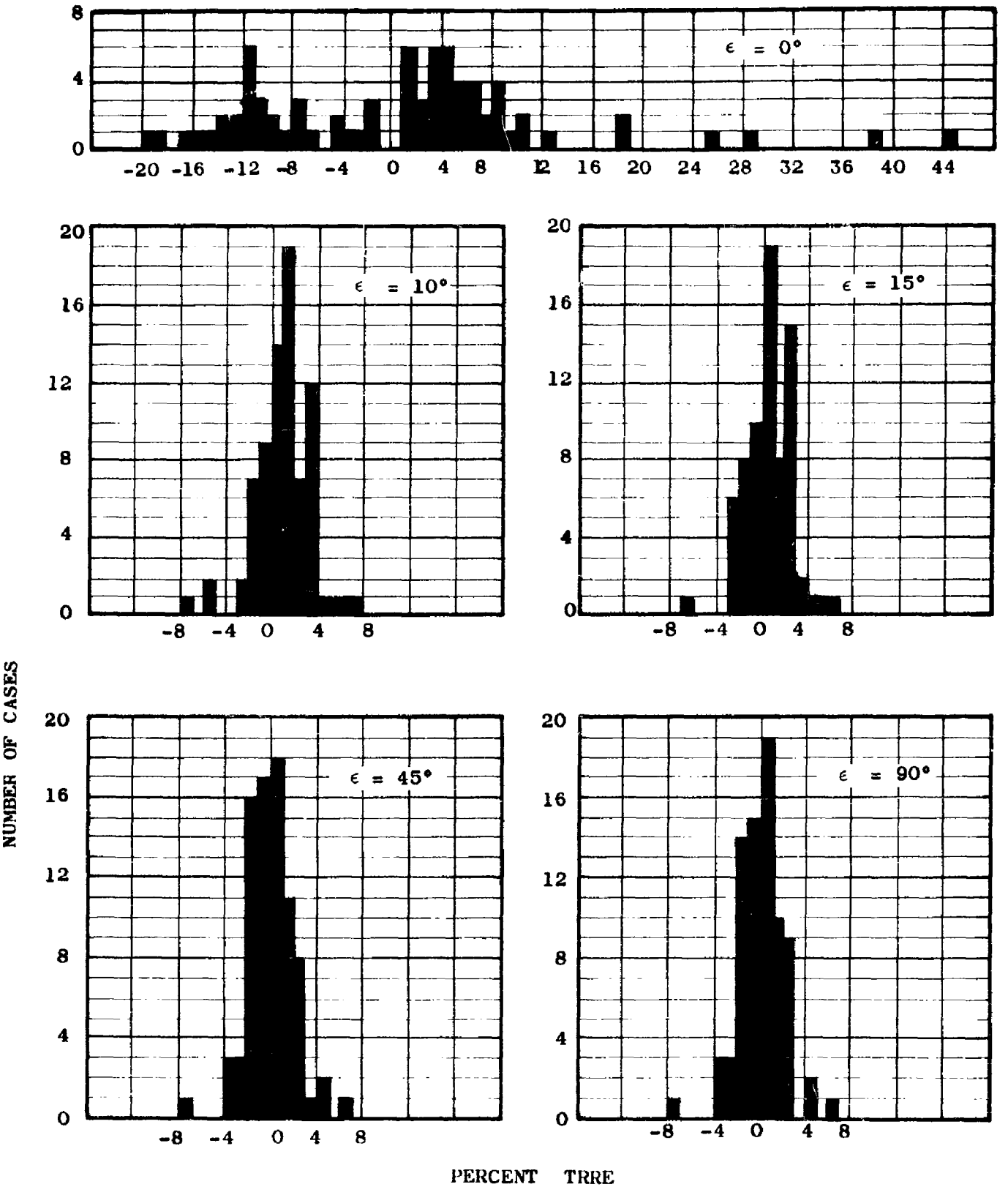

Figure 42. Histogram Showing Distribution of Percent Errors For 77 Profiles

caused by the calculation technique, in that the regression equation tends to underestimate large corrections and overestimate the small corrections. This leads to a preponderance of percent errors having the positive sign.

5.6.4.1 Expected Performance. The 77 actual profiles tested are not a statistical sample of average weather conditions. The class of ducting profiles represent conditions which occur only a small fraction of the time. The "MAX" and "LIN" profiles are for extreme values of N_S and will enclose a large population of profiles having intermediate values of N_S.

For this reason the results of an error correction technique based on this data will show a greater RMS residual error than should be expected when the same technique is applied to the general run of weather changes encountered at any one tracking site. The quoted errors, therefore, are to be treated as being pessimistic and conservative.

5.7 SUMMARY, LIMITATIONS, AND RECOMMENDATIONS

5.7.1 Summary

The above effort may be recapitulated by the following statements:

a. The magnitude of the tropospheric range aberration has been examined for 77 representative profiles covering a wide range of geographical and meteorological conditions. It has been observed that for low elevation angles, particularly, the range of aberrations is so great that it is impractical to attempt a correction based on a mean or average value of the aberration.

b. The dependence of the aberration upon surface-accessible parameters has been examined, and a significant correlation between TRA and N_S, Grad N, and H_S has been found. It has been determined that statistical regression techniques leading to a linear equation utilizing only these parameters provide an adequate correction for tropospheric range effects without requiring knowledge of the upper atmosphere.

c. Justification has been found (see Appendix III) for a recommendation that whenever possible, tracking sites be located at high altitudes in a dry climate.

d. Consideration of the effect of changing elevation angles and of the effects of diurnal and seasonal variations in the weather lead to the conclusion that a real-time solution for the tropospheric range correction is required.

e. A proposed correction technique has been presented which is readily applicable (by means of straight-forward analog computing devices) to a practical tracking station. This technique leaves a residual range error due to tropospheric effects of less than 2.5 percent of the total aberration down to a tracking angle of ten degrees. This same technique still gives reasonably adequate correction at tracking angles below ten degrees.

5.7.2 Effects Not Included in This Study

Ionospheric effects have not been studied in detail in this initial phase of the study. The magnitude of range aberration at microwave frequencies due to the ionosphere is a second-order effect compared to the tropospheric range aberration. Consideration of potential corrections for ionospheric refraction should be included, however, in any extension of this work.

The range-rate effects of turbulence and "blobs" or inhomogeneities in the atmosphere have not been included in this study.

The mathematical analysis used for the tropospheric aberration does not include the slight difference between a straight ray delayed by the troposphere and a curved ray which is bent, as well as delayed, by the atmosphere. (This effect has been shown by several investigators to be negligible in comparison to the total TRA.)

The possibility of ray trapping in an atmospheric duct was not included in the integration process used to obtain the values of TRA employed in the regression analysis.

Calculations have not been made for the reduced corrections required if the target being tracked lies within the troposphere. It has been assumed that all targets considered during this study were above 100,000 feet altitude.

All calculations have been made assuming a spherically stratified atmosphere. This ignores the fact that, at angles other than the vertical, the ray passes through an atmosphere which is somewhat different from the profile above the station where the weather data was obtained. Bean and Cahoon (Reference III-14) have shown that, at elevation angles down to about four degrees, this effect is entirely negligible.

5.7.3 Recommended Further Efforts

At the end of the study contract period several promising areas of investigation had not been analyzed. It is recommended that an extension of this effort be undertaken to include the following:

a. Current efforts to provide a profile form factor (utilizing weighted segments of the profile) to obtain TRC (0) should be continued.

b. An investigation of the improvement in accuracy obtainable by utilizing a combination of profile form factor data (taken at periodic intervals) and real-time data on the changes in surface parameters should be undertaken. Acquisition and analysis of a large number of time-spaced profiles, for a statistically significant number of other stations should be initiated.

c. The computer program for the statistical regression analysis should be re-examined to determine the feasibility of including the effect of cross product and other second-order terms.

d. Additional work should be expended on improving the functional relationship between elevation angle and tropospheric correction. This would involve deriving the equation in such a way that the errors could be matched at 90 degrees and 10 degrees (instead of at 90 degrees and 0 degrees), or a derivation which would include a weighting factor to accommodate the increased contribution of the low-altitude part of the atmosphere at low elevation angles.

e. The range error contribution by ionospheric effects should be evaluated, and suitable correction techniques developed.

f. The error in range-rate due to atmospheric turbulence and "blobs" should be investigated in some detail, and the resultant error contributions included in the tracking system model analysis.

SECTION VI

CONCLUSIONS

6.1 The major conclusions to be drawn from this study can be summarized as follows:

(1) For the baseline lengths considered (200- to 3,000- nautical miles) and the current state of the art in the area of time synchronization (1.0 microsecond), tracking systems which measure only range yield significantly greater accuracy in tracking cisluna spacecraft than can be attained by systems which measure range sums or range differences.

(2) The effect of inaccuracies in surveying the location of the tracking stations of a three-range-only tracking system produces a significant degradation in tracking accuracy. In other words, a tracking system surveyed-in with the best of classical geodetic techniques shows errors in spacecraft position which are an order of magnitude larger than those of the same system with zero survey error.

(3) The employment of a geodetic satellite for surveying-in the tracking system appears to offer a significant improvement in surveying accuracy and thus in the over-all tracking accuracy.

(4) The residual RMS error (after real time correction) in the radio measurement of slant range (due to tropospheric propagation effects) can be made sufficiently small to be negligible, e.g., less than one foot at slant range elevation angles down to 10 degrees. The residual RMS error can be kept to less than 13 feet for elevation angles down to 2 degrees.

SECTION VII

BIBLIOGRAPHY

I. TRACKER SYSTEM ERROR MODEL AND SIMULATION

I-1. Chuji, Tsuboi, A New and Simple Method of Calculating the Deflections of the Vertical from Gravity Anomalies with the Aid of the Bessel Fourier Series, Proced. of Japan Acad., Vol. 30, 1950, No. 6.

I-2. Davis, T. L. and Doherty, R. H., Widely Separated Clocks with Microsecond Synchronization and Independent Distribution Systems, 1969 IRE WESCON Convention Record, Part 5, Pages 3-17.

I-3. Hermes Electronics Co., Proposal for Accurate Time Synchronization Utilizing Meteor Burst Techniques, 17 April 1959.

I-4. Morgan, A. H., Precise Time Synchronization of Widely Separated Clocks, National Bureau of Standards, Boulder, Colorado, Tech. Note No. 22, July 1959.

I-5. Reder, F. H. and Winkler, G. M. R., World-Wide Clock Synchronization, IRE Trans. on Military Electronics, Vol. MIL-4, No.'s 2-3, Pages 336-376, April-July 1960.

I-6. Wills, A. P., Vector Analysis with an Introduction to Tensor Analysis, Prentice Hall Inc., New York, 1931, Chapter 7.

II. SURVEYING OF THE TRACKING SYSTEM WITH AN EARTH SATELLITE

II-1. Encyclopedia of Physics, Vol. XXIV, 1956, Page 31.

II-2. Davis, R. J., Whipple, F. L., and Zirker, J. B., The Orbit of a Small Earth Satellite, Van Allen, ed., Scientific Uses of Earth Satellites, Pages 1-22.

II-3. Heiskanen, W. A., New Era of Geodesy, Science, Lancaster, Pa. 121, 48 (1955) Symposium: New Era of Geodesy Bull. Geod. 1955, Nr. 36,55.

II-4. Johns, R. K. C., Geodetic Applications of Artificial Satellites, Lab. for Electronics, Boston.

BIBLIOGRAPHY (Continued)

II-5. Vaisala, Y., An Astronomical Method of Triangulation, Sitz. d. finnischen Akad. Wiss. 1946, Pages 99-107.

II-6. Veis, G., Geodetic Applications of Observations of the Moon, Artificial Satellites, and Rockets, 1958 Thesis, Ohio State Univ., Page 165.

II-7. Veis, G., Geodetic Uses of Artificial Satellites, Smithsonian Contribution to Astrophysics, 1960, Vol. 3, No. 9.

II-8. Whitney, C. A. and Veis, G., A Flashing Satellite for Geodetic Studies, Smithsonian Astrophysics Obs. Spec. Rep. 1958, No. 19, Pages 9-19.

III. TROPOSPHERIC PROPAGATION EFFECTS

III-1. Ament, W. S., Airborne Radiometeorological Research, Proceedings of the IRE, Vol. 47, No. 5, Part I, May 1959, Pages 756-761.

III-2. Anderson, J. J., Symposium on Present and Future Uses of Refractive Index Data for Radio Propagation Purpose, IRE Transactions on Antennas and Propagation 1957, Page 147.

III-3. Anderson, Beyer & Fanin, Comparison of Computed with Observed Atmospheric Refraction IRE Trans, AP-7, July 1959, Page 258.

III-4. Archer, Douglas H., Absorption and Refraction of Electromagnetic Waves in an Ionized Atmosphere, General Electric Report RM-59 TMP-11, 13 February 1959, ASTIA AD 230277.

III-5. Archer, Douglas H., Refraction of Electromagnetic Waves in an Absorbing Medium, General Electric Report RM 59 TMP-27, 10 June 1959, ASTIA AD-230-276.

III-6. Birnbaum, G. and Bussey, H. E., Amplitude, Scale, and Spectrum of Refractive Index Inhomogenieties in the First 125 Meters of the Atmosphere, Reprinted from the Proceedings of the IRE, Vol. 43, No. 10, October 1955, Pages 1412-1418.

III-7. Bean, B. R., Atmospheric Bending of Radio Waves, Electromagnetic Wave Propagation, Academic Press, Pages 163-181.

III-8. Bean, B. R., First Meeting on Radio Climatology, Proceedings of the IRE, Vol. 46, No. 7, July 1958.

BIBLIOGRAPHY (Continued)

III-9. Bean, B. R., Climatology of Ground-Based Radio Ducts, Journal of Research of the National Bureau of Standards - D. Radio Propagation, Vol. 63D, No. 1, July-August 1959, Pages 29-34.

III-10. Bean, B. R., The Geographical and Height Distribution of the Gradient of Refractive Index, Proceedings of the IRE, Vol. 41, No. 4, April 1953, Page 549.

III-11. Bean, B. R., Prolonged Space-Wave Fadeouts at 1,046 MC Observed in Cheyenne Mountain Propagation Program, Proceedings of the IRE, Vol. 42, No. 5, May 1954, Pages 848-853.

III-12. Bean, B. R. and Cahoon, B. A., A Note on the Climatic Variation of Absolute Humidity, Bulletin of the American Meteorological Society, Vol. 38, No. 7, September 1957, Pages 395-398.

III-13. Bean, B. R. and Cahoon, B. A., Effect of Atmospheric Horizontal Inhomogeneity Upon Ray Tracing, Journal of Research of the National Bureau of Standards-D. Radio Propagation, Vol. 63D, No. 3, November-December 1959, Pages 287-292.

III-14. Bean, B. R. and Cahoon, B. A., The Use of Surface Weather Observations to Predict the Total Atmospheric Bending of Radio Waves at Small Elevation Angles, Proceedings of the IRE, Vol. 45 No. 11, November 1957.

III-15. Bean, Cahoon & Thayer, Tables for the Statistical Prediction of Radio Bending and Elevation Angle Error, Using Surface Refractivity. N.B.S. Technical Note No. 44, 16 March 1944.

III-16. Bean, B. R. and Dutton, E. J., On the Calculation of the Departures of Radio Wave Bending From Normal, Journal of Research of the National Bureau of Standards - D. Radio Propagation, Vol. 63D, No. 3, May-June 1960, Pages 259-263.

III-17. Bean, B. R. and Horn, J. D., Radio-Refractive Index Climate Near the Ground, Journal Research NBS - Radio Propagation, Vol. 63D, No. 3, November-December 1959, Page 259.

III-18. Bean, B. R. and Horn, J. D., On the Climatology of the Surface Values of Radio Refractivity of the Earth's Atmosphere, NBS Report 5559, 3 March 1958, Pages 3, 5, Table II and Fig. 8.

III-19. Bean, B. R., Horn, J. D. and Riggs, L. P., Telecommunication Performance Standard Tropospheric Systems, Vol. 5 of 6, Chapter 3: Radio-Meteorological, Section 1: Introduction, Section 2: Radio Refractive Index Climatology, PM 83-30-1.

BIBLIOGRAPHY (Continued)

III-20. Bean, B. R., Horn, J. D. and Riggs, L. P., National Bureau of Standards Tropospheric Systems, Vol. 5 of 6, Chapter 3, Radio Meteorological Standards, Section 3. Climatology of Ground-Based Radio Ducts and Section 4. Synoptic Radio Meteorology.

III-21. Bean, B. R., Horn, J. D. and Riggs, L. P., Telecommunications Performance Standard Tropospheric Systems, Vol. 5 of 6, Chapter 3 Radio-Meteorological Standards, Section 5 Techniques for Computing Bending, Section 6 The Exponential Reference Atmosphere, Appendix B, NBS Memo Report PM-83-30-3.

III-22. Bean, B. R., Horn, J. D. and Riggs, L. P., Telecommunications Performance Standards, Chapter 3, Radio-Meteorological Standards, Section 7 Fading Regions Within the Horizon, Section 8 Attenuation of Microwaves, PM-83-30-4, June 30, 1960.

III-23. Bean, B. R. and Meaney, F. M., Some Applications of the Monthly Median Refractivity Gradient in Tropospheric Propagation, Proceedings of the IRE, Vol. 43, No. 10, October 1955, Pages 1419-1431.

III-24. Bean, B. R. and Ozanich, Jr., Climatology of the Radio Refractive Index Near the Ground for the United States, National Bureau of Standards Report 6030, Project 8380-12-8885, December 17, 1958.

III-25. Bean, B. R. and Riggs, L. P., Synoptic Variation of the Radio Refractive Index, Journal Res. NBS - D. Radio Propagation, Vol. 63D, No. 1, July-August 1959, Pages 91-97.

III-26. Bean, B. R., Riggs, L. P. and Horn, J. D., Synoptic Study of the Vertical Distribution of the Radio Refractive Index, Jour. Res. NBS - D. Radio Propagation, Vol. 63D, No. 2, September-October 1959, Pages 249-258.

III-27. Bean, B. R. and Thayer, G. D., A Model Radio Refractive Atmosphere NBS Report 5576, 9 June 1958.

III-28. Bean, B. R. and Thayer, G. D., Models of the Atmospheric Radio Refractive Index, Proceedings of the IRE, Vol. 47, No. 5, Part I, May 1959, Pages 740-755. Also issued as NBS Report 6025, 21 November 1958.

III-29. Bean, B. R. and Thayer, G. D., Models of Atmospheric Radio Refractive Index, (A Rebuttal to a letter by P. Misme in same issue) Proceedings of IRE Correspondence Section, Vol. 48, No. 8 August 1960, Page 1498.

BIBLIOGRAPHY (Continued)

III-30. Bean, B. R. and Thayer, G. D., Central Radio Propagation Laboratory Exponential Reference Atmosphere, Journal of Research of the National Bureau of Standards - D. Radio Propagation Vol. 63D, No. 3 November-December 1959, Pages 315-317.

III-31. Bean, B. R. and Thayer, G. D., A Model Radio Refractivity Atmosphere, NBS Project 8380-11-8361, Report N. 5576, June 9, 1958, Pages 3, 23, 28, 33, 39, 42, 43, 44-64, and 75.

III-32. Bean, B. R., Thayer, G. D. and Cahoon, B. A., Methods of Preciting the Atmospheric Bending of Radio Rays, Journal of Research of the National Bureau of Standards - D. Radio Propagation, Vol. 64D, No. 5, September-October 1960, Pages 487-492.

III-33. Bremmer, H., Mode Expansion in the Low-Frequency Range for Propagation Through a Curved Stratified Atmosphere, Journal of Research of the National Bureau of Standards - D. Radio Propagation, Vol. 63D, No. 1, July-August 1959, Page 75.

III-34. Buck, G., Schipper, R. J. & Kline, F. W., Improvements in Refraction Correction and Height Accuracy For Radar Height Finders AVCO Mfg. Co. Report.

III-35. Carroll, T. J. and Ring, R. M., Propagation of Short Radio Waves In A Normally Stratified Troposphere, Proceedings of the IRE, Vol. 43, No. 10, October 1955, Pages 1384-1390.

III-36. Counter, V. A., Propagation of Radio Waves Through the Troposphere and Ionosphere, Lockheed A/C Corp. Missile System Division, Palo Alto, Report 2066-R1 (U) 14 May 1958.

III-37. Counter, V. A. and Riedel, E. Paul, Calculations of Ground-Space Propagation Effects, LMSD-2461, 22 May 1958 (U) Lockheed Aircraft Corp., Missile Systems Division, Sunnyvale, Calif.

III-38. Crain, C. M., Deam, A. P., and Gerhardt, J. R., Measurement of Tropospheric Index-of-Refraction Fluctuations and Profiles, Proceedings of the IRE, Vol. 41, Jan-June 1953, Pages 284-290.

III-39. Crain, C. M., Gerhardt, J. R. and Williams, C. E., A Preliminary Survey of Tropospheric Refractive Index Measurements for US Interior and Coastal Regions, Transactions of the IRE Vol. 2, A-P No. 1, January 1954, Page 15.

BIBLIOGRAPHY (Continued)

III-40. Crain, C. M., Straiton, A. E. and Von Rosenberg, C. W., A Statistical Survey of Atmospheric Index of Refraction Variation, IRE Transactions - Antennas and Propagation, Vol. AP-1, No. 1, 1953-54, Pages 43-45.

III-41. Eshleman, V. R., Barthle, R. C. and Gallagher, P. B., Theory of Radar Studies of the Cislunar Medium, Radio Propagation Lab., Stanford Res. Inst. Scientific Reports No. 5, 8 July 1959, AFC RC-TN-59-381, ASTIA AD-220389.

III-42. Fannin, B. M. and Jehn, K. H., A Study of Radar Elevation-Angle Errors Due to Atmospheric Refraction, IRE Transactions on Antennas and Propagation 1957, Page 71.

III-43. Hazeltine Research Corporation, Studies Pertaining to Application of Precision Oscillators to Guidance Functions, 2nd Quarterly Progress Report (Report No. 7649) February 1960, Contract AF33 (616)-6690, WGL-WADC/ARDC.

III-44. Herbstreit, J. W. and Thompson, M. C., Measurements of the Phase of Radio Waves Received Over Transmission Paths with Electrical Lengths Varying as a Result of Atmospheric Turbulence, Proceedings of the IRE, Vol. 43, No. 10, October 1955, Pages 1391-1401.

III-45. Hermes Electronics Co., Precision of Compensated Tracking Systems, Report No. M-810, AFCRC-TR-59-356, ASTIA-AD-230096, 5 November 1959.

III-46. Ikegami, F., Influence of an Atmospheric Duct on Microwaves Fading Trans IRE AP-7, No. 3, Page 252; July 1959.

III-47. IRE Committee on Wave Propagation and its Sub-Committee on the Theory and Application of Tropospheric Propagation. Tropospheric Propagation: A Selected Guide to the Literature, Proceedings of the IRE, Vol. 41, January-June 1953, Pages 588-594.

III-48. Janes, H. B., Stroud, J. C. and Decker, M. T., Analysis of Propagation Measurements Made at 418 Megacycles per Second Well Beyond the Radio Horizon (A Digest), Journal of Research of the National Bureau of Standards-D. Radio Propagation Vol. 64D, No. 3, May-June 1960, Pages 255-257.

III-49. Janes, H. B. and Wells, P. I., Some Tropospheric Scatter Propagation Measurements Near the Radio Horizon, Proceedings of the IRE, Vol. 43, No. 10, October 1955, Pages 1336-1340.

BIBLIOGRAPHY (Continued)

III-50. Joint Technical Advisory Committee JTAC Radio Transmission by Ionospheric and Tropospheric Scatter, I. Ionospheric Scatter Transmission, II. Long-Range Tropospheric Transmission, III. Proceedings of IRE, Vol. 48, No. 1, January 1960, Pages 4-44.

III-51. Kirby, R. S. and Maloney, L. J., Telecommunications Performance Standards, Tropospheric Systems, National Bureau of Standards PM-83-34, Vol. 5 of 6, Chapter 7 Siting. (SIC.)

III-52. Kirby, R. S. and Rice, R. L., Telecommunication Performance Standards in Tropospheric Systems, Vol. 5 of 6, Chapter 2 Propagation Mechanisms, Preliminary NBS Report PM-83-29, November 1960.

III-53. McCracken, Leslie G., Ray Theory vs. Normal Mode Theory in Wave Propagation Problems, IRE Transactions on Antennas and Propagation, 1957, Page 137.

III-54. McGavin, R. E., Peterson, C. F., Barghausen, A. F., Wilber, R. W., Guiraud, F. O. and Murahata, S., Telecommunications Performance Standards, Tropospheric Systems, Vol. 5 of 6 NBS Memo Report PM-83-32-1, Chapter 5 Equipment Characteristics Affecting System Performance, June 30, 1960.

III-55. Millman, George H., Atmospheric Effects on VHF and UHF Propagation Proceedings of the IRE, Vol. 46, No. 8, August 1958, Pages 1492-1501.

III-56. Muchmore, R. B. and Wheelon, A. D., Line-of Sight Propagation Phenomena--I. Ray Treatment, Proceedings of the IRE, Vol. 43, No. 10, October 1955, Pages 1437-1449.

III-57. Norton, Kenneth A., System Loss in Radio Wave Propagation, Journal of Research of the National Bureau of Standards - D. Radio Propagation, Vol. 63D, No. 1, July-August 1959, Page 53.

III-58. Norton, K. A., Rice, P. L., Janes, H. B. and Barsis, A. P., The Rate of Fading in Propagation Through A Turbulent Atmosphere, Proceedings of IRE, Vol. 43, No. 10, October 1955, Pages 1341-1353.

III-59. Norton, K. A., Rice, P. L., and Vogler, L. E., The Use of Angular Distance in Estimating Transmission Loss and Fading Range for Propagation Through a Turbulent Atmosphere Over Irregular Terrain, Proceedings of the IRE, Vol. 43, No. 10, October 1955, Pages 1488-1526.

BIBLIOGRAPHY (Continued)

III-60. Pied Piper 2nd Quarterly Progress Report LMSD Report MSE-1481, (S) 15 January 1956.

III-61. Ricke, P. L., Barsis, A. P., Longley, A. G., Dougherty, H. T. and Kirby, R. S., Telecommunications Performance Standards Tropospheric Systems, Vol. 5 of 6, Chapter 6 - Predicting the Performance of Communication Circuits, NBS Memo Report PM-83-33, June 30, 1960.

III-62. Saastad, A. and Forbes, F. C., Processing and Analysis of Azusa Mark II Data, Convair Astronautics Report No. AE 60-0117, June 10, 1960.

III-63. Smith, E. K., and Weintraub, S., The Constants in the Equation for Atmospheric Refractive Index at Radio Frequencies, Proceedings of the IRE, Vol. 41, Pages 1035-37, August 1953.

III-64. Space Technology Laboratories, Inc., Tropospheric Scintillations, Part II GM-TM-0165-00308, 24 October 1958.

III-65. Space Technology Laboratories, Inc., Studies in Electromagnetic Propagation, STL Report GM-TM-0165-00307 (U) Part I, Refractive Corrections, Applied Physics Department Electronics Lab., 31 December 1958.

III-66. Swingle, Donald M., Nomograms for the Computation of Tropospheric Refractive Index, Proceedings of the IRE, Vol. 41, Jan.-June 1953, Pages 385-391.

III-67. Taylor, Capt. Fred S., III, Plane Electromagnetic Wave Propagation and Reflection in Non-Absorbing, Inhomogeneous Media, Thesis, September 1959, USAF Institute of Technology, ASTIA AD 227974.

III-68. Taylor, Paul B. and Engler, Nicholas A., Charts of Corrections to Radar Observations for Refraction by Terrestrial Atmospheres, WADC Technical Report 59-619, Research Report 427-71, Research Institute, U. of Dayton, Ohio, February 1960, Aerial Reconnaissance Lab., Wright Air Development Div., Air Res. and Development Command, U.S.A.F., Wright-Patterson A.F. Base.

III-69. Thompson, Moody, C., Jr., Janes, Harris B., and Treethey, Frank E., Atmospheric Limitations on Electronic Distance-Measuring Equipment, Reprint from Journal of Geophysical Research, Vol. 65, February 1960, No. 2, Pages 389-393.

BIBLIOGRAPHY (Continued)

III-70. Thompson, M. C., Jr. and Janes, H. B., Measurements of Phase Stability Over A Low-Level Tropospheric Path, Journal of Research of the National Bureau of Standards-D. Radio Propagation, Vol. 63D, No. 1, July-August 1959, Pages 45-51.

III-71. Thompson, M. C., Jr., Janes, H. B.,and Kirkpatrick, A. W., An Analysis of Time Variations in Tropospheric Refractive Index and Apparent Radio Path Length, Reprint from Journal of Geophysical Research, Vol. 65, No. 1, January 1960.

III-72. Toman, K., Focusing, Defocusing, and Refraction in A Circularly Stratified Atmosphere, Journal of Research of the National Bureau of Standards - D. Radio Propagation, Vol. 64D, No. 3, May-June 1960, Pages 287-289.

III-73. Villars, F. and Weiskopf, V. F., On the Scattering of Radio Waves by Turbulent Fluctuations of the Atmosphere, Proceedings of the IRE, Vol. 43, No. 10, October 1955, Pages 1232-1239.

III-74. Weisbrod, S. and Anderson, L. J., Simple Methods for Computing Tropospheric and Ionospheric Refractive Effects on Radio Waves Proceedings of the IRE, Vol. 47, No. 10, October 1959, Pages 1770-1777.

III-75. Wheelon, A. D., Note on Scatter Propagation with A Modified Exponential Correlation, Proceedings of the IRE, Vol. 43, No. 10, October 1955, Pages 1381-1383.

III-76. Wheelon, A. D., Radio-Wave Scattering by Tropospheric Irregularities, Journal of Research of the National Bureau of Standards-D. Radio Propagation, Vol. 63, No. 2, September-October 1959, Page 205.

III-77. Wheelon, A. D. and Muchmore, R. B., Line-Of-Sight Propagation Phenomena, II. Scattered Components, Proceedings of the IRE, Vol. 43, No. 10, October 1955, Pages 1450-1458.

IV MICROWAVE REFRACTOMETERS

IV-1. Cogdell, John R., Temperature Compensation and Transient Response of 403 Mc/s Coaxial Cavities, Master's Thesis, The University of Texas, 10 July 1959.

IV-2. Crain, C. M., Apparatus for Recording Fluctuations in the Refractive Index of the Atmosphere, The Review of Scientific Instruments, Vol. 21, May 1950, Pages 213-219, No. 5.

BIBLIOGRAPHY (Continued)

IV-3. Crain, C. M., Survey of Airborne Microwave Refractometer Measurements Proceedings of the IRE, Vol. 43, No. 10, October 1955, Pages 1405-1411.

IV-4. Crain, C. M. and Deam, A/P., An Airborne Microwave Refractometer, The Review of Scientific Instruments, Vol. 23, April 1952, Pages 149-191, No. 4.

IV-5. Deam, A. P., An Expendable Atmospheric Radio Refractometer, Electrical Engineering Research Laboratory, Report No. 108, The University of Texas, 15 May 1959.

IV-6. Deam, A. P., Status Report of the Development of an Expendable Atmospheric Radio Refractometer, Electrical Engineering Research Laboratory, Report No. 5-32, The University of Texas, 15 April 1958.

IV-7. Deam, A. P. and Staley, R. C., The Use of Balloon Borne Refractometer Observations in Studying Problems Relating to Telemetry Propagation from Space Vehicles, Electrical Research Laboratory Report No. 5-36, The University of Texas, 15 June 1959.

IV-8. Greenspan, Martin and Thompson, Moody C., Jr., An Eleven Megacycle Interferometer for Low Pressure Gases, Reprinted from the Journal of the Accoustical Society of America, Vol. 25, No. 1, January 1953, Pages 92-96.

IV-9. Thompson, M C., Jr., Freethey, Frank E., and Waters, Donald M., Fabrication Techniques for Ceramic X-Band Cavity Resonators, Reprinted from the Review of Scientific Instruments, Vol. 29, No. 10, October 1958, Pages 865-868.

IV-10. Thompson, M. C., Jr., Freethey, F. E. and Waters, D. M., End Plate Modification of X-Band TE_{011} Cavity Resonators, Reprinted from IRE Transactions on Microwave Theory and Techniques Vol. MTT-7, No. 3, July 1959.

IV-11. Thompson, M. C., Jr. and Vetter, M. J., Compact Microwave Refractometer For Use in Small Aircraft, Reprinted from The Review of Scientific Instruments, Vol. 29, No. 12, December 1958, Pages 1093-1096.

APPENDIX I

ERROR MODEL EQUIVALENCE

1.1 REDUCTION OF TRACKING SYSTEMS TO RANGE-ONLY EQUIVALENTS.

The demonstration of error model equivalence in generalized notation proceeds as follows:

The spacecraft coordinates are X, Y, Z, and the tracker coordinates are:

$$X_n,\ Y_n,\ Z_n \qquad n = 1,\ 2,\ 3.$$

Then, the missile position is determined by the equations

$$R_n^2 = (X - X_n)^2 + (Y - Y_n)^2 + (Z - Z_n)^2 \qquad n = 1,\ 2,\ 3$$

If sums or differences of ranges sufficient to determine (X, Y, Z) are measured, then they are also sufficient to determine all R_n, which may usually be found by linear equations

$$R_n = a_{n1} S_1 + a_{n2} S_2 + a_{n3} S_3 \qquad n = 1,\ 2,\ 3 \tag{I-1}$$

Now, since $X = X(R_n)$ and $R_n = R_n(S_1, S_2, S_3)$

$$\frac{\partial X}{\partial S_m} = \frac{\partial X}{\partial R_1}\ \frac{\partial R_1}{\partial S_m} + \frac{\partial X}{\partial R_2}\ \frac{\partial R_2}{\partial S_m} + \frac{\partial X}{\partial R_3}\ \frac{\partial R_3}{\partial S_m} \qquad m = 1,\ 2,\ 3 \tag{I-2}$$

Also, if ΔS_m is an error made in S_m,

$$\Delta S_m = \frac{\partial S_m}{\partial R_1}\ \Delta R_1 + \frac{\partial S_m}{\partial R_2}\ \Delta R_2 + \frac{\partial S_m}{\partial R_3}\ \Delta R_3 \tag{I-3}$$

and if ΔX is an error in X

$$\Delta X = \frac{\partial X}{\partial S_1}\ \Delta S_1 + \frac{\partial X}{\partial S_2}\ \Delta S_2 + \frac{\partial X}{\partial S_3}\ \Delta S_3 \tag{I-4}$$

Putting (I-2) and (I-3) in (I-4) we get

$$\Delta X = \left(\frac{\partial X}{\partial R_1}\frac{\partial R_1}{\partial S_1} + \frac{\partial X}{\partial R_2}\frac{\partial R_2}{\partial S_1} + \frac{\partial X}{\partial R_3}\frac{\partial R_3}{\partial S_1}\right)\left(\frac{\partial S_1}{\partial R_1}\Delta R_1 + \frac{\partial S_1}{\partial R_2}\Delta R_2 + \frac{\partial S_1}{\partial R_3}\Delta R_3\right)$$
$$+ \left(\frac{\partial X}{\partial R_1}\frac{\partial R_1}{\partial S_2} + \frac{\partial X}{\partial R_2}\frac{\partial R_2}{\partial S_2} + \frac{\partial X}{\partial R_3}\frac{\partial R_3}{\partial S_3}\right)\left(\frac{\partial S_2}{\partial R_1}\Delta R_1 + \frac{\partial S_2}{\partial R_2}\Delta R_2 + \frac{\partial S_2}{\partial R_3}\Delta R_3\right)$$
$$+ \left(\frac{\partial X}{\partial R_1}\frac{\partial R_1}{\partial S_3} + \frac{\partial X}{\partial R_2}\frac{\partial R_2}{\partial S_3} + \frac{\partial X}{\partial R_3}\frac{\partial R_3}{\partial S_3}\right)\left(\frac{\partial S_3}{\partial R_1}\Delta R_1 + \frac{\partial S_3}{\partial R_2}\Delta R_2 + \frac{\partial S_3}{\partial R_3}\Delta R_3\right) \qquad \text{(I-5)}$$

Differentiating (I-1) with respect to S_m we obtain

$$\frac{\partial R_n}{\partial S_m} = a_{nm} \qquad m = 1, 2, 3 \qquad n = 1, 2, 3 \qquad \text{(I-6)}$$

and

$$\frac{\partial S_m}{\partial R_n} = b_{nm} \qquad \text{(I-7)}$$

where b_{nm} is the number of R_n paths in sum S_m.

Using (I-6) and (I-7) and rearranging (I-5)

$$\Delta X = \frac{\partial X}{\partial R_1}\Delta R_1\left(a_{11}b_{11} + a_{12}b_{12} + a_{13}b_{13}\right) + \frac{\partial X}{\partial R_2}\Delta R_2\left(a_{21}b_{21} + a_{22}b_{22} + a_{23}b_{23}\right) + \frac{\partial X}{\partial R_3}\Delta R_3\left(a_{31}b_{31} + a_{32}b_{32} + a_{33}b_{33}\right) +$$
$$\frac{\partial X}{\partial R_1}\Delta R_2\left(a_{11}b_{21} + a_{12}b_{22} + a_{13}b_{23}\right) +$$
$$\frac{\partial X}{\partial R_1}\Delta R_3\left(a_{11}b_{31} + a_{12}b_{32} + a_{13}b_{33}\right) +$$

$$\frac{\partial X}{\partial R_2}\Delta R_1\left(a_{21}b_{11}+a_{22}b_{12}+a_{23}b_{13}\right)+\frac{\partial X}{\partial R_2}\Delta R_3\left(a_{21}b_{31}+a_{22}b_{32}+a_{23}b_{33}\right)+\frac{\partial X}{\partial R_3}\Delta R_1\left(a_{31}b_{11}+a_{32}b_{12}+a_{33}b_{13}\right)+\frac{\partial X}{\partial R_3}\Delta R_2\left(a_{31}b_{21}+a_{32}b_{22}+a_{33}r_{23}\right) \quad \text{(I-8)}$$

However, since (I-1) must be an identity, we may formulate the relationships between a_{nm} and b_{nm} which must be true to make it an identity.

These are:

$$a_{11}b_{11}+a_{12}b_{12}+a_{13}b_{13}=1$$

$$a_{11}b_{21}+a_{12}b_{22}+a_{13}b_{23}=0$$

$$a_{11}b_{31}+a_{12}b_{32}+a_{13}b_{33}=0$$

$$a_{21}b_{11}+a_{22}b_{12}+a_{23}b_{13}=0$$

$$a_{21}b_{21}+a_{22}b_{22}+a_{23}b_{23}=1$$

$$a_{21}b_{31}+a_{22}b_{32}+a_{23}b_{33}=0$$

$$a_{31}b_{11}+a_{32}b_{12}+a_{33}b_{13}=0$$

$$a_{31}b_{21}+a_{32}b_{22}+a_{33}b_{23}=0$$

$$a_{31}b_{31}+a_{32}b_{32}+a_{33}b_{33}=1$$

Putting these in (I-8) we obtain

$$\Delta X=\frac{\partial X}{\partial R_1}\Delta R_1+\frac{\partial X}{\partial R_2}\Delta R_2+\frac{\partial X}{\partial R_3}\Delta R_3 \quad \text{(I-9)}$$

which is exactly the error expression used in the range-only case.

Therefore, all tracking systems of the type which measure range, range sum, range difference, or combinations of these just sufficient to determine missile position may be reduced to range-only equivalents. Consequently, in all hybrid systems of this type the range errors associated with electric path are identical to those of their range-only equivalent.

1.2 THE GEOMETRICAL PARTIAL DERIVATIVES

The geometrical partial derivatives required to compute $M_{\bar{T}}$ and $M_{\dot{\bar{T}}}$ may be formed by simple vector-matrix operations involving the following 3×3 matrices:

$$R = \left[\bar{R}_1 \; \bar{R}_2 \; \bar{R}_3\right]^*$$

$$S_{X'} = \begin{bmatrix} \bar{1}_{X_1'} \cdot \bar{R}_1 & 0 & 0 \\ 0 & \bar{1}_{X_2'} \cdot \bar{R}_2 & 0 \\ 0 & 0 & \bar{1}_{X_3'} \cdot \bar{R}_3 \end{bmatrix}$$

$$S_{Y'} = \begin{bmatrix} \bar{1}_{Y_1'} \cdot \bar{R}_1 & 0 & 0 \\ 0 & 1_{Y_2'} \cdot \bar{R}_2 & 0 \\ 0 & 0 & \bar{1}_{Y_3'} \cdot \bar{R}_3 \end{bmatrix}$$

$$S_{Z'} = \begin{bmatrix} \bar{1}_{Z_1'} \cdot \bar{R}_1 & 0 & 0 \\ 0 & \bar{1}_{Z_2'} \cdot \bar{R}_2 & 0 \\ 0 & 0 & \bar{1}_{Z_3'} \cdot \bar{R}_3 \end{bmatrix}$$

$$T = \begin{bmatrix} R_1 & 0 & 0 \\ 0 & R_2 & 0 \\ 0 & 0 & R_3 \end{bmatrix}$$

$$U = \begin{bmatrix} \dot{R}_1 & 0 & 0 \\ 0 & \dot{R}_2 & 0 \\ 0 & 0 & \dot{R}_3 \end{bmatrix}$$

$$V = \left[\bar{V} \quad \bar{V} \quad \bar{V}\right]^*$$

* Denotes the transpose of the matrix

$$W_{X'} = \begin{bmatrix} \bar{1}_{X'_1} \cdot \bar{V} & 0 & 0 \\ 0 & \bar{1}_{X'_2} \cdot \bar{V} & 0 \\ 0 & 0 & \bar{1}_{X'_3} \cdot \bar{V} \end{bmatrix}$$

$$W_{Y'} = \begin{bmatrix} \bar{1}_{Y'_1} \cdot \bar{V} & 0 & 0 \\ 0 & \bar{1}_{Y'_2} \cdot \bar{V} & 0 \\ 0 & 0 & \bar{1}_{Y'_3} \cdot \bar{V} \end{bmatrix}$$

$$W_{Z'} = \begin{bmatrix} \bar{1}_{Z'_1} \cdot \bar{V} & 0 & 0 \\ 0 & \bar{1}_{Z'_2} \cdot \bar{V} & 0 \\ 0 & 0 & \bar{1}_{Z'_3} \cdot \bar{V} \end{bmatrix}$$

With these matrices then the partial derivative of missile position with respect to ranges 1, 2, and 3 is

$$P_R = R^{-1}T = \begin{bmatrix} \frac{\partial X}{\partial R_1} & \frac{\partial X}{\partial R_2} & \frac{\partial X}{\partial R_3} \\ \frac{\partial Y}{\partial R_1} & \frac{\partial Y}{\partial R_2} & \frac{\partial Y}{\partial R_3} \\ \frac{\partial Z}{\partial R_1} & \frac{\partial Z}{\partial R_2} & \frac{\partial Z}{\partial R_3} \end{bmatrix}$$

The partial derivative of missile position with respect to east coordinate of trackers 1, 2, and 3 is

$$P_\lambda = R^{-1}S_{X'} = \begin{bmatrix} \frac{\partial X}{\partial X'_1} & \frac{\partial X}{\partial X'_2} & \frac{\partial X}{\partial X'_3} \\ \frac{\partial Y}{\partial X'_1} & \frac{\partial Y}{\partial X'_2} & \frac{\partial Y}{\partial X'_3} \\ \frac{\partial Z}{\partial X'_1} & \frac{\partial Z}{\partial X'_2} & \frac{\partial Z}{\partial X'_3} \end{bmatrix}$$

The partial derivative of missile position with respect to north coordinate of trackers 1, 2, and 3 is

$$P_\phi = R^{-1}S_{Y'} = \begin{bmatrix} \frac{\partial X}{\partial Y'_1} & \frac{\partial X}{\partial Y'_2} & \frac{\partial X}{\partial Y'_3} \\ \frac{\partial Y}{\partial Y'_1} & \frac{\partial Y}{\partial Y'_2} & \frac{\partial Y}{\partial Y'_3} \\ \frac{\partial Z}{\partial Y'_1} & \frac{\partial Z}{\partial Y'_2} & \frac{\partial Z}{\partial Y'_3} \end{bmatrix}.$$

The partial derivative of missile position with respect to vertical coordinate at trackers 1, 2, and 3 is

$$P_r = R^{-1}S_{Z'} = \begin{bmatrix} \frac{\partial X}{\partial Z'_1} & \frac{\partial X}{\partial Z'_2} & \frac{\partial X}{\partial Z'_3} \\ \frac{\partial Y}{\partial Z'_1} & \frac{\partial Y}{\partial Z'_2} & \frac{\partial Y}{\partial Z'_3} \\ \frac{\partial Z}{\partial Z'_1} & \frac{\partial Z}{\partial Z'_2} & \frac{\partial Z}{\partial Z'_3} \end{bmatrix}.$$

The partial derivative of missile velocity with respect to ranges 1, 2, and 3 is

$$V_R = R^{-1}\left[U - VP_R\right] = \begin{bmatrix} \frac{\partial \dot{X}}{\partial R_1} & \frac{\partial \dot{X}}{\partial R_2} & \frac{\partial \dot{X}}{\partial R_3} \\ \frac{\partial \dot{Y}}{\partial R_1} & \frac{\partial \dot{Y}}{\partial R_2} & \frac{\partial \dot{Y}}{\partial R_3} \\ \frac{\partial \dot{Z}}{\partial R_1} & \frac{\partial \dot{Z}}{\partial R_2} & \frac{\partial \dot{Z}}{\partial R_3} \end{bmatrix}.$$

The partial derivative of missile velocity with respect to range rates 1, 2, and 3 is

$$V_{\dot{R}} = R^{-1}T = \begin{bmatrix} \frac{\partial \dot{X}}{\partial R_1} & \frac{\partial \dot{X}}{\partial R_2} & \frac{\partial \dot{X}}{\partial R_3} \\ \frac{\partial \dot{Y}}{\partial R_1} & \frac{\partial \dot{Y}}{\partial R_2} & \frac{\partial \dot{Y}}{\partial R_3} \\ \frac{\partial \dot{Z}}{\partial R_1} & \frac{\partial \dot{Z}}{\partial R_2} & \frac{\partial \dot{Z}}{\partial R_3} \end{bmatrix}.$$

The partial derivative of missile velocity with respect to east coordinate of trackers 1, 2 and 3 is

$$V_\lambda = R^{-1}\left[W_{X'} - VP_\lambda\right] = \begin{bmatrix} \frac{\partial \dot{X}}{\partial X_1'} & \frac{\partial \dot{X}}{\partial X_2'} & \frac{\partial \dot{X}}{\partial X_3'} \\ \frac{\partial \dot{Y}}{\partial X_1'} & \frac{\partial \dot{Y}}{\partial X_2'} & \frac{\partial \dot{Y}}{\partial X_3'} \\ \frac{\partial \dot{Z}}{\partial X_1'} & \frac{\partial \dot{Z}}{\partial X_2'} & \frac{\partial \dot{Z}}{\partial X_3'} \end{bmatrix}.$$

The partial derivative of missile velocity with respect to north coordinate of trackers 1, 2 and 3 is

$$V_\phi = R^{-1}\left[W_{Y'} - VP_\phi\right] = \begin{bmatrix} \frac{\partial \dot{X}}{\partial Y_1'} & \frac{\partial \dot{X}}{\partial Y_2'} & \frac{\partial \dot{X}}{\partial Y_3'} \\ \frac{\partial \dot{Y}}{\partial Y_1'} & \frac{\partial \dot{Y}}{\partial Y_2'} & \frac{\partial \dot{Y}}{\partial Y_3'} \\ \frac{\partial \dot{Z}}{\partial Y_1'} & \frac{\partial \dot{Z}}{\partial Y_2'} & \frac{\partial \dot{Z}}{\partial Y_3'} \end{bmatrix}.$$

The partial derivative of missile velocity with respect to vertical coordinates of trackers 1, 2 and 3 is

$$V_r = R^{-1}\left[W_Z' - VP_r\right] = \begin{bmatrix} \frac{\partial \dot{X}}{\partial Z_1'} & \frac{\partial \dot{X}}{\partial Z_2'} & \frac{\partial \dot{X}}{\partial Z_3'} \\ \frac{\partial \dot{Y}}{\partial Z_1'} & \frac{\partial \dot{Y}}{\partial Z_2'} & \frac{\partial \dot{Y}}{\partial Z_3'} \\ \frac{\partial \dot{Z}}{\partial Z_1'} & \frac{\partial \dot{Z}}{\partial Z_2'} & \frac{\partial \dot{Z}}{\partial Z_3'} \end{bmatrix}.$$

1.3 THE REDUCTION OF TRACKER MEASUREMENTS TO CARTESIAN COORDINATES IN REAL TIME

The mathematical methods employed in the computer program for simulating tracker performance are directly useful in the real-time coordinate reduction of an operational tracking system. The application is outlined in the following paragraphs.

The tracking configurations under consideration measure a_1, a_2, a_3, $\dot{a}_1$, $\dot{a}_2$ and $\dot{a}_3$. In all systems, the rate measurements are range rates, that is:

$\dot{a}_i = \dot{R}_i$ (i = 1, 2, 3), determined from the Doppler frequency shift at the receivers.

The systems considered here measure a_1, a_2, and a_3, where

$$a_1 = b_{11} R_1 + b_{12} R_2 + b_{13} R_3 \qquad \text{(I-10)}$$

$$a_2 = b_{21} R_1 + b_{22} R_2 + b_{23} R_3$$

$$a_3 = b_{31} R_1 + b_{32} R_2 + b_{33} R_3,$$

or in matrix notation,

$$\begin{bmatrix} a_1 \\ a_2 \\ a_3 \end{bmatrix} = B \begin{bmatrix} R_1 \\ R_2 \\ R_3 \end{bmatrix} \qquad \text{(I-10a)}$$

The solution of (I-10) for R_i (i = 1, 2, 3) is therefore given by

$$\begin{bmatrix} R_1 \\ R_2 \\ R_3 \end{bmatrix} = B^{-1} \begin{bmatrix} a_1 \\ a_2 \\ a_3 \end{bmatrix} \qquad \text{(I-11)}$$

The matrix B is formed using equation (I-10) and the definitions of a_i (i = 1, 2, 3) so that for:

1. Three Range Only,

   B = identify matrix;

2. Three Range Sums (transmitters at all sites);

$$B = \begin{bmatrix} 1 & 1 & 0 \\ 0 & 1 & 1 \\ 1 & 0 & 1 \end{bmatrix}, \text{ and}$$

$$B^{-1} = \begin{bmatrix} .5 & -.5 & .5 \\ .5 & .5 & -.5 \\ -.5 & .5 & .5 \end{bmatrix}$$

3. One Range, Two Range Differences,

$$B = \begin{bmatrix} 1 & 0 & 0 \\ 1 & -1 & 0 \\ 1 & 0 & -1 \end{bmatrix} \quad \text{, and}$$

$$B^{-1} = \begin{bmatrix} 1 & 0 & 0 \\ 1 & -1 & 0 \\ 1 & 0 & -1 \end{bmatrix}$$

4. One Range, Two Range Sums,

$$B = \begin{bmatrix} 1 & 0 & 0 \\ 1 & 1 & 0 \\ 1 & 0 & 1 \end{bmatrix} \quad \text{, and}$$

$$B^{-1} = \begin{bmatrix} 1 & 0 & 0 \\ -1 & 1 & 0 \\ -1 & 0 & 1 \end{bmatrix}$$

The locations of the three trackers are assumed to be given, from surveys, in some coordinate system, and are denoted $\bar{r}_1$, $\bar{r}_2$, and $\bar{r}_3$.

The unit vectors, (see Figure 43)

$$\bar{1}_\xi = \frac{\bar{r}_2 - \bar{r}_1}{|\bar{r}_2 - \bar{r}_1|} = \frac{\bar{r}_2 - \bar{r}_1}{b_{12}} ,$$

$$\bar{1}_\eta = \frac{\bar{r}_3 - \bar{r}_1}{|\bar{r}_3 - \bar{r}_1|} = \frac{\bar{r}_3 - \bar{r}_1}{b_{13}} ,$$

$$\bar{1}_\zeta = 1_\xi \times \bar{1}_\eta \div \left| \bar{1}_\xi \times \bar{1}_\eta \right|$$

are formed as constants of the tracking system. Next, the reciprocal vectors of these unit vectors are formed and stored:

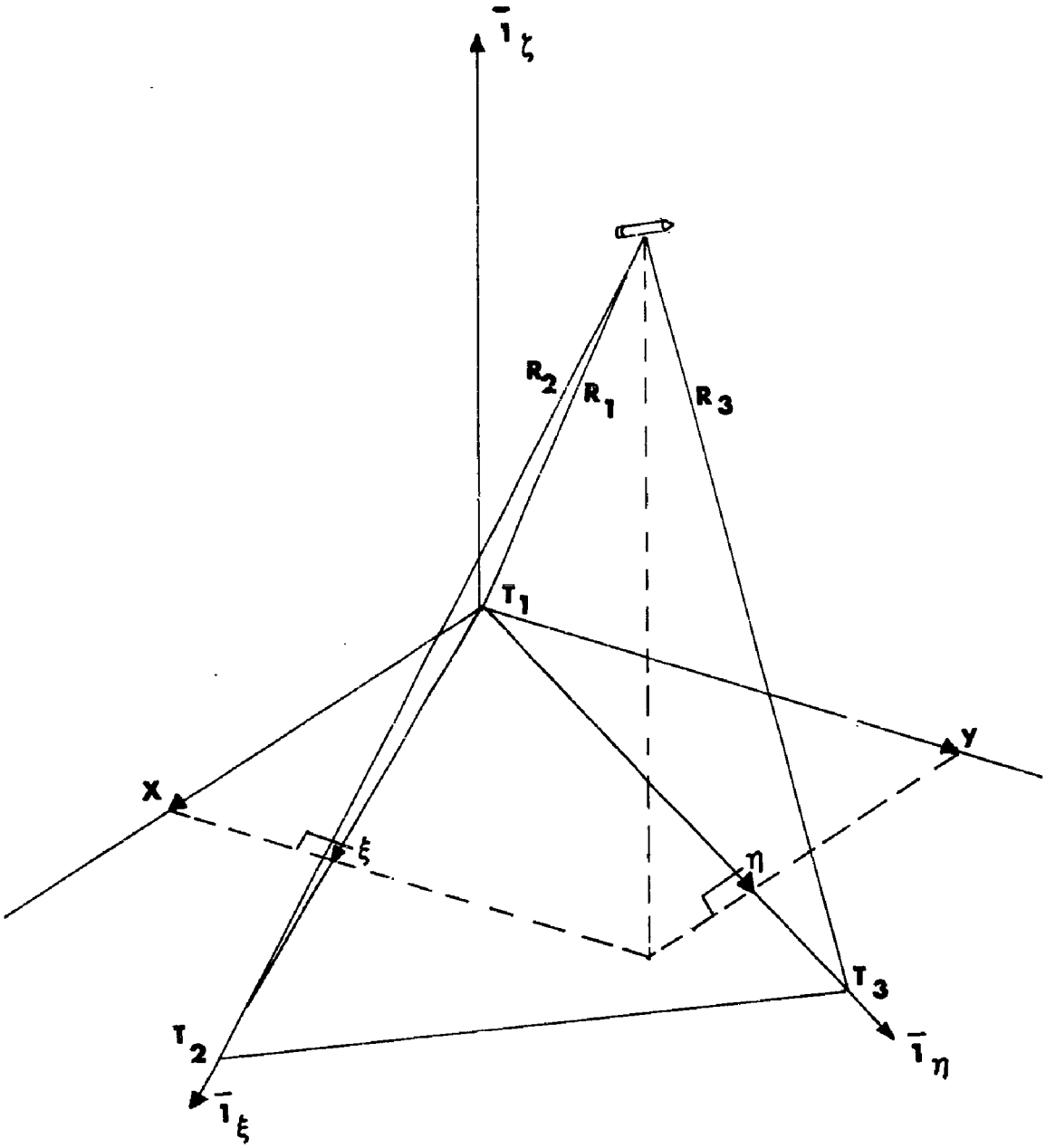

Figure 43. Non-Orthogonal Coordinate Relationships

$$\overline{U} = \frac{\overline{I}_\eta \times \overline{I}_\zeta}{\overline{I}_\xi \times \overline{I}_\eta \times \overline{I}_\zeta}$$

$$\overline{V} = \frac{\overline{I}_\zeta \times \overline{I}_\xi}{\overline{I}_\xi \times \overline{I}_\eta \times \overline{I}_\zeta}$$

Since the type of measurements made have been determined before tracking commences, the values of the elements of B^{-1} are stored in the memory, so that as measurements commence, R_1, R_2, R_3, $\dot{R}_1$, $\dot{R}_2$, $\dot{R}_3$ may be immediately computed from equations (I-11) and are available for real time reduction. From the law of cosines the quantities:

$$\xi = \frac{R_1^2 - R_2^2 + b_{12}^2}{2\,b_{12}} \quad ,$$

$$\eta = \frac{R_1^2 - R_3^2 + b_{13}^2}{2\,b_{13}} \quad ,$$

$$\dot{\xi} = \frac{1}{b_{12}} \quad (R_1 \dot{R}_1 - R_2 \dot{R}_2),$$

$$\dot{\eta} = \frac{1}{b_{13}} \quad (R_1 \dot{R}_1 - R_3 \dot{R}_3).$$

are determined.

Then the vector position and velocity, $\overline{r}$ and $\overline{v}$, which have components (X, Y, Z) and $(\dot{X}, \dot{Y}, \dot{Z})$ respectively, are given by:

$$X = X' U_X + Y' V_X$$

$$Y = X' U_Y + Y' V_Y$$

$$Z = + \left[R_1^2 - X^2 - Y^2\right]^{1/2}$$

$$\dot{X} = \dot{X}' U_X + \dot{Y}' V_X$$

$$\dot{Y} = \dot{X}' U_Y + \dot{Y}' V_Y$$

$$\dot{Z} = \frac{1}{Z} \quad (R_1 \dot{R}_1 - X \dot{X} - Y \dot{Y}) \quad .$$

There are thus thirteen scalar equations to be solved (with this method), in real time.

1.4 ERROR ANALYSIS OF A TRACKING COMPLEX WHICH MEASURES THREE RANGE DIFFERENCES

With the addition of a fourth station to a three-station tracking complex, an un-cooperative space vehicle, (if it is transmitting a suitably modulated signal) may be tracked and its location determined. The three time differences between the time of signal reception at one station and the times of reception at the other three, converted to three range differences, yield a unique solution for the vector position of the space vehicle

The measurements are therefore: D_1, D_2, D_3, where

$$D_1 = R_1 - R_4$$

$$D_2 = R_2 - R_4$$

$$D_3 = R_3 - R_4.$$

In the computations outlined, the same coordinate systems and notation are used as in the three-range-only analysis. Likewise, the same uncertainties are used, e.g., σ_c arising from uncertainty in the speed of light, σ_t , dependent upon the ability to synchronize time between stations, etc. The covariance matrices in spacecraft position resulting from the tracking process and from the survey of the tracking sites are computed, formed separately, and added together to obtain the system characteristics. Assuming an input position $\bar{r}$, and velocity, $\bar{w}$, of a vehicle, the partial derivatives of the coordinates with respect to the measurements are formed as follows:

$$\bar{R}_i = \bar{r} - \bar{r}_i \qquad (i = 1, 2, 3, 4)$$

$$R_i = \text{magnitude of } \bar{R}_i \qquad (i = 1, 2, 3, 4)$$

$$\bar{1}_{Ri} = \bar{R}_i \div R_i \qquad (i = 1, 2, 3, 4)$$

$$\bar{1}_{R1} - \bar{1}_{R4} = \bar{p}_1$$

$$\bar{1}_{R2} - \bar{1}_{R4} = \bar{p}_2$$

$$\bar{1}_{R3} - \bar{1}_{R4} = \bar{p}_3$$

$$P = \begin{bmatrix} \frac{\partial X}{\partial D_1} & \frac{\partial X}{\partial D_2} & \frac{\partial X}{\partial D_3} \\ \frac{\partial Y}{\partial D_1} & \frac{\partial Y}{\partial D_2} & \frac{\partial Y}{\partial D_3} \\ \frac{\partial Z}{\partial D_1} & \frac{\partial Z}{\partial D_2} & \frac{\partial Z}{\partial D_3} \end{bmatrix} = \left[\begin{bmatrix} p_1, & p_2, & p_3 \end{bmatrix}^* \right]^{-1}$$

The assumed system measurement error model is:

$$\begin{aligned}
\Delta\bar{r} = {} & \Delta C \left[D_1 \frac{\partial \bar{r}}{\partial D_1} + D_2 \frac{\partial \bar{r}}{\partial D_2} + D_3 \frac{\partial \bar{r}}{\partial D_3} \right] \\
& + \Delta t_1 \left[(C + \dot{R}_1) \frac{\partial \bar{r}}{\partial D_1} \right] + \Delta t_2 \left[(C + \dot{R}_2) \frac{\partial \bar{r}}{\partial D_2} \right] \\
& + \Delta t_3 \left[(C + \dot{R}_3) \frac{\partial \bar{r}}{\partial D_3} \right] - \Delta t_4 \left[(C + \dot{R}_4) \bar{T} \right] \\
& + \Delta t_b \left[(\dot{R}_1 - \dot{R}_4) \frac{\partial \bar{r}}{\partial D_1} + (R_2 - R_4) \frac{\partial \bar{r}}{\partial D_2} + (\dot{R}_3 - \dot{R}_4) \frac{\partial \bar{r}}{\partial D_3} \right] \\
& + k_b \left[\left(f(\epsilon_1) - f(\epsilon_4) \right) \frac{\partial \bar{r}}{\partial D_1} + \left(f(\epsilon_2) - f(\epsilon_4) \right) \frac{\partial \bar{r}}{\partial D_2} \right. \\
& \qquad \left. + \left(f(\epsilon_3) - f(\epsilon_4) \right) \frac{\partial \bar{r}}{\partial D_3} \right] \\
& + k_1 \left[\frac{\partial \bar{r}}{\partial D_1} f(\epsilon_1) \right] + k_2 \left[\frac{\partial \bar{r}}{\partial D_2} f(\epsilon_2) \right] \\
& + k_3 \left[\frac{\partial \bar{r}}{\partial D_3} f(\epsilon_3) \right] - k_4 \left[\bar{T} f(\epsilon_4) \right] ,
\end{aligned}$$

where

$$\bar{T} = \begin{bmatrix} \frac{\partial X}{\partial D_1} + \frac{\partial X}{\partial D_2} + \frac{\partial X}{\partial D_3} \\ \frac{\partial Y}{\partial D_1} + \frac{\partial Y}{\partial D_2} + \frac{\partial Y}{\partial D_3} \\ \frac{\partial Z}{\partial D_1} + \frac{\partial Z}{\partial D_2} + \frac{\partial Z}{\partial D_3} \end{bmatrix} ,$$

and $f(\epsilon)$ is of the same form as in the three-range-only model. The $\dot{R}_i$ ($i = 1, 2, 3, 4$) are formed by

$$\dot{R}_i = \bar{v} \cdot \bar{1}_{Ri} .$$

Before finding the expected value of $\Delta\bar{r}$, note the following nomenclature:

$$\bar{D} = \begin{bmatrix} D_1 \\ D_2 \\ D_3 \end{bmatrix}, \qquad \dot{\bar{D}} = \begin{bmatrix} \dot{R}_1 - \dot{R}_4 \\ \dot{R}_2 - \dot{R}_4 \\ \dot{R}_3 - \dot{R}_4 \end{bmatrix},$$

$$\bar{f}(\Delta\epsilon) = \begin{bmatrix} f(\epsilon_1) - f(\epsilon_4) \\ f(\epsilon_2) - f(\epsilon_4) \\ f(\epsilon_3) - f(\epsilon_4) \end{bmatrix} \quad : \text{ also,}$$

any diagonal matrix with elements a_1, a_2, a_3 will be denoted

$$\begin{bmatrix} a_1 & 0 & 0 \\ 0 & a_2 & 0 \\ 0 & 0 & a_3 \end{bmatrix} = \left\{a_i\right\} .$$

Then the covariance of $\Delta\bar{r}$ (due to the tracking operation) will be given by:

$$\Sigma_{\Delta\bar{r}} = \begin{bmatrix} \sigma X^2 & \sigma XY & \sigma XZ \\ \sigma YX & \sigma Y^2 & \sigma YZ \\ \sigma ZX & \sigma ZY & \sigma Z^2 \end{bmatrix} =$$

$$P \left[\sigma\bar{C}^2 \bar{D}\bar{D}^* + \sigma t^2 \left\{(C + \dot{R}_i)^2\right\} + \sigma tb^2 \dot{\bar{D}}\dot{\bar{D}}^* + \sigma kb^2 \bar{f}(\Delta\epsilon)\bar{f}(\Delta\epsilon)^* + \sigma k^2 \left\{f^2(\epsilon_i)\right\} \right] P^* + \left[\sigma t^2 (C + \dot{R}_4)^2 + \sigma k^2 f^2(\epsilon_4) \right] \bar{T}\bar{T}^* .$$

In analyzing the errors contributed by the survey of the tracking system, two covariance matrices in $\bar{r}$ are formed, one arising from the totally correlated errors between stations and the other from the totally uncorrelated errors. The equations relating the position of the vehicle to the locations of the stations are:

$$(D_i + R_4)^2 = (X - X_i)^2 + (Y - Y_i)^2 + (Z - Z_i)^2, \quad (i = 1, 2, 3).$$

* Denotes the transpose of the matrix

Forming the partial derivatives of these equations with respect to all the r_k, ϕ'_k, λ_k (K = 1, 2, 3, 4), and using the relationship

$$R_4^2 = (X - X_4)^2 + (Y - Y_4)^2 + (Z - Z_4)^2$$

to eliminate the terms of the form $\frac{\partial R_4}{\partial \phi_i}$,

one may compute P_i, given by:

$$P_i = \left[\frac{\partial \bar{r}}{\partial r_i}, \frac{\partial \bar{r}}{\partial \phi'_i}, \frac{\partial \bar{r}}{\partial \lambda_i}\right] \qquad (i = 1, 2, 3, 4).$$

The variances in r_i, ϕ'_i, λ_i $(i = 1, 2, 3, 4)$ are:

σ_{ri}^2 from the input $(i = 1, 2, 3, 4)$

$$\sigma_{\phi i}^2 = \frac{\sigma N^2}{r_i^2} \qquad (i = 1, 2, 3, 4)$$

$$\sigma_{\lambda i}^2 = \frac{\sigma E^2}{r_i^2 \cos^2 \phi'_i} \qquad (i = 1, 2, 3, 4).$$

Therefore, the covariance, $M_{\bar{r}}$ arising from survey errors is given by:

$M_{\bar{r}}$ = sum over i = 1 to 4 of

$$\left[P_i\right]\begin{bmatrix} \sigma_{ri}^2 & 0 & 0 \\ 0 & \sigma_{\phi' i}^2 & 0 \\ 0 & 0 & \sigma_{\lambda i}^2 \end{bmatrix}\left[P_i^*\right].$$

APPENDIX II

DETERMINING THE EARTH RADIUS AT THE TRACKING SITES BY USE OF THE ORBIT OF AN EARTH SATELLITE

2.1 BASIC EQUATION OF MOTION

The potential of the earth's gravitational field can be expressed as follows:

$$U = \frac{fM}{r}\left[1 + \frac{B-A}{2Mr^2}\,(1-3\sin^2\Theta) + P(r, \Theta, \phi)\right] \qquad \text{(II-1)}$$

where:

M is the mass of the earth,

B and A are the moments of inertia with respect to the earth's principal axes,

f is the gravity constant,

r is the distance from the earth's mass center,

and Θ is the angle of latitude.

The term $P(r, \Theta, \phi)$ represents the higher-order harmonic components and local gravity anomalies.

If the time of observation is limited to a relatively short period (less than 30 minutes) the term $P(r, \Theta, \phi)$ may be omitted, because its integrated effect over the interval is small.

The value of the coefficient $\frac{B-A}{M} = 0.001106a^2$ (a = equatorial radius) has been internationally adopted, so that, equation (II-1) can be rewritten, using $fM = 3.9871175 \times 10^{14} m^3/sec^2$, as:

$$U_{(meters^2/sec^2)} = \frac{3.987\ 117\ 5 \times 10^{14}}{r}\left[1 + \frac{2.250 \times 10^{10}}{r^2}\,(1-3\sin^2\Theta)\right] \qquad \text{(II-2)}$$

For the sake of simplicity we introduce the abbreviation:

$$fM = k = 3.9871175 \times 10^{14} \ m^3 \ sec^{-2} \tag{II-3}$$

$$\frac{B-A}{2M} = n = 2.250 \times 10^{10} \ m^2 \tag{II-4}$$

The gravitational acceleration of the potential field (II-1) is the gradient of the potential function,

$$\bar{g} = \text{grad } U \tag{II-5}$$

Substituting II-3 and II-4 in II-2 and taking the gradient, in spherical coordinates, the gravitational vector can then be expressed as follows:

$$\bar{g} = -\bar{e}_r \frac{k}{r^2} \left\{1 + \frac{3n}{r^2}(1-3\sin^2\Theta)\right\} \ -\bar{e}_\Theta \frac{6kn}{r^4} \sin\Theta \cos\Theta \tag{II-6}$$

where: $\bar{e}_r$ is the unit vector in the radial direction and $\bar{e}_\Theta$ is the unit vector in the meridian plane, perpendicular to the radius vector.

The motion of a satellite moving under influence of the gravitational field (equation II-6) can be characterized by the following set of equations:

$$\ddot{r} - r\dot{\Theta}^2 - r\dot{\phi}^2\cos^2\Theta = -\frac{k}{r^2}\left\{1 + \frac{3n}{r^2}(1 - 3\sin^2\Theta)\right\} \tag{II-7}$$

$$r\ddot{\Theta} + 2\dot{r}\dot{\Theta} + r\dot{\phi}^2 \sin\Theta\cos\Theta = \frac{6kn}{r^4}\sin\Theta\cos\Theta \tag{II-8}$$

$$r\ddot{\phi}\cos\Theta + 2\dot{r}\dot{\phi}\cos\Theta - 2r\dot{\phi}\dot{\Theta}\sin\Theta = 0 \tag{II-9}$$

This set of equations is non-linear, and rigorous solutions cannot be obtained by elementary methods. In this report an attempt is made to solve this equation by means of perturbation methods.

2.2 UNPERTURBED SOLUTIONS

The gravitational vector (equation II-6) can be considered as being composed of a primary term, which is the Newtonian force field, and some fairly small terms which distort the Newtonian field slightly. A Newton force field is generated around a mass point or a spherically shaped body having either uniform or concentric mass density distribution. Such a field has concentric, constant-potential surfaces with its center coinciding with the center of the sphere. Equation II-6 represents a Newtonian field for $n = 1/2 \frac{B-A}{M} = 0$ in

accordance with the definition. The term $\sqrt{\frac{B-A}{M}}$ which sometimes is referred to as "mechanical ellipticity" is a fictitious distance corresponding to the radius of gyration of the difference in the moments of inertia along the polar axis and an equatorial line. This distance is about 3.3 percent of the earth radius. Since terms containing the factor n enter the right hand side of equations II-7 and II-8, only small deviations will result from an orbit based on the Newtonian field. The orbit-theory of a body in the Newtonian field is well established and known as the Keplerian motion. Keplerian motion is therefore defined by equations II-7, II-8, and II-9 when $n = 0$ so that:

$$\ddot{r} - r\dot{\theta}^2 - r\dot{\phi}^2 \cos^2\theta = -\frac{k}{r^2} \tag{II-10}$$

$$r\ddot{\theta} + 2\dot{r}\dot{\theta} + r\dot{\phi}^2 \sin\theta\cos\theta = 0 \tag{II-11}$$

$$r\ddot{\phi}\cos\theta + 2\dot{r}\dot{\phi}\cos\theta - 2r\dot{\phi}\dot{\theta}\sin\theta = 0. \tag{II-12}$$

Solutions of this set of equations are obtainable by means of elementary methods. (Despite the fact that we know the solutions to conic sections, we do not hesitate in finding solutions of equations II-10 to II-12. The expressions gained will be used when the perturbed problem is treated.)

Equation II-12 can be integrated immediately after division by $r\dot{\phi}\cos\theta$, yielding the result:

$$r^2\dot{\phi}\cos^2\theta = C \tag{II-13}$$

where C represents a constant of integration.

By means of equation II-13 the quantity $\dot{\phi}$ in equation II-11 can be eliminated so that:

$$r\ddot{\theta} + 2\dot{r}\dot{\theta} + \frac{C^2\sin\theta}{r^3\cos^3\theta} = 0.$$

A solution to this equation is:

$$r^2\dot{\theta} = \sqrt{K - \frac{C^2}{\cos^2\theta}} \tag{II-14}$$

where K is another constant of integration.

Equations (II-13) and (II-14) together represent Kepler's first law which, of course, can be obtained in a simpler way when different coordinates are used. Kepler's first law says:

A mass point moving in a Newtonian field moves in a plane such that the radius vector sweeps out equal areas in equal time-periods.

This result can be expressed by:

$$r^2 \dot{\chi} = C' \tag{II-15}$$

where $\dot{\chi}$ represents the angular velocity of the radius vector $\bar{r}$. Figure 44 shows the orbital plane cutting out a great circle on a sphere of reference whose center coincides with the center of mass of the earth. The nodal line common to the orbital plane as well as the equatorial plane is the y axis of the cartesian coordinate system. Angle YOS is the true anomaly, χ ; angle YOT is the angle of azimuth, ϕ ; and angle TOS is the angle of latitude, Θ . The inclination of the orbital plane, with respect to the equatorial plane, is the angle α, measured at point Y.

For the spherical triangle YST the following three relationships exist:

$$\tan \phi = \cos \alpha \tan \chi \tag{II-16}$$

$$\cos \chi = \cos \Theta \cos \phi \tag{II-17}$$

$$\sin \Theta = \sin \alpha \sin \chi \tag{II-18}$$

Differentiating (II-16) with respect to time and using (II-15) and (II-17) yields the relationship:

$$r^2 \dot{\phi} \cos^2 \Theta = C' \cos \alpha \tag{II-19}$$

Comparison with equation (13) shows that:

$$C = C' \cos \alpha \ . \tag{II-20}$$

A relation corresponding to (II-14) can be obtained when (II-18) is differentiated and introduced into (II-15):

$$r^2 \dot{\chi} = r^2 \dot{\Theta} \frac{1}{\sqrt{1 - \dfrac{\cos^2 \alpha}{\cos^2 \Theta}}} = C' \tag{II-21}$$

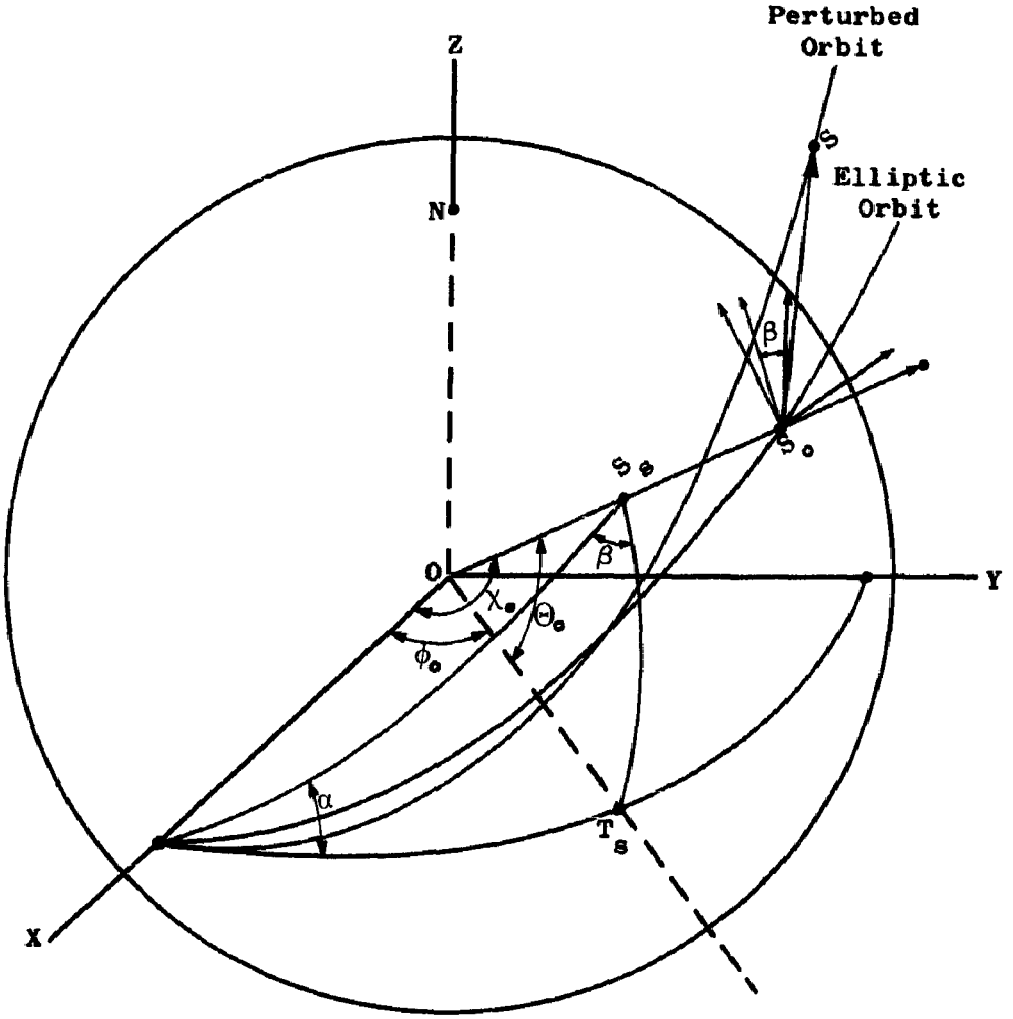

Figure 44. Orbital Cutting Plane and Reference Sphere

which, on combining with (II-14) yields:

$$K = \sqrt{C'} \quad . \tag{II-22}$$

Next we have to solve equation (II-10). Introducing (II-19) and (II-21) into (II-10) yields the following equation:

$$\ddot{r} - r \left[\frac{C'^2}{r^4} \left(1 - \frac{\cos^2 \alpha}{\cos^2 \Theta} \right) + \frac{C'^2}{r^4} \frac{\cos^2 \alpha}{\cos^2 \Theta} \right] = - \frac{k}{r^2}$$

or

$$\ddot{r} - \frac{C'^2}{r^3} + \frac{k}{r^2} = 0$$

Multiplying by dr and integrating, results in:

$$\frac{dr}{dt} = \frac{1}{r} \sqrt{2kr - C'^2} \quad . \tag{II-23}$$

Together with (II-15) the last equation becomes:

$$\frac{dr}{d\chi} = \frac{r}{C'} \sqrt{2kr - C'^2} \quad . \tag{II-24}$$

Integration of (II-24) results in:

$$r_o = \frac{P}{1 + \epsilon \cos (\chi_o - \chi_{o_A})} \quad , \tag{II-25}$$

the analytical expression of a conic section, where (p = parameter of conic section, ϵ = eccentricity, χ_{o_A} = angular distance of apogee.

2.3 PERTURBED PROBLEM

To determine the effects of small perturbing forces on satellite motion we can introduce in the radius vector, $\bar{r}_o$, of the unperturbed motion a small incremental vector $\overline{\Delta r}$. The

radius vector of the perturbed case thus becomes:

$$\bar{r} = \bar{r}_o + \overline{\Delta r} \quad . \tag{II-26}$$

Let us introduce the unit vector $\bar{e}_r$ in the radial direction and $\bar{e}_{\perp R}$, a unit vector perpendicular to the orbital plane and rewrite equation (II-26) as follows:

$$\bar{r} = \bar{e}_r r_o + \bar{e}_r \Delta r + r_o \Delta \bar{e}_r \quad . \tag{II-27}$$

According to (II-25), the quantity r_o in this equation is the radial distance and is a function of time. The incremental vector $\overline{\Delta e}_r$ has to be perpendicular to $\bar{e}_r$ since total differentiation of the identity $(\bar{e}_r)^2 = 1$, yields the dot product $2\ (\bar{e}_r \cdot \Delta \bar{e}_r) = 0$. Figure 44 shows the incremental vector $\overline{\Delta r}$ in relation to the instantaneous orbital position. (II-2)

The incremental component $r_o \overline{\Delta e}_r$ can be resolved along the unit vectors $\bar{e}_\theta$ and $\bar{e}_\phi$ of the local spherical coordinate system. In this fashion we get:

$$r_o \overline{\Delta e}_r = \bar{e}_\theta r_o \Delta\theta + \bar{e}_\phi r_o \cos\theta_o \Delta\phi \quad . \tag{II-28}$$

Equation (II-27) therefore becomes:

$$\bar{r} = \bar{e}_r r_o + \bar{e}_r \Delta r + \bar{e}_\theta r_o \Delta\theta + \bar{e}_\phi r_o \cos\theta_o \Delta\phi \quad . \tag{II-29}$$

This result exhibits all three incremental components of the difference vector between the perturbed radius vector and the unperturbed (elliptic orbit) radius vector. We shall note that equation (II-26) has been considered at the moment, t; therefore, time is an independent variable of all quantities in (II-29).

In order to get the three incremental components, we have to find Δr, $\Delta\theta$ and $\Delta\phi$ as a function of time. These three quantities are controlled by equations (II-7) to (II-9). The three variables of these equations can be written as follows:

$$r = r_o + \Delta r \tag{II-30}$$

$$\theta = \theta_o + \Delta\theta \tag{II-31}$$

$$\phi = \phi_o + \Delta\phi \quad . \tag{II-32}$$

These three terms substituted into sets of equations II-7, II-8, and II-19 (the solution of II-9), result in the desired set of equations for the new variables Δr, $\Delta \Theta$, and $\Delta\phi$. Because of the small order of those quantities, we can ignore all terms of the order higher than one. The equations in Δr, $\Delta\Theta$, and $\Delta\phi$ therefore will be linear type differential equations.

First we introduce equations II-30, II-31, and II-32 into II-19 and obtain:

$$(r_o + \Delta r)^2 \left[\dot{\phi}_o + (\Delta\phi)^{\cdot}\right] \cos^2 (\Theta_o + \Delta\Theta) = C' \cos\alpha \quad .$$

Expanding all the binomials and ignoring higher order terms:

$$\dot{\phi}_o r_o^2 \cos^2\Theta_o + \left[\dot{r}_o^2 (\Delta\phi)^{\cdot} + 2 r_o \dot{\phi}_o \Delta r\right] \cos^2\Theta_o$$
$$- 2\sin\Theta_o \cos\Theta_o \dot{\phi}_o r_o^2 \Delta\Theta = C' \cos\alpha \quad . \qquad \text{(II-33)}$$

Equation II-19 is also valid for the unperturbed system, consequently the equation:

$$\dot{\phi}_o r_o^2 \cos^2\Theta_o = C' \cos\alpha$$

reduces II-33 to the relation:

$$r_o \cos\Theta_o (\Delta\phi)^{\cdot} + 2\dot{\phi}_o \cos\Theta_o \Delta r - 2 r_o \dot{\phi}_o \sin\Theta_o \Delta\Theta = 0. \qquad \text{(II-34)}$$

Before we introduce equations II-30 to II-32 into equation II-8 we multiply II-8 by $2r^3\dot{\Theta}$ and obtain:

$$(r^4 \dot{\Theta}^2)^{\cdot} + 2 r^4 \dot{\phi}^2 \dot{\Theta} \sin\Theta\cos\Theta = \frac{12kn}{r} \sin\Theta\cos\Theta\ \dot{\Theta} \quad .$$

We can substitute $\dot{\phi}$ by means of the solution of (II-9) which happens to be identical with (II-19). In this way we obtain, after performing some small identical transformations:

$$r^4\dot{\Theta}^2 + C'^2 \frac{\cos^2\alpha}{\cos^2\Theta} = 6kn \int \frac{d(\sin^2\Theta)}{r} + C'^2 \quad . \qquad \text{(II-35)}$$

Now, introducing equations II-30 to II-32 into II-35, we obtain:

$$(r_o^4 + 4r_o^3 \Delta r)\left[\dot{\Theta}_o^2 + 2\dot{\Theta}_o (\Delta\Theta)^{\cdot}\right] + C'^2 \frac{\cos^2\alpha}{\cos^2(\Theta_o + \Delta\Theta)}$$
$$= 6kn \int \frac{d\left[\sin^2(\Theta_o + \Delta\Theta)\right]}{r_o} \left(1 - \frac{\Delta r}{r_o}\right) + C'^2 \quad .$$

or, taking into account only linear incremental terms:

$$r_o^4 \dot{\theta}_o^2 + \frac{C'^2 \cos^2\alpha}{\cos^2\theta_o}(1 - 2\cos\theta_o \sin\theta_o \Delta\theta) + 4r_o^3 \dot{\theta}_o^2 \Delta r$$

$$+ 2r_o^4 \dot{\theta}_o (\Delta\theta)^{\cdot} = 6kn \int \frac{d \sin^2\theta_o}{r_o} + C'^2 \quad . \tag{II-36}$$

The unperturbed solution obeys II-14, which can be rewritten as:

$$r_o^4 \dot{\theta}_o^2 + \frac{C'^2 \cos^2\alpha}{\cos^2\theta_o} = C'^2 \tag{II-37}$$

which, on combining with II-36, yields a second relation between the incremental quantities:

$$2C'^2 \cos^2\alpha \tan\theta_o \Delta\theta + 4r_o^3 \dot{\theta}_o^2 \Delta r + 4r_o^4 \dot{\theta}_o (\Delta\theta)^{\cdot}$$

$$= 6kn \int \frac{d(\sin^2\theta_o)}{r_o} \quad . \tag{II-38}$$

The left hand side of equation II-38 can be easily integrated. By means of II-18 and II-25 we obtain:

$$\int \frac{d(\sin^2\theta_o)}{r_o} = \frac{\sin^2\alpha}{p} \int (1 + \epsilon \cos\{\chi_o - \chi_{oA}\}) \; d(\sin^2\chi_o)$$

$$= \frac{\sin^2\alpha \sin^2\chi_o}{p} + \frac{\epsilon}{p} \sin^2\alpha \int \cos(\chi_o - \chi_{oA}) \, d(\sin^2\chi_o) =$$

$$\frac{\sin^2\alpha}{p}\left[\sin^2\chi_o - \frac{\epsilon}{3}\left(2\cos\chi_{oA} \cos^3\chi_o - \sin\chi_{oA} \sin^3\chi_o\right)\right] \quad . \tag{II-39}$$

Equation II-38 therefore can be rewritten as:

$$C'^2 \cos^2\alpha \tan\theta_o \Delta\theta + 2r_o^3 \dot{\theta}_o^2 \Delta r + r_o^4 \dot{\theta}_o (\Delta\theta)^{\cdot}$$

$$= \frac{3kn}{p} \sin^2\alpha \left[\sin^2\chi_o - \frac{\epsilon}{3}\left(2\cos\chi_{oA} \cos^3\chi_o - \sin\chi_{oA} \sin^3\chi_o\right)\right] \quad . \tag{II-40}$$

A third equation can be obtained by introducing equations II-30 to II-32 into equation II-7. In this way we get:

$$\ddot{r}_o + (\Delta r)^{\cdot\cdot} - (r_o + \Delta r)\left[\dot{\theta}_o^2 + 2\,\dot{\theta}_o\,(\Delta\theta)^{\cdot}\right]$$

$$- (r_o + \Delta r)\left[\dot{\phi}_o^2 + 2\,\dot{\phi}_o\,(\Delta\phi)^{\cdot}\right]\cos^2\theta_o\,(1 - \tan\theta_o\,\Delta\theta) =$$

$$-\frac{k}{r_o^2}\left(1 - 2\frac{\Delta r}{r_o}\right)\left\{1 + \frac{n}{r_o^2}\left(1 - 2\frac{\Delta r}{r_o}\right)\left[1 - 3\sin^2\theta_o\,(1 + 2\cot\theta_o\,\Delta\theta)\right]\right\}.$$

After expanding the bracket expressions and ignoring higher than first order terms we obtain:

$$\ddot{r}_o + r_o\,\dot{\theta}_o^2 - r_o\,\phi_o^2\cos^2\theta_o + (\Delta r)^{\cdot\cdot} - \dot{\theta}_o^2\,\Delta r - 2r_o\,\dot{\theta}_o\,(\Delta\theta)^{\cdot}$$

$$- \dot{\phi}_o^2\cos^2\theta_o\,\Delta r - 2r_o\,\dot{\phi}_o\cos^2\theta_o\,(\Delta\phi)^{\cdot} + r_o\,\dot{\phi}_o^2\cos\theta_o\sin\theta_o\,\Delta\theta$$

$$= -\frac{k}{r_o^2}\left\{1 + \frac{n}{r_o^2}(1 - 3\sin^2\theta_o)\right\} + \frac{2k}{r_o^3}\left\{1 + \frac{2n}{r_o^2}(1 - 3\sin^2\theta_o)\right\}\Delta r$$

$$+ 6\frac{kn}{r_o^4}\sin\theta_o\cos\theta_o\,\Delta\theta \quad .$$

Since the quantities r_o, θ_o, and ϕ_o obey equation II-10, the last equation reduces to:

$$(\Delta r)^{\cdot\cdot} - (\dot{\theta}_o^2 + \dot{\phi}_o^2\cos^2\theta_o)\,\Delta r - 2r_o\,\dot{\theta}_o\,(\Delta\theta)^{\cdot}$$

$$- 2r_o\,\phi_o\cos^2\theta_o\,(\Delta\phi)^{\cdot} + r_o\,\dot{\phi}_o^2\cos\theta_o\sin\theta_o\,\Delta\theta =$$

$$-\frac{kn}{r_o^4}\left[1 - 3\sin^2\theta_o - 4\frac{\Delta r}{r_o}(1 - 3\sin^2\theta_o) - 6\sin\theta_o\cos\theta_o\,\Delta\theta\right]$$

$$+ \frac{2k}{r_o^3}\,\Delta r \quad .$$

The terms $\frac{4\Delta r}{4_o}$ and $\Delta\Theta$ are $\ll 1$. Therefore we can bring this equation to the form:

$$(\Delta r)^{\cdot\cdot} - (\dot{\Theta}_o^2 + \dot{\phi}_o^2 \cos^2\Theta_o + \frac{2k}{r_o^3})\Delta r - 2r_o\dot{\Theta}_o(\Delta\Theta)^{\cdot}$$

$$- 2r_o\dot{\phi}_o\cos^2\Theta_o\ (\Delta\phi)^{\cdot} + r_o\dot{\phi}_o^2\sin\Theta_o\cos\Theta_o\Delta\Theta$$

$$= -\frac{kn}{r_o^4}(1 - 3\sin^2\Theta_o)\ . \qquad \text{(II-41)}$$

In equation II-41 we must specify all the coefficients containing derivatives. By means of II-19 and II-21 we obtain:

$$\dot{\Theta}_o^2 + \dot{\phi}_o^2\cos^2\Theta_o = \frac{C'^2}{r_o^4} \qquad \text{(II-42)}$$

$$r_o\dot{\Theta}_o = \frac{C'}{r_o}\sqrt{1 - \frac{\cos^2\alpha}{\cos^2\Theta_o}} \qquad \text{(II-43)}$$

$$\dot{\phi}_o = \frac{C'\cos\alpha}{r_o^2\cos^2\Theta_o} \qquad \text{(II-44)}$$

and on combining these equations with II-41:

$$(\Delta r)^{\cdot\cdot} - \frac{\Delta r}{r_o^3}\,2k\left[1 + \frac{C'^2}{2kr_o}\right] - \frac{2C'}{r_o}\sqrt{1 - \frac{\cos^2\alpha}{\cos^2\Theta_o}}\ (\Delta\Theta)^{\cdot}$$

$$+ \frac{\Delta\Theta}{r_o^3}C'^2\frac{\cos^2\alpha}{\cos^2\Theta_o}\,\mathrm{tg}\,\Theta_o\Delta\Theta - 2\frac{C'\cos\alpha}{r_o}(\Delta\phi)^{\cdot} \qquad \text{(II-45)}$$

$$= -\frac{kn}{r_o^4}(1 - 3\sin^2\Theta_o).$$

In the same fashion we can reduce II-40 and II-34, which yields:

$$C'^2 \cos^2\alpha \tan\Theta_o \Delta\Theta + \frac{2C'^2}{r_o}\left(1 - \frac{\cos^2\alpha}{\cos^2\Theta_o}\right)\Delta r$$

$$+ r_o^2 C' \sqrt{1 - \frac{\cos^2\alpha}{\cos^2\Theta_o}}\,(\Delta\Theta)^{\cdot}$$

$$= \frac{3kn}{p} \sin^2\alpha \left[\sin^2\chi_o - \frac{\epsilon}{2}\left(2\cos\chi_{oA}\cos^3\chi_o - \sin\chi_{oA}\sin\chi_o\right)\right] . \qquad \text{(II-46)}$$

Finally we obtain from II-34 the modified equation:

$$(\Delta\phi)^{\cdot} = 2\frac{C'\cos\alpha}{r_o^2\cos^2\Theta_o}\left(\tan\Theta_o\,\Delta\Theta - \frac{\Delta r}{r_o}\right) \qquad \text{(II-47)}$$

which on combining with equation II-45 obtains:

$$(\Delta r)^{\cdot\cdot} - \Delta r \frac{2k}{r_o^3}\left[1 + \frac{C'^2}{2kr_o}\left(1 - \frac{4\cos^2\alpha}{\cos^2\Theta_o}\right)\right] - \frac{2C'}{r_o}\sqrt{1 - \frac{\cos^2\alpha}{\cos^2\Theta_o}}\,(\Delta\Theta)^{\cdot}$$

$$- 3\frac{C'^2\cos^2\alpha}{r_o^3\cos^2\Theta_o}\Theta_o\Delta\Theta = -\frac{kn}{r_o^4}\left(1 - 3\sin^2\Theta_o\right) . \qquad \text{(II-48)}$$

Now we can introduce the incremental component of perturbation in the direction of the local meridian circle. This quantity shall be denoted by Δp. Next, we define the incremental component Δq, parallel to the equatorial plane. From II-29 we get the relations:

$$\Delta p = r_o \Delta\Theta \qquad \text{(II-49)}$$

$$\Delta q = r_o \cos\Theta_o \Delta\phi . \qquad \text{(II-50)}$$

Differentiating equation II-49:

$$(\Delta p)^{\cdot} = \dot{r}_o \Delta\theta + r_o (\Delta\theta)^{\cdot}$$

or

$$(\Delta\theta)^{\cdot} = \frac{1}{r_o}(\Delta p)^{\cdot} - \frac{\dot{r}_o}{r_o}\Delta p \quad . \tag{II-51}$$

We can modify equations II-46, II-47 and II-48 by introducing II-49, II-50 and II-51. Equation II-48 changes to:

$$(\Delta r)^{\cdot\cdot} - \Delta r \frac{2k}{r_o^3}\left[1 + \frac{C'^2}{2kr_o}\left(1 - \frac{4\cos^2\alpha}{\cos^2\theta_o}\right)\right] - \frac{2C'}{r_o^2}\frac{\tan\chi_o}{\tan\theta_o}(\Delta p)^{\cdot}$$

$$- \left[\frac{3C'^2\cos^2\alpha}{r_o^4\cos^2\theta_o}\tan\theta_o - \frac{2C'\dot{r}_o\tan\chi_o}{r_o^2\tan\theta_o}\right]\Delta p = -\frac{kn}{r_o^4}(1 - 3\sin^2\theta_o) \tag{II-52}$$

and II-46 becomes:

$$2\frac{C'^2}{r_o}\frac{\tan\chi_o}{\tan\theta_o}\Delta r + r_o C'\frac{\tan\chi_o}{\tan\theta_o}(\Delta p)^{\cdot}$$

$$+\left[\frac{C'^2}{r_o}\cos^2\alpha\tan\theta_o - r_o\dot{r}_o C'\frac{\tan\chi_o}{\tan\theta_o}\right]\Delta p$$

$$= \frac{3kn}{p}\sin^2\alpha\left[\sin^2\chi_o - \frac{\epsilon}{2}(2\cos\chi_{oA}\cos^3\chi_o - \sin\chi_{oA}\sin^3\chi_o)\right] \quad . \tag{II-53}$$

This is a set of linear differential equations between the two components of perturbation Δr and Δp. All the coefficients involved are functions of time, since the quantities χ_o, θ_o, and r_o are known functions of time. From equation II-47 we obtain the incremental component Δq directly.

$$\Delta q = \frac{2C'\cos\alpha}{r_o\cos\theta_o}\int_o^t \frac{\tan\theta_o\Delta p - \Delta r}{r_o^3\cos^2\theta_o}\,dt' \tag{II-54}$$

$\Delta\Theta$ and Δr are solutions of Eqs. II-52 and II-53, and therefore functions of time. We finally come to the conclusion that finding solutions of Eqs. II-52 and II-53 is the essential part in finding the perturbing components.

Since we have to express r_o as a function of time we obtain that function by integration of II-23.

$$t - t_o = \int_{r_{oA}}^{r_o} \frac{\rho d\rho}{\sqrt{2k\rho - C'^2}} = \frac{1}{3k^2} \sqrt{2kr_o - C'^2} \left[kr_o + C'^2 \right] - A .$$

Squaring r_{oA} this equation turns out a third-order algebraic equation for r_o:

$$2k^3 r_o^3 + 3C'^2 k^2 r_o^2 - \left[C'^2 + 9k^4 (t - t_o + A)^2 \right] = 0 \qquad \text{(II-55)}$$

which can be solved for r_o in terms of t. The parameter A is given by:

$$A = \frac{1}{3k^2} \sqrt{2kr_{oA} - C'^2} \left[kr_{oA} + C'^2 \right] \qquad \text{(II-56)}$$

where r_{oA} is the radial distance at $t = 0$ (or $\chi_o = 0$).

According to II-25:

$$r_{oA} = \frac{p}{1 + \epsilon \cos \chi_{oA}} . \qquad \text{(II-57)}$$

Now we can express χ_o in terms of r_o by means of:

$$\chi_o(t) = \chi_{oA} + \arccos \left\{ \frac{1}{\epsilon} \left[\frac{p}{r_o(t)} - 1 \right] \right\} \qquad \text{(II-58)}$$

where $r_o(t)$ is a solution of II-55.

Finally, the angle Θ_o can be expressed with respect to time according to II-18:

$$\Theta_o(t) = \arcsin \left\{ \sin\alpha \left[\sin \chi_{oA} \sqrt{1 - \frac{1}{\epsilon^2} \left[\frac{p}{r_o(t)} - 1 \right]^2} + \frac{1}{\epsilon} \left(\frac{p}{r_o(t)} - 1 \right) \cos \chi_{oA} \right] \right\} . \qquad \text{(II-59)}$$

Equations II-55, II-58, and II-59 exhibit the fact that the coefficients of the differential equations II-52 and II-53 are functions of the parameters ϵ (eccentricity), p (parameter of the ellipse), α (inclination angle of the plane of ellipse), χ_{oA} (true anomaly of reference line with respect to perigee), as well as, t (time), the independent variable.

2.4 PERTURBATION OF A CIRCULAR POLAR ORBIT

Equations II-52 and II-53 become linear equations with constant coefficients for circular polar orbits.

The circular polar orbit is characterized by:

$$\alpha = \frac{\pi}{2} \quad , \quad \epsilon = 0, \quad p = r_o = \text{constant}$$

$$C' = \frac{2\pi r_o^2}{T} \qquad (T = \text{revolution time})$$

$$k = g_o R^2$$

$$\chi_o = \Theta_o = 2\pi \frac{t}{T} \tag{II-60}$$

(Assuming that we consider orbit perturbation starting at the equator plane.)

Equation II-52 simplifies to:

$$(\Delta r)'' - \Delta r \frac{g_o R^2}{r_o^3} \left(1 + \frac{4\pi^2 r_o^3}{2T^2 g_o R^2}\right) - \frac{4\pi}{T} (\Delta p)'$$

$$= - \frac{g_o R^2}{r_o^4} n \left(1 - 3 \sin^2 2\pi \frac{t}{T}\right) \tag{II-61}$$

and equation II-53 to:

$$\Delta r + \frac{T}{4} (\Delta p)' = \frac{3 g_o R^2 T^2}{8\pi^2 r_o^4} n \sin^2 2\pi \frac{t}{T} \quad . \tag{II-62}$$

This set of equations (II-61 and II-62) can be solved by applying elementary methods. Combining II-62 with II-61 yields the linear equation:

$$(\Delta p)''' - \frac{4\pi^2}{T^2}\left(\frac{3}{2} - \frac{4}{\pi}\right)(\Delta p)' = \frac{4(4\pi^2)^{4/3} n}{(g_o R^2)^{1/3} T^{1/3}}\left(1 - \frac{45}{16}\sin^2 2\pi\frac{t}{T}\right) . \qquad \text{(II-63)}$$

If we consider the orbit to be circular at the equator plane, in other words $\Delta p = (\Delta p)' = 0$ at $t = 0$, then we obtain the following solution of II-63:

$$\Delta p = \frac{(4\pi^2)^{1/3} n}{2\pi\left(\frac{3}{2} - \frac{4}{\pi}\right)^{3/2} (g_o R^2 T^2)^{1/3}} \left\{ - \frac{\pi + 32}{11\pi - 8}\left(1 - e^{\omega_o \sqrt{\frac{3}{2} - \frac{4}{\pi}}\, t}\right) \right.$$

$$\left. + \frac{13\pi}{4}\sqrt{\frac{3}{2} - \frac{4}{\pi}}\,\frac{t}{T} - \frac{45\pi}{8(11\pi - 8)}\left(\frac{3}{2} - \frac{4}{\pi}\right)^{3/2} \sin\frac{4\pi}{T} t \right\} . \qquad \text{(II-64)}$$

By means of II-62 we get for Δr:

$$\Delta r = \frac{(4\pi^2)^{1/3} n}{2(g_o R^2 T^2)^{1/3}} \left\{ \frac{23\pi - 96}{8(3\pi - 8)} + \frac{(32 + \pi)\pi}{(11\pi - 8)(3\pi - 8)} e^{-\frac{2\pi}{T}\sqrt{\frac{3}{2} - \frac{4}{\pi}}\, t} \right.$$

$$\left. - \frac{3}{8}\,\frac{29\pi - 32}{11\pi - 8}\cos 2\,\frac{2\pi}{T} t \right\} . \qquad \text{(II-65)}$$

From II-54 we get:

$$\Delta q = 0 \qquad \text{(II-66)}$$

This result leads to the conclusion that a polar orbit remains a polar orbit if the only perturbation is that due to the ellipticity of the earth acting upon the satellite. One comes immediately to this conclusion on considering the fact that no force component perpendicular to the polar orbit plane exists. Figures 45 and 46 show the components Δr and Δp of perturbation versus time for a number of different orbits.

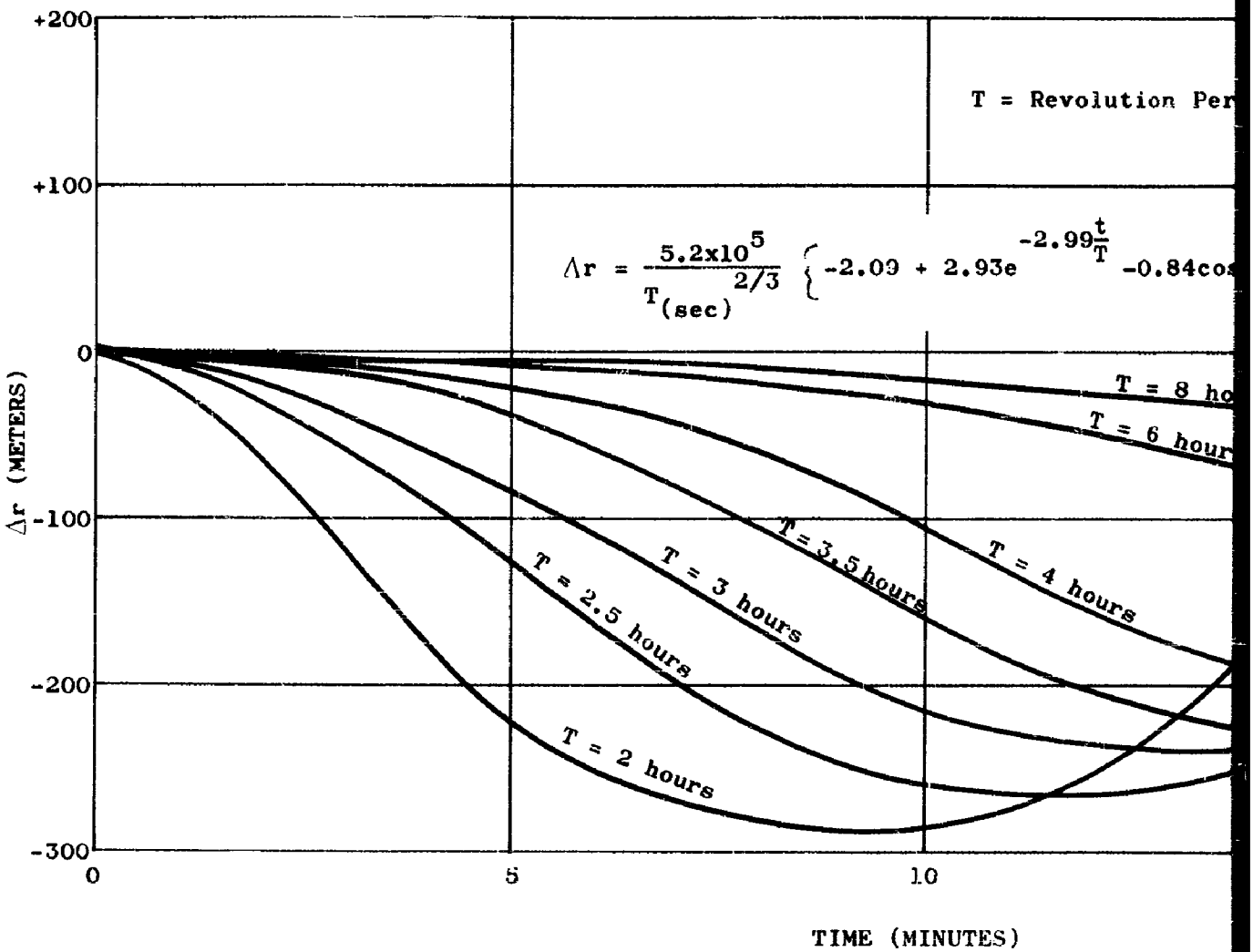

1

Figure 45. Radial Perturbatio

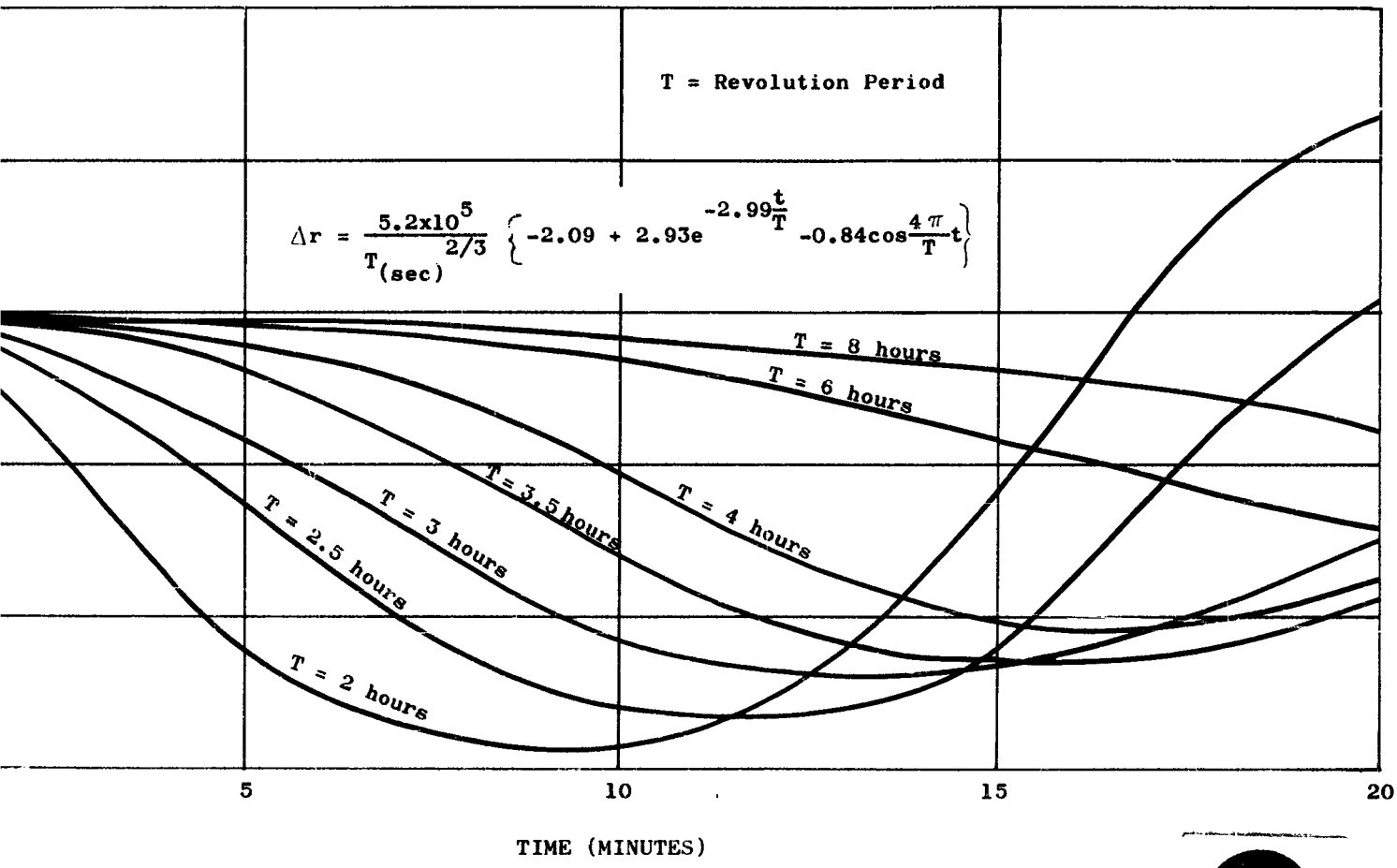

Figure 45. Radial Perturbation of a Circular Polar Orbit

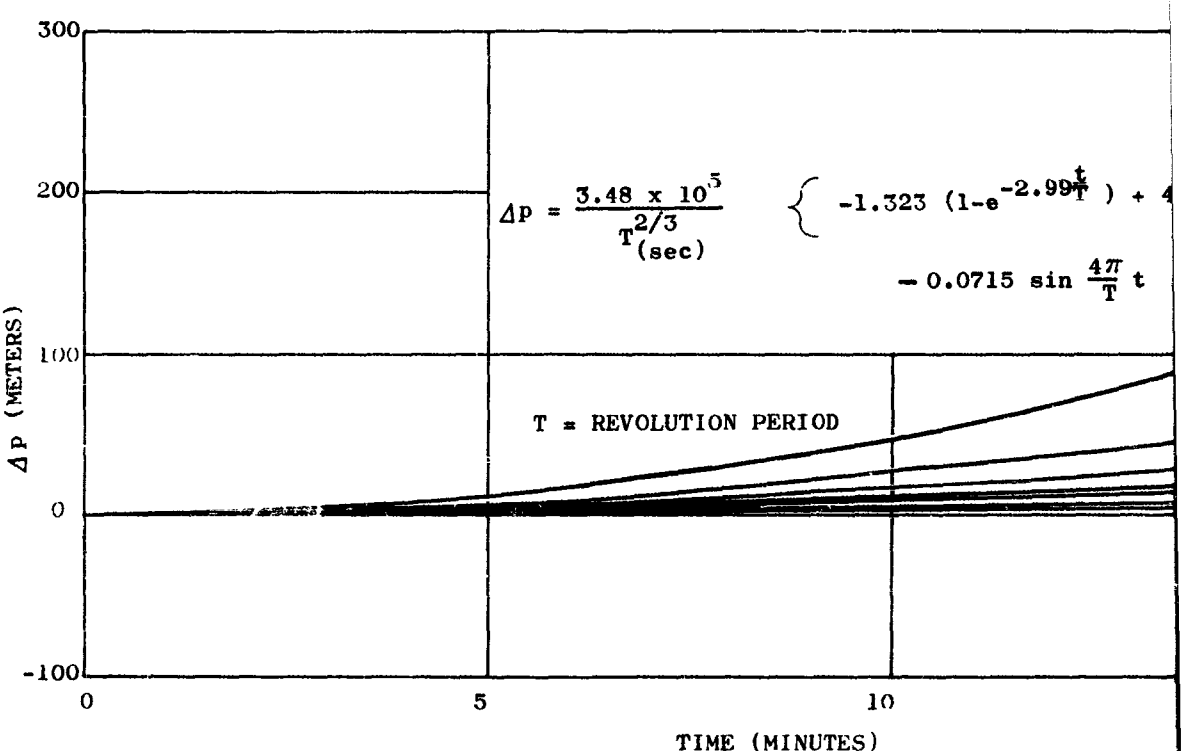

Figure 46. Meridional Perturba

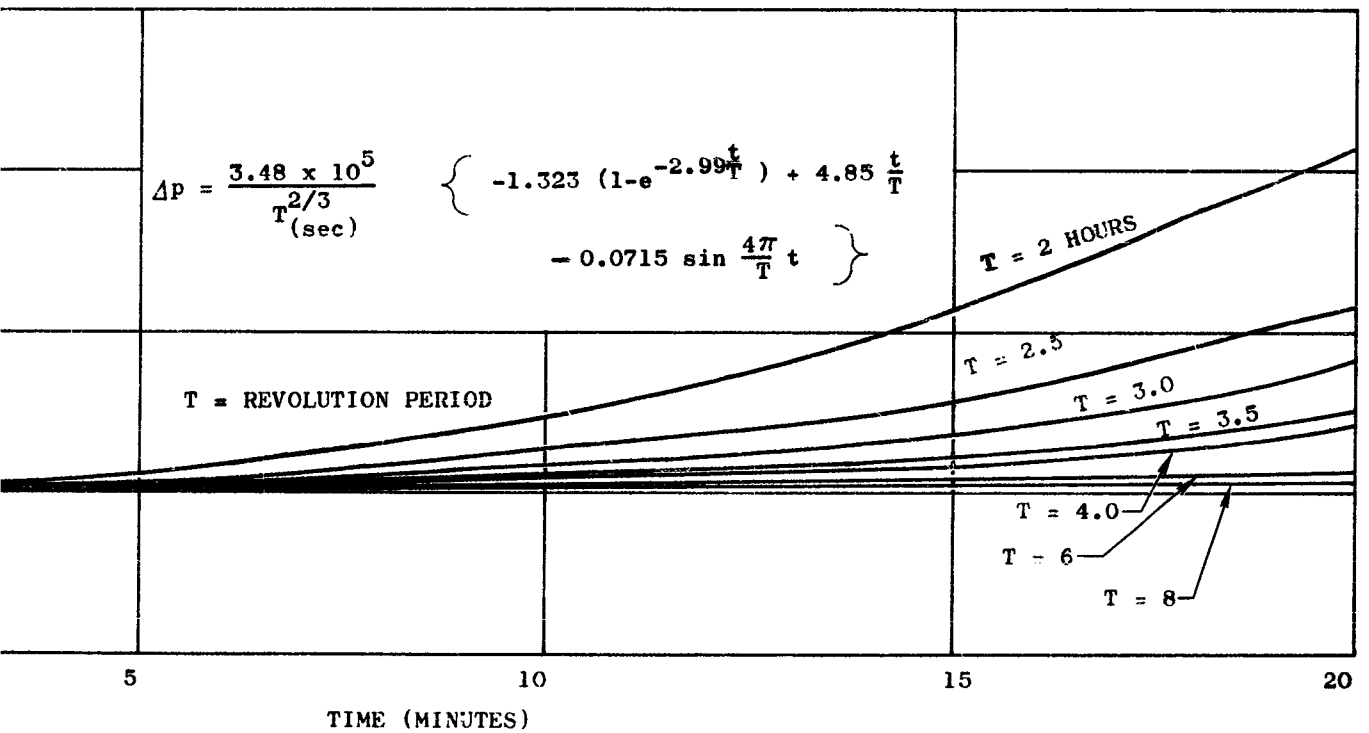

Figure 46. Meridional Perturbation of a Circular Polar Orbit

APPENDIX III

TROPOSPHERIC PROPAGATION

3.1 CONTRIBUTIONS OF SURFACE PARAMETERS

The investigation of the possibility of making fixed corrections for tropospheric range aberration (TRA), based on single parameters such as site location, surface refractivity, time of day, or season, led to the conclusion (as presented in the main body of the report) that a tropospheric range correction (TRC) based on a combination of data be employed.

The following discussions of these separate effects have been included in this appendix to support the fundamental conclusion.

3.1.1 Effect of Station Height

Early in the investigation it became apparent that the optimum location for tracking station sites would be at high and dry locations. This conclusion was reached for several different reasons.

World-wide values of surface refractivity versus altitude are plotted in Figure 47. This figure is taken from a report by Bean, Horn and Riggs (Reference III-19) of the Central Radio Propagation Laboratories (CRPL). It can be seen from the figure that the range of mean values of surface refractivity between different stations tends to decrease as the station elevation increases. It should also be noted that, since the absolute value of the surface refractivity is lower, and since there is less total atmosphere above the station, there is less tropospheric range aberration to be considered. In paragraph 3.2 of this appendix the diurnal and seasonal range of surface refractivity at a given station is also found to be less for high-altitude stations.

The required tropospheric range correction versus station elevation for several different values of elevation angle (ϵ) is plotted in Figure 48. The calculations for these curves were based on the CRPL reference profile having the world-wide mean value of sea-level refractivity, N_0, equal to 330 and assume that the atmosphere above any given station would correspond to that portion of the atmosphere lying above the reference profile at that altitude intercept.

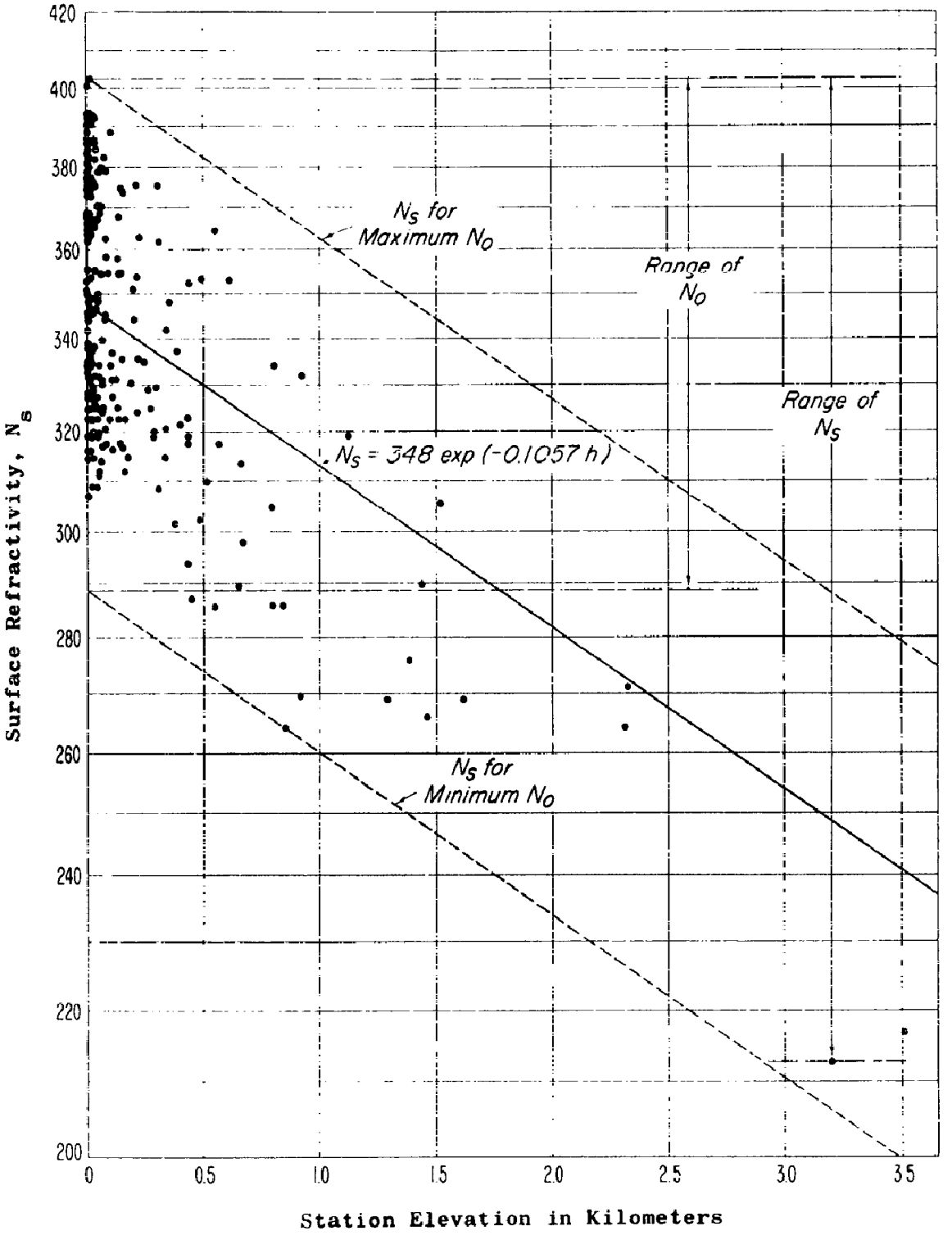

Figure 47. World-Wide Values of Surface Refractivity (N_S) vs. Height for August

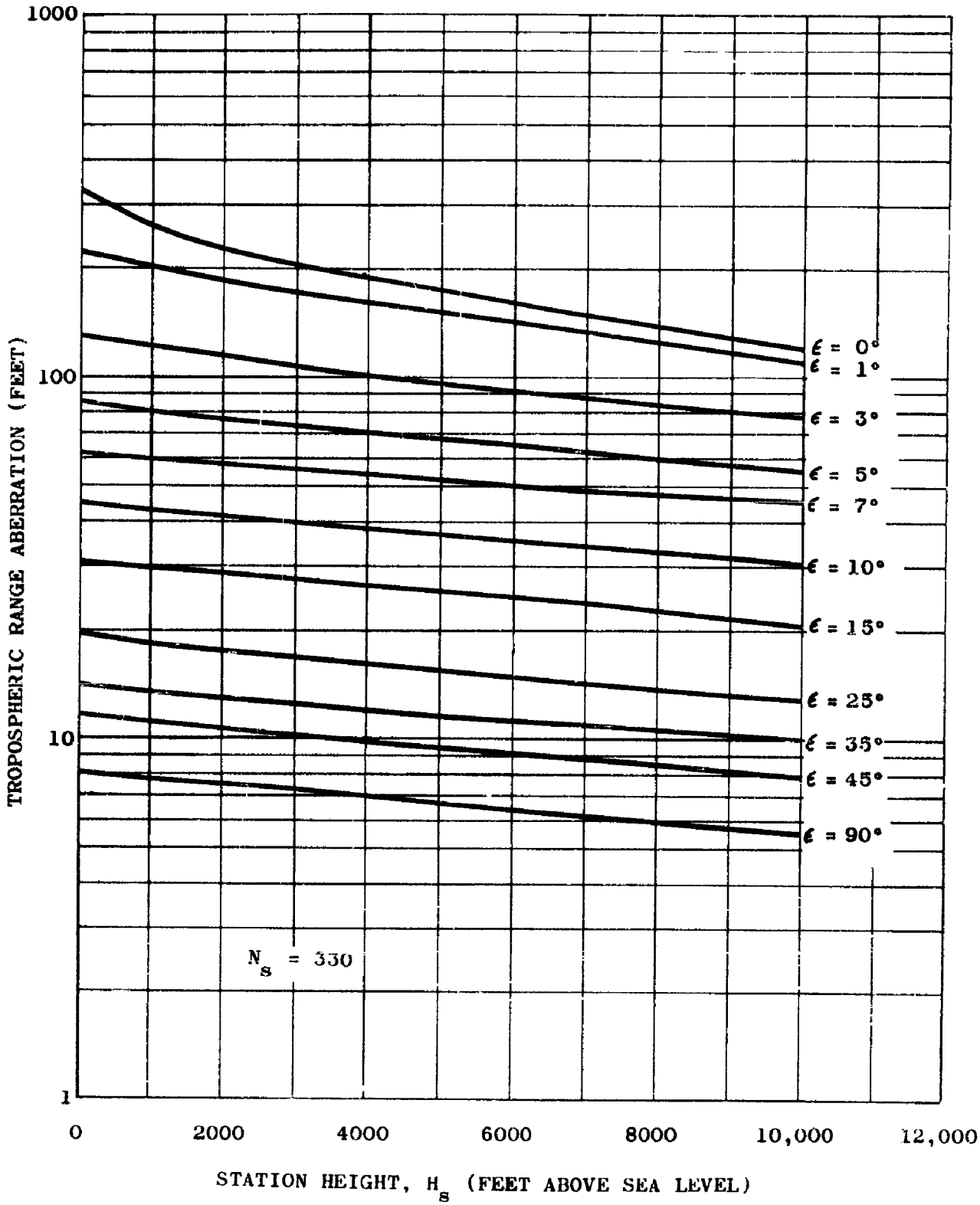

Figure 48. Tropospheric Range Aberration vs. Station Elevation for CRPL Reference Atmosphere - 1958 with $N_s = 330$

Having calculated the tropospheric range aberration for each of the 77 profiles supplied by the National Bureau of Standards, the rather close dependence of TRA upon the elevation of the station, H_S, was immediately apparent. Figure 49 is a scatter diagram of the total range aberration for each of the 77 stations plotted, versus H_S. It can be observed that there is reasonably good agreement between this figure and Figure 48. The values of the actual TRA at 45 degrees seem to be about one foot greater that the values of the TRA as calculated for the reference profile.

The refractivity, N, is composed of a dry term, D, plus a wet term, W. Bean and Ozanich (Reference III-24) quote these as being:

$$D = \frac{77.6\ P}{T}$$

$$W = \frac{3.73 \times 10^5\ e_s\ RH}{T^2}$$

Where: P is total atmospheric pressure in millibars

T is temperature in degrees Kelvin

e_s is the saturation vapor pressure in millibars

RH is the percent relative humidity

The dry term depends chiefly on altitude, while the wet term depends on the type of air mass above the site. To reduce the total refractivity and its variation (which will then reduce the aberration produced in the troposphere and the errors in any chosen correction scheme), it is desirable to reduce both the dry and wet terms. Choosing a site having a dry climate the year round is, of course, the best way to reduce the TRA contribution of the wet term.

Many authorities have pointed out that the amount of stratification in the atmosphere is much greater below 5,000 feet altitude above mean sea level. Since the variations in refractivity are much less below this altitude, the conclusion may be drawn that for a reduction in range errors due to tropospheric effects, trackers should be situated at sites chosen to give the highest, dryest climate possible.

3.1.2 Effect of Surface Refractivity, N_S

Many workers in the field of tropospheric propagation have suggested that the correlation between tropospheric range aberration and surface refractivity is a satisfactory means of obtaining (at least as a first approximation) an appropriate correction for tropospheric effects. Figures 50 and 51 give a scatter diagram plot of the values of the tropospheric

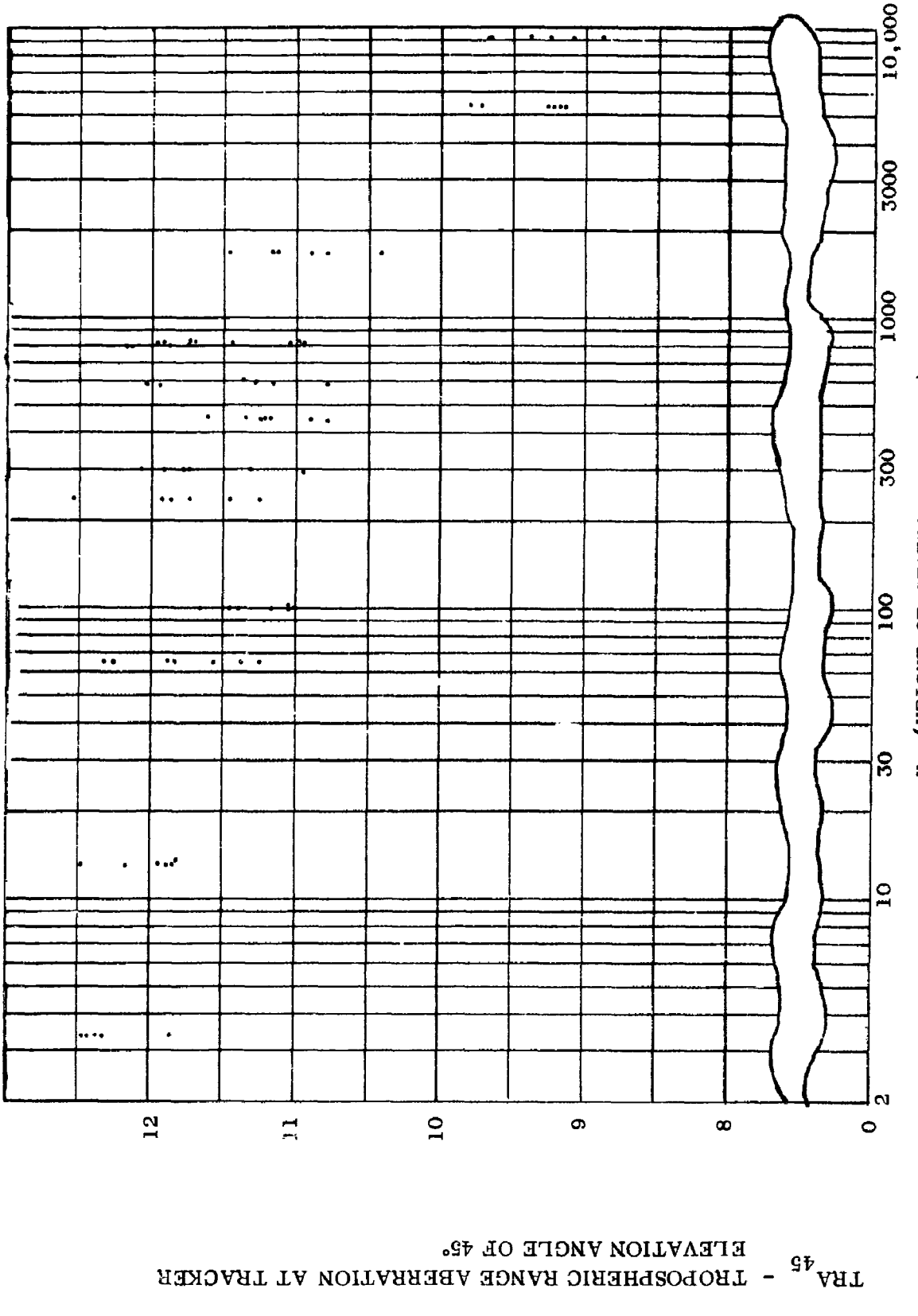

Figure 49. Tropospheric Range Aberration at $\epsilon = 45°$ vs. Station Elevation for 77 Actual Profiles at 13 Stations

range aberration as a function of surface refractivity for each of the 77 sets of profile data that were examined. It is seen that the correlation of the needed correction with N_S is very pronounced at low elevation angles, but that there is still quite a sizeable residual error. The solid lines drawn on the graphs of Figures 50 and 51 represent the regression line of TRA upon N_S. The RMS residual error when N_S is used as the only means of predicting tropospheric range aberration is 42.5 feet at 0 degree-elevation angle, 0.374 feet at 45 degree-elevation angle and 0.266 feet at 90 degree-elevation angle.

Bean and Horn (Reference III-18) state that a mean value of surface refractivity N_S for stations at any altitude may be obtained by using the formula:

$$N_S = 330 \exp(-0.03222H)$$

where N_S is the mean surface refractivity at an altitude, H, in thousands of feet, and 330 is the world-wide mean sea-level refractivity, N_O. A closer approximation to the value of N_S for any particular station can be obtained by replacing the 330 in this equation with a specific value of N_O as a function of location as given in Section 2 of Reference III-19.

Having obtained an appropriate value of N_S for a station at a location under consideration, the approximate value of the tropospheric range aberration can then be obtained by reference to Figures 50 and 51 which give TRA as a function of N_S alone.

3.2 EFFECT OF CLIMATE

There is a large amount of information in the literature showing the variations in the index of refraction as a function of geographic location, time of day, and season of the year. Coupled with the dependence of TRA upon N_S, these variations show that it is necessary to include a correction for tropospheric range aberration as a function of either the climate and time of day, or as a function of the instantaneous value of N_S.

Figures 52 and 53 are taken from a report by Bean, Horn and Riggs (Reference III-19) and serve to illustrate typical variations to be expected at different seasons, times and locations. Figure 52 gives data for Miami, Florida, and shows that the range of surface refractivity goes from a low of 288 in January at 1400 local time, to a high of 397 in August at 0200 local time. Reference to Figures 50 and 51 shows that this will cause a predicted variation in TRA at a 45 degree-tracking angle of 10.25 to 12.65 feet. The lower portions of this chart show that the range of N_S deviations with time of day are greater in the winter months than in the summer for this station.

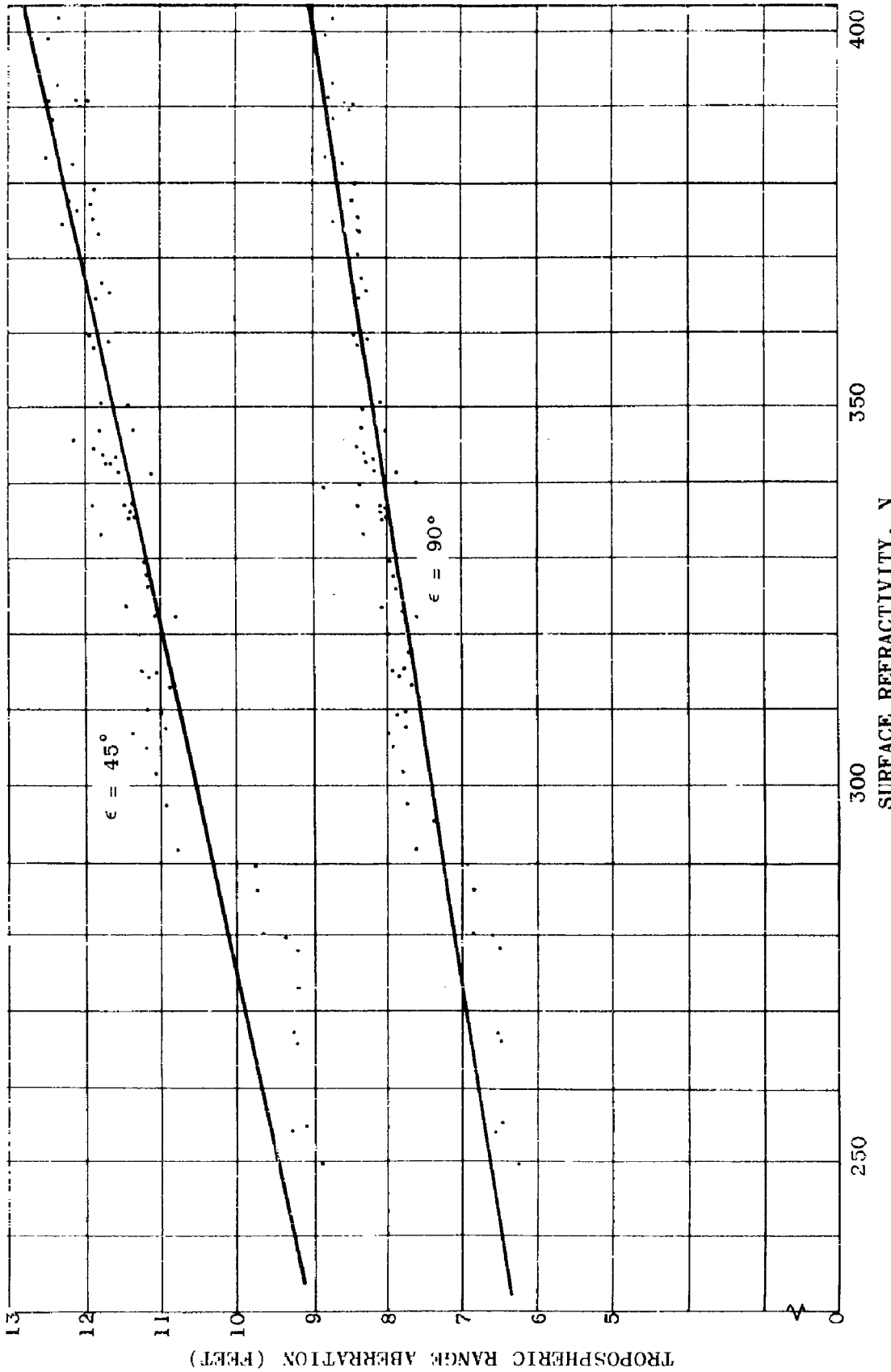

Figure 50. Tropospheric Range Aberration vs. Surface Refractivity for 77 Profiles (ϵ = 45° and 90°)

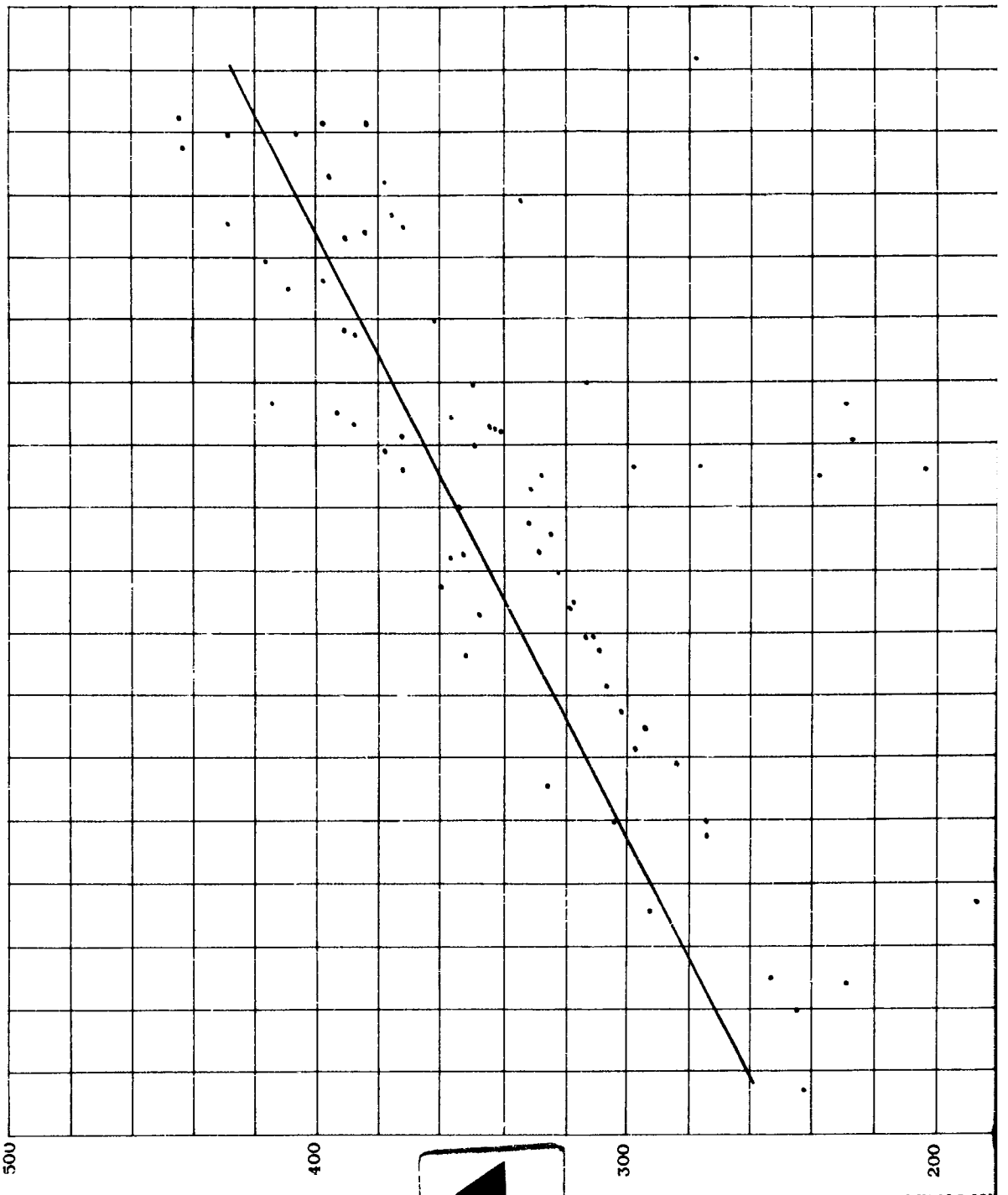

Figure 51. Tr
Refr

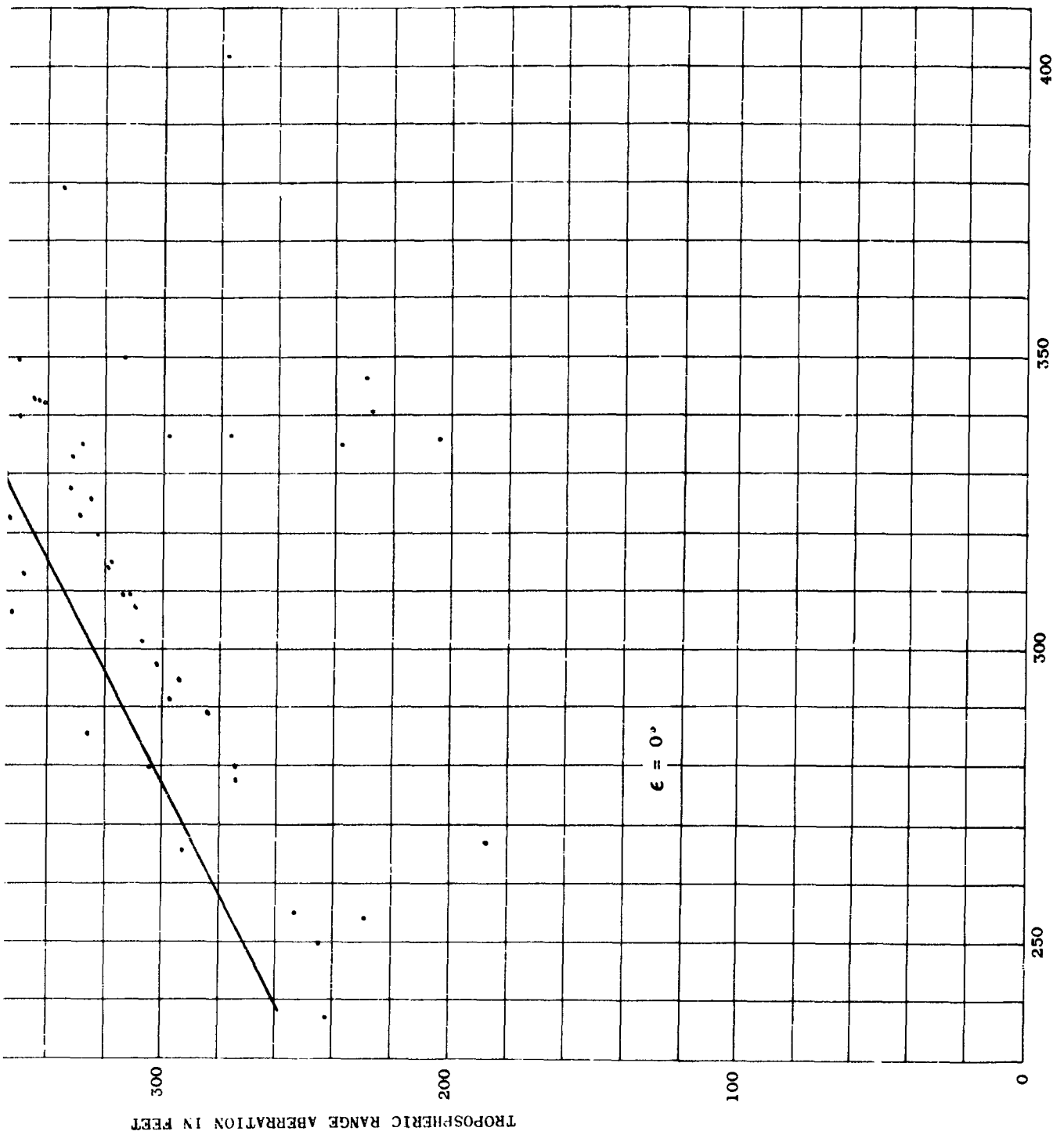

Figure 51. Tropospheric Range Aberration vs. Surface Refractivity for 77 Profiles ($\epsilon = 0°$)

Figure 53 shows the seasonal and diurnal variations in N_S for a high-altitude station (Colorado Springs, Colorado). Again, reference to Figures 50 and 51 shows that the minimum value of N_S of 213 in April at 1400 local time would give a 45-degree TRA of 8.6 feet, while the maximum value of 302 in August at 0200 local time would give a 45-degree range aberration of 10.6 feet. Comparison of this data with the data previously quoted for the sea level station shows that the higher and dryer site locations not only give smaller tropospheric range corrections but also give smaller variations in the corrections required.

From these figures it may be concluded that the seasonal and diurnal variations in the surface refractivity (and associated tropospheric range aberration) are large enough to make it desirable to include a real-time correction for changes in surface refractivity whenever precision range radar tracking is required. The rate of change of refractivity (as judged from charts such as those in Figure 52) is great enough to show definite advantages in the use of a real-time correction for N_S, as opposed to manual fixed corrections that would be made on the basis of intermittent measurements of its value.

3.3 EFFECT OF ELEVATION ANGLE ON TRC

Figure 54 shows the variation of the tropospheric range aberration for the CRPL Reference Profile-1958, as the elevation angle, ϵ , changes. The vertical bars represent the spread in TRA for the 77 different actual profiles tested. For all but the crudest range tracking systems (limited to tracking angles above 30 degrees) a real-time correction for TRA as a function of ϵ is required.

3.3.1 The Cosecant Expression

Several means of accomplishing this elevation correction have been considered. The simplest way would be to use a cosecant-potentiometer pickoff on the tracking antenna, where the zenith value of correction (TRC_{90}) is then substituted in the following equation:

$$TRC\ (N, \epsilon) = TRC_{90}\ (N) \times \csc \epsilon\ .$$

This cosecant expression gives a reasonably good fit to the data for elevation angles above 15 degrees. It was compared to the results of the IBM 7090 calculation for the CRPL Reference Profile-1958, based on $N_S = 330$, and gave less than one percent error for this one profile down to $\epsilon = 15$ degrees. At lower angles the error rises rapidly, being 2.1 percent at 11 degrees, 10.3 percent at 5 degrees, and 109.5 percent at 1 degree. In Figure 55 this data is plotted against elevation angle. The circles and crosses are equivalent data for two representative actual profiles.

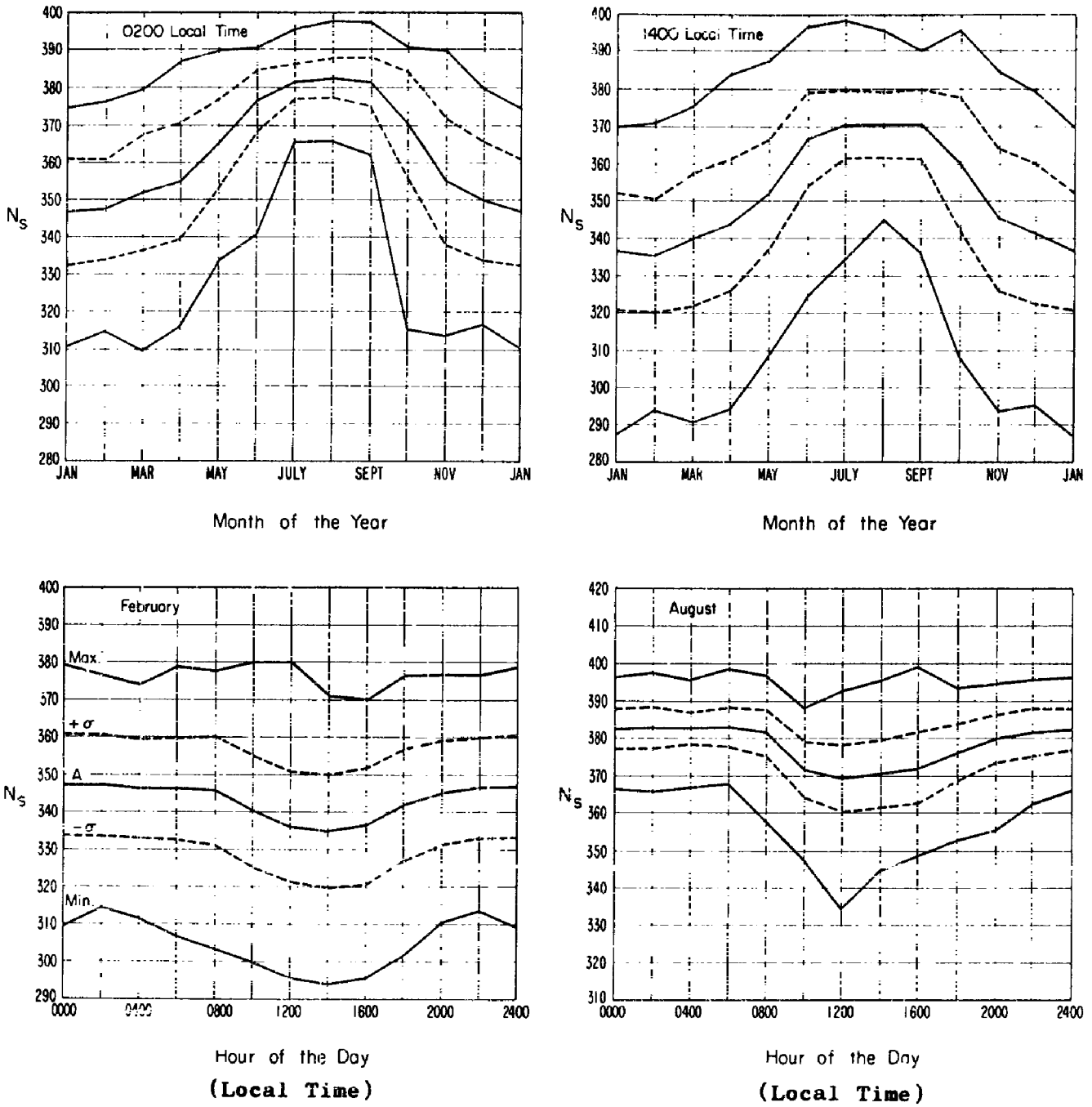

Figure 52. Variation in Surface Refractivity - Miami, Florida

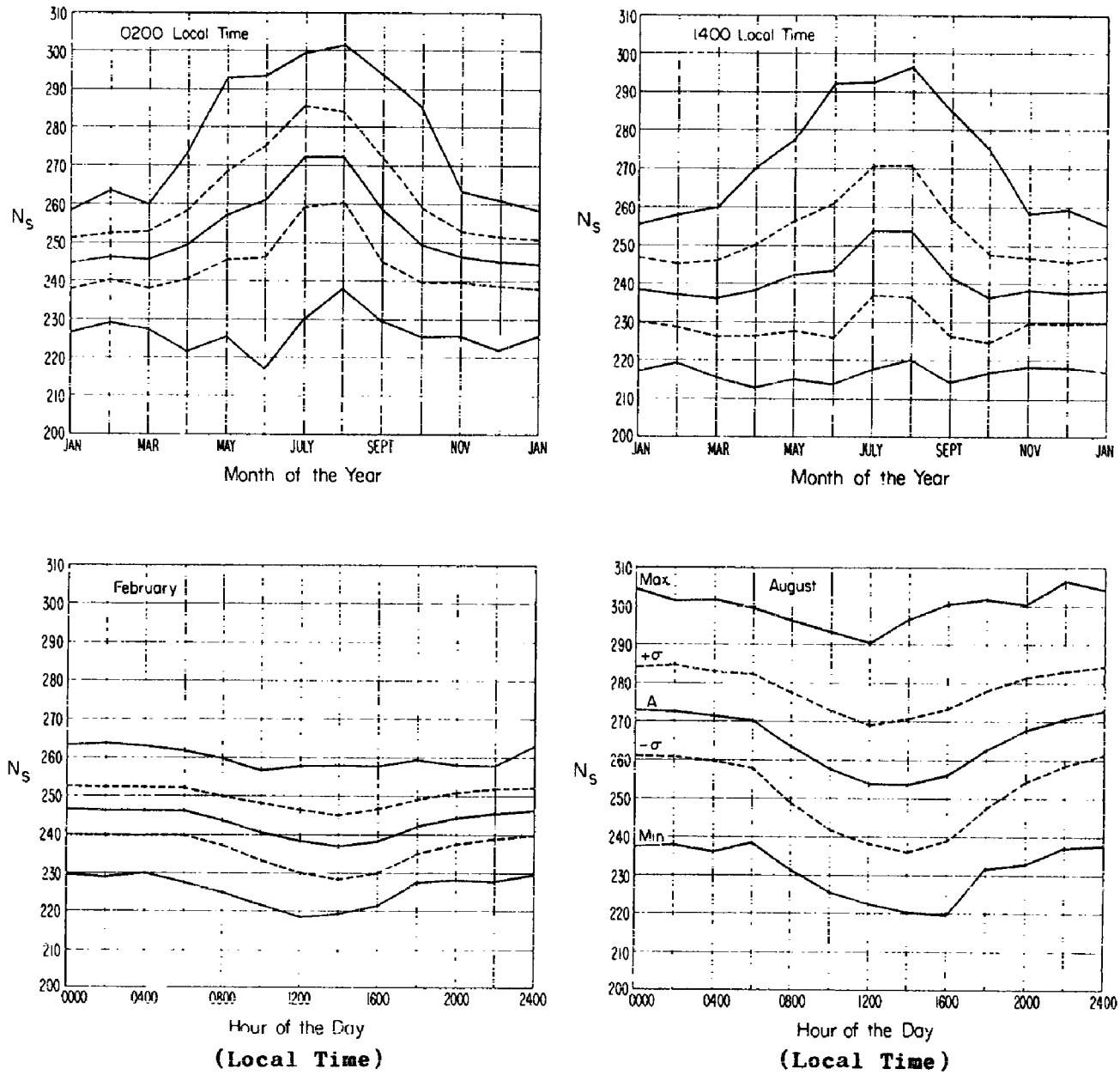

Figure 53. Variation in Surface Refractivity - Colorado Springs, Colorado

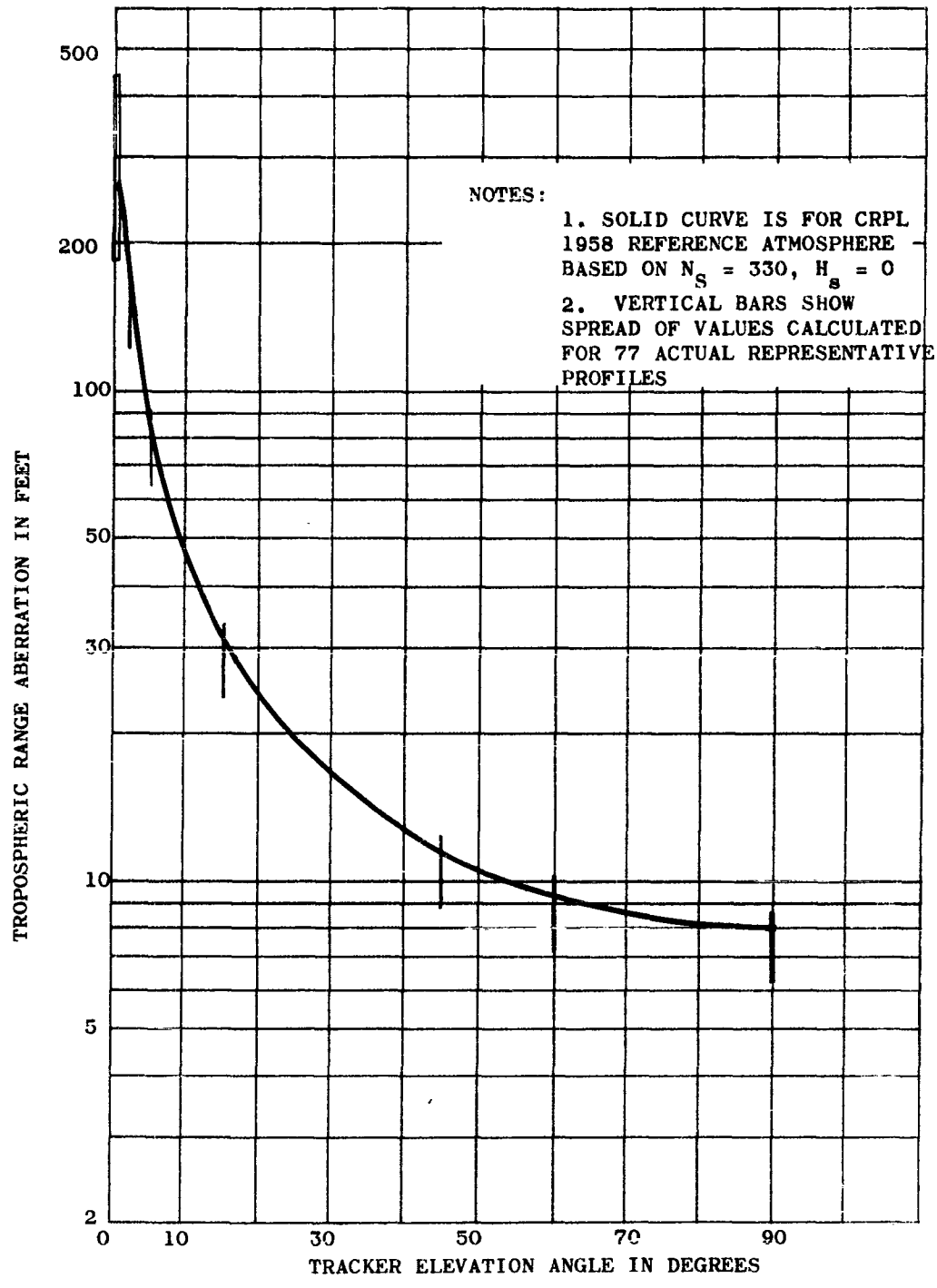

Figure 54. Tropospheric Range Aberration vs. Tracker Elevation Angle

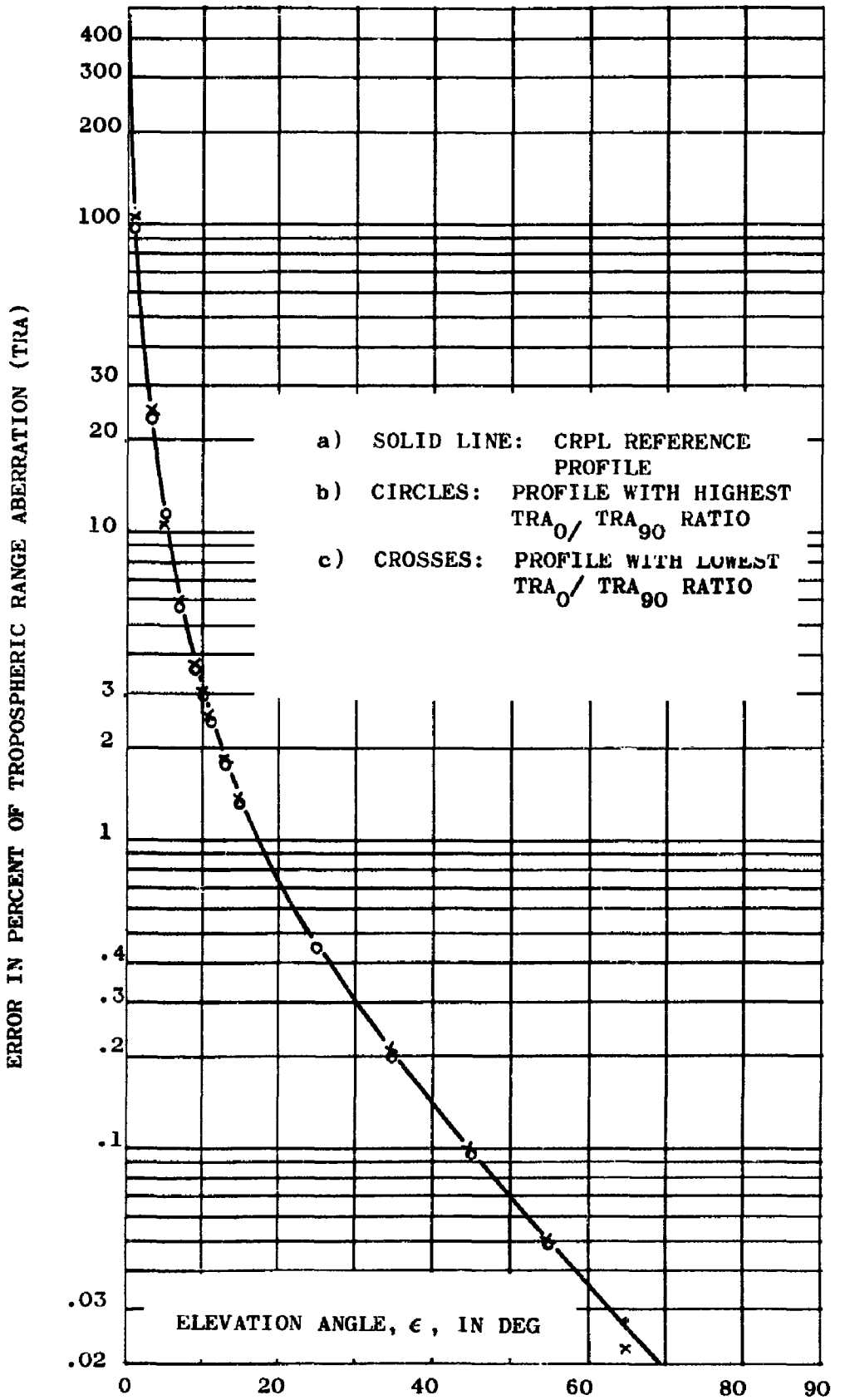

Figure 55. Cosecent Expression for f(ϵ) Percent Error vs. Elevation Angle

The cosecant expression assumes constant ratios between the values of TRA (0°) and TRA (90°). As has already been seen, these ratios are not constant. The ratio of TRA (0°)/TRA (90°) varies from a minimum of 24.96 to a maximum of 50.63 over the 77 actual profiles that were tested. The primary reason for the inability of the cosecant expression to handle this situation is that the cosecant expression assumes that the atmosphere is homogeneous, and that it lies uniformly over a flat earth. This, of course, is not true, so that a better function of elevation angle, f (ϵ), is required.

3.3.2 Bowers' Expression

The following function of elevation angle was derived by Dr. Robert Bowers, of the Convair-Astronautics Flight Performance and Guidance Analysis Group. A brief version of his derivation is contained in paragraph 3.3.3 of this appendix.

$$TRC\ (\epsilon) = \sqrt{\left(\frac{E_0^2 - E_{90}^2}{2\,E_0\,E_{90}}\right)^2 \sin^2 \epsilon + 1} - \left(\frac{E_0^2 - E_{90}^2}{2E_0\,E_{90}}\right) \sin \epsilon$$

where:

E_0 = Tropospheric Range Correction at $\epsilon = 0°$

E_{90} – Tropospheric Range Correction at $\epsilon = 90°$

ϵ = Tracker elevation angle

This expression assumes that the atmosphere is spherically-stratified over a curved earth. The percentage difference between this f (ϵ) and the IBM 7090 calculations for the two actual profiles having the largest and the smallest ratios TRA (0°)/TRA (90°), and for the CRPL Reference-1958 profile based on N_s = 330 is plotted in Figure 56.

The Bowers' expression gives a much better fit to the real function of elevation angle than does the cosecant function, primarily because it "forces" the error to be zero at both ends of the function. (Note the 10:1 scale change between graphs.)

Due to the fact that the atmosphere is not homogeneous, and because a low-angle ray spends a greater percentage of its atmosphere transit-time in the lower, denser layers of atmosphere, this f (ϵ) departs significantly from ideal performance below 10 degrees. Attempts to correct this by weighting the contribution of the lower parts of the atmosphere, or by fitting the expression to the data at E_{90} and E_{10} (instead of at E_{90} and E_0) have, to date, resulted in expressions of such complexity as to be unsuited for real-time elevation angle correction.

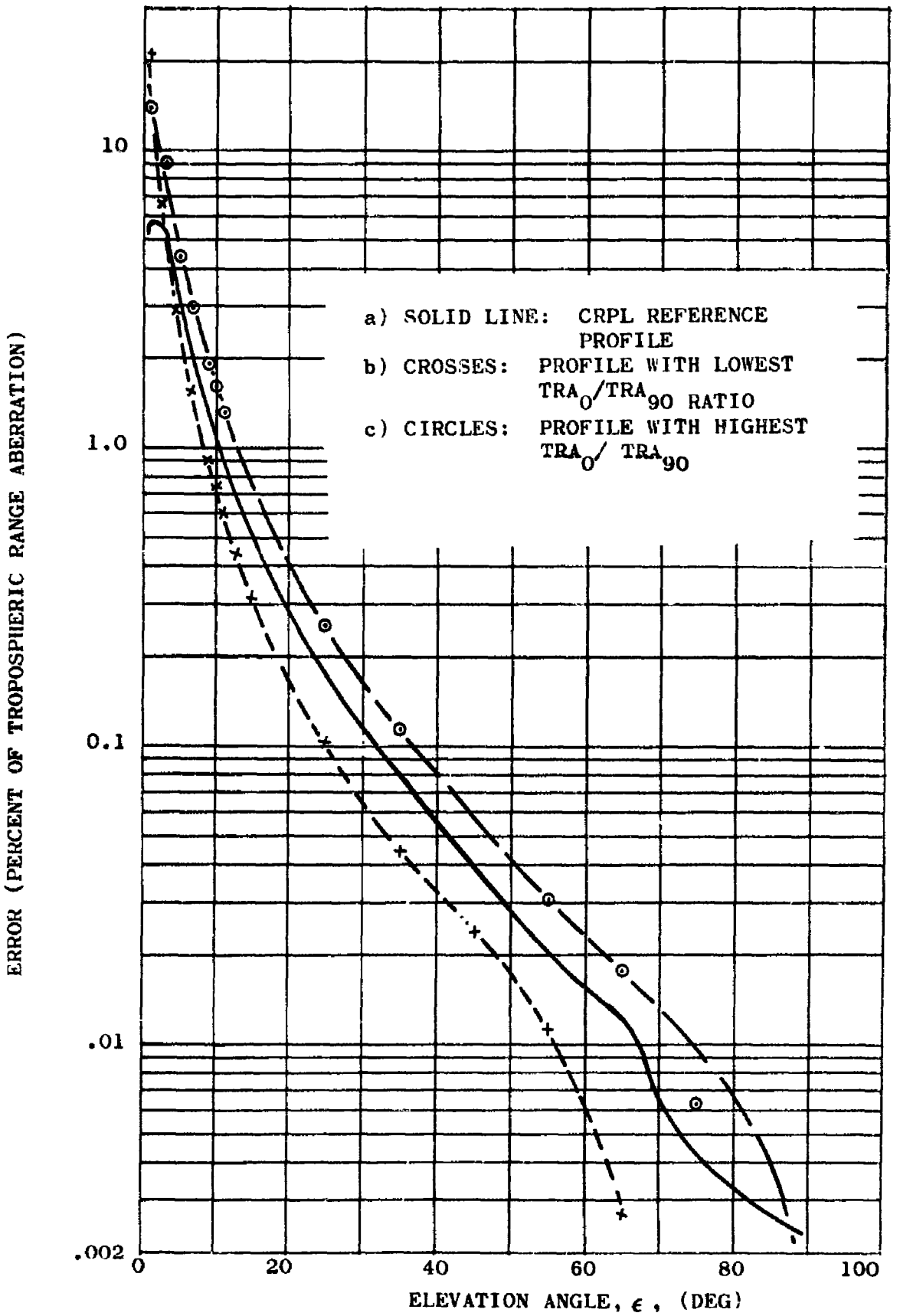

Figure 56. Bowers' Expression for f(ϵ) Percent Error vs. Elevation Angle

If the effects of angle are to be completely minimized, other, more complex techniques can be employed. A "table look-up" solution employing a digital computer has been suggested, with computer-interpolation of values between closely-spaced, pre-calculated tabular data for various profile types. The expense and bulk of this method is not felt to be justifiable in most cases, since the error due to the angle function is a small part of the entire residual tropospheric range error.

3.3.3 Derivation of Bowers' Expression

In determining the tropospheric range correction (TRC) as a function of elevation angle, ϵ, it is desirable to obtain a reasonably good approximation function, so that the integration of paragraph 5.2 of Section 5 need not be repeated for every profile at each angle.

A first approximation often used is the cosecant expression:

$$\text{TRC}(\epsilon) = \text{TRC}(90) \csc \epsilon$$

This relationship assumes:

a) the atmosphere is homogeneous and has some effective thickness, t, and that

b) the atmosphere lies over a flat earth.

Since neither of these assumptions is valid, the errors in the cosecant expression rise rapidly at low tracking angles, (see Figure 55), approaching infinity as ϵ approaches zero.

An expression which forces the error to be zero at both the zenith and the horizon has been derived by Dr. Robert Bowers. An outline of that derivation follows.

Figure 57 illustrates the geometry involved. This relationship also assumes that the actual atmosphere can be replaced by an effective, homogeneous atmosphere of effective thickness, t, but includes the effects of earth curvature.

By the cosine law:

$$\cos \phi = \frac{\rho_o^2 + \rho^2 - \ell^2}{2\rho_o \rho}$$

and:

$$\cos \phi = \frac{OR}{OQ} = \frac{\rho_o + \ell \sin \epsilon}{\rho}$$

Therefore:

$$\ell^2 + (2\,\rho_o \sin\epsilon)\ell + (\rho_o^2 - \rho^2) = o$$

and, by the quadratic formula (since $\rho = \rho_o + t$):

$$\ell\,(\epsilon) = \ell = \sqrt{\rho_o \sin\epsilon + 2\rho t + t^2} - \rho_o \sin\epsilon$$

Equation III-2 gives an accurate expression for the straight-line path length through an atmosphere of effective homogeneous thickness, t. Since the effective thickness is not known, and since it varies from profile to profile (note the 2:1 range in the value of TRA(0)/TRA(90) in Table 6 of Section 5), equation III-2 must be manipulated so as to eliminate t.

The zenith correction, E_{90}, is given by:

$$E_{90} = TRA_{90} = 10^{-6} \int_{h=0}^{h \text{ at } N=0} N(h)\,dh = kt \qquad \text{(III-3)}$$

Where the variable, k, is defined as:

$$k = \frac{E_{90}}{t} \qquad \text{(III-4)}$$

If we make the approximation that the correction, TRC (ϵ), in the assumed homogeneous atmosphere of effective thickness, t, is proportional to the path length traversed in this fictitious atmosphere, we can write:

$$TRC\,(\epsilon) = k\ell\ (\epsilon)$$

$$= k\left[\sqrt{(\rho_o \sin\epsilon)^2 + 2\rho_o t + t^2} - \rho_o \sin\epsilon\right] \qquad \text{(III-5)}$$

At the horizon this reduces to:

$$E_o = TRC(0) = k\left[2\rho_o t + t^2\right]^{1/2} = kt\left[\frac{2\rho_o}{t} + 1\right]^{1/2} \qquad \text{(III-6)}$$

$$E_0 = E_{90}\left[\frac{2\rho_o}{t} + 1\right]^{1/2} \qquad \text{(III-7)}$$

Substituting III-4 into III-5 we get:

$$TRC(\epsilon) = E_{90}\left[\sqrt{\left(\frac{\rho_o}{t}\right)^2 \sin^2\epsilon + \frac{2\rho_o}{t} + 1} - \frac{\rho_o}{t}\sin\epsilon\right] \qquad \text{(III-8)}$$

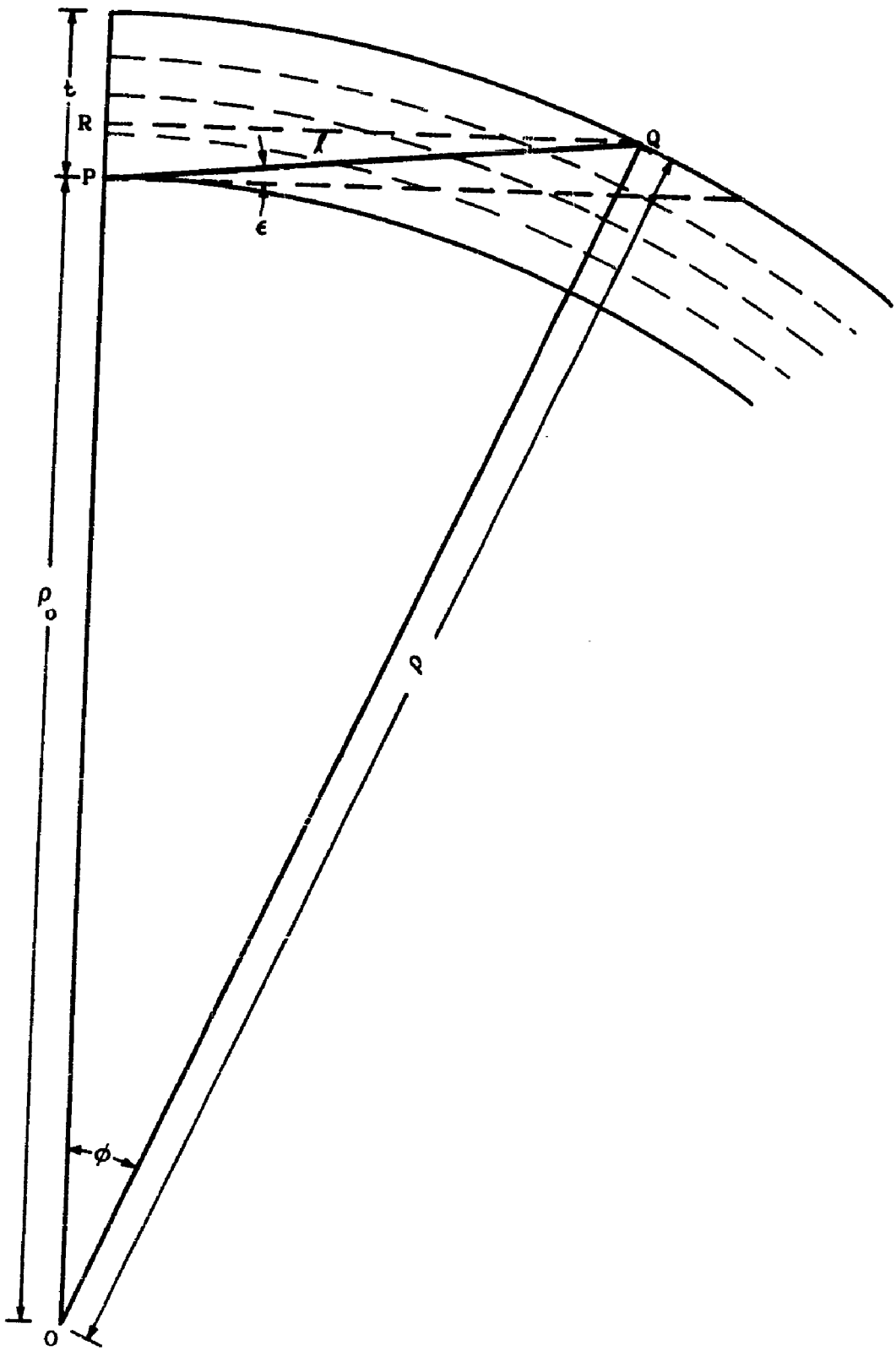

Figure 57. Geometry Used in Approximate Ray Tracking

Now, momentarily introducing the ratio, M, and observing each of the following relationships with the several different terms of III-5 and III-8;

$$M \equiv \frac{E_0}{E_{90}} = \left(\frac{2\rho_o}{t} + 1\right)^{1/2} \tag{III-9}$$

$$M^2 = \frac{2\rho_o}{t} + 1 \tag{III-10}$$

$$\frac{\rho_o}{t} = \frac{M^2 - 1}{2} = \frac{E_0^2 - E_{90}^2}{2E_{90}^2} \tag{III-11}$$

$$\frac{\rho_o^2}{t^2} = \left[\frac{E_0^2 - E_{90}^2}{2E_{90}^2}\right]^2 \tag{III-12}$$

Now substituting III-10, III 11, and III-12, we obtain

$$TRC(\epsilon) = E_{90}\left[\sqrt{\left(\frac{E_0^2 - E_{90}^2}{2E_{90}^2}\right)^2 \sin^2\epsilon + \left(\frac{E_0}{E_{90}}\right)^2} - \left(\frac{E_0^2 - E_{90}^2}{2E_{90}^2}\sin\epsilon\right)\right] \tag{III-13}$$

Which, on factoring $\frac{E_0}{E_{90}}$ from within the brackets gives

$$TRC(\epsilon) = E_0\left[\sqrt{\left(\frac{E_0^2 - E_{90}^2}{2E_0E_{90}}\right)^2 \sin^2\epsilon + 1} - \left(\frac{E_0^2 - E_{90}^2}{2E_0E_{90}}\right)\sin\epsilon\right] . \tag{III-14}$$

If we now define:

$$A = \frac{E_0^2 - E_{90}^2}{2E_0E_{90}} , \tag{III-15}$$

we obtain the desired function of elevation angle in the form:

$$TRC(\epsilon) = E_0\left[\sqrt{(A\sin\epsilon)^2 + 1} - A\sin\epsilon\right] \tag{III-16}$$

The quantities E_0 (the correction required for the horizontal ray) and E_{90} (the zenith correction) may be determined by any suitable technique (such as regression equations on surface refractivity and initial gradient, or upon form factors, etc.). Equation III-16 is easily adaptable for use in a simple analog computer.

The lack of rigor in the above equation is the assumption that the atmosphere behaves as through it were homogeneous throughout some effective thickness, t. As can be noted in Figure 62, the ray spends an increasing percentage of its time in the low-altitude section of the profile as the elevation angle approaches zero. It is proposed to extend this type of analysis to a stratified atmosphere in an effort to reduce the 6-to-20 percent error incurred at very low angles (around 1 degree).

3.4 VARIATIONS ALONG A BASE LINE

Because of the nature of the tracking system model used to analyze the over-all system errors, it was desirable to obtain quantities representative of the correlated and uncorrelated components of tropospheric range aberration as a function of base line distance. As has been seen in the section on the effects of climate (paragraph 2.1, of this appendix), the tropospheric range aberration fluctuates widely with the time of day and the type of air mass over the site. It was felt, however, that working with mean values of surface refractivity would give an indication of the magnitude of the variation in TRA to be expected between two stations along a given base line.

Figures 58 and 59 were taken from a report by Bean, Horn and Riggs on Radio Refractive Index Climatology (Reference III-19). Having plotted a typical 2,000-mile base line diagonally across the United States on each of these figures, the values of mean sea-level refractivity (N_0) were then plotted on Figure 60. Also plotted on this figure is the value of surface refractivity (N_s). The value of N_s for the chart was obtained by using the relationship, N_s $N_s = N_0 \exp(-0.1057h)$, see Figure 47.

Using the values of N_s from Figure 60 and the relationship between N_s and total range aberration, as given in Figures 50 and 51, the upper (solid) curve of Figure 61 was plotted. This curve shows the expected mean value of tropospheric range aberration for an antenna-pointing angle of 45 degrees. The lower curve of Figure 61 is a plot of the values of deviation of N_s as taken from Figure 59. The dashed curves surrounding the mean value of TRA in the upper curve are the 1-sigma variations in range aberration corresponding to the indicated variations in surface refractivity.

The root-mean-square variation in the values of N_s on Figure 60 equals 311 N-units (around a mean value of 313 N-units). At 0 degree elevation angle this corresponds to an RMS variation of 31 feet, out of 335 feet total range aberration. At the zenith this corresponds to an RMS variation of 0.5 foot out of 7.6 feet TRA. If the correction to be applied for tropospheric range effects were to be based only on average values of N_s, these figures for RMS variation could be used for the uncorrelated part of the error. Most of the variation in TRA shown in Figure 61 will be compensated for by the more complete correction technique now proposed. It seems logical to assume that the uncorrelated portion of the tropospheric effect is that part of the aberration which is not completely compensated for by the correction. As was shown in Table 9 in Section 5 of this report, the residual error varies from 0.12 foot

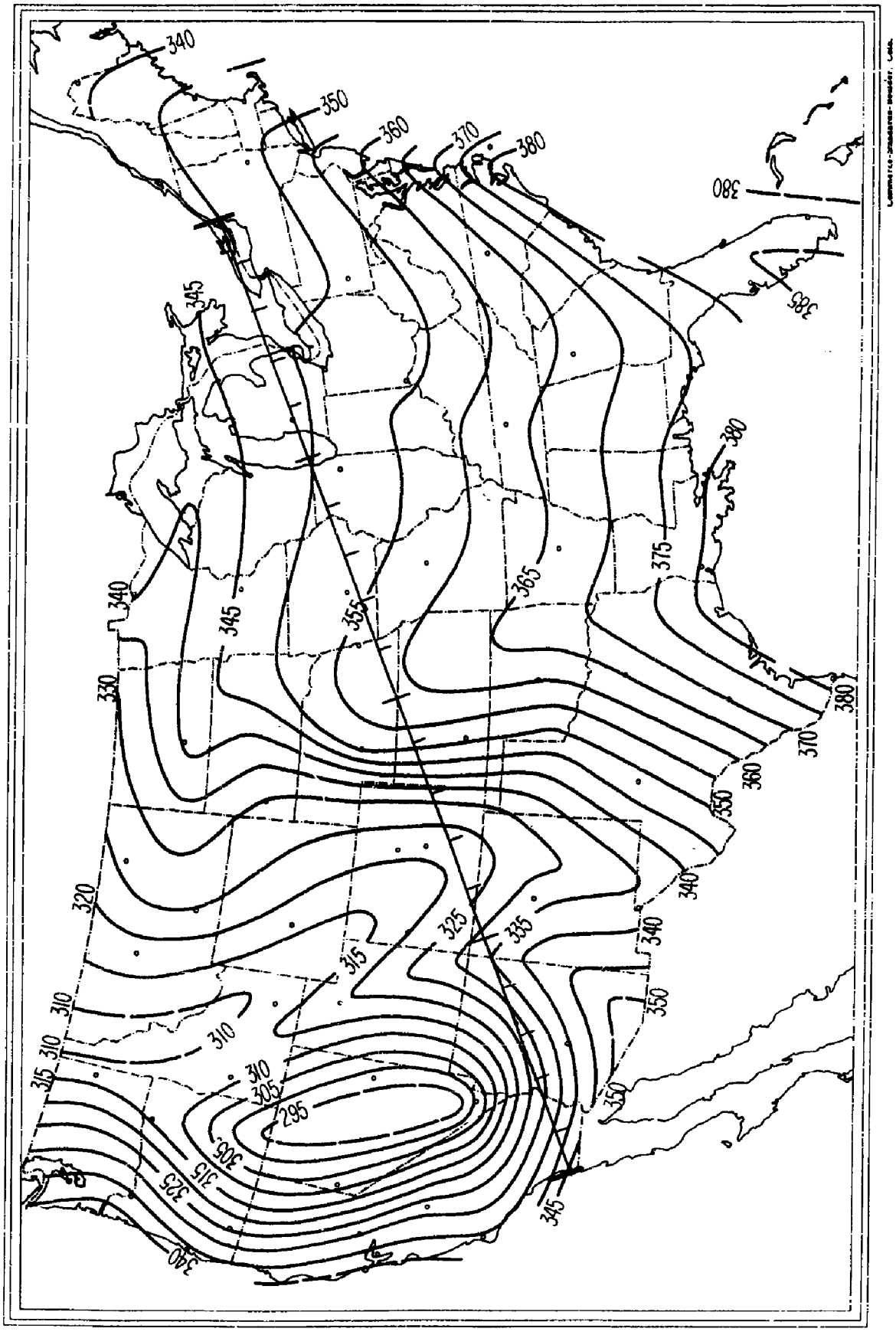

Figure 58. Mean Sea Level Refractivity (N_o) August, 0800

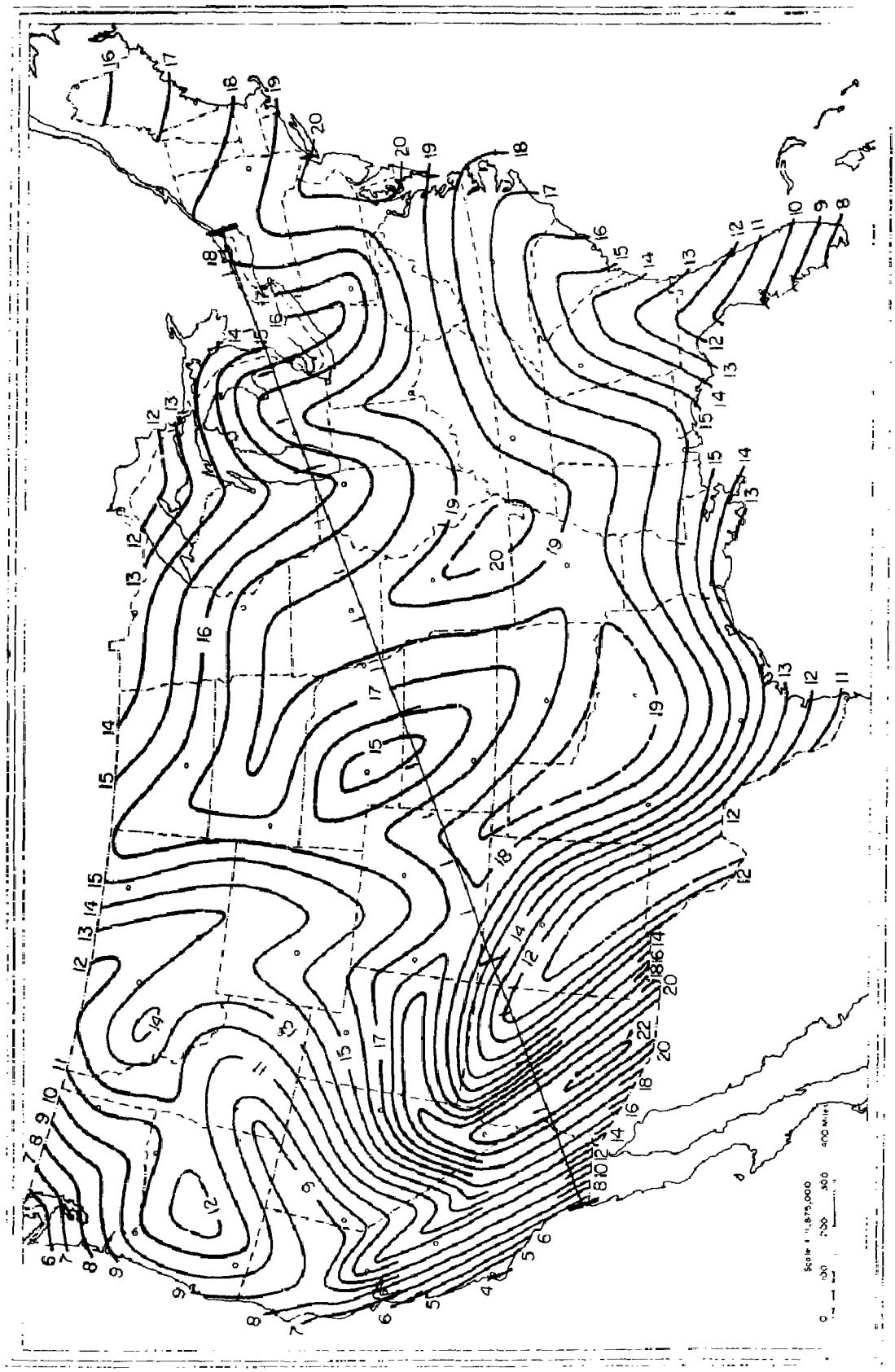

Figure 59. Standard Deviation of Surface Refractivity (N_s) August, 1400

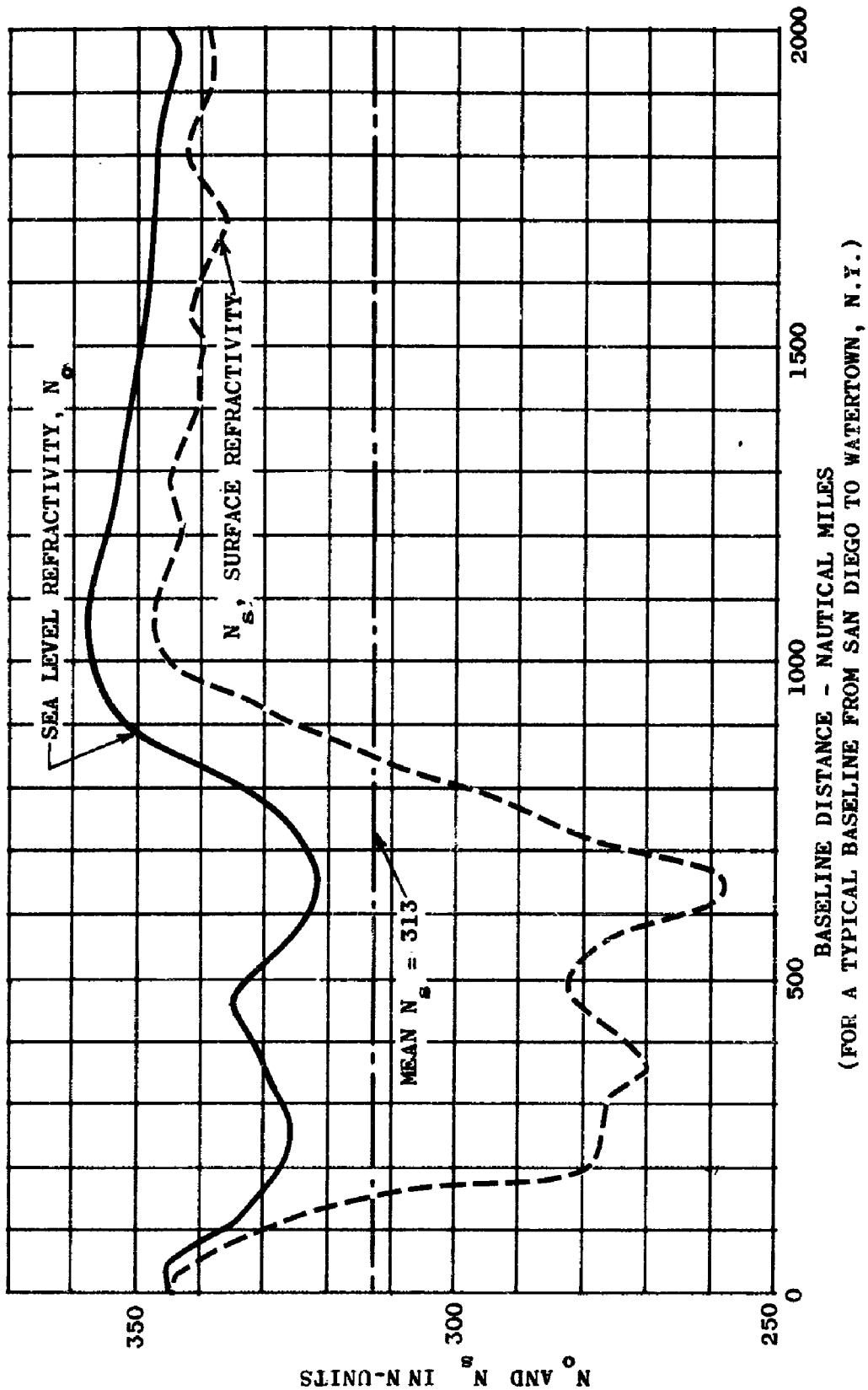

Figure 60. Refractivity vs. Location Along a Typical Baseline

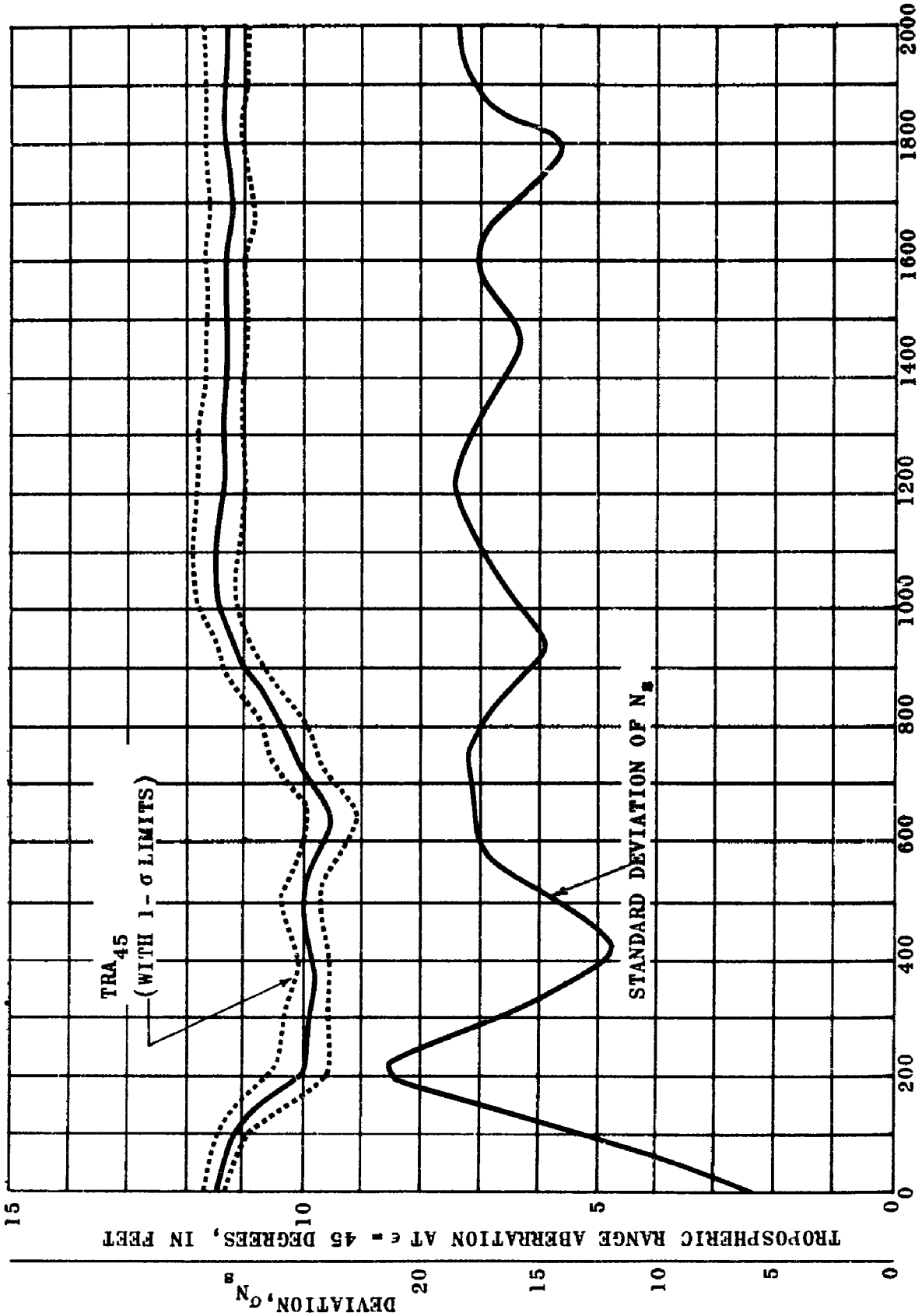

Figure 61. 45° Range Aberration Changes Along a Typical Baseline

at the zenith to 29.3 feet at the horizon, both values being mean values of the magnitude of the residual error. A more useful estimate of the uncorrelated portion of the effect is that, at the zenith the RMS residual error is 2.02 percent, while at the horizon it is 11.87 percent.

3.5 FORM FACTOR

It can be shown that, at a 90-degree elevation angle, the tropospheric range aberration is given by:

$$TRA_{90} = \int_{\text{surface}}^{\text{top of troposphere}} N\,dh \times 10^{-6}$$

If a plot of radiosonde data for N vs. h is integrated (by use of a planimeter, etc.) the value of the required correction, TRC_{90}, can be readily determined in the field.

3.5.1 Vertical Form Factor

Since it is a straightforward matter to obtain the integral of N dh, we have defined a vertical form factor (VFF) as follows:

$$VFF = \sum_{N=0}^{N=N_s} N_i\ \Delta h_i \times 10^{-6} = E_{90}$$

The value of VFF can then be used in place of E_{90} in the $f(\epsilon)$ expression for total range correction at angles other than the zenith.

3.5.2 Horizontal Form Factor

It is desirable that a means of obtaining an equivalent expression for E_O for substitution in the f (ϵ) expression (paragraph 3.2) be obtained in a manner analogous to the vertical form factor (VFF). At the present time the possibility of providing an arbitrary weighting factor for various altitude increments of a radiosonde profile is being investigated in order to obtain a horizontal form factor (HFF).

3.5.3 Combinations of Form Factor with Surface Parameters

The total tropospheric range aberration depends on the instantaneous values of the complete profile of refractivity vs. altitude. The complete profile is very difficult to obtain at frequent intervals and is impossible to obtain in real time or instantaneously. Changes in the value of this profile are due to variations in the type of air mass above a station and to variations in the temperature, etc., at the ground. The most significant changes in the tropospheric range aberration are due to changes in the lower portions of the profile. These changes can be inferred partially by evaluation of surface refractivity and initial gradient of refractivity.

It is considered probable that an evaluation of TRA in terms of form factors (as determined by radiosonde information taken at spaced intervals, perhaps four times a day) will initially be subject to much less error than determination of tropospheric range aberration based upon surface refractivity and initial gradient, alone. This error will gradually increase with time as atmospheric conditions progressively change. Since surface refractivity and initial gradient can be obtained on a continuous basis (indicating at least the direction of these progressive changes) it would seem feasible to attempt to combine the effects of periodic profile data with the effects of instantaneous changes in the surface parameters.

3.5.4 Proposed Future Efforts

It is proposed, therefore, that an extension of the present effort be undertaken to permit an analysis of an error model of the following type:

$$TRA(t) = A(FF_O) + B\ (N_{s_t} - N_{s_O}) + C\ (\text{grad } N_t - \text{grad } N_O) + D\ H_s$$

where·

TRA(t) is a total range aberration at a selected angle at a time, t, following the time of radiosonde ascent,

FF_O is the form factor obtained from the radiosonde at time zero,

N_{s_t} is the surface refractivity at a time, t, after the radiosonde ascent,

N_{s_O} is the surface refractivity at the time of the radiosonde ascent,

grad N_t is the low-altitude gradient of refractivity at the time, t, after the radiosonde data was obtained,

grad N_O is the initial gradient present at the time radiosonde data was obtained, and

H_s is the altitude of the tracking station.

The coefficients A, B, C and D are the weighting factors to be determined by regression analysis.

To perform this type of analysis requires refractivity profile information which is not presently on hand. The data must be obtained from a statistically significant number of stations and be taken at a succession of time intervals. The form factor to be used can then be evaluated from a profile chosen at time t_O, and the differences in the surface refractivity and refractivity gradient can be evaluated over a time internal, t. The regression analysis would then be performed by utilizing values of TRA by accurate integration of a complete profile taken at time t_2. The errors in the result would then be evaluated by comparing the regression-equation calculated corrections, with the actual integrated tropospheric range aberration, obtained from a profile taken at some intermediate time, t_1.

The profiles used in the current effort are not profiles taken over a span of time, as would be required for the proposed analysis. It has, however, been determined that the necessary number and type of profile information is available from the Central Radio Propagation Laboratories of the National Bureau of Standards at Boulder, Colorado. Arrangements have been made to obtain the required number of profiles.

The technique to be used following such an analysis would be to determine, from a radiosonde profile, the value of HFF (the horizontal form factor) using appropriate weighting coefficients, the value of VFF (the vertical form factor) using simply the integral of N(h), and the instantaneous values of N_s and $N_{0.1}$

A small, relatively simple analog calculator would then accept as manually-set inputs the two form factors, N_{s_O}, grad N_O, and the fixed coefficients, A through D; and, as analog variables the values of N_{s_t}, $N_{0.1(t)}$ and ϵ_t. From these factors it would calculate the appropriate value of TRC. Any of the appropriate functions of elevation angle could be readily employed. The resultant information would then combine the advantages of real-time sensitivity to weather changes plus the increased accuracy obtainable by using complete profile refractivity information, rather than refractivity information related to the surface alone.

3.6 ARTIFICIAL TROPOSPHERIC PROFILES

It was felt by the present investigators that since the relationships between surface refractivity and angular bending, and between surface refractivity and signal strength loss have been established, it was worthwhile investigating the degree of the relationship between surface refractivity and total range aberration. In order to test the above hypothesis, several available expressions for refractivity as a function of altitude were investigated.

The following equations are arbitrary expressions presented by various investigators as describing typical profiles of refractivity, N, vs. altitude, h.

Average Profile, by Fannin and Jehn (Reference III-42)

$$N_A = 542.9 + 4.8544h - 100.859\sqrt{h + 3.9187}$$

$$(0 \leq h \leq 103.87)$$

where h is in thousands of feet.

Wet-Day Profile, by Millman (Reference III-55)

$$N_{W_L} = 338 - 1.55 \times 10h + 4.09 \times 10^{-1}h^2 - 6.96 \times 10^{-3}h^3 + 6.16 \times 10^{-5}h^4 - 1.584 \times 10^{-7}h^5$$

$$(0 \leq h \leq 32.8)$$

$$N_{W_H} = 338\ e^{\frac{-h}{25}}$$

where h is in thousands of feet.

Dry-Day Profile, by Millman (Reference III-55)

$$N_{D_L} = 262 - 7.65\,h + 8.55 \times 10^{-2}h^2 - 4.56 \times 10^{-4}h^3 + 8.64 \times 10^{-7}h^4$$

$$(0 \leq h \leq 32.8)$$

$$N_{D_H} = 262\ e^{\frac{-h}{25}}$$

$$(32.8 \leq h \leq 200)$$

where h is in thousands of feet

Hot Moist Air Mass Profile, by Buck, Schipper & Kline (Reference III-34)

$$N_{HMA} = 654.693 + 7.053\ h - 131.540\sqrt{h + 4.1}$$

(h in thousands of feet)

Medium-Dry, Warm Air Profile, by Buck, Schipper & Kline (Reference III-34)

$$N_{DWA} = 586.981 + 5.884\ h - 114.064\sqrt{h + 4.1}$$

(h in thousands of feet)

Moist Cold Air Mass Profile, by Buck, Schipper & Kline (Reference III-34)

$$N_{MCA} = 495.199 + 3.854\ h - 86.993\sqrt{h + 4.1}$$

(h in thousands of feet)

Dry Hot Air Mass Profile, by Buck, Schipper & Kline (Reference III-34)

$$N_{DHA} = 431.987 + 2.433\ h - 67.89\sqrt{h + 4.1}$$

(h in thousands of feet)

In their paper (Proceedings of the IRE, 47 No. 5, May 1959), Bean and Thayer describe the following, 3-segmented atmospheric representation, which has been titled "The CRPL Reference Atmosphere - 1958" (Reference III-28)

Low Altitude $(O \leq h \leq h_s + 1\ Km)$

$$N_L\ (h) = N_s - (h - h_s)\ 7.32\ (e^{+\ 0.005577 N_s})$$

Medium Altitude $(h_s + 1 \leq h \leq 9\ Km)$

$$N_M\ (h) = N_1 \left(e^{-\frac{(h - h_s - 1)}{8 - h_s}\ \ln \frac{N_1}{105}} \right)$$

High Altitude ($h \geq 9$ Km)

$$H_H\ (h) = 105\ e^{-0.1424\ (h\ -\ 9)}$$

where:

h = height in kilometers

$N_1 = N_s + \Delta N$ = Value at $h = h_s + 1$

$$N = -7.32\ e^{0.005577\ N_s}$$

N_s = Surface Refractivity

In the same paper Bean and Thayer present their "CRPL Exponential Radio Refractive Atmosphere" which, although it deviates from physical reality at high altitudes, has the advantage of being straightforward to handle mathematically. The mathematical expression for this exponential reference atmosphere is:

$$N_{ER}\ (h) = N_s\ e^{-C_e\ (h\ -\ h_s)}$$

where:

$$C_e = \ln \frac{N_s}{N_1} = \ln \frac{N_s}{N_s + \Delta N}$$

and other terms are as defined above.

All of the preceding profile descriptions are for relatively smooth variation of N vs. h. In order to simulate effects of super-refractive layers, surface and elevated ducts, etc., as listed in Table 4 in Section V of this report, the perturbations in Table 11 were applied to the two types of reference profiles.

Table 11. Perturbations*

TYPE	INFLECTION POINTS	N
1. MGL	0 ft	0
	2,000 ft	-46 N-units
	at higher values	$-50\ e^{-3.22h \times 10^{-5}}$
2. MAX	0 ft	+64
Maximum Surface	8,000	+10
	18,000	+ 0
3. LIN	None	$-100\ e^{-3.22h \times 10^{-5}}$
Minimum Surface		
4. E.D.	0	+62
Elevated Duct	5,200	+20
	5,600	+ 5
	10,000	+ 0
5. Duct	0	+65
	700	0

*Applied only to reference atmospheres, and only with unperturbed values of N_S = 330 at sea level.

Table 11. Perturbations* (Continued)

TYPE	INFLECTION POINTS	N
6. Comb	0	0
	1,500	-32
(MGL + E.D.)	5,200	-20
	5,800	$-60\ e^{-3.22h \times 10^{-5}}$

*Applied only to reference atmospheres, and only with unperturbed values of N_S = 330 at sea level.

Figure 62 illustrates the perturbations that were applied to the CRPL-1958 reference atmosphere. The various artificial atmospheres that were tested are listed in Table 12. The CRPL 1958 reference atmosphere was tested over a wide range of elevation angles, while the other atmospheres were tested at a limited number of ray-path angles.

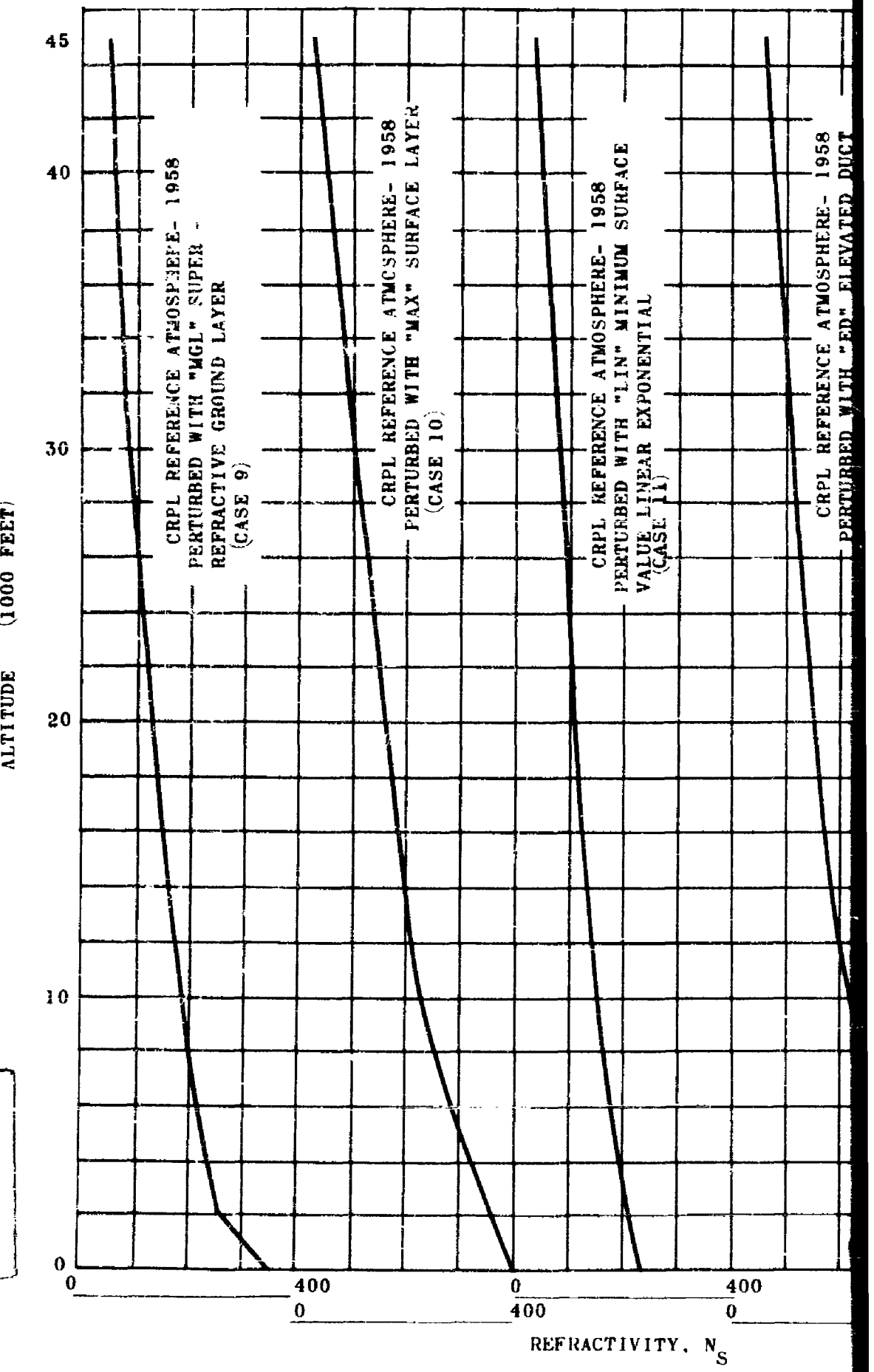
CRPL REFERENCE ATMOSPHERE- 1958
PERTURBED WITH "MGL" SUPER -
REFRACTIVE GROUND LAYER
(CASE 9)
CRPL REFERENCE ATMOSPHERE- 1958
PERTURBED WITH "MAX" SURFACE LAYER
(CASE 10)
CRPL REFERENCE ATMOSPHERE- 1958
PERTURBED WITH "LIN" MINIMUM SURFACE
VALUE LINEAR EXPONENTIAL
(CASE 11)
CRPL REFERENCE ATMOSPHERE- 1958
PERTURBED WITH "ED" ELEVATED DUCT
ALTITUDE (1000 FEET)
45
40
30
20
10
0
0
400
0
400
0
400
0
REFRACTIVITY, N_S

Figure 62. R

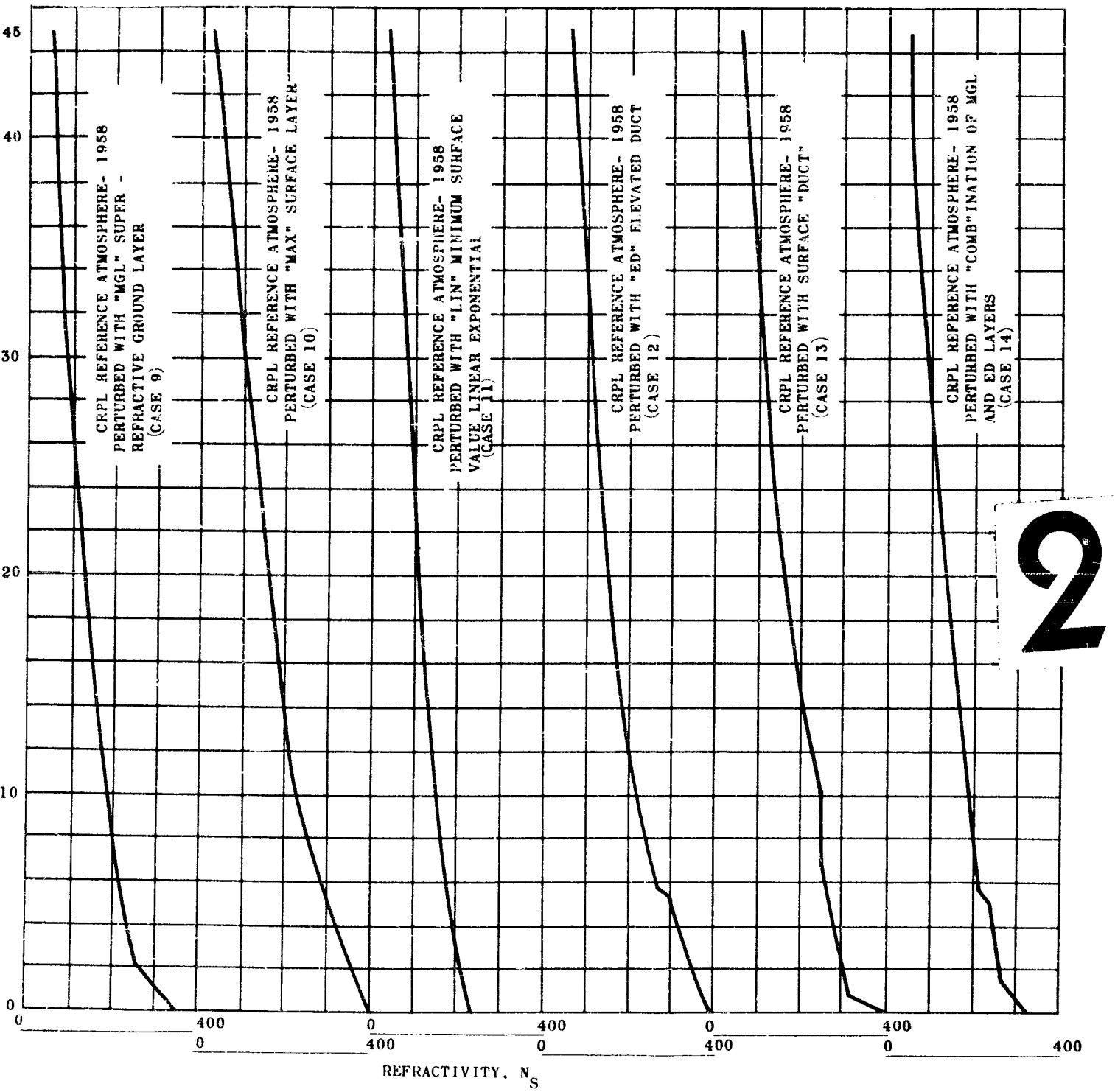

Figure 62. Refractivity vs. Altitude

Table 12. List of Artificial Profiles Tested

CASE NO.	PROFILE	PERTURBATION*	SURFACE REFRACTIVITY	RAY PATH ANGLES IN DEGREES
1.	Bean & Thayer Exponential	None	330	From 1 to 15 degrees in 2-degree increments
2.	CRPL Reference, 1958	None	330	From 15 to 85 degrees in 10-degree increments
3.	CRPL Reference, 1958	None	300	
4.	CRPL Reference, 1958	None	330	10, 45
5.	CRPL Reference, 1958	None	350	10, 45
6.	CRPL Reference, 1958	None	400	10, 45
7.	CRPL Reference, 1958 (Surface Alt. 5000 ft.)	None	250	10, 45
8.	CRPL Reference, 1958 (Surface Alt. 5000 ft.)	None	300	10, 45
9.	CRPL Reference, 1958	MGL	330	10, 45, 45
10.	CRPL Reference, 1958	MAX	394	10, 45, 85
11.	CRPL Reference, 1958	LIN	230	10, 45, 85
12.	CRPL Reference, 1958	ED	330	10, 45, 85
13.	CRPL Reference, 1958	DUCT	395	10, 45, 85
14.	CRPL Reference, 1958	COMB	330	10, 45, 85

Table 12. List of Artificial Profiles Tested (Continued)

CASE NO.	PROFILE	PERTURBATION*	SURFACE REFRACTIVITY	RAY PATH ANGLES IN DEGREES
15.	CRPL Exponential Reference	None	330	10, 45
16.	CRPL Exponential Reference	MGL	330	10, 45
17.	CRPL Exponential Reference	ED	330	10, 45
18.	CRPL Exponential Reference	DUCT	395	10, 45
19.	CRPL Exponential Reference	COMB	330	10, 45
20.	Fannin & Jehn, Average	None	343.2	45
21.	Millman	Wet Day	338	45
22.	Millman	Dry Day	262	45
23.	Buck, Schipper & Kline	Hot Moist Air	388.3	45
24.	Buck, Schipper & Kline	Medium Dry Warm Air	356	45
25.	Buck, Schipper & Kline	Moist Cold Air	319	45
26.	Buck, Schipper & Kline	Dry Hot Air	294.5	45

* See Table 4, Section V of this report for definitions of terms.

GLOSSARY OF TERMS USED IN TROPOSPHERIC RANGE CORRECTION DISCUSSIONS

A_i = value of constant used in regression equations (subscript when present indicates type of regression)

B_i = value of coefficient of N_s used in regression equations

C_i = value of coefficient of grad_0 N (the initial N gradient) used in regression equations

D_i = value of coefficient of Δ N (the refractivity change in the first kilometer) used in regression equations

Δ N = change in refractivity in first kilometer above the tracking station

E_i = value of coefficient of H_s (station altitude) used in regression equations

FFH = horizontal form factor - a means of evaluating the effect of a particular profile of "N" vs "h" upon tropospheric range aberrations for zero elevation angle

FFV = vertical form factor = $\int N(h)\ dh \times 10^{-6}$ feet (a means of evaluating a particular profile of N vs h for its effect on range aberration at the zenith)

E_0 = the tropospheric range correction for a given profile, evaluated at an elevation angle $\epsilon = 0°$ by any of the several correction techniques presented

T = temperature in degrees centigrade

TRA = total range aberration for general case

TRA(ϵ) = total range aberration at tracker elevation angle indicated by subscript

TRA_0 = TRA at horizon

TRA_{90} = TRA at zenith

$TRC_{i,\epsilon}$ = tropospheric range correction to be applied.
subscripts (if present) mean:

- i = method used for determining the correction
- ϵ = tracker elevation angle at which correction is used

$TRRE_{i,\epsilon}$ = tropospheric range residual errors after correction, subscripts (if present) mean:

i = method used for determining the correction having this [illegible]

ϵ = tracker elevation angle at which the residual error is [illegible]

E_{90} – the tropospheric range correction for a given profile evaluated at the zenith (ϵ = 90°) by any of the available techniques presented

ϵ = tracker elevation angle

Grad N = initial gradient of N vs h (refractivity vs height) profile, in N units per kilometer, (taken as equal to change in refractivity in lowest 1 kilometer for this report)

H_s – height of tracking station above sea-level, in feet

$L(\epsilon)$ = a function of effective ray path length through the atmosphere

$$\sqrt{\left(\frac{TRA_0^2 - TRA_{90}^2}{2\,TRA_0\,TRA_{90}}\right)^2 \sin^2\epsilon + 1} - \frac{TRA_0^2 - TRA_{90}^2}{2\,TRA_0\,TRA_{90}} \sin\epsilon$$

η – index of refraction $\eta = 1 + N \times 10^{-6}$

N – refractivity (in N-units) = $N = (\eta - 1) \times 10^6$

N_s – surface refractivity at tracking site, in N-units

N (h) – refractivity aloft at elevation h' above station

N_0 – refractivity at sea level

$N_0 = N_s \exp + 0.03222h$, where h is in kilofeet

$N_{0.1}$ – refractivity at 0.1 km above the tracking site

N_1 – refractivity at 1 km above the tracker

ρ_i – geocentric distance to bottom of atmospheric layer "i"

ρ_o = mean radius of earth

= 20,877,130 ft